Renewable and Sustainable Polymers

ACS SYMPOSIUM SERIES **1063**

Renewable and Sustainable Polymers

Gregory F. Payne, Editor
University of Maryland

Patrick B. Smith, Editor
Michigan Molecular Institute

**Sponsored by the
ACS Division of Polymer Chemistry**

American Chemical Society, Washington, DC

Distributed in print by Oxford University Press, Inc.

The paper used in this publication meets the minimum requirements of American National Standard for Information Sciences—Permanence of Paper for Printed Library Materials, ANSI Z39.48n1984.

PRINTED IN THE UNITED STATES OF AMERICA

Foreword

The ACS Symposium Series was first published in 1974 to provide a mechanism for publishing symposia quickly in book form. The purpose of the series is to publish timely, comprehensive books developed from the ACS sponsored symposia based on current scientific research. Occasionally, books are developed from symposia sponsored by other organizations when the topic is of keen interest to the chemistry audience.

Before agreeing to publish a book, the proposed table of contents is reviewed for appropriate and comprehensive coverage and for interest to the audience. Some papers may be excluded to better focus the book; others may be added to provide comprehensiveness. When appropriate, overview or introductory chapters are added. Drafts of chapters are peer-reviewed prior to final acceptance or rejection, and manuscripts are prepared in camera-ready format.

As a rule, only original research papers and original review papers are included in the volumes. Verbatim reproductions of previous published papers are not accepted.

ACS Books Department

Chapter 1

The Emergence of Renewable and Sustainable Polymers

Patrick B. Smith[*,1] **and Gregory F. Payne**[2]

[1]Michigan Molecular Institute, 1910 West St. Andrews Road, Midland, MI 48640
[2]Center for Biosystems Resources and Fischell Department of Bioengineering, 5115 Plant Sciences Building, University of Maryland, College Park, MD 20742
[*]smith@mmi.org

These are exciting times for biofuels and renewable chemicals! A sense of urgency is driving a frenzy of activity on both research and commercialization fronts. Presciently, the ACS selected "Chemistry for a Sustainable World" as the theme for the Spring 2010 national meeting within which we organized a symposium entitled "Renewable and Sustainable Polymers". The following chapters provide a sampling of the promising opportunities and research directions currently underway across the globe. Included are chapters on the synthesis of materials from seed oils, carbohydrates, protein-based materials, and natural monomers using chemical and biocatalytic processes. In this introductory chapter we provide a broad perspective on the motivation for these activities and an overview of the likely paths forward. We especially focus on reviewing the explosion of commercialization activities in the hope that this static snapshot can provide a glimpse of an incredibly dynamic situation.

Introduction

Throughout history, humans have enlisted biological polymers – especially proteins and polysaccharides - to meet their needs for food, fuel, clothing and shelter. This situation changed dramatically during the last century.

Stunning technical advances enabled petroleum to be recovered and processed inexpensively providing cheap fuels that powered the economic growth for much of the world. Further advances in industrial organic chemistry allowed the petroleum feedstock to be processed into a handful of building blocks (e.g., ethylene, propylene, benzene, toluene and xylene) for the synthesis of petroleum-derived chemicals for applications ranging from consumer goods to agricultural chemicals. Many of these building blocks also became the monomers for the generation of synthetic polymers. In some cases, these synthetic polymers offered inexpensive alternatives to biological polymers and in other cases, these synthetics enabled entirely new capabilities (e.g., engineering plastics and non-stick coatings for frying pans). From the perspective of the early 21st century, it is easy to overlook the impact that advances in petroleum processing had on our way of life.

The Push Away from Fossil Resources

As we project into the future, there are growing concerns that a significant reliance on petroleum (or other fossil resources) is not sustainable for a variety of reasons. First, the fossil resources themselves are finite. Recent estimates indicate that oil production will peak by the next decade (*1*) and while "peak production" is not equivalent to "resource depletion" it does indicate a point of price inelasticity. When supply can no longer be adjusted to meet increasing demand, economics predicts that prices will be prone to substantial increases and fluctuations in response to the market.

Thus, the second concern for the un-sustainability of petroleum is economic. As the price of petroleum increases the search for alternatives will become more urgent – at both the individual and the national levels. Importantly, the petroleum reserves are not distributed equally, as the OPEC-producing nations control nearly 80% of the world's oil reserves (*1*). Nations that rely on substantial oil imports to maintain their economies will face particularly difficult policy decisions when prices escalate. Obviously, other fossil resources could be considered (e.g., coal, shale and natural gas), but accessing and processing these alternatives are less convenient and more costly than petroleum.

The third concern for the un-sustainability of fossil resources is the cost/risk to safety, health and the environment. Much of the discussion has focused on links among fossil fuel consumption, greenhouse gas emission and global warming, and what actions could/should be taken. Yet the recovery and processing of fossil resources presents additional costs/risks. Sadly, 2010 has also been marked by numerous deaths in coal mining accidents and by the worst oil spill in US history.

The Likely Path Forward

It seems likely that the 20th century-trend to an increasing reliance on fossil resources for fuels, chemicals and materials will not continue into the 21st century. This change in paradigm, however, does not mark a demise but rather a transition. This transition cannot reasonably be expected to be rapid as it is difficult (or

impossible) to imagine completely replacing US consumption of fossil fuels in the near term. Even if the US meets the ambitious target for producing 35 billion gallons of ethanol by 2017 (*2*), this would only represent about 12% of the annual US petroleum consumption.

We anticipate three features of the transition from fossil to renewable resources for chemicals and materials. The first expectation is that many of the renewable chemicals and polymers will be driven by successes in biofuels production. Historically, the success of petroleum-based fuels relied on inexpensive large-scale processing. Once the refining capabilities were in place, then they provided an inexpensive supply of building block chemicals that could drive developments in the petrochemical industry. By analogy, advances in the processing of renewable feedstocks (e.g., cellulosics) for biofuels should enable the generation of inexpensive building blocks for value-added chemical and polymeric products. While this "biorefinery" concept is not new it has considerable appeal for "extracting" value from the raw material. In fact, each of the major US grain processing companies, Cargill, Archer Daniels Midland and Tate&Lyle, have built major renewable chemicals manufacturing facilities within their existing grain processing facilities in order to leverage the cost advantages of integration within the site. Cargill has done this with its NatureWorks™ poly(lactic acid) facility in Blair, NE, ADM with its Mirel™ poly(hydroxyalkanoate) plant in Clinton, IA, and Tate&Lyle with its Bio-PDO™ 1,3-propanediol production facility in Loudon, TN.

The second expectation is that the development of renewable chemicals and polymers will significantly benefit from the previous advances in industrial chemistry. In some cases, the transition to renewable polymers may simply mean a switch in raw materials. Examples include the dehydration of fermentation-derived ethanol and 3-hydroxypropionic acid to yield ethylene and acrylic acid, respectively. Once these intermediates are generated, previously-established processing methods (e.g., free-radical polymerization) can be enlisted to yield products for existing markets. In other cases, new products will be generated from renewable resources by extending existing chemical approaches (e.g., ring-opening polymerization for polylactide synthesis).

A third expectation is that biology will play an increasingly-important role in the generation of chemical and material products. Biotechnology transformed the practice of medicine in part by providing capabilities for the biosynthesis of protein-based therapeutics (e.g., insulin) and these capabilities are being enlisted for lower-value applications. Already, protein engineering is yielding improved enzymes (e.g., cellulases) for feedstock processing while metabolic engineering is providing intermediates that cannot be readily obtained through chemical routes (e.g., 1, 3-propanediol for polyester production). Potentially, synthetic biology will provide even more capabilities to access complex feedstocks and generate low-cost intermediates and products with superior functionality.

Potential Chemical Building Blocks Derived from Biofuels

The development of technology for the biofuels market will likely, as stated earlier, provide feedstocks for the chemical industry. If the processes and target molecules currently under development are any indication, trends in this field might provide direction for the nascent renewable chemicals industry. The biomass conversion technologies being commercially developed today are based on three main types of processes; fermentation, thermochemical and algal processes, but there are many variants within them. Table 1 lists many of the companies active in biofuels technology, categorizing them within the conversion technology framework. Most of the information included in this table came from company web pages. This table is not meant to include all the companies in this area because the list would change almost weekly, but rather, it is meant to help define trends. Some of the companies listed are also active in more than one conversion technology.

The primary target biofuels for the fermentation-based conversion technologies are ethanol and butanol although there are recent efforts to develop hydrocarbon-based biofuels. For instance, the small company LS9 is using a fermentative approach to convert carbohydrates to fatty acid intermediates which are upgraded to hydrocarbon fuels enzymatically (*3*). Others, such as Amyris, are commercializing a carbohydrate fermentation to produce polyfarnesene-based hydrocarbons (*4*). Similarly, biofuels from algal conversion technologies often target ethanol and oils for biodiesel and green diesel production. Thermochemical biomass conversion technologies most often produce syngas or bio-oil which can be upgraded to fuels using conventional crude oil refining processes such as hydroforming/hydrotreating, catalytic upgrading and Fisher Tropsch processes. Some technologies produce syngas which is then fermented to ethanol (*5*, *6*). As renewable biofuels become less expensive and more available they will also become attractive feedstocks for generating renewable chemicals and polymers.

In order not to be overly optimistic about the future of biofuels and renewable chemicals, it should be noted that the US renewable fuels business is still somewhat in a state of flux due to several factors. These factors include the substantial fluctuations in the price of oil, the uncertainty of federal tax supports, the food versus fuel debate and issues surrounding carbon dioxide emissions. Ethanol production, primarily from corn in the US, appears to be viable because reformulated transportation fuels require an oxygenate and ethanol is the oxygenate of choice. However, the US ethanol business, even with the federal tax credits, was only marginally profitable when the price of oil dropped below $70 per barrel. With oil prices well above that level today and trending upward, this business is expected to continue to grow. Biodiesel, on the other hand, has seen considerable capacity reduction in 2009 and 2010 in the US as a result of the loss of federal tax credits.

Ethanol from sugar cane or corn starch and biodiesel from seed oils are the low cost renewable fuels in production today, but much research is devoted to the commercialization of the so-called second (cellulosic feedstocks), third (algal) and fourth (thermochemical) generation biofuels. There are many hurdles to the commercialization of these next generation processes, their business success

depending on breakthrough technologies which will significantly reduce their costs. The future cost of oil is another unknown but fossil fuels are a limited resource. In our opinion, the transition from this limited resource to renewable fuels is inevitable. The only question is with regard to the timing. And as the biofuels industry grows, we believe there will be a synergistic growth in the commercialization of chemicals and materials from renewable resources.

Renewable Chemicals and Polymers

There is also increasing interest in obtaining chemicals from renewable resources and this has spurred a myriad of commercial activities. Table 2 lists many of the commercial organizations active in this area and the renewable chemicals they are targeting. (Table 2 has the same disclaimers associated with Table 1.) As indicated, much of the interest in renewable chemicals is targeted towards polymers. For instance, many of the small molecules (lactic, acrylic and adipic acids) are being investigated as monomers for polymer synthesis. This situation is analogous to the petrochemical industry where a substantial fraction of the industrial activity is devoted to monomer synthesis and subsequent polymerization.

To put these commercial activities into perspective, renewable plastics still represent less than 1% of the total plastics market (*7*) but it is a segment of the market with excellent projected growth rates of nearly 13% over the period between 2009 and 2014 (*8*). Obviously, the growth potential of renewable polymers is motivating the commercial activity outlined in Table 2.

The primary feedstocks for the renewable chemical industry today are carbohydrates such as glucose (sugar cane) and starch (primarily corn), seed oils (soy, castor, palm, etc.), glycerol from biodiesel production and ethanol. There have been several reviews on specific chemicals from renewable feedstocks (*9, 10*), glycerol as a feedstock (*11–13*) and renewable polymers (*14–17*). There are also several recent books written on the subject of renewable and biodegradable polymers (*18–22*).

Renewable polymers are chemically diverse and can be categorized based on their source/synthesis. Traditionally, renewable polymers were obtained from natural sources and these pre-formed polymers could be subsequently modified to adjust properties. Pre-formed renewable polymers include carbohydrates (e.g., starch, cellulose and chitin), proteins (e.g. gelatin), natural rubber and lignin. More recently, chemical-synthesis methods were developed to generate polymers from renewable monomers. Examples include poly(lactic acid), PLA, and poly(butylene succinate), PBS. Also, fermentation-derived 1, 3-propane diol is being converted to poly(propylene terephthalate), PPT, and the dehydration of ethanol provides the monomer for renewable polyethylene, PE. A third category of renewable polymers are those that are generated from renewable substrates via fermentation processes. The classic example of a fermentation-derived renewable polymer is xanthan gum while the emerging example is poly(hydroxyalkanoate), PHA, that is produced by engineered bacteria to make copolymers which do not exist in nature.

Table 1. Companies Active in Biofuels Production

Fermentation	Thermochemical	Algae
Abengoa	Biofine (Maine Bioproducts)	Aurora Biofuel
AltraBiofuels	Clearfuels Technology	Algenol Biofuels
Bluefire Ethanol	ConocoPhillips	Joule Unlimited, Inc.
BP Biofuels	Coskata	LiveFuels
Cobalt Technologies	Dynamotive	PetroAlgae
Codexis, Inc.	Emery Energy Co	Sapphire Energy
DuPont Danisco	Enerkem	Synthetic Genomics
Florida Crystals	Ensyn Technologies	
Ginkgo BioWorks	Gas Technologies Inst.	
ICM, Inc.	Greenfield Ethanol	
Iogen	Haldor Topsoe, Inc.	
KL Energy Corp.	INEOS New Planet Bioenergy	
LS9, Inc.	PetroBras	
Logos Tecnologies, Inc.	Range Fuels	
Lurgi	Renewable Energy Inst.	
Mascoma	Rentech	
OPX Biotechnologies	Sundrop Fuels Inc.	
POET	ThermoChem Recovery Intl.	
Pure Energy Corp.	UOP	
Qteros	Virent	
Shell, Cosan	Woodland Biofuels	
SunOpta BioProcess, Inc.		
Valero		
Verenium		
ZeaChem		

Advances in biotechnology and chemical catalysis have greatly reduced the costs of producing these renewable polymers. Nevertheless, we believe there remains considerable room for further cost reduction. One challenge for renewable polymers, compared to petrochemically-derived polymers, is that processing must often be achieved in aqueous environments. Thus, advances in aqueous-based separations technologies (e.g., to recover monomers from fermentation broths) and aqueous-based catalysis (e.g., to convert renewable monomers) could substantially improve the economics for renewable polymers.

Emerging Trends in Commercialization

The information in Table 2 can be used to identify some major trends in this industry in terms of the molecules and processes being targeted, as well as many of the companies active in the renewable chemicals space. One macro-trend is that renewable chemicals and materials will not displace petrochemical-based materials overnight. There are some good reasons for this, but on average, the growth rate in renewable chemicals and materials is substantially greater than that for petrochemicals.

Table 2. Companies Active in Commercialization of Renewable Chemicals and Polymers

Renewable Chemicals	Target Molecules
Segetis	Levulinic ketal esters
Elevance Renewable Sciences	Natural oil-based waxes, functional oils, solvents, lubricants
Rivertop Renewables	Glucaric acid
Amyris	Polyfarnesene building blocks
Genencor, Danisco	Bioiosprene
Genomatica	1, 4-butanediol, methylethyl ketone
Gevo	Butanol
DNP, Bioamber	Succinic Acid
BASF	Ecovio™ PLA blend, succinic acid
Mitsubishi Chemical	Poly(butylene succinate)
Showa High Polymer	Poly(butylene succinate)
Draths	Caprolactam, resorcinol
Novomer	CO_2-based polycarbonates, acrylic acid
Bioenergy International	D-lactic acid
Telles, (Metabolix and ADM)	Poly(hydroxyalkanoates)
Tianan Biologic	Poly(hydroxyalkanoates)
Shenzhen Ecomann	Poly(hydroxyalkanoates)
Tianjin Green Bioscience and DSM	Poly(hydroxyalkanoates)
ADM	Propylene glycol, ethyl acrylate
Novozymes, Cargill	3-Hydroxypropionic acid (to acrylic acid)
NatureWorks (Cargill)	Poly(lactic acid)
Tate&Lyle	1,3-propane diol (with DuPont)

Continued on next page.

Table 2. (Continued). Companies Active in Commercialization of Renewable Chemicals and Polymers

Renewable Chemicals	Target Molecules
DuPont	Poly(propylene terephthalate), 1,3-propane diol,
Synthezyme	ω-hydroxy fatty acids, sophorolipids
Arkema	Poly(acrylic acid)
OPX Biotechnologies	Acrylic acid
Dow	Epichlorohydrin, oleochemical-based coatings
Dow, Crystalsev	Polyethylene
Solazyme	Oils from algae
Verdezyne	Adipic acid
OPX Biotechnologies	Acrylic acid
Braskem	Polyethylene, polypropylene (with Novozymes)
Purac	D- and L-lactic acid, succinic acid
Roquette, DSM	Succinic acid
Solvay Chemicals	Epichlorohydrin

A small group of materials is receiving most of the attention in the renewable plastics segment. They include PLA, which is by far the largest renewable polymer in production today other than starch-based plastics and cellulosics. The primary producer of PLA is NatureWorks (Cargill) who introduced its Ingeo™ product line in 2003. New producers are entering the market including Bioenergy International, Purac and others.

Another very interesting trend is the conversion of fermentation-derived alcohols to olefins. Renewable polyethylene derived from bioethanol dehydration has been announced by Braskem and Dow/Crystalsev, both in Brazil. Braskem, in collaboration with Novozymes, is also targeting a carbohydrate fermentation process for propanol which can be dehydrated to propylene. There also appears to be much interest in isoprenoid building blocks. Amyris' polyfarnesene technology comes from this source as does Danisco's bioisoprene.

Poly(hydroxyalkanoates) are being commercialized by Telles, a joint venture between Metabolix and Archer Daniels Midland (ADM) in the US, PHB Industrial of Brazil and Tianan Biologic in China. 1, 3-propanediol, the building block of DuPont's Sorona™ PPT polyester material is also a fermentation product.

Several companies have announced acrylic acid and acrylates as target molecules from renewable feedstocks. Cargill and Novozymes are collaborating to develop a fermentation route to 3-hydroxypropionic acid which can be dehydrated to acrylic acid. Arkema has announced a catalytic process for acrylic acid with glycerol as the feedstock (*23*). OPX Biotechnologies and Novomer are also developing processes that target acrylic acid. ADM has also announced the

construction of a corn stover biorefinery to produce, among other things, ethyl acrylate (*24*).

Several firms have announced their intention to produce succinic acid and PBS. These include Showa High Polymer which is producing PBS today from petro feedstocks, Mitsubishi, DNP/Bioamber and Roquette. A process for epichlorohydrin, a building block for epoxy resins utilizing glycerol as the feedstock, has been announced by both Dow and Solvay.

There are some other more or less conventional processes which might impact the renewable plastics industry as well. For example, several of the companies listed in Table 1 which have developed thermochemical processes to convert biomass to syngas, also possess technology to upgrade the syngas to higher hydrocarbons by Fischer-Tropsch or other catalytic processes common in the petrochemical industry. Some of them are targeting benzene, toluene, xylene, or BTX feedstocks, which form the basis for much of the petrochemical plastics industry today.

In summary, the major bio-plastics currently in large scale production include PLA, PHA, PBS, PPT and polyethylene. All of these rely on fermentation either for monomer generation or polymer formation. Those being commercialized in the near future include poly(acrylic acid), polyisoprenoids, polypropylene, epichlorohydrin-based epoxy resins and 1,4-butanediol-based polyols and polyurethanes. Some, but not all, are fermentation products. Thermochemical processes to produce syngas and bio-oils may provide economical routes to BTX products which could yield a renewable source for conventional petrochemical building blocks. Thus, realistic renewable technology is in current development to produce the great majority of today's petrochemical-based commodity plastics as well as several new bioplastics. It will be very interesting to see how this field develops.

Goals and Organization of This Book

The intention of the symposium at the Spring 2010 National ACS meeting on "Renewable and Sustainable Polymers" was to bring together the diverse perspectives of authors representing industry, national labs and the academy in an attempt to capture perspectives on emerging technologies, products in development and projects that were in the commercial phase, in other words, from start to finish. Topics in this book include the synthesis of materials from seed oils, carbohydrates, proteins and other natural monomers, polymerization methods, renewable polymer additives and the biodegradation of these materials. We hope this treatise will be of benefit to you.

References

1.   Nashawi, I. S.; Malallah, A.; Al-Bisharah, M. *Energy Fuels* **2010**, *24*, 1788−1800.
2.   *C&EN*, April 27, **2009**, 9−13.
3.   http://www.ls9.com/.

In Renewable and Sustainable Polymers; Payne, G., et al.;
ACS Symposium Series; American Chemical Society: Washington, DC, 2011.

4. Graham, M. J.; McPhee, D. J. U.S. Patent 7655739, 2010.
5. http://coskata.com/.
6. http://inpbioenergy.net/.
7. Shen, L.; Haufe, J.; Patel, M. P. Product Overview and Market Projection of Emerging Biobased Plastics; PRO-BIP; Utrecht University: The Netherlands, 2009.
8. CEH Marketing Research Report 580.0280 A; *Biodegradable Polymers*; January 2010.
9. Van Haveren, J.; Scott, E. L.; Sanders, J. *Biofuels, Bioprod. Biorefin.* **2008**, *2*, 41–57.
10. Bozell, J. J.; Petersen, G. R. *Green Chem.* **2010**, *12*, 539–554.
11. Zhou, C.-H.; Beltramini, J. N.; Fan, Y.-X.; Lu, G. Q. *Chem. Soc. Rev.* **2008**, *37*, 527–549.
12. Katrynoik, B.; Paul, S.; Capron, M.; Dumeignil, F. *ChemSusChem.* **2009**, *2*, 719–730.
13. Kenar, J. A. *Lipid Technol.* **2007**, *19*, 249−253. Zheng, Y.; Chen, X.; Shen, Y. *Chem. Rev.* **2008**, *108*, 5253−5277.
14. CEH Marketing Research Report 580.0280 A; *Biodegradable Polymers*; January 2010.
15. Gross, R. A.; Kalru, B. *Science* **2002**, *297*, 803–807.
16. Shen, L.; Worrell, E.; Patel, M. *Biofuels, Bioprod. Biorefin.* **2010**, *4*, 25–40.
17. Gandini, A. *Macromolecules* **2008**, *41*, 9491–9504.
18. *Handbook of Biodegradable Polymers*; Bastioli, C., Ed.; Smithers Rapra Publishing: Shropshire, U.K., 2005.
19. Platt, D. K. *Biodegradable Polymers*; Smithers Rapra Publishing: Shropshire, U.K., 2006.
20. *Biodegradable Polymer Blends and Composites*; Yu, L., Ed.; John Wiley & Sons, Ltd.: New York, 2009.
21. *Monomers, Polymers and Composites from Renewable Resources*; Belgacem, M. N., Gandini, A., Ed.; Elsevier: Amsterdam, 2008.
22. *Polymers from Renewable Resources*; Karlsson, S., Ed.; Smithers Rapra Publishing: Shropshire, U.K., 2010.
23. *C&EN*, May 24, **2010**, 20−21.
24. http://www.ADM.com.

Chapter 2

Copolyester Synthesis Using Glycerol from Biodiesel Production

Massoud J. Miri,[*,1] **Keelyn E. Nori,**[1] **Rebecca M. Andrew,**[1] **and Changfeng Ge**[2]

[1]Department of Chemistry, Rochester Institute of Technology, Rochester, NY 14623
[2]Department of Packaging Science, Rochester Institute of Technology, Rochester, NY 14623
[*]E-mail: mjmsch@rit.edu. Ph.: (585) 475-6004. Fax: (585) 475-7800.

Copolyesters were produced with semi-purified biodiesel based glycerol and either sebacic acid or dodecanedioic acid as comonomer. The biodiesel based glycerol was purified by an inexpensive method involving neutralization with hydrochloric acid, the removal of soap by centrifugation, and the removal of methanol and water by distillation. To avoid gel formation, the polyesterifications were conducted at two stoichiometric glycerol/acid-ratios, 1:2 and 2:1, and run to relatively low conversions. Reagent grade glycerol was used in control runs. Polymerizations were conducted in bulk using dibutyl-tin(IV)oxide as a catalyst at 150 °C. The effect of the biodiesel based glycerol on the conversion, degree of branching, and molecular weight is described. The copolyesters were characterized by IR, ^{1}H NMR, ^{13}C NMR, GPC, DSC, TGA and solvent extraction.

Sustainability of the Utilization of Biodiesel Based Glycerol

Biodiesel represents fuel obtained from biomass, such as soybeans, corn, palm trees, algae, animal waste, or cooking oil waste. It is a viable alternative source of energy, because in contrast to fossil fuels, it is renewable and its use has more beneficial effects on the environment. Biodiesel is more readily available, making countries with low resources of fossil fuels less dependent on them. In

2008, approximately 20 million tonnes of biodiesel were produced worldwide, and the growth is forecasted to stay at the minimum at 40%. Most biodiesel is produced in Europe; however, the United States government also has encouraged the manufacturing of biodiesel. The volume of biodiesel produced in the United States skyrocketed between 2003 and 2008, amounting to 700 million gallons in 2008. Different grades of biodiesel are offered in the market; for example, B20, which contains 20 % biodiesel and 80 % regular diesel. Biodiesel is currently more expensive than regular diesel (\$ 2.54). For example in 2009, the nationwide price for a gallon of B20 was about 15 ¢ higher, while the price of fuel containing 99 - 100 % biodiesel (B99-100) was about 50 ¢ higher. However, with the continually increasing prices of fossil fuels, biodiesel also should become economically favorable in the near future. (*1–3*).

Biodiesel is particularly more sustainable because of its ecological advantages. It burns more efficiently than untreated biomass, and performs better than many grades of petroleum based diesel both in terms of efficiency and carbon emissions. Biodiesel has a lower sulfur content than conventional diesel, and as an oxygenated fuel also has better lubrication properties. Using biodiesel results in less water usage and contamination than with fossil fuels. In terms of the social aspects of sustainability, biodiesel that is produced from non-food stock would be preferable, because it would not trigger an increase of food prices.

The biodiesel used in this work was produced from microalgae. Compared to other sources of biomass algae have several important advantages. First, algae grow faster and are more efficient in photosynthesis than regular crops. For example, it is estimated that the growth of algae is 50 times faster than that of switchgrass, the latter being one of the fastest naturally growing crops. Second, the oil content of algae is relatively high, with typically 20 to 50%, and in certain cases even 80%. Third, since algae are not a major food, such as edible fats or oils, they do not cause negative effects on the food supply. Fourth, algae production is easier to control than growing conventional crops. Finally, the costs for maintaining the algae production are relatively low compared to harvesting crops (*4*).

Biodiesel represents fuel that is obtained by transesterification of the triglycerides in biomass, as shown in Figure 1.

The oil or fat source should contain only little fatty acids or water to avoid excess soap formation with the alkali. Therefore, an acid catalyzed esterification preceding the base catalyzed transesterification is frequently applied (*5*). For every ten pounds of biodiesel that is produced, about one pound of glycerol is formed as a by-product. Close to two-thirds of the glycerol produced worldwide originates from biodiesel (*2*). Glycerol is an important feedstock in the organic, pharmaceutical, food and cosmetic industry. It is used as solvent, antifreeze, detergent, emollient and sweetener. The purity of the glycerol in particular for the latter applications has to be high. As the price of glycerol has been significantly dropping with the increase of biodiesel production, there is a major trend to find new applications for the low-cost glycerol (*5–8*).

In Renewable and Sustainable Polymers; Payne, G., et al.;
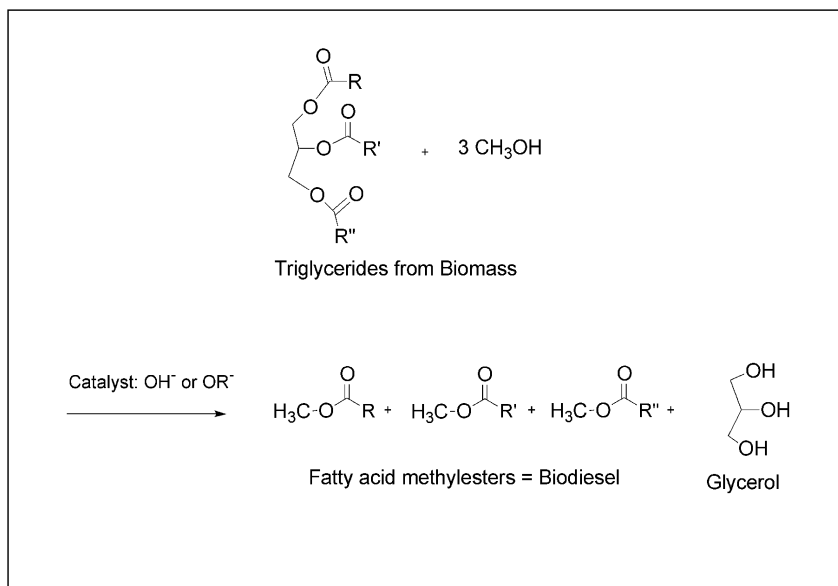ACS Symposium Series; American Chemical Society: Washington, DC, 2011.

Figure 1. Transesterification of triglycerides leading to glycerol as by-product.

One attractive option is to use glycerol as a comonomer for the production of polyesters. Conversion of glycerol to 1,3-propanediol either by organic synthesis or biochemical fermentation has been reported (*9–11*). However, it would be more economical, if the synthesis steps could be kept to a minimum, and the glycerol could be used directly as a comonomer in the polymerization. As part of a growing trend towards sustainability in the plastics industry there is a search for processes and products that are not only based on efficient and renewable energy, but are more sustainable as a whole. The glycerol/diacid copolyesters have indeed the advantage that they could be depolymerized by fungi that occur in soil once their life cycle has ended, and by being biodegradable would not contribute to waste in landfills.

Several research groups published work on the copolymerization of glycerol with diacids to form copolyesters. Almost all of these used reagent grade glycerol and not glycerol formed in biodiesel production (*12–20*). They particularly used adipic acid, but other dicarboxylic acids have also been applied as comonomers. No reference could be found describing the chemical synthesis of polyglyceroldodecanedioates. In an article prepared by medical professionals, Migneco, et al. mentioned the "fabrication" of this copolymer at 1:1 ratio without describing any detail about its synthesis or characterization of chemical properties, such as the microstructure or molecular weight properties of the polymer (*21*). Gross et al. discussed, in detail, the use of a lipase catalyst for the synthesis of polyglyceroladipates. Jose et al. reported the syntheses of copolyesters with biodiesel based glycerol, however it is unclear how and if this biodiesel glycerol was purified, and what the difference in polymerization behavior to regular, reagent grade glycerol was (*22*, *23*).

Our main objective was to produce a series of copolyesters based on biodiesel based glycerol that would lead to mostly uncrosslinked, thermoplastic polymers. Such products would have, for example, the potential to be used as inexpensive adhesives or laminates in packaging. We intended the majority of the polymer to be linear. However, branched structures in the polymer would be still acceptable, contributing usually to a decrease in crystallinity. As was shown earlier, the addition of small amounts, e.g. 1%, of glycerol can lead to a low degree of crosslinking, which could have the advantage of reinforcing the mechanical strength of the still essentially thermoplastic polymer (*18*, *20*). We selected two types of aliphatic and linear diacids for the binary copolymerizations with the glycerol: sebacic acid and dodecanedioic acid. The structures of the two acids are quite similar; however, it was hoped that the additional methylene groups in dodecanedioic acid would lead to a higher crystallinity. Polymerizations with reagent grade glycerol were to be performed as control runs to determine the effects of the ingredients in the biodiesel based glycerol after some basic purification. Our initial findings were mentioned in a preprint (*24*).

Theoretical Background of Glycerol Copolymerization

The copolymerization of diacids with glycerol represents an A_2B_3-type system with potential for gelation depending on stoichiometric ratios and conversion of the monomers. The related theory has been described by two methods (*25*); while Carothers derived his equations based on the kinetics of the reactions (*26*), Flory approached the concept from a statistical view (*12*, *27*). The two basic approaches result in different values for the critical conversion, p_c, at and above which gelation should occur.

In Table 1 the theoretically expected values for the critical conversion are given, as suggested by different approaches. The first two rows in Table 1 are based on equivalent stoichiometric ratios of the diacid to glycerol based on moles basis and on functional groups, i.e. 1:1 or 1:1.5, respectively. The last two rows are calculated for the corresponding ratios used in this work. We applied the diacid/glycerol-ratio of 2:1, because the p_c-values exceed those at the other ratios, and, therefore, gelation can be more easily avoided. We also applied the 1:2 diacid/glycerol-ratio to experimentally test the scenario in which the glycerol is *starved* from acid comonomer and, thereby, would reduce condensation of the less reactive secondary OH-group, and as a result, should lead to more linear polymer.

Results obtained using Carothers's and Flory's equations are given in column 1 and 3 of Table 1, respectively (*26*, *27*). The difference in the reactivities of the primary OH- groups to the secondary OH-group of the glycerol had been addressed early on by Kienle, and others tried to adjust their formulas for the critical conversion accordingly (*12*, *13*). Durand found that the critical conversions were slightly higher (depending on the [COOH]/[OH] ratio by 2 to 3%) when the secondary hydroxyl group was differentiated from the two primary groups due to its lower reactivity (*28*).

Table 1. Functionalities and Critical Conversions Obtained by Different Methods

Molar A/B -Ratio	[COOH] /[OH] -Ratio r	Carothers[1] (26)		Pinner[2] (27)		Flory[3] (12)		Stafford[4] (30)	
		f_{ave}	p_c	f_{ave}	p_c	f	p_c	f_{ave}	p_c
1:1	0.67	2.50	0.80	2.00	1.00	3.00	0.58	2.60	0.77
1.5:1	1.00	2.40	0.83	2.40	0.83	3.00	0.71	2.50	0.80
2:1	1.33	2.33	0.86	2.00	1.00	3.00	0.82	2.43	0.82
1:2	0.33	2.67	0.75	1.33	1.00[5]	3.00	0.41	2.75	0.73

A: diacid; B: glycerol; f_i: functionality of monomer i; f_{ave}: average functionality; N_i: moles of monomer i; X_i: mole fraction of monomer i.

$$1 \quad f_{ave} = \frac{\sum (N_i f_i)}{\sum N_i} \; ; \quad p_c = \frac{2}{f_{ave}}$$

$$2 \quad f_{ave} = \frac{2 N_L f_L}{\sum N_i} \quad \text{for monomer L being the limiting agent;} \quad p_c = \frac{2}{f_{ave}}$$

$$p_c = \sqrt{\frac{1}{2} r}$$

[3] f = functionality of branching unit;

$$4 \quad f_{ave} = f_A + (f_B - f_A) \frac{f_B X_B}{f_B X_B + f_A X_A} \; ; \quad p_c = \frac{2}{f_{ave}}$$

[5] Calculated value is 1.50; however max. value of p_c is 1.

As mentioned by Pinner, the average functionality needs to be corrected when non-stoichiometric ratios of the reactants are applied, basing them only on the functional groups that are part of the limiting reagent, such as with the two carboxylic groups at the 1:2 diacid/glycerol ratio. This treatment leads to much higher critical conversions than those obtained by the original kinetic

15

approach (*29*). The corresponding results for the average functionality and critical conversion are given in column 2 of Table 1. Furthermore, particularly with larger diacid molecules, there is some likelihood for intramolecular cyclization, which would consume monomer and, thereby, result in higher than expected conversions. Several further attempts were made to improve the theoretical models over the following decades, in particular by applying an average functionality also for Flory's model (*30*). Stafford applied average functionalities depending on the molar ratios of the monomers, included in column 4 of Table 1. While some argue that the statistical theory leads to closer results to experimental values (*31*), others believe the kinetic approach is more accurate (*29, 32*).

Ultimately experimental work is necessary to study these polymerizations with the main concern of avoiding significant gel formation, while still obtaining sufficiently high molecular weight copolymers.

Experimental

Materials

Reagent grade glycerol, sebacic acid, dodecanedioic acid, titanium(IV) isopropoxide were purchased from Sigma Aldrich. Argon was obtained from Airgas. The biodiesel glycerol derived from algae was provided by Gaiergy Corp.

Purification of Biodiesel Based Glycerol

The dark-brown, highly viscous glycerol was diluted approximately by 50 v/v % with distilled water. Under stirring concentrated hydrochloric acid was added dropwise to the basic mixture until the pH reached 7. A less dense yellowish layer of potassium carboxylate, or soap, began to separate and form on top of the glycerol. The mixture of soap and glycerol was centrifuged to remove the soap. Most of the water/methanol mixture was distilled off. Over several days potassium chloride crystals precipitated, most of which were not transferred to the polymerization system.

Polymerizations

As preliminary tests a set of small scale glycerol/diacid polymerizations was carried out without catalyst for up to 48 hours, to determine if gelation would occur and the times until gelation occurred. For each of the main polymerization runs (shown in the subsequent Table 2), the reaction apparatus was purged with argon. A 500 ml reaction flask was equipped with a magnetic stirrer and condenser with a collecting flask. For Entry 1, 90.4 g (= 0.45 mol) of sebacic acid were added to the reaction flask. The flask was heated above the melting point of the diacid and 20.6 g (= 0.22 mol) glycerol were added followed by dibutyltin(IV) oxide catalyst (0.1 g = 0.4 mmol). The reaction then was heated to 150 °C. The polymerization was continued at this temperature for about 6 h. A slight vacuum (ca. 0.1 torr) was created to remove water or excess glycerol for at least two hours at 90 °C.

Characterization

IR spectra of solid samples were obtained using a Shimadzu IR Prestige21 FTIR. ^{1}H NMR spectra were run in deuterated chloroform with instruments from Bruker at 300 and 400 MHz. Inverse gated and decoupled ^{13}C NMR spectra were recorded using a 5 s pulse delay. Comparative measurements with a 10 s pulse delay did not result in significantly different peak intensities. Trifluoroacetic acid, deuterated DMSO, and deuterated chloroform were initially used as solvents and the main measurements were carried out with the last solvent, because of better peak separations. DSC data were obtained with a TA Instrument 210 DSC at a heating rate of 10 °C/min up to 300 °C, recording the second heating. TGA was performed on a TA TGA 2050. A 10-18 mg sample was heated under a nitrogen flow of 100 cm[3]/min from room temperature to 900 °C at 10 °C/min. Molecular weight distributions were obtained by size-exclusion chromatography in tetrahydrofuran and mostly provided by Eastman Kodak. Molecular weight distributions and averages were calculated as polystyrene equivalents from a calibration curve constructed from retention volume data for 15 narrow distribution polystyrene standards. Some molecular weight measurements were provided by Polyanalytik Inc. at similar conditions.

To remove unreacted acid from the polymer, vigorous mixing with the organic solution of the polymer in tetrahydrofuran or chloroform was performed. Solvent extractions to determine gel content were measured according to ASTM D2765-01 (*33*). For this method, tetrahydrofuran was used as solvent at 66 °C. For each sample 2 g of polymer were placed in a steel wire container immersed in the solvent and refluxed for 8 hours. After separating the gel and soluble fraction the compounds were dried at 70°C until a constant weight was reached. Typically this took at least 24 hours.

Results and Discussion

Effectiveness of Purification of the Biodiesel Based Glycerol

Biodiesel based glycerol typically contains a large number of compounds, aside from the glycerol (*34–36*). Glycerol separates easily from the biodiesel because of the different polarities of the two compounds. Depending on the source of the biodiesel, close to half of the glycerol phase contains pure glycerol. Most residual methanol, which was applied in the biodiesel production, remains with the glycerol. The glycerol phase also contains some biodiesel, i.e. esters, which are mostly mono- and dimethylglycerides of fatty acids, and free fatty acids. A significant amount of soaps form due to alkali metal hydroxide or alkoxide, which was added as catalyst during the biodiesel synthesis. Among the fatty acids, oleic acid, linoleic acid and linolenic acid, are prevalent. Some alkali hydroxide or alkoxide may be present as well. Usually 0.5 to 3% of ash remains after these components have been removed (*34*).

Glycerol has a relatively high boiling point (290 °C at 1 atm) and is viscous (1500 cpoise), making it difficult to distill. Particularly, the crude glycerol from biodiesel processing is highly viscous. Many techniques have been applied to

separate glycerol from the impurities; for example, thin film evaporation or ion exchange to remove salts. However, these methods are generally expensive. The purification of the biodiesel glycerol by the method described in the Experimental Part turned out to be simple, inexpensive and efficient. For our studies it also would have been trivial if the biodiesel based glycerol would have been completely purified, since it then would have had to react exactly like reagent grade glycerol. One of the initial questions of interest for us was how much of the residual impurities in the biodiesel based glycerol the polymerization system could tolerate to yield useful polymers at reasonable rates.

While the untreated biodiesel glycerol was coffee-like dark brown, had a high viscosity resembling molasses and was heterogeneous, the semi-purified material was amber in color, had a viscosity similar to a light oil and had a uniform consistency. The appearances of these materials are shown in Figure 2.

In Figure 3 the IR spectra of the untreated biodiesel glycerol, the semi-purified type, and reagent grade material are shown.

The peaks that are characteristic for glycerol are the broad and large peak at 3300 to 3500 cm^{-1} caused by stretching vibrations of the hydroxyl groups. The medium strong peaks between 1150 and 1500 cm^{-1} are due to bending vibrations of the C-H bonds and hydroxyl groups. The strong peak at 1040 cm^{-1} is caused by another mode of bending vibrations of the hydroxyl groups. Glycerol readily absorbs water producing a broad peak at about 1650 cm^{-1}. The latter peak is present in the untreated and semi-purified glycerols which were processed in direct contact with aqueous solutions, while the reagent grade glycerol was hardly exposed to water.
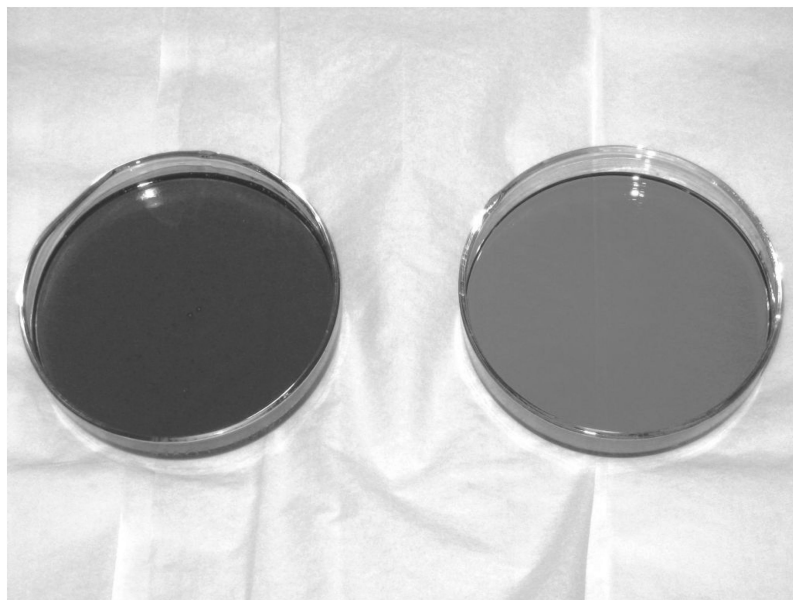
Figure 2. Original, untreated biodiesel based glycerol (left) and semi-purified material (right).
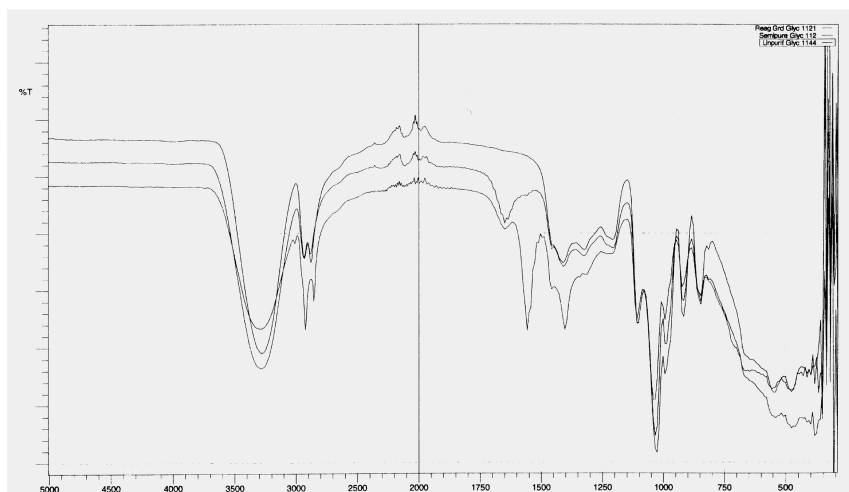
*Figure 3. IR spectra of reagent grade glycerol (top), semi-purified version
(center) and untreated biodiesel based glycerol (bottom).*

The different peak assignments of the free fatty acids, the fatty acid esters,
and their salts for IR spectroscopy have been published (*37–43*). The untreated
biodiesel glycerol has a strong carbonyl peak at ca. 1570 cm $^{-1}$, which is
characteristic for the fatty acid salts or soaps. The position of these types of
carbonyl peaks can vary depending on several factors such, as the presence of
salt crystallites and the pH (*42, 43*). There is no indication in any of the three
spectra in Figure 3 that free fatty acids or their esters are present in a detectable
amount. By comparing the spectra on the top and center of Figure 3, it becomes
apparent that the applied purification process resulted in the removal of most of
the soap, since the corresponding peak at 1570 cm^{-1} has decreased significantly
in the spectrum of the semi-purified glycerol. One can observe a small buckle
on the right shoulder of the broad peak at ca. 1650 cm^{-1} In the spectrum of the
semi-purified glycerol. This is due to traces of the soaps that remained in the
glycerol after the purification step.

The ^{1}H NMR spectra of the two types of glycerol are shown in Figure 4.

The main peaks of glycerol in its ^{1}H NMR spectrum are those of the methylene
protons at 3.32 – 3.38 ppm, of the methine proton at ca. 3.47 ppm, and of the
hydroxyl proton at 4.8 – 5.2 ppm. The chemical shift of the hydroxyl based peak
varies depending on the pH and the presence of water. The soaps, esters and the
free form of the fatty acids produce two large peaks at 1.22 and 0.82 ppm, which
are caused by the methylene and methyl groups at the hydrophobic end of the
fatty acid components, respectively. They also have peaks between ca. 2.00 and
2.50 ppm, which are specific for the derivatives of each type of fatty acid. Esters
have an additional high and narrow peak at about 3.63 ppm associated with the
methylene protons at the carbon atom, which is single-bonded to the oxygen atom
of the ester (*44, 45*).
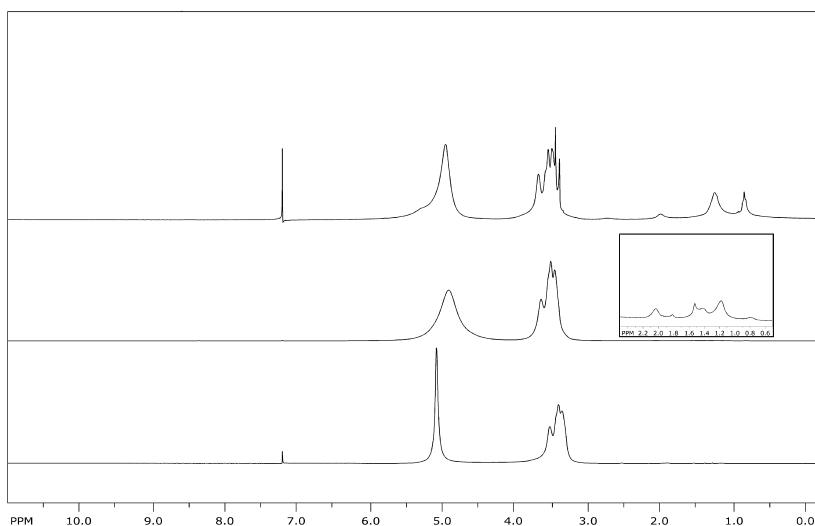
Figure 4. ¹H NMR spectra of untreated biodiesel based glycerol (top), semi-purified material (center) with insert of region between 0.5 and 2.5 ppm magnified by ca. 40, and reagent grade version (bottom).

A comparison of the three spectra in Figure 4 reveals that the untreated biodiesel glycerol contains a large amount of fatty acid compounds indicated by the peaks at 0.81, 1.23, and 1.97 ppm. The small peak at ca. 2.71 ppm would be indicative of linoleic acid derivatives. The glycerol peaks between 3.0 and 3.5 ppm are virtually identical in the semi-purified and the reagent grade glycerol, in contrast to those peaks in the unpurified glycerol. Hardly any of the peaks of the fatty acid derivatives can be observed in the spectrum of the semi-purified glycerol (center in Figure 4). However, they can be detected when the spectrum is magnified a factor of about 40. The absence of fatty acid esters is also verified by ¹H NMR spectroscopy, since no peak at 3.63 ppm is observed. Though the acidic proton of free fatty acids produces only a very small peak at low field (ca. 11 ppm), there is also no evidence that these would be present even in the untreated biodiesel glycerol.

As mentioned above, the applied purification process results in the formation of potassium chloride crystals. The salt forms during the purification step as the potassium hydroxide is neutralized with hydrochloric acid. Neither IR nor NMR spectroscopy can be used to detect the presence of this salt in the semi-purified biodiesel. The salt cannot be observed by IR spectroscopy because no vibrations occur in that wavenumber range, and since it is a solid it cannot be detected by regular solution based NMR spectroscopy. However, we were able to verify the presence of potassium chloride as a precipitate in the semi-purified biodiesel glycerol. The presence of chloride in the salt was proven by precipitation with silver nitrate. Potassium was detected by a flame test of the aqueous salt solution resulting in a purple flame color. Though most of the precipitated salt was removed from the glycerol, some was also transferred to the polymerization apparatus.
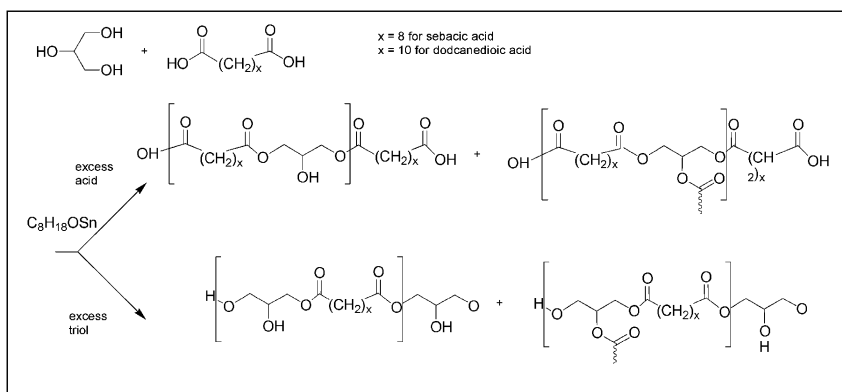
Scheme 1. Step-Growth Polymerization of Glycerol with Either Sebacic Acid or Dodecanedioic Acid

Table 2. Polymerization Conditions and Conversions

Entry No.	Glycerol Source	Diacid	Glycerol /Diacid Mol-Ratio	t_p (h)	p (%)
1	RG	SA	1:2	6	82
2	BD	SA	1:2	5	84
3	RG	DDA	1:2	16	84
4	BD	DDA	1:2	5	81
5	RG	SA	2:1	8	52
6	BD	SA	2:1	8	65
7	RG	DDA	2:1	5	59
8	BD	DDA	2:1	5	70
9	BD	DDA	2:1	8	93

RG: reagent grade; BD: biodiesel; SA: sebacic acid; DDA: dodecanedioic acid; t_p: polymerization run time; T: 150 °C, catalyzed by dibutyltin(IV) oxide.

Polymerizations

In Scheme 1 the polymerization reactions are shown. Each linear acid, sebacic or dodecanedioic, was directly polymerized with the glycerol without use of a solvent. As mentioned above, polymerizations were conducted at two different stoichiometric ratios of glycerol to diacid: 1:2 and 2:1. It could be anticipated that with the excess of acid terminal carboxylic groups would prevail, while with excess glycerol most terminal groups would bear the alcohol functionality.

The set of polymerizations that were conducted with the more detailed stoichiometric ratios and polymerization conditions are given in Table 2.

Initially a couple of test runs were conducted that led to major formation of gel (not included in Table 2). For example, using sebacic acid at a 1:2 triol/ diacid ratio, gelation was observed after 7 h and beyond. In the subsequent runs, polymerization was stopped about an hour before gelation had occurred in the prior runs. Entry 3 was run at a relatively long polymerization time, and was included as a case, which was expected to lead to a higher gel content and could be used for comparison.

The conversions were estimated by comparing the peak areas for the residual monomers and the polymer from GPC diagrams, which are discussed in more detail further below. The direct method of the determination of the conversion from the GPC data was preferred to yield determination, followed by isolation of the neat polymer and subsequent acid titration, because the latter method involves more measurement errors overall. The data in Table 2 indicate that it is easier to reach high conversions with excess acid rather than excess glycerol. This is likely caused by the higher concentration of the diacid and the self-catalyzing catalytic effect of the diacid on the polymerization, which is generally true for polyesterifications (*25*).

Remarkably, the conversions of all polymerizations using the semi-purified biodiesel based glycerol are higher than the corresponding runs with reagent grade glycerol. It is possible that the remaining soap and KCl residues in the semi-purified biodiesel caused this increase in conversion by reacting with the applied dibutyltinoxide catalyst. In the simpler, small scale polymerizations which were performed without catalyst, no significant difference in the polymerizations between reagent grade and biodiesel based glycerol was observed.

Polymer Microstructure Determination by Spectroscopy

In Figure 5 the structures that can be formed based on the polymerization reactions shown in Scheme 1 are formally shown with their notations similar to those given in other literature references (*14, 16*). The chain length of the branches or the crosslinks is typically longer than shown here in the simple overview.
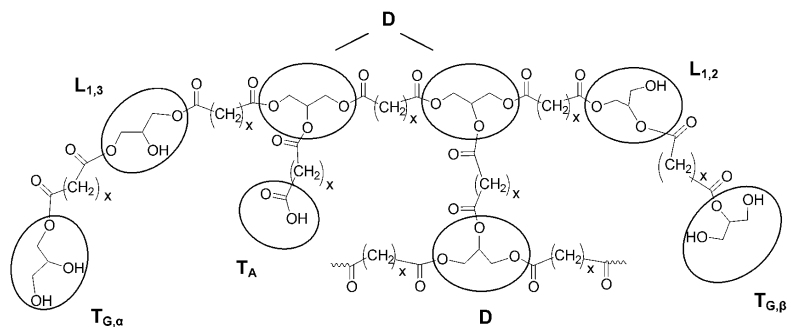
Figure 5. Types of structural units than can occur in copolyesters formed from glycerol with diacids (x = 8 for sebacic acid and x = 10 for dodecanedioic acid).

In Renewable and Sustainable Polymers; Payne, G., et al.;
ACS Symposium Series; American Chemical Society: Washington, DC, 2011.

Glycerol can form two types of linear units, $L_{1,3}$ and $L_{1,2}$, and correspondingly two types of terminal units $T_{G,\alpha}$ and $T_{G,\beta}$, depending on if the primary hydroxyl groups or the secondary hydroxyl group undergo condensation, respectively. The diacid may form a terminal group, T_A, as well. The structural unit with only one dendritic unit (D) connected here to a terminal unit (Figure 5, center towards the left) is an example of a branch and, if dominant, can lead to hyperbranching. The structural unit between two dendritic units of two long chain segments (Figure 5, center towards the right) represents crosslinking. The methylene groups in the diadid segments can be also distinguished by spectroscopy have; however,they have not been labeled in Figure 5. There distinctions will be mentioned further below.
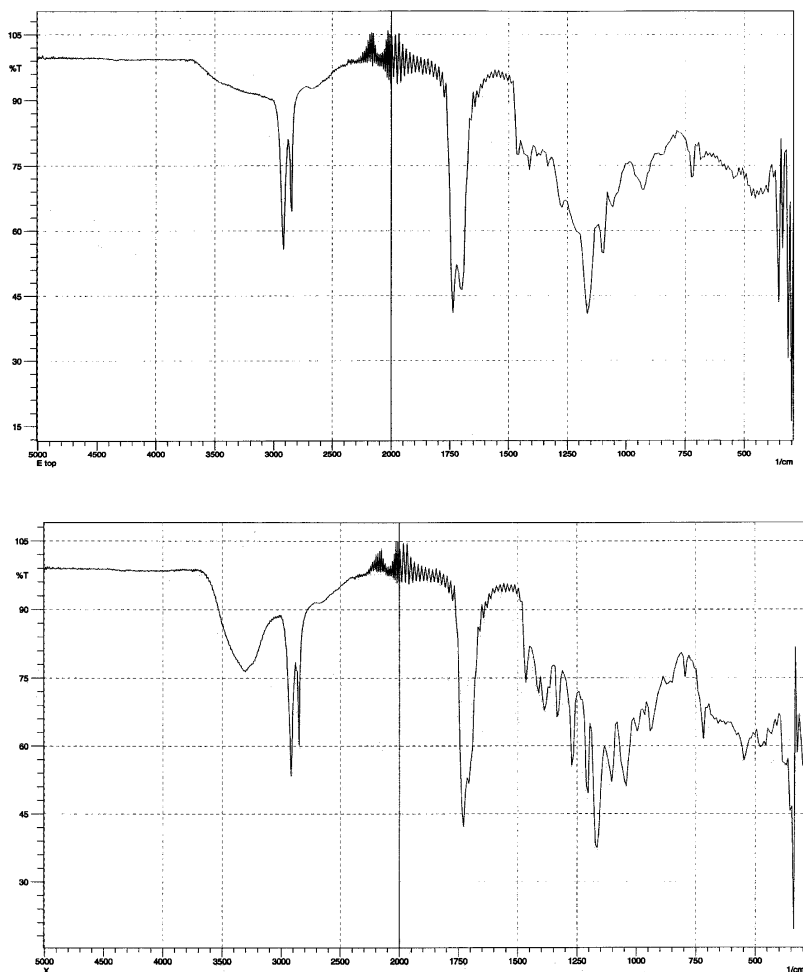
Figure 6. IR spectra of two types of polygyceroldodecanedioate, glycerol/acid ratio used for synthesis on the top: 1 : 2 (Entry 4), on the bottom: 2 : 1 (Entry 8).

In Figure 6 the infrared spectra of two copolyesters are compared. In both spectra, two characteristic carbonyl peaks can be found, one at ca. 1725 to 1740 cm^{-1} stemming from the carbonyl of the ester group and another at 1695 to 1710 cm^{-1}, which is associated with free carboxyl groups (T$_A$), as also mentioned elsewhere (*22*). The particular polymer shown in Figure 6 on the top (Entry 4), which had been made at a low triol/diacid ratio, was purified by vigorous mixing with warm water and is therefore free of any excess acid. Prior to washing the polymer with water, the height of the peak at ca. 1695 cm^{-1} exceeded that of the neighboring ester related peak on its left. The remaining intensity of the peak at 1695 cm^{-1} is caused by terminal acid groups of the polymer. There is a second larger peak due to the the ester group at ca. 1150 cm^{-1}. In addition, the acid produces several peaks due to its methylene groups in the regions at about 2900, 1465 and 722 cm^{-1}.

In the IR spectrum on the bottom of Figure 6, which was obtained from the polygyceroldodecanedioate made at the high triol/diacid ratio (Entry 8), the peak for the free carboxylic group at 1695 cm^{-1} has clearly shrunk, since hardly any polymer chains were terminated by the acid. The incorporated glycerol is more easily detected by the very broad peak at ca. 3300 cm^{-1} caused by the OH-bond. The large peak at ca. 1110 cm^{-1} stems from the C—O bonds from the secondary C-atoms, and one peak to its left at ca. 1170 cm^{-1} from the C—O bond at the tertiary C-atom of the L$_{1,3}$ units. In addition, the glycerol units produce several other peaks in the aliphatic region between 1000 and 1400 cm^{-1} resulting also from terminal groups and L$_{1,2}$ units. These peaks become more prominent in the lower spectrum because of the applied high glycerol/acid ratio.

Dendritic units can be detected semi-quantitatively in the ^{1}H NMR spectra, as shown in Figure 7.

The advantage of the use of the ^{1}H NMR spectroscopy is that one can quickly determine if the polymer is linear or branched and possibly crosslinked. Dendritic groups appear between 5.25 and at 5.35 ppm, and linear segments at 5.10 and 5.20 ppm. However, the ratios obtain by ^{1}H NMR are quantitatively not reliable.

^{13}C NMR spectroscopy is more valuable in terms of both qualitative and quantitative information. Figure 8 shows the ^{13}C NMR spectra of a copolyester produced with excess acid (Entry 2) and below of a copolyester produced with excess glycerol (Entry 6).

To observe the peaks associated with the diacid almost the entire area of the spectrum needs to be observed. The polyglycerolsebacate synthesized with excess acid produces a peak at close to 180 ppm, characteristic for the terminal acid groups (T$_A$), which is in agreement with peak assignments mentioned in ref. (*46*). The analog polyester synthesized with excess glycerol does not show this peak at all. The three large peaks on the right are caused by methylene groups of the diacid. The peak at about 34.5 ppm is due to methylene directly attached to the carbonyl group of the acid (α-CH$_2$). The rightmost peak at 24.6 to 25.1 ppm is assigned to the methylene group in the β-position to the carbonyl group (β-CH$_2$). The center peak at about 29.4 ppm is caused by methylene groups in the center of the acid starting from the γ-position from the carbonyl group (γ$^+$-CH$_2$). Incidentally, the peak intensities for this peak are consistently larger for the polymers of the dodecanedioic acid, due to the two additional methylene groups it has compared

to the sebacic acid. However, since this difference is not simply apparent by viewing the heights of the peaks rather than their intensities, a spectrum of a polyglyceroldodecanedioate has not been included for the comparison of the diacid related peaks.
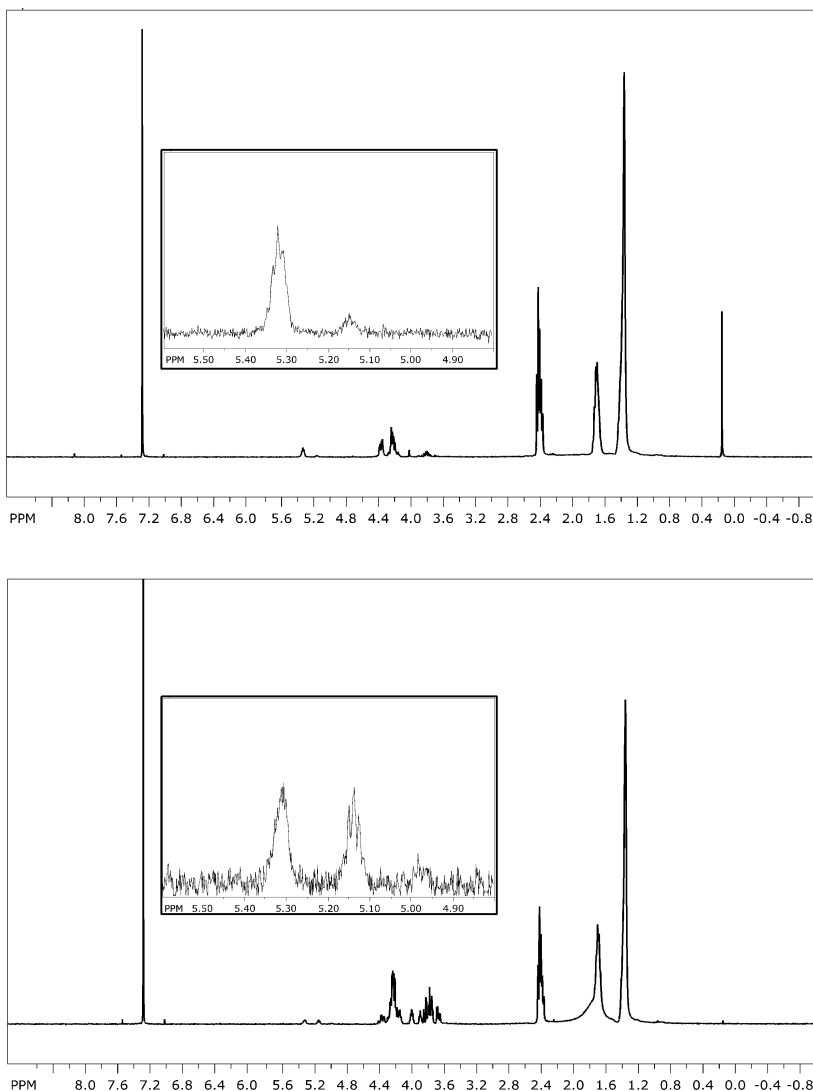

Figure 7. ^{1}H NMR spectra of two polyglyceroldodecanedioates with the region between 4.8 and 5.6 ppm expanded (top: Entry 3, bottom Entry 9).
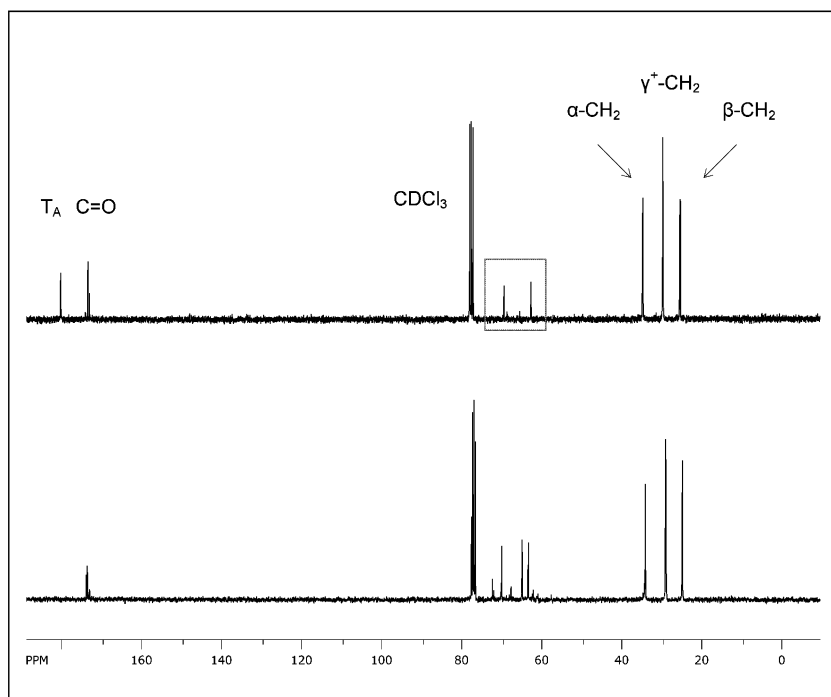
Figure 8. ^{13}C NMR spectra of polyglycerolsebacates synthesized with biodiesel based glycerol (top: Entry 2 and Bottom: Entry 6). The framed region containing peaks from the glycerol units is expanded and discussed below (see Figure 9).

It is also apparent from Figure 8 that there are hardly any peaks produced in the region characteristic for the glycerol for the polymer on the top (framed region in Figure 8, top, Entry 2). It indeed has only dendritic groups (D) and no linear types ($L_{1,3}$, $L_{1,2}$). Further details about the incorporation of the glycerol become evident by a closer look in the region between 72 and 60 ppm, shown in Figure 9.

Since each glycerol unit has two secondary C-atoms and one tertiary C-atom, there are typically pairs for each structural unit, except for the dendritic units. For example, two peaks are produced for the $L_{1,3}$-units, one at ca. 68 ppm assigned to the tertiary C-atom in the glycerol unit and the other at ca. 65 ppm assigned to the secondary C-atom in that unit. Generally, all tertiary carbon atoms are observed at lower field than the secondary carbon atoms, as was verified by ^{13}C DEPT 135 NMR studies.

The most striking difference between the spectra of the copolyesters is caused by the two applied stoichiometric glycerol/diacid ratios. This becomes apparent when comparing the expanded regions of the spectra characteristic for the differences in glycerol incorporation. The two polymers obtained with an excess of the dodecanedioic acid have dendritic structures (D) as the largest peak intensities (Figure 9, top and center, Entries 3 and 4, respectively). However, the corresponding copolyester obtained with the excess glycerol (Figure 9, bottom) has almost no dendritic structures. Instead it has large peaks indicating the

presence of terminal glycerols by reaction of an α-hydroxyl group, $T_{G,\alpha}$. In all polyesters, except those prepared with an excess of sebacic acid (Entries 1 and 2), linear glycerol groups due to unreacted secondary hydroxyl groups ($L_{1,3}$) are formed. In the cases of excess of glycerol, relatively small amounts of glycerol units in which the secondary hydroxyl group undergoes reaction ($L_{1,2}$) are also present. However, terminal groups formed via reaction of the secondary hydroxyl group, i.e. T_β, at about 72 ppm, are not observed (*16*).
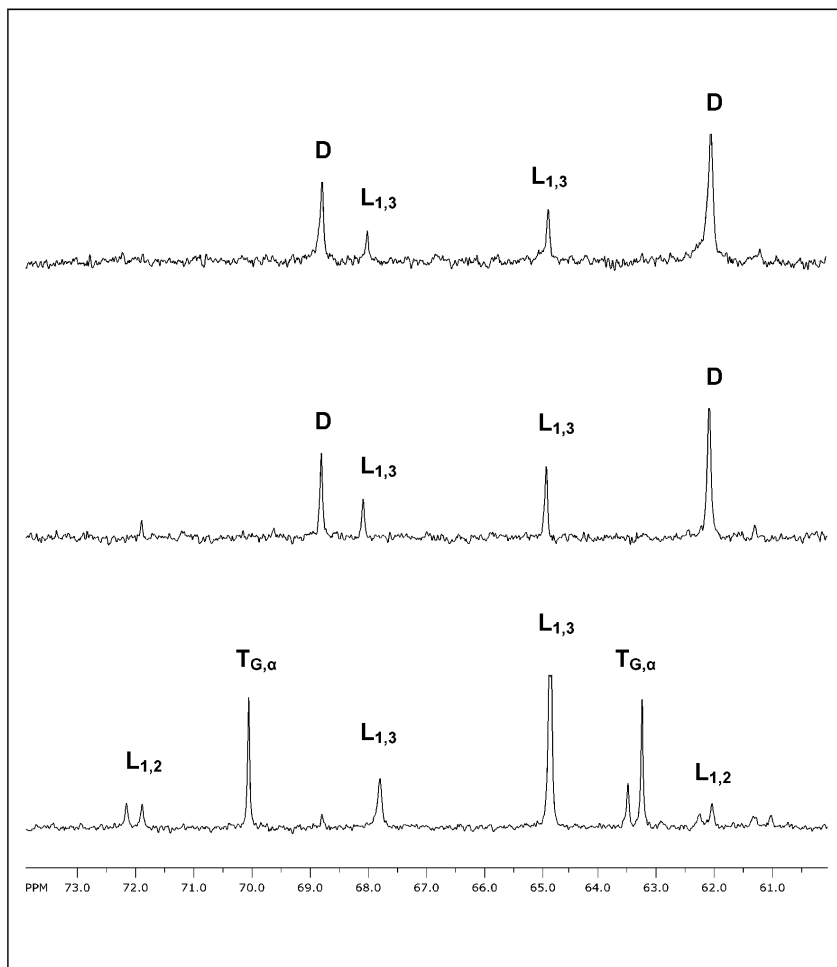
Figure 9. Expanded regions of ^{13}C NMR of three polyglyceroldodecanedioates (top: Entry 3, center: Entry 4, bottom: Entry 8) with peak assignments using the notation described above in Figure 4.

Table 3. Data on Copolymer Microstructure Obtained from C 13 NMR Spectroscopy

Entry No.	Acid	Glycerol			DB %
	COOH*	Sum L %	Sum T %	Sum D %	
1	0.06	0	0	100	100
2	0.05	0	0	100	100
3	0.04	17	0	83	83
4	0.05	18	0	82	82
5	0.02	44	53	3	8
6	0.00	48	46	6	11
7	0.02	42	58	0	0
8	0.02	53	47	0	0
9	0.00	51	28	21	29

* normalized intensities; DB: Degree of Branching.

By comparing the spectra on the top and center of Figure 9 (Entries 3 and 4) the effect of the residual impurities in the semi-purified biodiesel glycerol becomes apparent. The polymer produced with the biodiesel based glycerol (Entry 4) has a lower amount of dendritic groups relative to its linear structures. It appears that the residues in the semi-purified biodiesel may have caused reactions with the applied catalysts. It has been shown that the nature of the catalyst is influential on the degree of branching (*15*). However, such an effect of the residue could not be observed when a high glycerol/diacid ratio was used, probably because there was a lower tendency toward branching than at the high diacid/glycerol ratio.

The results of all ^{13}C NMR measurement are summarized in Table 3.

As expected with excess diacid, the intensity of terminal acid groups (TA, producing a peak at 180 ppm), is larger than in the set with excess glycerol. This is true even when unreacted acid is removed from the sample. The percentages of linear, terminal and dendritic groups were obtained by summing up the intensities for the corresponding peaks in the region from ca. 72 to 60 ppm. The degree of branching, DB, was calculated according to the modified equation of Frechet and Hawker (*47*):

$$DB = \frac{D}{D+L} \times 100$$

The polymers obtained at a low glycerol/diacid ratio are highly dendritic and as mentioned earlier obtained at relatively high conversions. Interestingly, sebacic acid leads to a higher degree of branching than dodecanedioic acid, when excess acid is applied (Entries 1 and 2). Even at the high glycerol/acid ratio the sebacic acid causes the formation of some dendritic units, while the dodecanedioic acid does not.

Table 4. Gel Content, Molecular Weight Properties and Glass and Melting Temperatures of Copolyesters

Entry No.	Gel -Content %	M_w g/mol	M_w/M_n	T_g °C
1	26	17,900	12.8	-101
2	12	22,500	14.3	-99
3	22	35,100	20.3	-86
4	0	5,620	4.0	-99
5	0	1,087	3.5	-101
6	0	1,802	4.3	-100
7	0	1,390	1.4	-99
8	0	2,160	1.7	-96
9	9	92,600	25.2	21

Table 4 shows the gel content, the molecular weight properties, and glass transition temperatures of the polymers. Measurements of the gel content, obtained by the extraction technique described in the Experimental Part, showed that even the 100% dendritic polymers were not totally insoluble or forming pure gels. The polymers appear not to be crosslinked, but only partially branched. Indeed only a maximum of 26% gel was obtained with the most dendritic polymer (Entry 1). Most of the dendritic units cause branching, but not necessarily crosslinks as distinguished in the two representative structures in Figure 5. In the case of excess acid, the biodiesel glycerol in both comparisons (Entries 1 and 2, and Entries 3 and 4) resulted in lower gel contents. In fact, the polymer produced with biodiesel glycerol and dodecanedioic acid at a 1:2 ratio (Entry 4) is exceptional in that it has 83 % dendritic units but forms no gel at all.

The copolyesters were, except for those containing gel totally soluble in tetrahydrofuran, chloroform, dimethylsulfoxide and trifluoroacetic acid. Acetone, dichloromethane, toluene and ethylacetate did not dissolve the material. To remove excess diacid the polymers can be dissolved in THF, and subsequently water can be added which results in a hazy solution. The polymer will then move to the upper phase, if not too high in molecular weight, and will float into a thin separate layer on top of the aqueous mixture. Alternatively, chloroform could be used to dissolve the polymer and after vigorous mixing with water dissolving the acid, the water can be separated from the emulsion.

Also shown in Table 4 are the glass transition temperatures of the polyesters, which are generally relatively low. This is likely due to the overwhelmingly low molecular weights of the polymers. This is further evidenced by Entry 9, which at the highest molecular weight also leads to the highest T_g values, similar to those reported in the literature for related polymers (*23*). The T_g values of the polyglyceroldodecanedioates are indeed slightly higher than those of the polyglycerolsebacates, due to the longer methylene chain in the prior acid,

causing slightly stronger dispersion forces between the polymer chains. Several DSCs of the polyesters show a number of small endothermic peaks between -20 and 110°C, while the products are still mostly amorphous. The DSC diagram of a copolyester is shown in Figure 10.
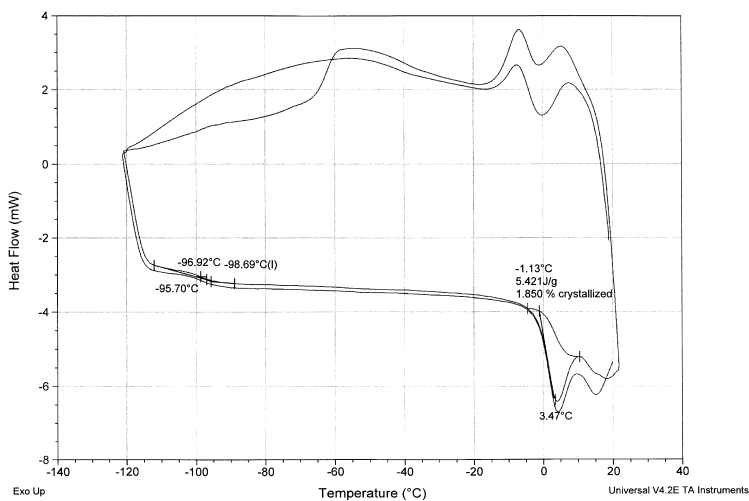
Figure 10. DSC diagram of a copolyester (Entry 5).
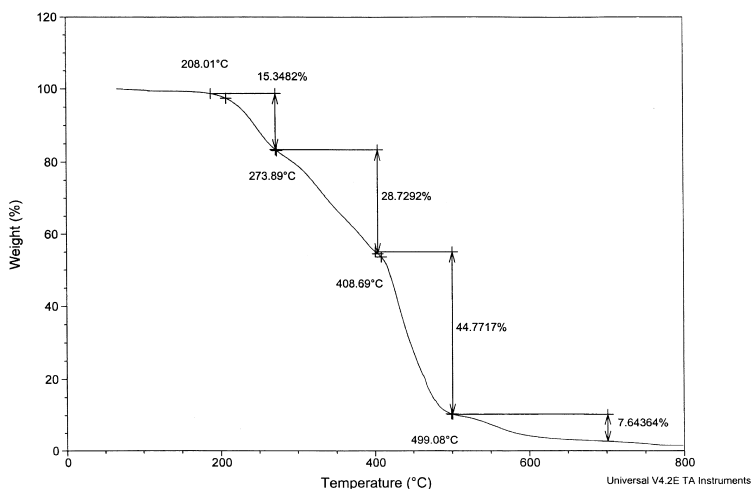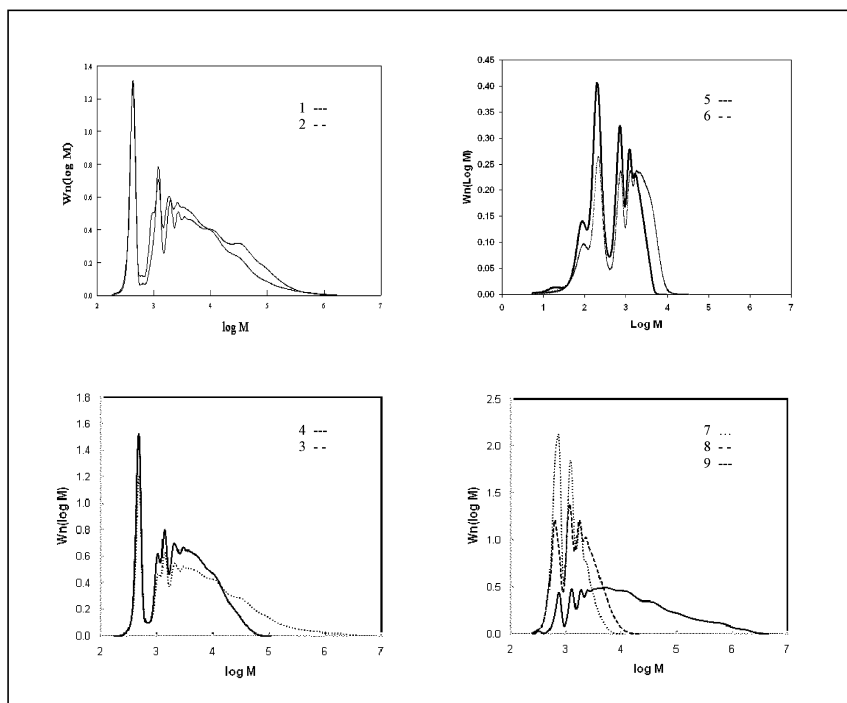

Figure 11. TGA diagram of a copolyester (Entry 4).

Figure 12. GPC Diagrams; top: Polyglycerolsebacates, bottom: Polyglyceroldodecanedioates; left: 1:2 glycerol/diacid ratio, right: 2:1 glycerol/diacid ratio (entry numbers given in legends).

A TGA diagram is shown in Figure 11. The unreacted monomer starts decomposing slightly above 200 °C, being in agreement with the above mentioned conversions. This is followed by the decomposition of oligomers, between 274 and about 400 °C. The higher molecular weight portion of the copolyesters generally decomposes starting at about 400 °C and ending at ca. 500°C. The TGA measurements also show that in the polyesters there is about 3 – 8% residue, which starts decomposing above 500° C. The percentage of these remaining ingredients is higher for the polymers made with biodiesel based glycerol as compared to those made with reagent grade glycerol. Such residues usually are composed of inorganic salts formed during the neutralization step with hydrochloric acids or metals which were applied in the biodiesel production.

Figure 12 shows the GPC diagrams of polymers grouped by the type and amount of applied diacid.

It is apparent that all GPC diagrams show the presence of residual monomer and of significant amounts of oligomers (log M for glycerol at ca. 2, log M for sebacic acid at ca. 2.3 and log M for dodecanedioic acid at ca. 2.4). The peaks close to 1000 g/mol represent examples of dimeric units. Except for Entries 5 and 6 the right tail extends to molecular weights of 100,000 g/mol. High acid/glycerol ratios also favor increase of the polydispersity compared to low acid/glycerol ratios. Another factor with significant influence on the molecular weight

distribution is the conversion. As a consequence of running at low conversions to avoid gelation, most of the obtained polymers have low molecular weights. This was particularly the case at high glycerol/acid ratios. For example, with sebacic acid only M_w of ca. 1000 g/mol was obtained in 8 h, while at the low glycerol/acid ratio M_w was as high as about 20,000 g/mol obtained in only 5 to 6 hours.

Figure 13 shows the dependence of the weight average molecular weight and the polydispersity, M_w/M_n, on the conversion. As expected the weight average molecular increases with conversion. It is also not surprising, that since M_n changes only little, the polymers with a higher M_w also have a broader distribution. However, M_{w-} increases sharply due to the branching of the polymer. The effect of the branching on the polydispersity is even more distinct. While for linear polymers the polydispersity only increases slightly with rising conversion (typically lying between 1.5 and 3), in the present case the polydispersity increases by almost twentyfold. Similar effects of branching on the molecular weight properties have been observed in other systems (*12*, *15*).

At similar conversions, the biodiesel based glycerol resulted in a larger molecular weight, both Mn and Mw, and a broadening of the molecular weight distribution compared to reagent grade glycerol. There is also a good correlation of the obtained molecular weights with the intensity of the terminal groups obtained by 13C NMR measurements. For the first series of copolyesters with mainly acid endgroups, TA, (Entries 1 to 4) the corresponding graph is shown in Figure 14, left. For the polymers with predominantly glycerol end groups, TG (here TG,α only), the graph is given in Figure 14, right.
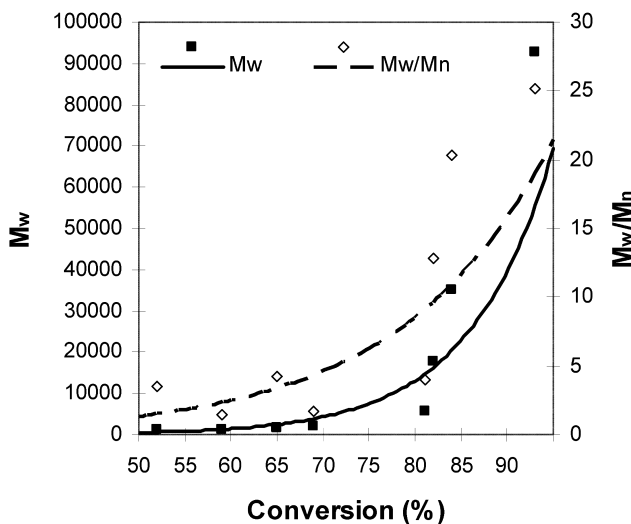
Figure 13. Increase of the weight average molecular weight and molecular weight distribution with conversion.
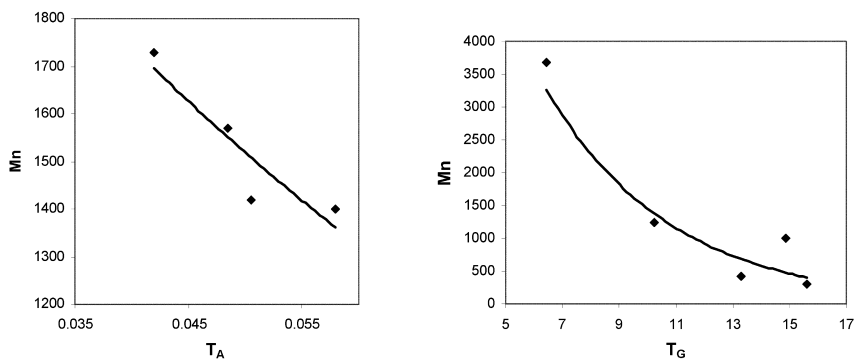
Figure 14. Relationship between the terminal endgroups and the number average molecular weight, Left: acid end groups, right: glycerol end groups.

Remarkably, a polyester with a M_w of 92,600 g/mol could be produced at the high glycerol/acid ratio also resulting in a relatively low gel content of 9%. As mentioned above, the residual soap and potassium chloride in the applied semi-pure glycerol very likely caused an increase in catalyst activity. In future related research, we plan to conduct studies on the specific effects of the found residues in the semi-purified biodiesel glycerol on the polymerization mechanism, which caused the higher conversions, the lower degree of branching and larger molecular weights of the obtained polymers

Conclusions

Copolyesters can be produced from linear diacids with biodiesel based glycerol, which was purified by a simple and inexpensive process. The residue in the semi-purified biodiesel, which was identified to be mainly traces of soap and potassium chloride, does not hinder polymerization or alter it in a disadvantageous manner. In fact, contrary to our expectations, conversions were higher with the biodiesel based glycerol, and for polymerizations with excess diacid, the biodiesel based glycerol led to less branching and lower gel formation. With excess glycerol, the linear groups dominated even when reagent grade glycerol was used. The molecular weights of the copolyesters produced with the biodiesel based glycerol were higher than those obtained with the reagent grade glycerol. Most polymers are amorphous and have low glass transition temperatures, whereby the T_g values for the polyglyceroldodecandioates were slightly higher than those for the polyglycerolsebacates. The obtained polymers could be useful as coatings, adhesives and laminates.

Acknowledgments

Company for providing the GPC data, and Dr. Sandip Sur of the University of Rochester and Kyle Rugg of RIT for their support with the NMR measurements.

References

1. U.S. Department of Energy, Clean Cities Alternative Fuel Price Report, July 2009. http://www.afdc.energy.gov/afdc/pdfs/afpr_jul_09.pdf (accessed July 2010).
2. McCoy, M. *Chem. Eng. News* **2009** (June 1), 16–17.
3. National Biodiesel Board. http://www.biodiesel.org/resources/faqs/ (accessed July 30, 2010).
4. Fan, X.; Burton, R. *Open Fuels Energy Sci. J.* **2009**, *2*, 100–109.
5. Vasudevan, P. T.; Briggs, M. *J. Ind. Microbiol. Biotechnol.* **2008**, *35*, 421–430.
6. Pachauri, N.; He, B. *Am. Soc. Agric. Biol. Eng. (ASABE)*; Paper No. 066223; July 2006. http://www.webpages.uidaho.edu/~bhe/pdfs/asabe066223.pdf (accessed August 15, 2010).
7. Pagliaro, M.; Rossi, M. *Future of Glycerol*; Series: RSC Green Chemistry Series; Springer, 2008.
8. Ashby, R. D.; Wyatt, V. T.; Foglia, T. A.; Solaiman, D. K. Y. In *Biocatalysis and Bioenergy*; Hou, C. T., Shaw, J.-F., Eds.; John Wiley & Sons, 2008; pp 131−154.
9. Kuorosaka, T.; Maruyama, H.; Naribayashi, I.; Sasaki, Y. *Catal. Commun.* **2008**, *9*, 1360–1363.
10. Wang, K.; Hawley, M. C.; DeAthos, S. J. *Ind. Eng. Chem. Res.* **2003**, *42*, 2913–2923.
11. Mu, Y.; Teng, H.; Zhang, D.-J.; Wang, W.; Xiu, Z.-L. *Biotechnol. Lett.* **2006**, *28*, 1755–1759.
12. Flory, P. *J. Am. Chem. Soc.* **1941**, *63*, 3083–3090.
13. Kienle, R. H. *J. Am. Chem. Soc.* **1939**, *61*, 2258–2268.
14. Kulshrestha, A. S.; Gao, W.; Gross, R. A. *Macromolecules* **2005**, *38*, 3193–3204.
15. Hu, J.; Gao, W.; Kulshrestha, A.; Gross, R. *Polym. Prepr.* **2006**, *47* (2), 279–280.
16. Stumbe, J.-F.; Bruchmann, B. *Macromol. Rapid Commun.* **2004**, *25*, 921–924.
17. Werry, B.; Fossum, B. *Polym. Prepr.* **2007**, *48* (1), 426–427.
18. Liu, Q.; Tian, M.; Ding, T.; Shi, R.; Feng, Y.; Zhang, L.; Chen, D.; Tian, W. *J. Appl. Polym. Sci.* **2007**, *103*, 1412–1419.
19. Wyatt, V. T.; Nunez, A.; Foglia, T. A.; Marmer, W. N. *J. Am. Oil Chem. Soc.* **2006**, *83*, 1033–1039.
20. Li, G.; Yang, S. L.; Jiang, J. M.; Wu, C. S. *Polymer* **2005**, *46*, 11142–11148.
21. Migneco, F.; Huang, Y.-C.; Birla, R. K.; Hollister, S. J. *Biomaterials* **2009**, *30*, 6479–6484.

22. de Mereiles Brioude, M.; Guimaraes, D. H.; da Paz Fiuza, R.; de Almeida Prado, L. A. S.; Boaventura, J. S.; Jose, M. M. *Mater. Res.* **2007**, *10*, 335–339.

23. Guimaraes, D. H.; de Mereiles Brioude, M.; da Paz Fiuza, R.; de Almeida Prado, L. A. S.; Boaventura, J. S.; Jose, M. M. *Mater. Res.* **2007**, *10*, 257–260.

24. Miri, M.; Nori, K.; Ge, C. *Polym. Prepr.* **2010**, *51* (1), 769–770.

25. Odian, G. *Principles of Polymerization*, 4th ed.; John Wiley & Sons: Hoboken, New Jersey, 2004.

26. Carothers, W. H. *Trans. Faraday Soc.* **1936**, *32*, 39–49.

27. Flory, P. *Principles of Polymer Chemistry*; Cornell University Press, Ithac, NY, 1953.

28. Durand, D.; Bruneau, C.-M. *Makromol. Chem.* **1978**, *179*, 147–157.

29. Pinner, S. H. *J. Polym. Sci* **1956**, *21*, 153–157.

30. Stafford, J. W. *J. Polym. Sci., Polym. Chem.* **1981**, *19*, 3219–3236.

31. Stockmayer, W. H. *J. Chem. Phys.* **1943**, *11*, 45–55.

32. Whiteway, S. G.; Smith, I. B.; Masson, C. R. *Can. J. Chem.* **1970**, *48*, 33–45.

33. ASTM D 2765-01 (Reapproved 2006); ASTM International: West Conshohocken, Pennysylvania.

34. Thompson, J. C.; He, B. B. *Appl. Eng. Agric.* **2006**, *22*, 261–265.

35. Komers, K.; Stloukal, R.; Machek, J.; Skopal, F. *Eur. J. Lipid Sci. Technol.* **2001**, *103*, 363–371.

36. McCurry, J. D.; Wang, C.-X. Analysis of Glycerin and Glycerides in Biodiesel (B100) Using ASTM D6584 and EN14105, 2007. http://www.chem.agilent.com/Library/applications/5989-7269EN.pdf (accessed August 15, 2010).

37. SDBS (Spectral Database for Organic Compounds) of AIST (National Institute of Advanced Industrial Science and Technology), Japan. http://riodb01.ibase.aist.go.jp/sdbs/cgi-bin/direct_frame_top.cgi (accessed August 15, 2010).

38. Sinclair, R. G.; McKay, A. F.; Myers, G. S.; Norman Jones, R. *J. Am. Chem. Soc.* **1952**, *74*, 2578–2585.

39. Ooi, T. L.; Yong, K. C.; Dzulkefly, K.; Wanyunus, W. M. Z.; Hazimah, A. H. *J. Oil Palm Res.* **2001**, *13*, 16–22Online.

40. O'Connor, R. T.; Duprie, E. F.; Feuge, R. O. *J. Am. Oil Chem. Soc.* **1955**, *32*, 88–93.

41. Holmgren, A.; Lindblom, G.; Johansson, L. B.-A. *J. Phys. Chem.* **1988**, *92*, 5639–5642.

42. Lynch, M. L. *Curr. Opin. Colloid Interface Sci.* **1997**, *2*, 495–500.

43. Gasgnier, M. *J. Mater. Sci. Lett.* **2001**, *20,* 1259–1262.

44. Knothe, G.; Kenar, J. A. *Eur. J. Lipid Sci. Technol.* **2004**, *106*, 88–96.

45. Satyarthi, J. K.; Srinivas, D.; Ratnasamy, P. *Energy Fuels* **2009**, *23*, 2273–2277.

46. Kricheldorf, H. R. *Makromol. Chem.* **1978**, *179*, 2133–2143.

47. Hawker, C. J.; Lee, R.; Frechet, J. M. J *J. Am. Chem. Soc.* **1991**, *113*, 4583–4588.

Chapter 3

Bioplastics, Biocomposites, and Biocoatings from Natural Oils

Rafael L. Quirino and Richard C. Larock*

Department of Chemistry, 2751 Gilman Hall, Iowa State University, Ames, IA 50011, USA
*larock@iastate.edu.

A range of new materials can be obtained by the cationic, free radical, or thermal copolymerization of natural and modified oils with a number of petroleum-based comonomers. These novel new biobased materials possess good thermal stabilities, good mechanical properties, and good damping and shape memory properties. Unique new bioplastics have also been prepared by the ring opening metathesis polymerization (ROMP) of modified oils and fatty alcohols in the presence of strained cyclic alkenes to form rubbery to hard materials. In order to improve the performance of these new bioplastics, inorganic fillers and natural fibers have been used to reinforce the cationic, free radical, and ROMP resins. Vegetable oil-based waterborne polyurethane dispersions (PUD's) have also been synthesized from vegetable oil polyols. In order to improve their properties, the PUD's have been copolymerized with an emulsion of vinyl or acrylic comonomers to form a series of polyurethane/acrylic hybrid latexes. Core-shell latexes have also been obtained by the emulsion copolymerization of PUD's with vinyl comonomers. All of these materials exhibit properties similar to or better than related petroleum-based products.

Introduction

With the tremendous commercial importance of the plastics and coatings industries, it is obvious that the replacement of petroleum-based materials by useful new bioplastics from inexpensive, renewable, natural materials, like vegetable oils and agricultural residues, will have an enormous impact economically, environmentally, and energy-wise. The advantages of biobased materials are the ready availability of large quantities of renewable starting materials, the usually competitive price of these starting materials in comparison to currently used petroleum-based monomers, the potential of producing more bio-degradable materials than virtually indestructible petroleum-based polymers, the possibility of producing new materials with properties not presently available in commercial petroleum-based products, and the overall intrinsic low toxicity of such biobased products.

The use of renewable resources in energy and material-related applications is receiving increasing attention in both industry and academia. A range of factors contributes to frequent dramatic fluctuations in the price of oil, which is reflected in the production cost of all petroleum-based goods. This situation creates an urgent need, from an industrial point of view, for renewable starting materials and biobased products that have the potential to replace petroleum-based materials. Thus, research and development of new biopolymers is extremely important in attaining oil independence and sustainable industrial development.

Currently, the most widely used renewable raw materials are vegetable oils, polysaccharides (cellulose and starch), wood, and proteins (*1*). A variety of chemicals have been prepared from these starting materials. Bio-oil and syngas are obtained by the pyrolysis of wood and agricultural wastes (*2*). Proteins are denatured and aligned during processing to make protein-based biopolymers (*3*), and vegetable oils find use in paints (*4*), biocoatings (*5–9*), biofuels (*10*), and as building blocks for biobased polymers (*11–13*).

Recently, a variety of vegetable oil-based polymers, with good thermal and mechanical properties, have been developed through the cationic (*14–16*), free radical (*17*, *18*), and thermal (*12*, *13*) copolymerization of regular and conjugated natural oils with several petroleum-based comonomers. In such systems, the reactive sites in the triglyceride units are the carbon-carbon double bonds. Overall, the reactivity of vegetable oils towards these polymerization processes can be significantly increased if the carbon-carbon double bonds in the fatty acid chains are isomerized and brought into conjugation (*19*, *20*). For the remainder of this chapter, the term "conjugated" refers to carbon-carbon double bonds that are conjugated (as in a 1,3-diene). Other polymerization methods, such as ring-opening metathesis polymerization (ROMP) (*21–23*) and acyclic diene metathesis (ADMET) (*24*), have also been recently employed to synthesize vegetable oil-based biopolymers.

Biobased materials with improved thermophysical and mechanical properties can be obtained by simply reinforcing the aforementioned polymeric matrices with inorganic fillers and natural fibers. The use of glass fiber (*25*) and organoclays (*26*) as reinforcements in biocomposites significantly improves the Young's modulus and tensile strength of the bio-materials. Along the same lines, various agricultural

residues and natural fibers, such as spent germ (*27*), soybean hulls (*28*), corn stover (*29*), wheat straw (*30*), rice hulls (*31*), and switch grass (*32*) have been added to the aforementioned vegetable oil-based resins to prepare biocomposites with up to 85 wt % of biobased content.

Promising biocoatings can also be obtained from vegetable oils. Indeed, soybean oil-based polyols have been successfully used in the preparation of anionic (*6*) and cationic (*7*) polyurethane dispersions. In order to improve the thermophysical and mechanical properties of these new soybean oil-based polyurethane dispersions (PUD's), hybrid latexes have been prepared by the emulsion copolymerization of PUD's with acrylates (*8*). Core-shell hybrid latexes have also been prepared by the emulsion copolymerization of PUD's from acrylated soybean oil polyols with vinyl comonomers, which results in biobased latexes with promising properties for use as coatings and adhesives (*9*).

The technology involved in these new natural oil-based materials is remarkably simple and should be readily adapted to the existing polymer and coating industries. The recent transition from petroleum to biobased products provides major economical advantages, and even more importantly, generates more environmentally friendly processes and products. This chapter focuses primarily on the research progress made on biobased plastics, composites and coatings derived from natural oils by the Larock group over the last 10 years and closely related work. No attempt has been made to report a comprehensive review of the development of new biopolymers.

Natural Oil-Derived Bioplastics

Natural oils are a renewable resource that can be extracted from animals and plants. Structurally, the oils consist of triglycerides with fatty acid side chains of varying length and degree of unsaturation. The general chemical representation of a triglyceride oil can be seen in Figure 1, while the fatty acid composition of the most common oils used as renewable starting materials for biopolymers is given in Table I (*11, 16*). The notation in parentheses ($C_{a:b}$), after the fatty acid name (Table I), denotes the number of carbon atoms (a), followed by the number of carbon-carbon double bonds (b) in the corresponding fatty acid. The carbon-carbon double bonds in these natural oils possess predominantly a *cis* configuration.
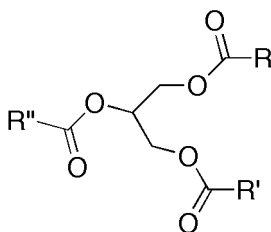
Figure 1. General triglyceride structure, where R, R', and R'' are linear alkyl chains with variable lengths and degrees of unsaturation depending on the oil involved.

Table I. Fatty Acid Composition of Commonly Used Natural Oils in the Preparation of New Biobased Materials

Oil	Linolenic acid ($C_{18:3}$) content (%)	Linoleic acid ($C_{18:2}$) content (%)	Oleic acid ($C_{18:1}$) content (%)	Stearic acid ($C_{18:0}$) content (%)	Palmitic acid ($C_{16:0}$) content (%)	Double bonds per triglyceride[a]
Tung[b]	-	9	4	-	6	7.9
Linseed	57	15	19	4	6	6.6
Walnut	3	73	18	1	5	5.5
Low saturation soybean	9	57	31	1	3	5.0
Safflower	-	78	12	2	7	5.0
Sunflower	1	54	37	3	5	4.7
Soybean	8	53	23	4	11	4.6
Corn	1	60	25	2	11	4.5
Grapeseed	-	63	27	3	7	4.5
Canola	9	21	61	2	4	3.9
Sesame	1	43	41	6	9	3.9
Peanut	-	32	47	2	11	3.3
Olive	1	6	80	3	9	2.9
Castor[c]	1	4	5	1	2	2.7
Fish[d]	-	-	11-25	-	10-22	-

[a] Average number of carbon-carbon double bonds per triglyceride. [b] Approximately 84 % of the fatty acid chains in tung oil are alpha-eleostearic acid, a naturally conjugated triene (*12*). [c] Approximately 85 % of the fatty acid chains in castor oil are ricinoleic acid, a $C_{18:1}$ acid with an hydroxyl group on carbon 12 of the fatty acid chain. [d] Fish oil presents a high percentage of polyunsaturated fatty acids, containing as many as 5-6 non-conjugated carbon-carbon double bonds (*14*).

Some fatty acids bear functional groups, like ricinoleic acid, which contains an hydroxyl (-OH) group attached to carbon 12 (C_{12}) in the fatty acid chain. Structural changes in the triglyceride moiety, such as the length of the fatty acid chains, the number of carbon-carbon double bonds, the configuration (*cis/trans*) of the carbon-carbon double bonds, and conjugation of the carbon-carbon double bonds directly affect the physical and chemical characteristics of the oil, such as its reactivity towards other reagents. Thus, vegetable oils can be classified as drying, semi-drying, and non-drying oils, depending on their ability to auto-oxidize in the presence of the oxygen in air.

Thermal polymerization process:
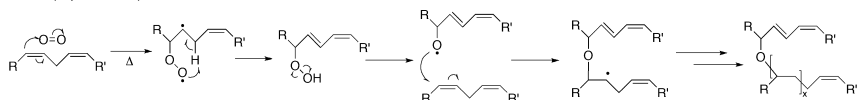
Free radical polymerization process:
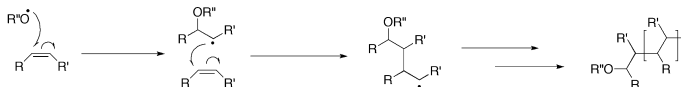
R"O• = Free radical initiator fragment

Cationic polymerization process:
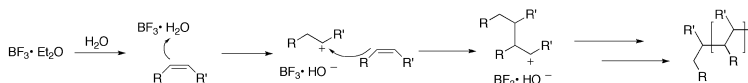
Figure 2. General reaction mechanisms for thermal, free radical and cationic polymerization.

Stabilization of a free radical:
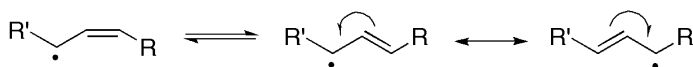
Stabilization of a carbocation:
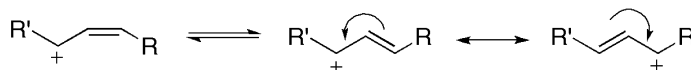
Figure 3. Resonance structures of a free radical and of a carbocation.

The carbon-carbon double bonds in triglycerides can be reacted in many different ways to form biobased polymers. The four main types of polymerizations discussed here are ROMP, cationic, free radical, and thermal polymerizations. While the free radical and thermal polymerizations of triglycerides follow essentially the same mechanism, differing only with respect to the initiation process, the cationic polymerization of triglycerides follows a different mechanism, initiated by a strong electrophile (*11*). The ROMP process involves still a different type of initiation process, which will be discussed in more detail later. Three out of the four polymerization mechanisms covered in this chapter are illustrated in Figure 2.

As expected thermodynamically, the intermediates formed during the free radical, thermal, or cationic polymerization of triglycerides can be further stabilized if the carbon-carbon double bonds are initially conjugated. In these cases, the intermediate free radicals and carbocations can be stabilized by the electrons on the adjacent double bonds, as shown in Figure 3. Thus, conjugated triglycerides are more readily polymerized than natural, non-modified oils.

Bioplastics from the Cationic Copolymerization of Natural Oils

As mentioned before and shown in Figure 2, a strong electrophile is required to promote the cationic polymerization of triglycerides and fatty acids. Lewis acids are the ideal species to initiate this process. Indeed, $AlCl_3$, $TiCl_4$, $SnCl_4$, $ZnCl_2$, $FeCl_3$, $SnCl_4 \cdot 5H_2O$, H_2SO_4 and $BF_3 \cdot OEt_2$ (BFE) have been used to initiate the cationic copolymerization of mixtures containing 50-94 wt % of regular or conjugated fish oil ethyl esters with divinylbenzene (DVB) and norbornadiene (NBD), or dicyclopentadiene (DCPD) under mild reaction conditions (*33*). Among the initiators tested, BFE is the most efficient (*33*) and is commonly used in the cationic copolymerization of natural oils with vinyl comonomers.

The cationic homopolymerization of either regular or conjugated fish oil ethyl esters affords only low molecular weight, viscous materials with limited utility (*33*). Therefore, the addition of reactive petroleum-based comonomers is crucial in order to obtain viable solid thermosets. The structure of the biobased starting material along with the nature and stoichiometry of the comonomers used during preparation of the bioplastics has an effect on the final properties of the polymer. The copolymerization of mixtures containing 30-60 wt % of a fish oil triglyceride, and regular or conjugated fish oil ethyl esters with various amounts of styrene (ST) and DVB affords materials ranging from soft rubbers to rigid plastics (*34*). It has been shown that the resulting fish oil triglyceride-containing polymeric material, due to its higher crosslink density, exhibits properties comparable to rigid plastics, while materials containing fish oil ethyl esters exhibit lower mechanical properties (*34*). Triglycerides have a branched structure that leads to extensive crosslinking. Each unsaturated fatty acid chain in the triglyceride can participate in the cationic reaction, thus a crosslinked, three-dimensional polymer network can be formed. Among the fish oil ethyl esters used, the conjugated esters exhibit overall better properties due to their higher reactivity (*34*). Likewise, the copolymerization of mixtures containing various amounts of conjugated fish oil triglycerides with DVB, NBD, or DCPD affords materials with overall better properties than the materials obtained from the cationic copolymerization of regular fish oil with the same comonomers (*14*). Overall, the fish oil-based bioplastics exhibit low creep-resistance at room temperature, but moduli comparable to those of conventional polyolefins (*35*). A comparison of the tensile properties of bioplastics made by the cationic copolymerization of various natural oils is presented in Table II (*16*, *34*, *36*, *40*).

The conjugated carbon-carbon double bonds in tung oil are responsible for its high reactivity in cationic polymerization. Very strong materials, with storage moduli at room temperature (as determined by DMA) of about 2 GPa, are obtained from the cationic copolymerization of 50-55 wt % of tung oil with DVB (*15*). The gel time can be controlled by the substitution of up to 25 wt % of the tung oil with less reactive vegetable oils, such as soybean (SOY), low saturation soybean (LSS), or conjugated low saturation soybean (CLS) oils (*15*). Similarly, mixtures containing 35-55 wt % of corn or conjugated corn oil with various amounts of DVB and ST afford polymeric materials whose mechanical properties range from soft and rubbery to rigid plastics, depending on the stoichiometry of the comonomers used (*36*). The gel times can also be affected by the stoichiometry

of the comonomers, with an exponential increase in time for increasing amounts of the oil, especially beyond 40 wt % (*36*). The gel times for resins containing conjugated corn oil are significantly shorter than for resins made from regular corn oil, indicating the higher reactivity of the conjugated oil (*36*). The cure temperatures also affect the gel time of the cationic resins. For example, when a resin containing 45 wt % of corn oil, 32 wt % of ST, 15 wt % of DVB, and 8 wt % of BFE initiator is cured at room temperature, the gel time observed is 116 minutes. At 15 °C, the same resin doesn't gel completely in 24 hours (*36*).

Table II. Tensile Properties of Bioplastics Made by the Cationic Polymerization of Various Natural Oils

Oil (wt %)	DVB (wt %)	Young's modulus (GPa)	Tensile strength (MPa)
Fish oil (*49*)	15	0.82	42.6
Fish oil ethyl ester (*49*)	15	0.08	5.5
Conjugated fish oil ethyl ester (*49*)	15	0.45	18.3
Corn oil (*45*)	15	0.05	4.6
Conjugated corn oil (*45*)	15	0.07	7.0
Conjugated low saturation soybean oil (*45*)	15	0.23	11.5
Low saturation soybean oil (*62*)	30	0.06	3.0
Soybean oil (*62*)	30	0.05	2.5
Olive oil (*62*)	30	0.03	1.2
Peanut oil (*62*)	30	0.04	1.7
Sesame oil (*62*)	30	0.04	2.2
Canola oil (*62*)	30	0.04	1.7
Linseed oil (*62*)	30	0.10	5.6
Grapeseed oil (*62*)	30	0.05	3.0
Sunflower oil (*62*)	30	0.05	3.0
Safflower oil (*62*)	30	0.06	3.1
Walnut oil (*62*)	30	0.06	3.8
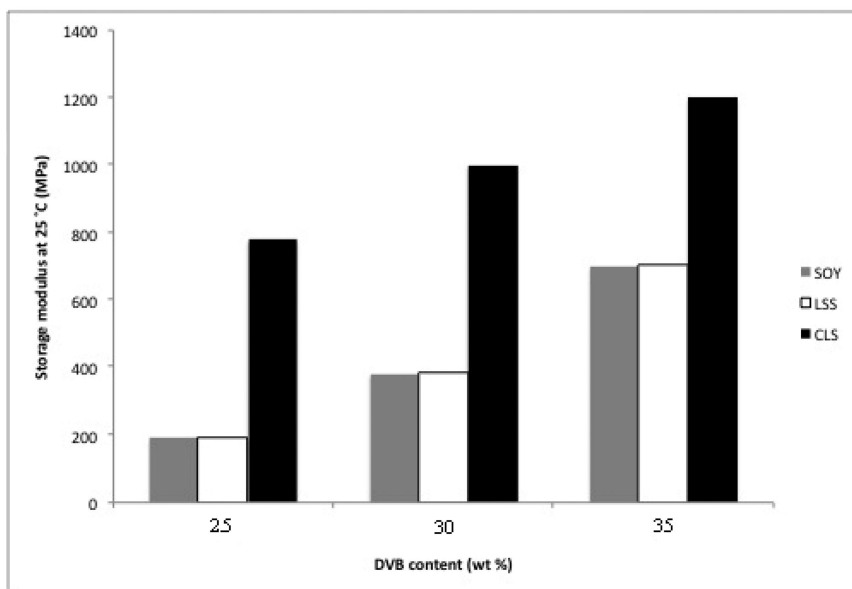
Figure 4. Storage modulus (as determined by DMA) as a function of divinylbenzene (DVB) content in soybean oil (SOY)-, low saturation soybean oil (LSS)-, and conjugated low saturation soybean oil (CLS)-based thermosets.

Extensive research has been conducted on the cationic copolymerization of SOY, LSS, and CLS with various crosslinking agents (*37–45*). Whenever 50-60 wt % of SOY, LSS, or CLS is copolymerized with DVB, a densely crosslinked polymer network, interpenetrated by 12-31 wt % of unreacted free oil or oligomers, is produced (*37*). The amount of unreacted free oil left after cure of the resin is directly dependent on the amount and reactivity of the oil initially employed in the preparation of the resin. Poor miscibility between the oil and the BFE initiator results in micro-phase separation in the SOY and LSS-based copolymers, with distinctly different crosslink densities in different parts of the bulk copolymer (*37*). Modification of the BFE initiator with other oils, especially with fish oil ethyl ester, helps in the homogeneous copolymerization of SOY, LSS, and CLS with DVB (*37*). The resulting bulk copolymers exhibit higher conversion of the oils into crosslinked thermosets than those utilizing the non-modified BFE initiator (*37*). With respect to the concentration of the comonomers, an increase in the room temperature storage modulus (as determined by DMA) of the final copolymer is seen when employing higher amounts of DVB in the original composition (*37*), as evidenced in Figure 4. For example, the storage modulus at room temperature increases from 0.78 GPa to 1.20 GPa when the DVB content increases from 25 wt % to 35 wt % in the CLS copolymers (*37*). The unreacted free oil or oligomers present in the final copolymers largely affects the thermal stability of the thermosets. The CLS polymers have the highest storage moduli and thermal stabilities, because they contain the least unreacted free oil (*37*).

To increase the structural uniformity of the crosslinked copolymers, the monofunctional monomer ST has been added to the original composition using

SOY, LSS, or CLS/DVB (*38*). With the substitution of 25-50 wt % of DVB by ST, the overall properties of the resulting plastics are significantly improved (*38*). The thermophysical properties of the thermosets are considerably affected by the crosslink density of the bulk copolymers and the yield of crosslinked material is strongly dependent on the concentration and reactivity of the crosslinking agent (DVB, DCPD, or NBD), and the reactivity of the oil used (*38–40*). Among the crosslinking agents used, DVB exhibits the highest reactivity and thus gives the most promising, crosslinked materials with good damping and shape memory properties (*38–42*). The overall properties of soybean oil-based thermosets are maximized when the concentration of the oil is equivalent to that of the other comonomers (*40*). An isothermal cure study of these systems established the ideal cure temperature to be in the range 12-66 °C, depending on the actual composition of the resin (*43*) and a DSC study of the cure of resins initiated by different concentrations of BFE revealed an optimum concentration of the Lewis acid equal to 2 wt % (*45*).

The cationic copolymerization of SOY and 100 % conjugated soybean oil (CSO) with DCPD in the presence of various modified BFE initiators has been studied and the results indicate that the commonly used fish oil ethyl ester modifier is unnecessary when the polymerization involves the more reactive CSO (*46*). It was also found that below a DCPD content of 42 wt %, the final thermosets behave as rubbers at room temperature (*47*).
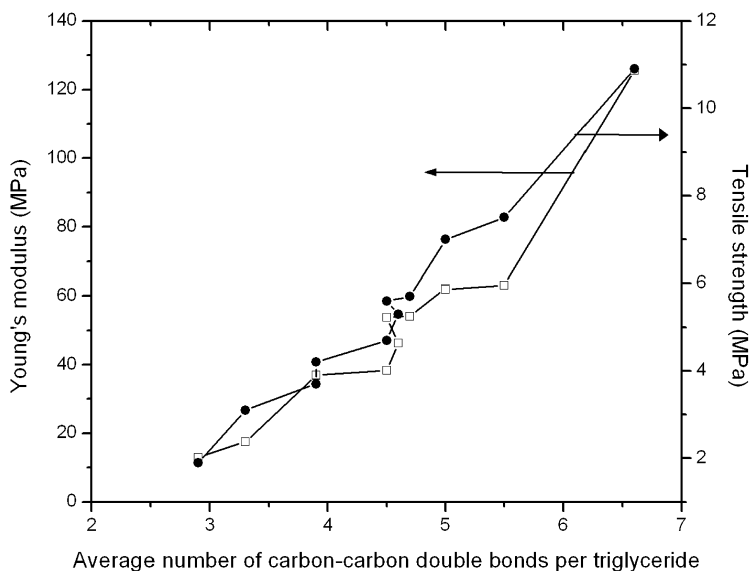
Figure 5. Young's modulus and tensile strength as a function of the average number of carbon-carbon double bonds per triglyceride in thermosets containing 45 wt % of vegetable oil, 32 wt % of styrene (ST), and 15 wt % of divinylbenzene (DVB).

A variety of other vegetable oils, including olive, peanut, sesame, canola, grapeseed, sunflower, safflower, walnut, and linseed oils have been cationically copolymerized with DVB and/or ST to form a range of thermosets with properties that can be tailored for specific applications (*48*). Overall, the properties of these new materials exhibit a gradual increase with the degree of unsaturation and thus increasing oil reactivity (*48*), as shown by the curves for the Young's modulus and tensile strength versus carbon-carbon double bond content shown in Figure 5. However, it has been found that the gelation times of these copolymers are independent of the degree of unsaturation of the vegetable oil used (*48*).

More recently, the products of the Diels-Alder reaction of linseed oil with cyclopentadiene (sold commercially as Dilulin), and the ene reaction between linseed oil and cyclopentadiene (sold commercially as ML189), have been copolymerized with DCPD (*49*). The structures of Dilulin and ML189 are represented in Figure 6. Due to the similar reactivity of DCPD and the modified linseed oils, homogenous thermosets containing 57-97 wt % of the biobased materials are obtained after their cationic copolymerization (*49*). As observed for thermosets prepared by the cationic copolymerization of SOY, LSS, and CLS with DVB (*37, 40*), the Dilulin and ML189/DCPD thermosets exhibit mechanical properties that increase with an increase in the amount of the crosslinking agent, DCPD. Overall, the cationic thermosets developed by the Larock group are dark brown in color, exhibit promising damping and shape memory properties, and may find applications in the substitution of petroleum-based plastics.
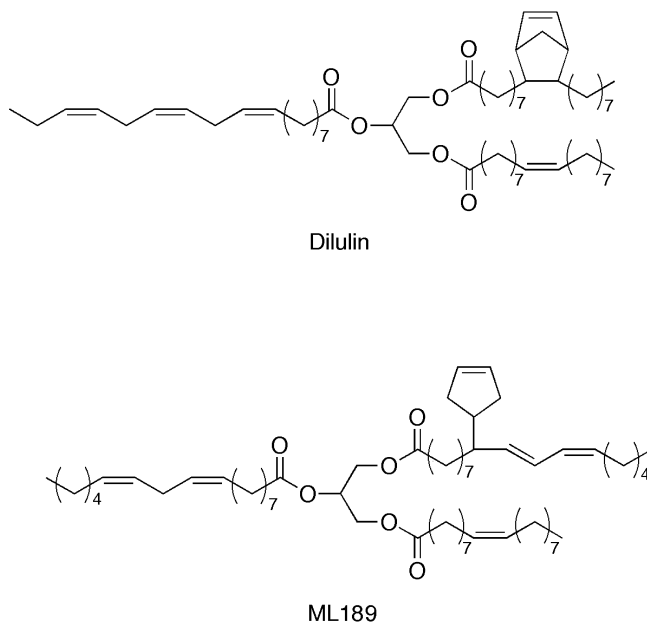
Dilulin

ML189

Figure 6. Chemical structures of Dilulin and ML189.

Bioplastics from the Free Radical Copolymerization of Vegetable Oils

Translucent vegetable oil-based thermosets have been obtained by the Larock group through the free radical copolymerization of reactive unsaturated triglycerides and vinyl comonomers (*17, 18*). The free radical copolymerization of vegetable oils with petroleum-based comonomers requires that the carbon-carbon double bonds in the oil be sufficiently reactive in order to form a homogeneous material. As discussed earlier, conjugated double bonds form more stable intermediates during free radical polymerization, suggesting that conjugated vegetable oils are better starting materials for the preparation of free radical biobased thermosets. The conjugation of a variety of vegetable oils can be easily achieved in the presence of a rhodium catalyst in a process developed by the Larock group and previously described in the literature (*19, 20*).

The bulk free radical copolymerization of mixtures containing 30-75 wt % of 100 % conjugated linseed oil with various amounts of acrylonitrile (AN) and DVB affords a range of materials from flexible to rigid thermosets (*17*). The free radical reaction, in this case, is initiated by 1 wt % of azobisisobutyronitrile (AIBN) (*17*). Although the materials exhibit promising thermophysical and mechanical properties, Soxhlet extraction with methylene chloride for 24 hours revealed that only 61-96 wt % of the oil, initially employed in the synthesis, is retained in the final thermoset (*17*). Alternatively, benzoyl peroxide has been used as a free radical initiator for the preparation of rigid thermosets containing 30-65 wt % of regular linseed oil, ST, and DVB (*50*). Independent of the free radical initiator used, there is a tendency for the properties to decrease when increasing the vegetable oil content in the thermosets (*17, 50*).

Soybean oil-based thermosets have been prepared by the copolymerization of mixtures containing 40-85 wt % of CLS with various amounts of AN, DVB, and/or DCPD in the presence of AIBN (*18*). The copolymers obtained exhibit 100 % incorporation of the CLS when the amount of oil initially added ranges from 40 wt % to 65 wt %, especially for the DCPD-containing thermosets (*18*). This higher oil incorporation in DCPD-containing thermosets is related to the similar reactivity of both components. When the oil content exceeds 70 wt %, a large amount of unreacted oil is recovered from the final thermoset after Soxhlet extraction with methylene chloride (*18*). A wide range of thermal and mechanical properties have been obtained by simply changing the stoichiometry of the resin components.

Bioplastics from the Thermal Copolymerization of Vegetable Oils

Drying oils undergo auto-oxidation in the presence of oxygen, and form peroxides, which then undergo crosslinking through free radical recombination to form highly branched polymeric materials. This characteristic of drying oils makes them very useful biorenewable materials for the coatings industry. It has been shown that vegetable oil-based free radical macroinitiators can be formed by a similar process using linseed and soybean oils (*50–52*). Such free radical macroinitiators have been used to initiate the polymerization of methyl methacrylate (MMA) and *n*-butyl methacrylate (BMA) to form polymeric linseed (*52*) and soybean oil (*51*) grafted copolymers, respectively. One of the advantages

of these new materials is their partial biodegradability and biocompatibility when compared to standard PMMA and PnBMA (*51*, *52*).

In 1940, a tung oil-styrene copolymer was produced by simply heating these two compounds at 125 °C for 3 days (*53*). However, tung oil constituted only 0.1-2.0 % of the copolymer in that work (*53*). Thermosets containing 30-70 wt % of tung oil (TUN) have been prepared by the Larock group through the thermal copolymerization of TUN with various amounts of ST and DVB at temperatures ranging from 85 °C to 160 °C (*12*). The materials prepared range from rubbery polymers to tough and rigid plastics (*12*). These fully cured thermosets, initiated by simply heating the mixture, exhibit higher crosslink densities and overall better properties when metallic salts of Co, Ca, and Zr are added as catalysts during the cure (*12*). Similar materials have been prepared using 30-70 wt % of a commercially available 87 % conjugated linseed oil (*13*). Once again, materials ranging from rubbers to hard plastics are obtained by simply varying the stoichiometry of the comonomers (*13*). The use of a less reactive oil, compared to TUN, resulted in the appearance of two distinct glass transition temperatures (T_g's), which indicates a microphase separation into oil-rich and DVB-rich phases (*13*). A scanning electron microscopy (SEM) analysis of solvent extracted samples of such thermosets revealed that the soluble components consist mainly of unreacted oil, which is well distributed throughout the polymer matrix, leaving evenly distributed nanopores after extraction (*13*). As observed for the TUN-based thermally produced thermosets (*12*), the use of increasing amounts of cobalt drying catalysts, during the cure, results in increasingly higher crosslink densities (*5*).

Bioplastics from the Ring Opening Metathesis Polymerization (ROMP) of Modified Vegetable Oils

In the ROMP process, strained, unsaturated cyclic molecules are opened at the carbon-carbon double bond, by interaction with a ruthenium carbene catalyst. Subsequent coordination of a new molecule of the strained ring and metathesis of the carbon-carbon double bonds results in an unsaturated polymer (*54*) that can be additionally crosslinked through thermal reaction of the remaining carbon-carbon double bonds. A step-wise illustration of the ROMP process is provided in Figure 7, using norbornene as an example of a strained, unsaturated ring. If more than one type of strained, unsaturated ring is present in the reaction medium, a copolymer is formed.

(I) = Grubbs' catalyst
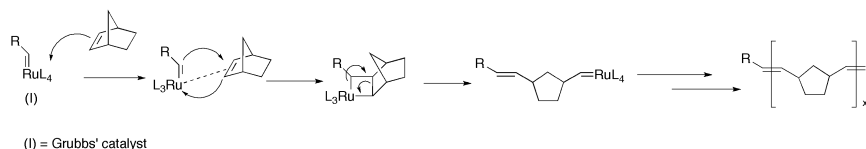
Figure 7. Step-wise ring opening metathesis polymerization (ROMP) mechanism using norbornene as an example.

In order for vegetable oils to participate in ROMP, modification of the fatty acid chains is necessary. As mentioned earlier, the Diels-Alder reaction of cyclopentadiene and linseed oil produces a commercially available product, Dilulin, which has been used, by the Larock group, in ROMP with a norbornene-based crosslinking agent (*22*). As the content of the crosslinking agent increases from 0 wt % to 50 wt %, increases in the thermal stability and the crosslink density of the resulting thermosets are observed (*22*). Quantitative incorporation of Dilulin in the polymer network is attained even in the presence of lower amounts of the crosslinking agent (*22*). DCPD has also been employed as a crosslinking agent in ROMP with Dilulin, but unlike the results obtained with the norbornene-based crosslinking agent (*22*), the maximum oil incorporation was only 80 wt % (*55*). The 20 wt % of unreacted free oil acts as a plasticizer in the final thermoset (*55*). Decreasing the DCPD content in those thermosets results in materials with lower T_g's (*55*).

Castor oil, where approximately 90 % of the fatty acid chains bear an hydroxyl group on C12, has also been modified for use in ROMP reactions (*21*). It has been reacted with bicyclo[2.2.1]hept-5-ene-2,3-dicarboxylic anhydride to give a norbornenyl-functionalized triglyceride, referred to as BCO and represented in Figure 8. Varying amounts of this modified oil (55-85 wt %) have been copolymerized with cyclooctene in the presence of 0.5 wt % of the 2nd generation Grubbs catalyst to afford transparent rubbery thermosets (*21*). An increase in the thermal stability of such thermosets has been observed when increasing the oil content (*21*). It has been shown that the thermal stability of ROMP thermosets is closely related to the presence of unreacted triglycerides in the final material (*21*).

A different approach to the preparation of biobased ROMP thermosets involves the use of vegetable oil-derived functionalized fatty alcohols (*23*). Norbornenyl-functionalized fatty alcohols from soybean oil (NMSA), Dilulin (NMDA), ML189 (NMMA) and castor oil (NMCA) have been prepared and polymerized in the absence of other comonomers (*23*). These fatty alcohols are represented in Figure 9. The number of norbornenyl groups appended to the fatty acid alcohols and their viscosity affect the final properties of the thermosets. Polymers obtained from the ROMP of NMDA and NMMA exhibit Young's moduli and ultimate tensile strengths comparable to HDPE and poly(norbornene), and show promise as high performance bioplastics (*23*). In order to avoid the problems associated with viscosity during the ROMP of biobased systems, novel norbornenyl-functionalized castor oil (NCO) and fatty alcohol (NCA), were developed by reacting castor oil and its fatty alcohol with norbornene carbonyl chloride (*56*). The chemical structures of NCO and NCA are shown in Figure 10. The ROMP of NCO and NCA results in rubbery to rigid transparent thermosets with increased crosslink densities and good thermophysical and mechanical properties, and thermal stabilities (*56*).
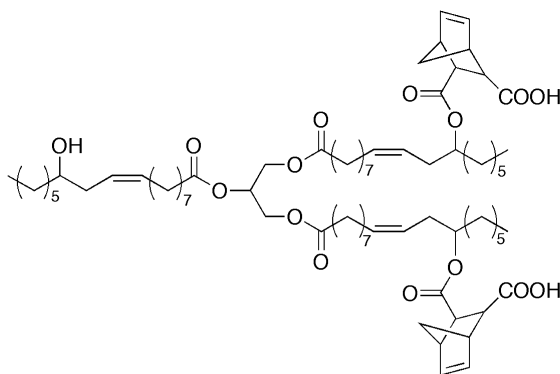
Figure 8. Chemical structure of BCO.
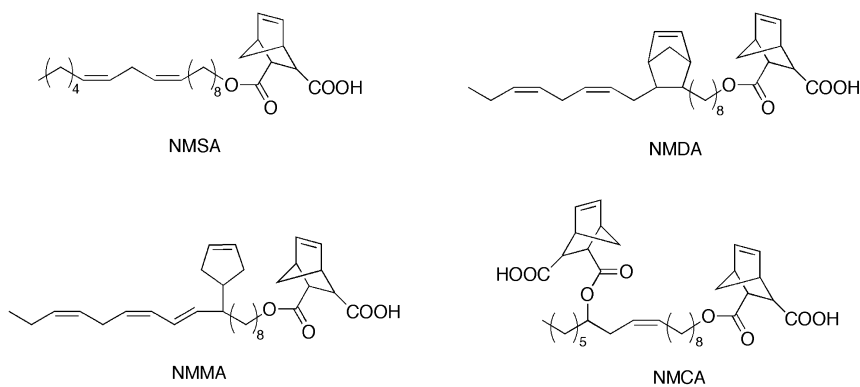
Figure 9. Chemical structures of NMSA, NMDA, NMMA, and NMCA.
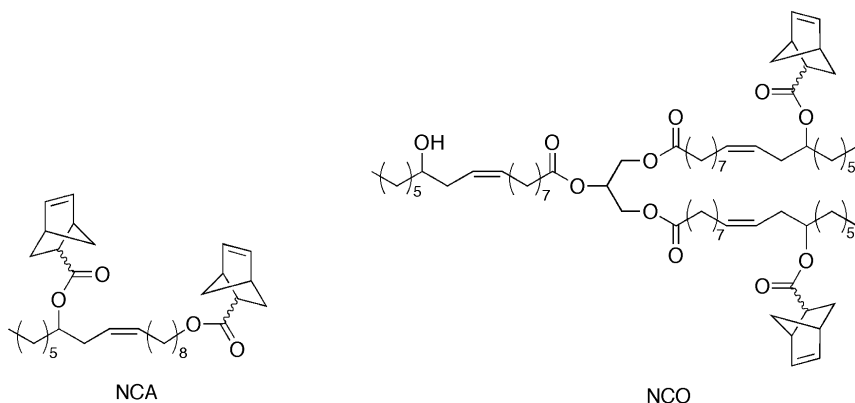
Figure 10. Chemical structures of norbornenyl-functionalized castor oil fatty alcohol (NCA) and norbornenyl-functionalized castor oil (NCO).

Biocomposites

In order to improve the thermophysical and mechanical properties of the biobased thermosets developed by the Larock group, the biobased polymeric matrices have been reinforced with inorganic fillers and natural fibers. The use of such fillers in the preparation of biocomposites significantly improves the Young's modulus and the tensile strength. Using natural fibers, high biobased content biocomposites, with a biorenewable content of up to 85 wt %, have been prepared.

Vegetable Oil-Based Biocomposites Reinforced with Inorganic Fillers

Particularly stiff materials have been obtained by reinforcing the cationic corn oil-based copolymers described previously (*36*) with continuous glass fibers (*25*). It has been shown that significant improvements in Young's modulus and tensile strength can be attained by using up to 45 wt % of glass fibers (*25*). Indeed, the Young's modulus increases from 4.1 MPa to 874 MPa and the tensile strength increases from 1.7 MPa to 8.4 MPa, when the glass fiber content is increased from 0 wt % to 45 wt % (*25*). Changes in the resin composition also affect the final properties of the composites (*25*). As discussed previously (*36*), increases in the DVB content of the resin result in an increase in the crosslink density of the thermoset, which has a positive effect in the thermophysical properties of the material. Also, the replacement of regular corn oil by conjugated corn oil results in a material with slightly better properties due to the higher reactivity of the conjugated system.

In similar work, soybean oil-based cationic resins have been reinforced with continuous glass fibers (*57*). SOY and LSS have been copolymerized with ST and DVB, in the presence of 0-50 wt % of continuous glass fibers, in a cationic process initiated by fish oil ethyl ester-modified BFE (*57*). As a result, significant increases in the Young's modulus from 0.15 GPa to 2.73 GPa, and in the tensile strength from 7.9 MPa to 76 MPa, have been obtained (*57*). The thermal stabilities and mechanical properties can also be improved by increasing the crosslink density of the matrix. Such materials have promise for use in housing and automotive applications.

Glass fibers have also been used as a reinforcement for Dilulin/DCPD ROMP resins, producing promising composites (*58*). Such resins have been described previously by the Larock group (*55*). They exhibit an increase in T_g values for the higher crosslink densities obtained by increasing the DCPD content in the original formulation (*55*). Since the presence of glass fibers has no effect on the crosslink density, no changes in either the T_g values or the thermal stability are detected when the pure resin is compared to the glass fiber composite (*58*). Although the presence of 40 wt % of glass fibers results in an increase in the Young's modulus from 29 MPa to 168 MPa, SEM revealed a weak interaction between the fibers and the matrix (*58*). Nevertheless, the ability of the fibers to reduce crack propagation and fracture results in an overall improvement in all of the mechanical properties (*58*).

A different class of biocomposites has been prepared by reinforcing cationic thermosets with a functionalized organoclay (*26*). The cationic thermosets have been prepared by the copolymerization of either conjugated soybean oil (CSO) or CLS with ST and DVB. The resin has been reinforced with a reactive organomodified montmorillonite clay (*26*). The filler has been prepared by the cationic exchange of sodium montmorillonite with (4-vinylbenzyl)triethylammonium chloride in aqueous solution (*26*). Wide angle X-ray (WAX) and transmission electron microscopy (TEM) experiments have revealed the nanocomposite character and the morphology of the composites prepared (*26*). The latter greatly depends on the amount of nanofiller added, with an intercalated and exfoliated morphology at organoclay loadings ranging from 1 wt % to 2 wt % (*26*). That loading range also results in the best overall properties, especially thermal stability (*26*). The use of the more unsaturated CLS oil over CSO results in even better composites (*26*).

The same organoclay filler has also been used as a reinforcement for corn oil-based cationic resins (*59*). The resin consisted of a copolymer of conjugated corn oil, ST, and DVB. In this system, optimum, intercalated composites have been obtained for clay loadings between 2 wt % and 3 wt % (*59*). Changes in the crosslink density result in an improvement in the mechanical properties (*59*).

Vegetable Oil-Based Biocomposites Reinforced with Agricultural Residues

Composites with a high biobased content have been prepared, by compression molding, using a variety of ligno-cellulosic fillers. Spent germ, the co-product of wet mill ethanol production, has been used, at different particle sizes, to reinforce a tung oil-based free radical resin, initiated by *t*-butyl peroxide (*27*). The resin consists of a copolymer of tung oil (50 wt %), BMA, and DVB (*27*). When compared to the pure resin, the reinforced thermosets exhibit higher storage moduli (as determined by DMA), and thermal stabilities compared with the filler and the resin alone (*27*). The use of shorter particles and higher DVB content results in better properties (*27*). When the filler load is increased from 40 wt % to 60 wt %, agglomeration and formation of micro-voids in the composite cause a decrease in the properties and an increase in the wear depth against diamond (*27*, *60*). This phenomenon can be compensated for by an increase in the molding pressure (*27*). An increase in the DVB content reduces the wear depth caused by a diamond probe (*60*). It was also found that residual corn oil from the spent germ acts as a plasticizer in the composite and if it is removed prior to preparation of the composite, better mechanical properties are obtained (*27*, *60*).

In similar work, a CSO-based free radical resin has been reinforced with soybean hulls (*28*). The concentration of the resin comonomers, BMA, DVB, and DCPD, has been varied, as well as the filler particle size, the filler load (50-60 wt %), and the molding pressure (*28*). The concentration of CSO in the resin has been kept constant at 50 wt % (*28*). An optimum cure sequence of 5 hours at 130 °C, followed by a post-cure of 2 hours at 150 °C, has been established by differential scanning calorimetry (DSC) (*28*). Whenever BMA or DVB are substituted by DCPD, the mechanical properties are compromised (*28*). In this particular system, a decrease in the properties was observed when an excessive

molding pressure of 368 psi was applied (*28*). As previously observed by the Larock group, when studying resins composed of comonomers with different reactivities, the appearance of two distinct T_g's implies that the resin is phase separated (*28*, *37*).

Free radical resins containing 50 wt % of either CSO or conjugated linseed oil (CLO), and various amounts of DVB and BMA have been reinforced with 20-80 wt % of corn stover (*29*). Increasing the amount of corn stover and decreasing the length of the fiber results in an overall improvement of the mechanical properties and a decrease in the thermal stability of the biocomposites (*29*). As expected, water uptake experiments have confirmed that water absorption increases with the fiber content of the composite (*29*).

Wheat straw has also been used as a natural filler in the preparation of a CLO-based biocomposite (*30*). The resin consisted of a copolymer containing 50 wt % of CLO and various amounts of DVB, BMA, and maleic anhydride (MA) (*30*). MA acts as a compatibilizer between the hydrophobic matrix and the hydrophilic resin, and incorporation of 5-15 wt % of MA in the composites' structure results in significant improvements in the mechanical properties (*30*). As noticed with other natural fillers studied by the Larock group, an increase in the filler load from 50 wt % to 90 wt % results in improvements in the mechanical properties and a decrease in the thermal stability (*30*).

A free radical resin composed of 50 wt % CLO, 35 wt % BMA, and 15 wt % DVB has been used to determine the optimal conditions for the preparation of rice hull biocomposites (*31*). The mechanical properties were optimized when a cure sequence of 5 hours at 180 °C under 600 psi of molding pressure was applied, followed by a post-cure of 2 hours at 200 °C under ambient pressure (*31*). Also, 70 wt % of dried rice hulls, at a particle size smaller than 1 mm diameter, afford the best composite properties (*31*). SEM along with X-ray mapping of the fractured composites revealed the presence of significant amounts of silica in the rice hulls, which may account for the high mechanical and thermal properties obtained (*31*). With the optimum parameters established for the preparation of rice hull biocomposites (*31*), changes in the resin composition were evaluated (*61*). It has been observed by SEM that the addition of MA to the resin significantly improves the filler-matrix interactions (*61*). Composites made from CLO exhibit better overall properties than those prepared from CSO, due to the higher degree of unsaturation of the CLO (*61*).

The same CLO-based free radical resin has been reinforced with switch grass (*32*). Improvements in the mechanical properties of the composites have been observed when increasing the load of the filler up to 70 wt % (*32*). Beyond that point, excessive agglomeration of the filler compromises the composites' properties.

Finally, a thorough study has been carried out of the effect of different natural oils and different natural fillers on the properties of cationic composites (*62*). Cationic resins made from CSO, CLO, conjugated corn, and fish oils have been reinforced with corn stover, wheat straw, and switch grass (*62*). The resins all possessed 50 wt % oil, while the concentrations of ST and DVB were varied. The oils with a higher degree of unsaturation resulted in composites with better

properties (*62*). With respect to the different fillers studied, wheat straw afforded composites with the most promising properties (*62*).

Vegetable Oil-Derived Biocoatings

The carbon-carbon double bonds in the fatty acid chains of vegetable oils can be epoxidized to form epoxidized triglycerides with various degrees of epoxidation (*63*). The epoxidized triglycerides can be reacted with various molecules to append different functional groups and increase the reactivity of the oil. Acrylated epoxidized soybean oil (AESO), synthesized from the reaction of acrylic acid and epoxidized soybean oil, has been extensively studied in polymers and composites (*64*) and is commercially available under the trade name of Ebecryl 860. Recently, AESO has been used to produce thermosetting foams with a high biobased content and mechanical properties comparable to semi-rigid industrial foams (*65*). Besides soybean oil, epoxidized methyl oleate has been acrylated and polymerized to afford pressure-sensitive adhesives (*66*). Only the work developed by the Larock group, related to the preparation of polyurethanes and latexes from epoxidized vegetable oils, will be covered in this section.

Polyurethane Dispersions from Vegetable Oil Polyols

Epoxidized vegetable oils can be converted into polyols by the ring opening reaction of the epoxide groups in the triglyceride. Such polyols can react with diisocyanates to give vegetable oil-based polyurethanes. Figure 11 illustrates the ring opening reaction of epoxidized soybean oil. Castor oil and ricinoleic acid, both of which contain hydroxyl groups, have been used in the preparation of polyurethanes directly or after modifications (*67–69*). Polyols based on a variety of epoxidized oils (sunflower, canola, soybean, corn, and linseed oils) have been polymerized with methylene diphenyl diisocyanate (MDI) to give polyurethanes (*70*). It has been found that the differences in the properties of these polyurethane networks results primarily from different crosslink densities, and less from the position of the reactive sites in the fatty acids.
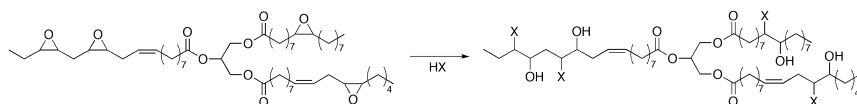
X = Cl, CH$_3$O, H$_2$C=CHCO$_2$

Figure 11. Ring opening reaction of epoxidized soybean oil.
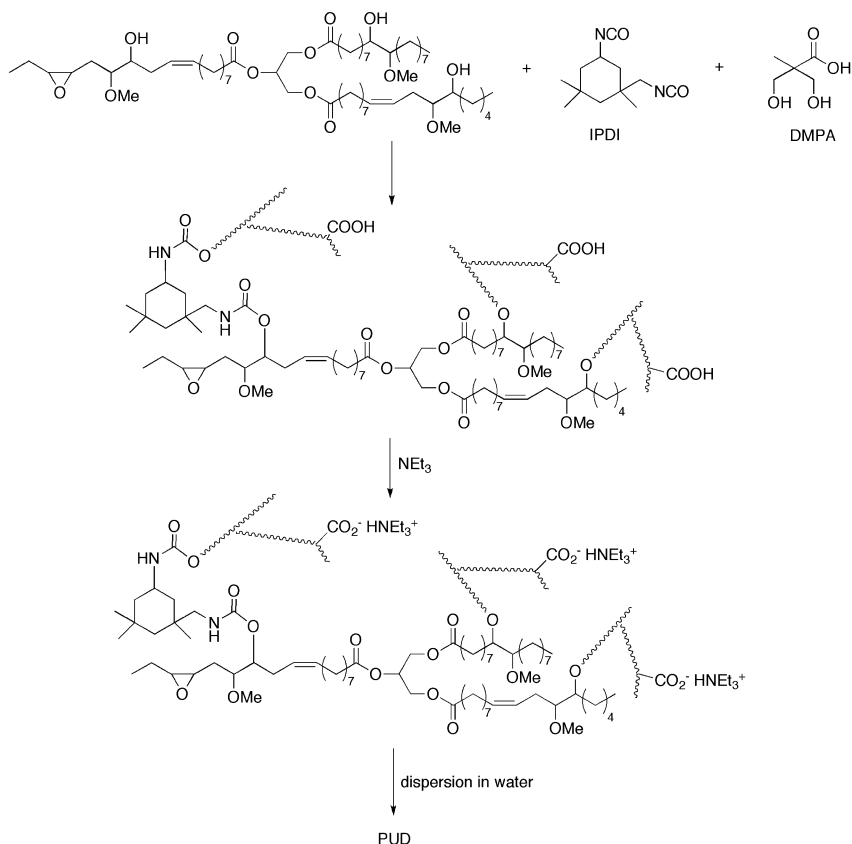
Figure 12. Preparation of a soybean oil-based anionic waterborne polyurethane dispersion (PUD).

Environmentally friendly, waterborne polyurethane dispersions (PUD's), containing no volatile organic compounds (VOCs), have found wide applications as coatings and adhesives, and related end uses. Methoxylated soybean oil polyols (MSOLs), prepared by ring opening epoxidized soybean oil by methanol, with hydroxyl numbers per triglyceride ranging from 2.4 to 4.0, have been used to prepare anionic PUD's with uniform particle sizes and biobased content ranging from 50 wt % to 60 wt % (*6*). These soybean oil-based waterborne PUD's have been obtained by the reaction of MSOLs with isophorone diisocyanate (IPDI) and dimethylolpropionic acid (DMPA), followed by neutralization with triethylamine and then dispersion in water (*6*). The reaction scheme is shown in Figure 12. Increased OH numbers in the MSOLs significantly increase the crosslink density of the polyurethanes, while increased hard segment content improves the interchain interactions caused by hydrogen bonding. Therefore, the structure and the properties of the resulting biorenewable polyurethanes greatly depend on these two factors (*6*).

Recently, the preparation of vegetable oil-based cationic PUD's with uniform particle sizes has been reported in the literature (*7*). Castor and methoxylated and

acrylated epoxidized soybean oil-based polyols have been reacted with *N*-methyl diethanol amine (MDEA) and MDI to form biobased polyurethanes containing tertiary amines (*7*). Hydrophilic groups were then formed by the addition of acetic acid and the resulting polyurethanes have been dispersed into water to give cationic PUD's (*7*). Compared to anionic PUD's, cationic PUD's exhibit very high adhesion to a variety of anionic substrates, such as leather and glass, which suggests wide application of these new materials as adhesives and coagulants.

Vegetable Oil-Based Hybrid Latexes

In order to increase the mechanical properties of the biobased polyurethanes developed by the Larock group, soybean oil-based anionic PUD's have been allowed to undergo emulsion copolymerization with acrylic comonomers, resulting in polyurethane-acrylic hybrid latexes with 15-60 wt % biobased content (*8*, *71*). The polyurethane dispersions employed in such hybrid latexes have been prepared from either a soybean oil-based polyol or AESO (*71*), toluene 2,4-diisocyanate, and DMPA. Butyl acrylate and methyl methacrylate have been grafted onto the soybean oil-based polyurethane network by the free radical reaction of the carbon-carbon double bonds in the fatty acid chains and the acrylates (*8*, *71*). The resulting hybrid latexes exhibit properties comparable to those of polypropylene glycol-based polyurethane/acrylic hybrid latex films indicating their potential application in the coatings industry.

Vegetable Oil-Based Core-Shell Latexes

Surfactant-free, core-shell hybrid latexes have been synthesized by seeded emulsion polymerization of 10-60 wt % vinyl monomers (styrene and butyl acrylate) in the presence of a soybean oil-based PUD as seed particles (*9*). The soybean oil-based PUD, synthesized by reacting IPDI with methoxylated soybean oil polyols and DMPA, forms the latex shell, and serves as a high molecular weight emulsifier, while the vinyl polymers form the core (*9*). The core-shell hybrid latex films show a significant increase in thermal stability and mechanical properties when compared to the pure polyurethane films, due to grafting and crosslinking in the hybrid latexes (*9*).

Conclusions

The technology developed in the Larock group over the last decade involves the use of natural oil-based materials in the preparation of diverse green products, such as bioplastics, biocomposites and biocoatings. The progress made in the last 10 years on the development of these new natural oil-based products has been substantial and is expanding rapidly. Biobased thermosets ranging from rubbery to hard plastics have been synthesized by the cationic, free radical, thermal, and ring opening metathesis copolymerization of a variety of natural oils with numerous petroleum-based comonomers. In general, a similarity in the reactivities of the

comonomers used in the preparation of the thermoset resins is of great importance in maximizing the oil incorporation and the homogeneity of the products obtained.

The biobased cationic, free radical, and ROMP resins have been reinforced with continuous glass fibers, functionalized organoclays, and a variety of natural fillers to afford high biobased content biocomposites. In comparison to the pure resins, significant improvements have been obtained in the mechanical properties by the addition of the fillers.

The preparation of anionic and cationic vegetable oil-based waterborne PUD's with uniform particle sizes has been achieved. Significant improvements in the thermophysical and mechanical properties have been attained by emulsion copolymerization of the PUD's with acrylates and vinyl comonomers, forming hybrid and core-shell latexes, respectively.

Current research in the Larock group on biobased materials includes improvements in the current processes, examination of other naturally occurring oils and commercially available comonomers, exploration of other polymerization processes, development of appropriate processing procedures, and examination of the new materials in various industrial applications.

References

1. Huber, G. W.; Iborra, S.; Corma, A. *Chem. Rev.* **2006**, *106*, 4044–4098.
2. Demirbas, A. *Energy Convers. Manage.* **2009**, *50*, 2782–2801.
3. Srinivasan, G.; Grewell, D. *67th ANTEC* **2009**, 2610–2614.
4. Van De Mark, M. R.; Sandefur, K. In *Industrial Uses of Vegetable Oil*; Erhan, S. Z., Ed.; AOCS Press: Peoria, IL, 2005; pp 143−162.
5. Kundu, P. P.; Larock, R. C. *Prog. Org. Coat.* **2009**, *65*, 10–18.
6. Lu, Y.; Larock, R. C. *Biomacromolecules* **2008**, *9*, 3332–3340.
7. Lu, Y.; Larock, R. C. *ChemSusChem* **2010**, *3*, 329–333.
8. Lu, Y.; Larock, R. C. *Biomacromolecules* **2007**, *8*, 3108–3114.
9. Lu, Y.; Xia, Y.; Larock, R. C. *Prog. Org. Coat.* **2010**, submitted.
10. Lima, D. G.; Soares, V. C. D.; Ribeiro, E. B.; Carvalho, D. A.; Cardoso, E. C. V.; Rassi, F. C.; Mundim, K. C.; Rubim, J. C.; Suarez, P. A. Z. *J. Anal. Appl. Pyrolysis* **2004**, *71*, 987–996.
11. Lu, Y.; Larock, R. C. *ChemSusChem* **2009**, *2*, 136–147.
12. Li, F.; Larock, R. C. *Biomacromolecules* **2003**, *4*, 1018–1025.
13. Kundu, P. P.; Larock, R. C. *Biomacromolecules* **2005**, *6*, 797–806.
14. Li, F.; Marks, D. W.; Larock, R. C.; Otaigbe, J. U. *Polymer* **2000**, *41*, 7925–7939.
15. Li, F.; Larock, R. C. *J. Appl. Polym. Sci.* **2000**, *78*, 1044–1056.
16. Andjelkovic, D. D.; Valverde, M.; Henna, P.; Li, F.; Larock, R. C. *Polymer* **2005**, *46*, 9674–9685.
17. Henna, P. H.; Andjelkovic, D. D.; Kundu, P. P.; Larock, R. C. *J. Appl. Polym. Sci.* **2007**, *104*, 979–985.
18. Valverde, M.; Andjelkovic, D.; Kundu, P. P.; Larock, R. C. *J. Appl. Polym. Sci.* **2008**, *107*, 423–430.

19. Larock, R. C.; Dong, X.; Chung, S.; Reddy, C. K.; Ehlers, L. E. *J. Am. Oil Chem. Soc.* **2001**, *78*, 447–453.

20. Andjelkovic, D. D.; Min, B.; Ahn, D.; Larock, R. C. *J. Agric. Food Chem.* **2006**, *54*, 9535–9543.

21. Henna, P. H.; Larock, R. C. *Macromol. Mater. Eng.* **2007**, *292*, 1201–1209.

22. Mauldin, T. C.; Haman, K.; Sheng, X.; Henna, P.; Larock, R. C.; Kessler, M. R. *J. Polym. Sci., Part A: Polym. Chem.* **2008**, *46*, 6851–6860.

23. Xia, Y.; Lu, Y.; Larock, R. C. *Polymer* **2010**, *51*, 53–61.

24. Rybak, A.; Fokou, P. A.; Meier, M. A. R. *Eur. J. Lipid Sci. Technol.* **2008**, *110*, 797–804.

25. Lu, Y.; Larock, R. C. *J. Appl. Polym. Sci.* **2006**, *102*, 3345–3353.

26. Lu, Y.; Larock, R. C. *Biomacromolecules* **2006**, *7*, 2692–2700.

27. Pfister, D. P.; Baker, J. R.; Henna, P. H.; Lu, Y.; Larock, R. C. *J. Appl. Polym. Sci.* **2008**, *108*, 3618–3625.

28. Quirino, R. L.; Larock, R. C. *J. Appl. Polym. Sci.* **2009**, *112*, 2033–2043.

29. Pfister, D. P.; Larock, R. C. *Bioresour. Technol.* **2010**, *101*, 6200–6206.

30. Pfister, D. P.; Larock, R. C. *Composites, Part A* **2010**, in press.

31. Quirino, R. L.; Larock, R. C., unpublished.

32. Pfister, D. P.; Larock, R. C., unpublished.

33. Marks, D. W.; Li, F.; Pacha, C. M.; Larock, R. C. *J. Appl. Polym. Sci.* **2001**, *81*, 2001–2012.

34. Li, F.; Perrenoud, A.; Larock, R. C. *Polymer* **2001**, *42*, 10133–10145.

35. Li, F.; Larock, R. C.; Otaigbe, J. U. *Polymer* **2000**, *41*, 4849–4862.

36. Li, F.; Hasjim, J.; Larock, R. C. *J. Appl. Polym. Sci.* **2003**, *90*, 1830–1838.

37. Li, F.; Hanson, M. V.; Larock, R. C. *Polymer* **2001**, *42*, 1567–1579.

38. Li, F.; Larock, R. C. *J. Appl. Polym. Sci.* **2001**, *80*, 658–670.

39. Li, F.; Larock, R. C. *J. Polym. Sci., Part B: Polym. Phys.* **2000**, *38*, 2721–2738.

40. Li, F.; Larock, R. C. *J. Polym. Sci., Part B: Polym. Phys.* **2001**, *39*, 60–77.

41. Li, F.; Larock, R. C. *Polym. Adv. Technol.* **2002**, *13*, 436–449.

42. Li, F.; Larock, R. C. *J. Appl. Polym. Sci.* **2002**, *84*, 1533–1543.

43. Li, F.; Larock, R. C. *Polym. Int.* **2003**, *52*, 126–132.

44. Li, F.; Larock, R. C. *J. Polym. Environ.* **2002**, *10*, 59–67.

45. Badrinarayanan, P.; Lu, Y.; Larock, R. C.; Kessler, M. R. *J. Appl. Polym. Sci.* **2009**, *113*, 1042–1049.

46. Andjelkovic, D. D.; Larock, R. C. *Biomacromolecules* **2006**, *7*, 927–936.

47. Andjelkovic, D. D.; Lu, Y.; Kessler, M. R.; Larock, R. C. *Macromol. Mater. Eng.* **2009**, *294*, 472–483.

48. Andjelkovic, D. D.; Valverde, M.; Henna, P.; Li, F.; Larock, R. C. *Polymer* **2005**, *46*, 9674–9685.

49. Xia, Y.; Henna, P. H.; Larock, R. C. *Macromol. Mater. Eng.* **2009**, *294*, 590–598.

50. Sharma, V.; Banait, J. S.; Larock, R. C.; Kundu, P. P. *eXPRESS Polym. Lett.* **2008**, *2*, 265–276.

51. Cakmakli, B.; Hazer, B.; Tekin, I. O.; Comert, F. B. *Biomacromolecules* **2005**, *6*, 1750–1758.

52. Cakmakli, B.; Hazer, B.; Tekin, I. O.; Kizgut, S.; Koksal, M.; Menceloglu, Y. *Macromol. Biosci.* **2004**, *4*, 649–655.
53. Stoesser, S. M.; Gabel, A. R., U.S. Patent 2,190,906, 1940.
54. Leitgeb, A.; Wappel, J.; Slugovc, C. *Polymer* **2010**, *51*, 2927–2946.
55. Henna, P.; Larock, R. C. *J. Appl. Polym. Sci.* **2009**, *112*, 1788–1797.
56. Xia, Y.; Larock, R. C. *Polymer* **2010**, *51*, 2508–2514.
57. Lu, Y.; Larock, R. C. *Macromol. Mater. Eng.* **2007**, *292*, 1085–1094.
58. Henna, P. H.; Kessler, M. R.; Larock, R. C. *Macromol. Mater. Eng.* **2008**, *293*, 979–990.
59. Lu, Y.; Larock, R. C. *Macromol. Mater. Eng.* **2007**, *292*, 863–872.
60. Bhuyan, S.; Sundarararajan, S.; Pfister, D.; Larock, R. C. *Tribol. Int.* **2010**, *43*, 171–177.
61. Quirino, R. L.; Larock, R. C., unpublished.
62. Pfister, D. P.; Larock, R. C., unpublished.
63. Park, S.; Jin, F.; Lee, J. *Macromol. Rapid Commun.* **2004**, *25*, 724–727.
64. Khot, S. N.; Lascala, J. J.; Can, E.; Morye, S. S.; Williams, G. I.; Palmese, G. R.; Kusefoglu, S. H.; Wool, R. P. *J. Appl. Polym. Sci.* **2001**, *82*, 703–723.
65. Bonnaillie, L. M.; Wool, R. P. *J. Appl. Polym. Sci.* **2007**, *105*, 1042–1052.
66. Bunker, S. P.; Wool, R. P. *J. Polym. Sci., Part A: Polym. Chem.* **2002**, *40*, 451–458.
67. Yeganeh, H.; Mehdizadeh, M. R. *Eur. Polym. J.* **2004**, *40*, 1233–1238.
68. Petrovic, Z. S.; Cvetkovic, I.; Hong, D.; Wan, X.; Zhang, W.; Abraham, T.; Malsam, J. *J. Appl. Polym. Sci.* **2008**, *108*, 1184–1190.
69. Somani, K. P.; Kansara, S. S.; Patel, N. K.; Rakshit, A. K. *Int. J. Adhes. Adhes.* **2003**, *23*, 269–275.
70. Zlatanic, A.; Lava, C.; Zhang, W.; Petrovic, Z. S. *J. Polym. Sci., Part B: Polym. Phys.* **2004**, *42*, 809–819.
71. Lu, Y.; Larock, R. C. *J. Appl. Polym. Sci.* **2008**, in press.

Chapter 4

Biofabrication: Enlisting the Unique Capabilities of Biological Polymers for Hierarchical Construction

Benjamin D. Liba,[1] India V. Aranha,[2] Eunkyoung Kim,[1] and Gregory F. Payne*,[1,3]

[1]Center for Biosystems Research, Univeristy of Maryland, 5115 Plant Sciences Building, College Park, MD 20742
[2]Gwynn Park High School (Science Dept.), Prince George's County Public Schools, 13800 Brandywine Road, Brandywine, MD 20613
[3]Fischell Department of Bioengineering, University of Maryland, College Park, MD 20742
*gpayne@umd.edu

Biological polymers can be obtained either from dedicated production (e.g., fermentation-derived xanthan gum) or as value-added byproducts (e.g., gelatin) from food or agricultural processing. While biological polymers have had difficulty displacing synthetics in low-cost applications, we contend that biopolymers often possess a unique combination of properties that can be enlisted for high-performance applications. Here, we review recent work with the aminopolysaccharide chitosan that illustrates how its properties enable it to perform complex functions that would be difficult to perform with existing polymer systems. Specifically, we illustrate two of chitosan's capabilities that facilitate the assembly of proteins at electrode interfaces for potential applications in biosensing, bioelectronics and lab-on-a-chip devices. First, chitosan's pH-responsive film-forming properties enable it to "recognize" locally-imposed electrical stimuli and respond by self-assembling as a stable hydrogel deposit. Chitosan's electrodeposition facilitates the spatially-selective and hierarchical assembly of proteins at specific electrode addresses. Second, chitosan's nucleophilic amines facilitate

conjugation to proteins that have been enzymatically activated by tyrosinase. Tyrosinase converts accessible tyrosine residues of proteins into electrophilic quinone residues that undergo non-enzymatic grafting to chitosan. Chitosan's electrodeposition and enzymatic-conjugation enable proteins to be assembled at electronic surfaces simply, rapidly and without the need for reagents. More broadly, this work illustrates that biopolymers often can undergo self-assembly and enzymatic-assembly for the precise biofabrication of structure and function.

Introduction

For millennia, humans relied on biological polymers (e.g., cellulose) and composites (e.g., wood) to meet many of their materials needs. This situation changed dramatically over the last century as technical advances in petroleum-processing allowed synthetic polymers to be created and analyzed in ways that were previously unimaginable. In some cases, polymers could be synthesized so cheaply that they enabled a range of low-value applications (e.g., single-use packaging) while in other cases, polymers could be generated with such unique properties that they enabled entirely new high-value applications (e.g., structural materials capable of replacing metals). Interestingly, the study of synthetic and biological polymers also diverged significantly over the last century. During that time, Nobel prizes were awarded for advances in polymer synthesis (e.g., Ziegler Natta catalysts); light scattering methods emerged for polymer characterization; and plastics became integral to many consumer goods. Also during that time, Nobel prizes were awarded for understanding biopolymer structure and function (e.g., Watson-Crick base pairing); molecular biology enabled detailed study of biopolymers; and recombinant proteins became common in high-value applications in medicine and industry (e.g., industrial enzymes).

In the 21st century, we anticipate a trend away from the use of synthetic polymers. An expected escalation in petroleum prices should erode the cost-advantages of synthetic polymers. Further, there are growing concerns for the accumulation of poorly degradable synthetic polymers in the environment (e.g., trash in our oceans and litter in our cities) and these concerns are beginning to result in restrictions/charges on items such as plastic grocery bags. We also anticipate that biological polymers will become more broadly utilized in a range of applications. As more groups study biological polymers there should be an increasing appreciation of the unique capabilities of these materials. In addition, the application of experimental and modeling tools from synthetic polymers promises to yield new insights into the structures and interactions of complex biological polymers such as polysaccharides and protein-polysaccharide conjugates.

Our group focuses on enlisting biological polymers and especially proteins and polysaccharides to perform high-value materials functions (*1–3*). In many cases, these biological polymers offer valuable performance capabilities not easily

attained from synthetic polymers. In particular, many biological polymers are stimuli-responsive and often form fibers, films and gels that allow hierarchical assembly from the nano- (i.e. macromolecular) scale to the macro-scale. Also, biological polymers can often serve as substrates for enzymes which can allow these selective catalysts to be employed to build macromolecular structure (e.g., increase molecular weight).

In particular, our group studies the use of biological polymers to build the interface between biological and microelectronic systems. Advances in both biology and microelectronics transformed our way of life but surprisingly, there has been little synergy between these two fields. We believe that if biology and electronics could be better integrated, then it would be possible to fabricate hand-held devices that could be taken into the field to analyze contaminants or to be employed by first-responders to assess a patient's status in-transit. In addition, the effective integration of biology with electronics might enable implantable devices that can communicate directly with the brain to restore lost neurological function. There are many challenges to realizing such dreams and our focus is to enlist the unique capabilities of biological materials and mechanisms to *biofabricate* the bio-device interface.

Materials and Methods

The following materials were purchased from Sigma Aldrich. Chitosan (85% deactylation from crab shells), human immunoglobulin G (IgG antibodies) labeled with fluorescein isothiocyanate (FITC) and tyrosinase (from mushroom). Glucose oxidase (GOx) from *Aspergillus niger* (activity ≈ 100,000 U g^{-1}) was purchased from Amresco. The chitosan solution was prepared by adding chitosan to 1% HCl, mixing overnight and filtering using a vacuum filter to remove undissolved particles. The antibody solution was prepared by diluting the purchased IgG antibody stock (1:1000) using 0.1 M phosphate buffered saline (PBS) with 0.05% Tween 20.

Electrodeposition was performed by immersing electrodes (either gold wires or gold-coated substrates) into chitosan solution. An alligator clip was used to connect the electrodes to a DC power supply (2400 Sourcemeter, Keithley). The electrodes were biased with a cathodic potential (a platinum wire was used as the counter electrode). Electrochemical conjugation of GOx was performed using a three electrode system (CHI 6273C electrochemical analyzer) with the gold-coated chip as the working electrode, a platinum wire as the counter electrode, and Ag/AgCl as the reference electrode. The chip was biased with an anodic potential of 0.9V (vs. Ag/AgCl). Fluorescent images were obtained using an Olympus MVX10 microscope.

Protein G was prepared as previously described (*4*). Briefly, an engineered gene for a modified protein G from *Streptococcus* was transformed into *E. coli* cells for protein expression. After cell lysis, the recombinant proteins were purified by Talon metal affinity resins (Clontech, Mountain View, CA). The final product was desalted by dialysis.

Results and Discussion

Chitosan's Stimuli-Responsive Film-Forming Properties Allow Electrodeposition

Chitosan is a stimuli-responsive film-forming aminopolysaccharide. As illustrated by the reaction in Figure 1, the primary amines of the glucosamine repeating units are protonated at low pH making chitosan a water-soluble cationic polyelectrolyte. As the pH is increased above 6, the amines are deprotonated, chitosan loses its charge and it can undergo a sol-gel transition to yield a transparent hydrogel. Chitosan's film-forming ability is illustrated by the photographs in Figure 1 which show a dip-cast chitosan film. The film was generated by dipping a gold-coated silicon wafer in a chitosan solution (2.5 %; pH 2), partially drying the film, neutralizing it by soaking in NaOH (1 M), and then peeling the film from the gold surface. The right-most image in Figure 1 illustrates that chitosan's pH-responsive film-forming properties allows the generation of a stable "free-standing film" or membrane.
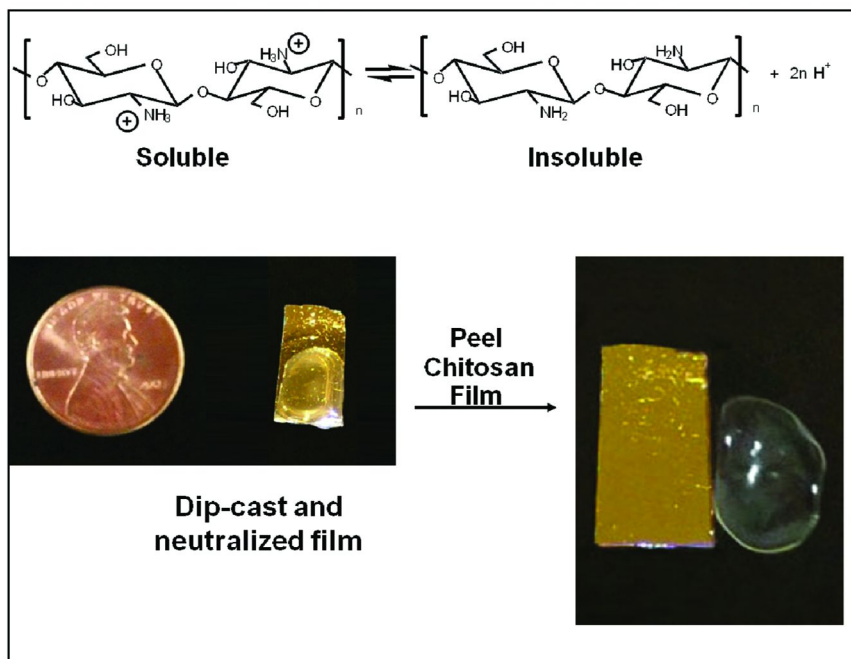
Figure 1. Chitosan's pH-responsive film-forming properties allow for stable films to be created (e.g., by casting and neutralization).
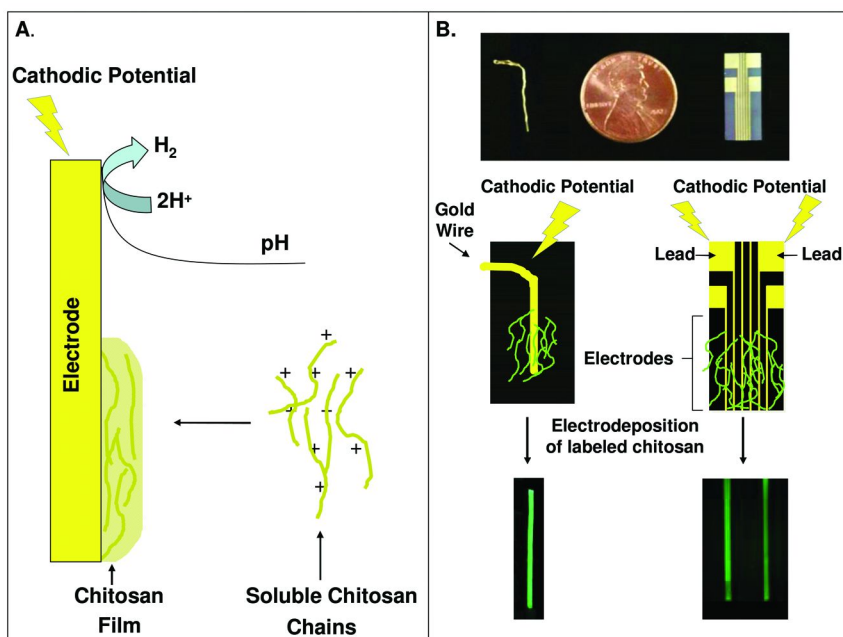
Figure 2. Chitosan electrodeposition. (A) Mechanism illustrating cathodic reactions create the pH gradient that triggers chitosan's sol-gel transition. (B) Deposition of fluorescein-labeled chitosan on a gold wire and a chip with patterned gold electrodes.

Recently, it was discovered that chitosan's stimuli-responsive film-forming properties enable it to "recognize" imposed electrical signals and respond by electrodepositing as a stable hydrogel film (*5–8*). Figure 2a illustrates the mechanism for chitosan electrodeposition: cathodic reactions generate the pH gradient that induces the localized sol-gel transition that results in the deposition of a thin film on the electrode surface. After rinsing, the film is stable in the absence of an applied potential provided the pH is retained above about 6.5 (chitosan will re-dissolve at lower pHs). Several studies have demonstrated that the thickness of the deposited chitosan film can be controlled by the deposition conditions (e.g., concentration and pH of the solution, and the deposition time) (*5, 7*).

Chitosan's electrodeposition provides a versatile mechanism for electrical signals (e.g., cathodic currents) to be employed to guide hierarchical film assembly. For instance, the left-most panels in Figure 2b illustrate that chitosan can be electrodeposited onto a gold wire. To facilitate visualization in this demonstration, we labeled chitosan with fluorescein and prepared a deposition solution containing fluorescein-labeled chitosan (1 %, pH 5.6). For electrodeposition, the gold wire was connected as the cathode to the power supply, partially-immersed in the deposition solution and a constant cathodic current density (4 A/m²) was applied for 1 min (a platinum wire served as the counter-electrode). After deposition, the chitosan-coated wire was rinsed and

imaged. The fluorescence photomicrograph at the bottom left in Figure 2b indicates good coverage of the gold wire by the fluorescently-labeled chitosan.

The right-most panel in Figure 2b illustrates the electrodeposition of fluorescein-labeled chitosan onto gold surfaces that had been patterned onto a silicon chip. Here, a chip with 6 electrically-independent gold electrodes was immersed in a solution of fluorescein-labeled chitosan (1 %, pH 5.6) and a cathodic current was applied ($4 A/m^2$ for 1 min) to two of the electrodes by connecting their leads to the power supply (Pt counter-electrode). The fluorescence photomicrograph at the lower right in Figure 2b demonstrates that chitosan electrodeposition can be achieved with high spatial selectivity (e.g., at the micron level) (9).

The utility of electrodeposition for assembling proteins at electrode surfaces is illustrated by the experiment in Figure 3. For this demonstration, we used the enzyme glucose oxidase (GOx) that is commonly employed for glucose analysis (e.g., from blood). Analysis is based on the recognition of glucose by GOx and generation of H_2O_2 that can be to an electrochemically detected by the following reactions:

GOx Reaction: Glucose + O_2 $\rightarrow$ Gluconic acid + H_2O_2

Anode Reaction: $H_2O_2 \rightarrow O_2 + 2H^+ + 2e^-$
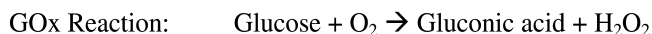
GOx was assembled at the electrode by blending GOx (680 U/ml) into the chitosan solution (1 %, pH 5.4) and co-depositing this enzyme at the gold electrode ($3 A/m^2$ for 1 min) as illustrated in Figure 3. While co-deposited GOx is entrapped within the chitosan network, we used a second assembly step, electrochemical conjugation, to covalently conjugate GOx to chitosan with the goal of reducing possible GOx-leakage from the film (10, 11). Electrochemical conjugation was achieved by immersing the GOx-functionalized chitosan-coated electrode in a salt solution (0.1 M NaCl in 0.1 M phosphate buffer pH 7) and applying an anodic potential of 0.9 V (vs Ag/AgCl) for 20 sec. To demonstrate the potential of the GOx-functionalized electrode for glucose detection, we immersed this electrode in buffer and added aliquots to yield 0.2 mM step-increases in glucose levels (aliquot additions are indicated by the vertical arrows in Figure 3b).

The plot in Figure 3b shows that each aliquot addition of glucose resulted in a step increase in observed anodic current. These experimental results can then be used to generate the standard curve illustrated in Figure 3c. In addition to providing a sensitive means for electrochemical detection, GOx also confers selectivity to detection. This selectivity is illustrated in Figure 3b which shows that the addition of aliquots of other sugars (fructose or sucrose) do not yield increases in anodic current
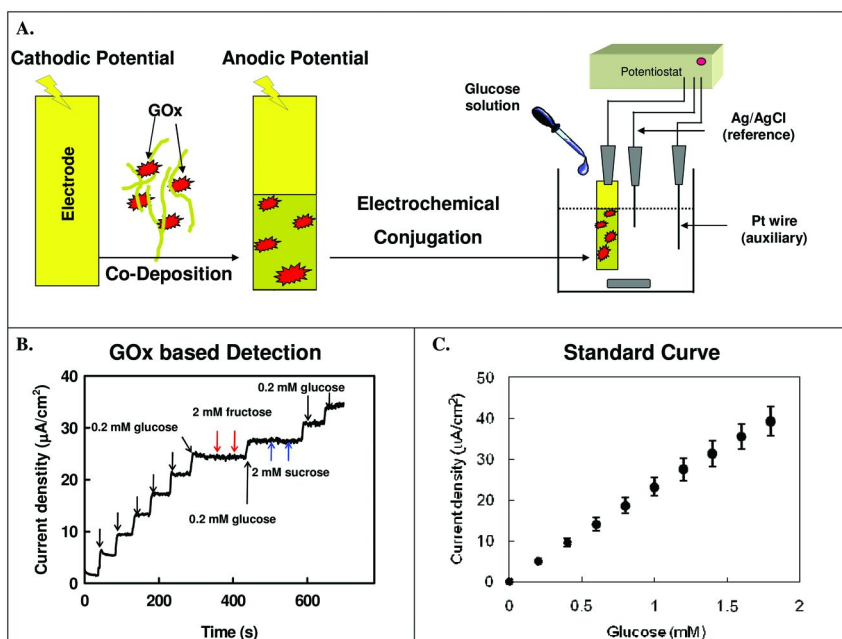
Figure 3. Electrodeposition to biofunctionalize chitosan film. (A) Co-deposition and electrochemical conjugation provide a simple means to generate GOx-based biosensor. (B) Glucose additions lead to step increases in current, while 10-fold larger additions of fructose and sucrose lead to no changes. (C) Standard curve between observed current and glucose (data from B).

In summary, chitosan's electrodeposition facilitates the assembly of proteins at electrode addresses. Importantly, protein assembly is achieved simply, rapidly and without the need for reactive reagents. Further, electrodeposition can be performed from within a covered microfluidic channel and thus provides unique capabilities for lab-on-a-chip applications compared to conventional protein assembly methods that require a line-of-sight (e.g., photolithographic methods) or direct access to the surface (e.g., printing methods) (*12*, *13*).

Chitosan's Nucleophilic Amines Allow Enzymatic Conjugation

There is considerable appeal to the use of enzymes for macromolecular synthesis because they are selective and can perform reactions under mild (e.g., aqueous) conditions. We have been examining the enzyme tyrosinase to conjugate proteins to chitosan (*14*, *15*). As illustrated in Figure 4, tyrosinase activates proteins for conjugation by converting accessible tyrosine residues into reactive quinone residues that undergo conjugation reactions with the nucleophilic amines of chitosan.

In Renewable and Sustainable Polymers; Payne, G., et al.;
ACS Symposium Series; American Chemical Society: Washington, DC, 2011.
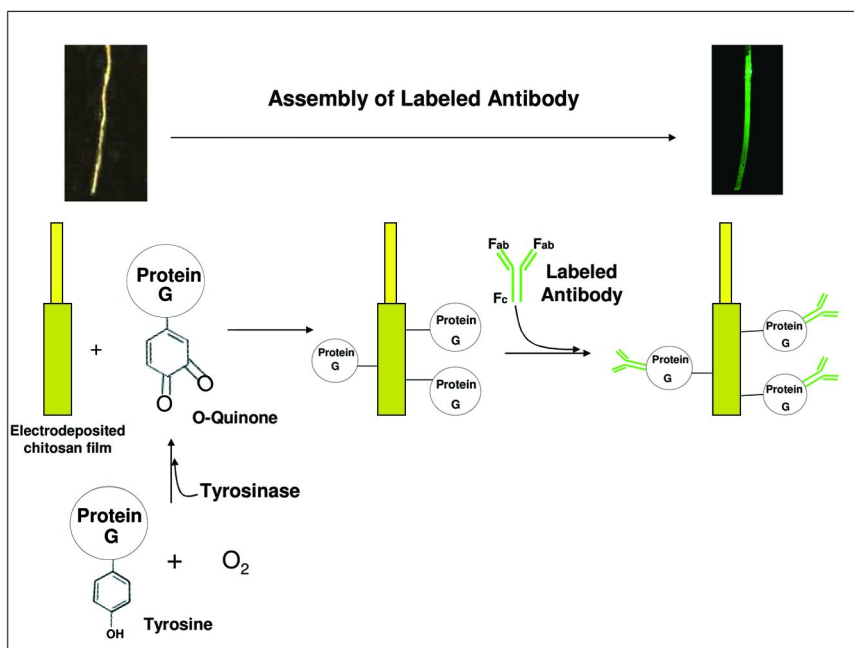
Figure 4. Enzymatic functionalization of chitosan using tyrosinase to initiate Protein G conjugation. Protein G can then bind to IgG antibodies.

For demonstration purposes, we conjugated a bacterial protein (Protein G) to a chitosan-coated gold wire (*4*). The Protein G was engineered with added tyrosine residues to promote tyrosinase-mediated conjugation. Protein G is an interesting biotechnological protein because it binds to the constant region (Fc) of antibodies and allows presentation of the antigen binding regions (Fab). To conjugate Protein G to a chitosan-coated wire, we first electrodeposited chitosan on the wire (1 %, pH 5.6, 4 A/m^2 for 1 min) and then incubated the chitosan-coated wire in a solution with Protein G (5 μM) and tyrosinase (100 U/mL). To demonstrate that the protein G-conjugated chitosan wire can bind antibodies, we contacted the wire with a solution containing fluorescently-labeled human IgG antibody (described in Materials and Methods) and then observed the resulting fluorescence. The fluorescence photomicrograph in Figure 4 indicates that antibody had been assembled onto the chitosan. This experiment suggests the potential for creating functionalized wires for immunodetection.

The above results indicate that tyrosinase can catalyze grafting to build macromolecular structure. More broadly, enzymes employ molecular recognition to confer catalytic selectivity (e.g., tyrosinase only activates tyrosine residues) and this capability may be advantageous compared to alternative methods that require reactive reagents or complex protection/deprotection strategies. Further the enzymes operate under mild conditions reducing environmental, health and safety concerns. One possible disadvantage of enzyme selectivity is that proteins that lack accessible tyrosine residues will not effectively react with tyrosinase. This is not a problem when the protein can be genetically engineered to provide

such residues (*15–17*). Thus, when genetic engineering can be applied, tyrosinase may provide a generic approach for protein assembly.

Conclusions

Biological polymers are renewable and biodegradable, and these sustainability attributes should become increasingly important over time. But biological polymers often offer high-performance properties that can make them cost-effective even today. The representative results provided above illustrate that the stimuli-responsive and film-forming properties of chitosan allow its electrodeposition, and this facilitates the assembly of proteins at electrode surfaces. While chitosan is the best-studied example, recent results indicate that other biological polymers can also be electrodeposited (*18–20*) and these observations could enable entirely different applications (e.g., the generation of composite coating (*18*) and thin film bioprocessing (*21*)). The second capability we highlighted is that biopolymers can often be acted-upon by enzymes and this provides a selective tool for grafting and crosslinking macromolecules. While we focused on tyrosinase, additional enzymes are also under investigation (*22*, *23*) and these include transglutaminases (*24–27*), peroxidases (*28*, *29*) and sortases (*30*, *31*). In a broader sense, this work illustrates that biofabrication – the use of biological materials and mechanisms for construction – offers opportunities for the precise assembly of high-performance materials under "green" conditions.

Acknowledgments

References

1. Yi, H. M.; et al. Biofabrication with chitosan. *Biomacromolecules* **2005**, *6* (6), 2881–2894.
2. Payne, G. F.; Raghavan, S. R. Chitosan: A soft interconnect for hierarchical assembly of nano-scale components. *Soft Matter* **2007**, *3* (5), 521–527.
3. Liu, Y.; et al. Biofabrication to build the biology-device interface. *Biofabrication* **2010**, *2* (2), 21.
4. Wu, H. C.; et al. Biofabrication of antibodies and antigens via IgG-binding domain engineered with activatable pentatyrosine pro-tag. *Biotechnol. Bioeng.* **2009**, *103* (2), 231–240.
5. Wu, L. Q.; et al. Voltage-dependent assembly of the polysaccharide chitosan onto an electrode surface. *Langmuir* **2002**, *18* (22), 8620–8625.
6. Redepenning, J.; et al. Electrochemical preparation of chitosan/ hydroxyapatite composite coatings on titanium substrates. *J. Biomed. Mater. Res., Part A* **2003**, *66* (2), 411–416.

7. Pang, X.; Zhitomirsky, I. Electrodeposition of composite hydroxyapatite-chitosan films. *Mater. Chem. Phys.* **2005**, *94* (2-3), 245–251.

8. Luo, X. L.; et al. A glucose biosensor based on chitosan-glucose oxidase-gold nanoparticles biocomposite formed by one-step electrodeposition. *Anal. Biochem.* **2004**, *334* (2), 284–289.

9. Buckhout-White, S. L.; Rubloff, G. W. Spatial resolution in chitosan-based programmable biomolecular scaffolds. *Soft Matter* **2009**, *5* (19), 3677–3681.

10. Shi, X. W.; et al. Reagentless protein assembly triggered by localized electrical signals. *Adv. Mater.* **2009**, *21* (9), 984–988.

11. Meyer, W. L.; et al. Chitosan-coated wires: Conferring electrical properties to chitosan fibers. *Biomacromolecules* **2009**, *10* (4), 858–864.

12. Park, J. J.; et al. Chitosan-mediated in situ biomolecule assembly in completely packaged microfluidic devices. *Lab on a Chip* **2006**, *6* (10), 1315–1321.

13. Luo, X. L.; et al. Programmable assembly of a metabolic pathway enzyme in a pre-packaged reusable bioMEMS device. *Lab on a Chip* **2008**, *8* (3), 420–430.

14. Chen, T. H.; et al. In vitro protein-polysaccharide conjugation: Tyrosinase-catalyzed conjugation of gelatin and chitosan. *Biopolymers* **2002**, *64* (6), 292–302.

15. Chen, T. H.; et al. Nature-inspired creation of protein-polysaccharide conjugate and its subsequent assembly onto a patterned surface. *Langmuir* **2003**, *19* (22), 9382–9386.

16. Lewandowski, A. T.; et al. Tyrosine-based "activatable pro-tag": Enzyme-catalyzed protein capture and release. *Biotechnol. Bioeng.* **2006**, *93* (6), 1207–1215.

17. Lewandowski, A. T.; et al. Protein assembly onto patterned microfabricated devices through enzymatic activation of fusion pro-tag. *Biotechnol. Bioeng.* **2008**, *99* (3), 499–507.

18. Cheong, M.; Zhitomirsky, I. Electrodeposition of alginic acid and composite films. *Colloids Surf., A* **2008**, *328* (1-3), 73–78.

19. Shi, X. W.; et al. Electroaddressing of cell populations by co-deposition with calcium alginate hydrogels. *Adv. Funct. Mater.* **2009**, *19*, 2074–2080.

20. Sun, F.; Zhitomirsky, I. Electrodeposition of hyaluronic acid and composite films. *Surf. Eng.* **2009**, *25* (8), 621–627.

21. Yang, X. H.; et al. In-film bioprocessing and immunoanalysis with electroaddressable stimuli-responsive polysaccharides. *Adv. Funct. Mater.* **2010**, *20* (10), 1645–1652.

22. Chen, T. H.; et al. Enzyme-catalyzed gel formation of gelatin and chitosan: potential for in situ applications. *Biomaterials* **2003**, *24* (17), 2831–2841.

23. Yang, X. H.; Liu, Y.; Payne, G. F. Crosslinking lessons from biology: Enlisting enzymes for macromolecular assembly. *J. Adhes.* **2009**, *85* (9), 576–589.

24. Yang, X. H.; et al. Orthogonal enzymatic reactions for the assembly of proteins at electrode addresses. *Langmuir* **2009**, *25* (1), 338–344.

25. Kamiya, N.; et al. Transglutaminase-mediated protein immobilization to casein nanolayers created on a plastic surface. *Biomacromolecules* **2005**, *6* (1), 35–38.

26. Villalonga, R.; et al. Transglutaminase-catalyzed synthesis of trypsin-cyclodextrin conjugates: Kinetics and stability properties. *Biotechnol. Bioeng.* **2003**, *81* (6), 732–737.

27. Jones, M. E. R.; Messersmith, P. B. Facile coupling of synthetic peptides and peptide-polymer conjugates to cartilage via transglutaminase enzyme. *Biomaterials* **2007**, *28* (35), 5215–5224.

28. Lee, F.; Chung, J. E.; Kurisawa, M. An injectable enzymatically crosslinked hyaluronic acid-tyramine hydrogel system with independent tuning of mechanical strength and gelation rate. *Soft Matter* **2008**, *4* (4), 880–887.

29. Sakai, S.; et al. An injectable, in situ enzymatically gellable, gelatin derivative for drug delivery and tissue engineering. *Biomaterials* **2009**, *30* (20), 3371–3377.

30. Parthasarathy, R.; Subramanian, S.; Boder, E. T. Sortase A as a novel molecular "stapler" for sequence-specific protein conjugation. *Bioconjugate Chem.* **2007**, *18* (2), 469–476.

31. Chan, L. Y.; et al. Covalent attachment of proteins to solid supports and surfaces via sortase-mediated ligation. *PLoS One* **2007**, *2* (11), 5.

Chapter 5

Polyurethanes from Hybrid Vegetable Oil/Petrochemical Polyester Polyols

Mihail Ionescu,[†] **Ye Ji,**[†] **William M. Shirley,**[‡] **and Zoran S. Petrović**[*,†]

**†Kansas Polymer Research Center, Pittsburg State University,
1701 South Broadway, Pittsburg, KS 66762
‡Chemistry Department, Pittsburg State University, 1701 South Broadway,
Pittsburg, KS 66762
*zpetrovi@pittstate.edu**

The synthesis and properties of a new family of hybrid vegetable oil-petrochemical polyester polyols and polyurethanes are described. Polyols are polyesters of vegetable oil polyols (castor oil, soybean polyol) with organic diacids (adipic, azelaic and sebacic acid) and glycols (diethylene glycol, 1,4-butanediol, 1,2-propanediol and 1,3-propanediol). Depending on the nature of diacids or glycols, the bio content of the polyester polyols studied varied from 30 at 100%. Polyols were used to make cast polyurethane elastomers and flexible polyurethane foams with good physical and mechanical properties. Hybrid polyester polyols are also suitable for applications of other elastic polyurethanes such as coatings, adhesives and sealants.

Keywords: polyols; polyesters; vegetable oil; castor oil; polyurethanes; flexible foams; cast elastomers

Introduction

Polyester polyols represent the second largest group of polyols for polyurethanes after polyether polyols. Linear polyester polyols are α,ω- telechelic polymers with terminal hydroxyl groups, obtained by polycondensation of diacids and glycols in excess. Branched polyester polyols are obtained by polycondensation of a diacid and a glycol in the presence of a high functionality polyol such as glycerol, trimethylolpropane or pentaerythritol. Polyfunctional

polyester polyols are important polyols for a range of flexible polyurethane foams and suitable for other elastic polyurethanes (cast elastomers, coatings, sealants). Generally the polyester polyols are obtained from petrochemical raw materials such as adipic acid, ethylene glycol, diethylene glycol and propylene glycol. The most important trifunctional polyester polyols for flexible polyurethane foams are based on adipic acid, diethylene glycol and trimethylolpropane as a branching agent. Concerns about sustainability, ecology and needs for responsible management of our resources are driving forces for greater utilization of biobased products. Hybrid bio-based/petrochemical polyether polyols were obtained by ring opening polymerization of propylene oxide and ethylene oxide initiated by a vegetable oil polyol as starter (castor oil, soybean polyol, etc.) in the presence of dimetallic catalysts (*1*, *2*). Polyester polyols may have advantages in special applications where higher oxidative stability and higher strength of polyurethanes is desired. Hybrid biobased-petrochemical polyester polyols derived from castor oil, adipic acid and diethylene glycol were synthesized earlier using a non-catalytic polyesterification process, and their application in polyurethanes was discussed (*3*). Unfortunately this kind of polyesterification reaction in the absence of any catalyst requires a very long time, around 36 hours, to complete (*3*). One issue when reacting difunctional and polyfunctional monomers is a possibility of gelation and another is the formation of linear polyester polyols together with polyfunctional polyols. In this work we describe a new family of branched polyester polyols obtained partially or completely from renewable raw materials, and their application in cast polyurethanes and flexible polyurethane foams. Polyols were made by catalytic polyesterification of diacids with glycols and vegetable oil polyols as branching agents. We have previously prepared biobased polyester triols of nominal molecular weight 1000-4000 from ricinoleic acid and trimethylolpropane and crosslinked them with isocyanate to get elastomers. We also have prepared triols by polycondensation of hydroformylated oleic acid and made polyurethanes (*4*, *5*).

Experimental

Raw Materials

- Castor Oil: OH# =162 mg KOH/g, functionality f=2.7 OH groups/mol.
- Polyol X-173 with secondary OH groups: OH#= 175 mg KOH/g, number average functionality f_n=3.3 OH groups/mol.
- Hydroformylation polyol (HF-polyol) with primary OH groups: OH#= 230 mg KOH/g, number average functionality f_n= 4 OH groups/mol.
- Adipic acid: M=146.14; 99%, Acros Organics.
- Azelaic acid: M= 188.22; 90%, Acros Organics.
- Sebacic acid: M=202.25; 95%, Aldrich.
- Ricinoleic acid: M=298.46; 95%, TCI.
- Diethylene glycol: M=106.12; 99% Fisher Scientific.
- 1,2 propanediol: M= 76.09; 99.5%, Aldrich.
- 1,3 propane diol: M=76.10; 99%, Alfa Aesar
- Titanium (IV) isopropoxide: M=284.26; 98% Acros Organics.

- MONDUR CD (Bayer): modified 4,4′ Diphenyl Methane Diisocyanate. NCO%=29.5.
  Toluene diisocyanate (TDI 80/20): NCO%= 48.
- Struksilon 8026: silicone surfactant, Cellchem International LLC.
- Dabco DC-193: silicone surfactant, Air Products.
- Niax A1: tertiary amine catalyst (dimethylamino diethyl ether), Air Products.
- DABCO A 33: tertiary amine catalyst (33% solution of diazo bicyclo octane in dipropylene glycol), Air Products.

Analytical Methods

- Hydroxyl number was determined by the phthalic anhydride method, according to ASTM D4272.
- Acid value was determined by IUPAC 2.201 method, using a 1:1(V:V) toluene/isopropanol mixture as solvent.
- Iodine value was determined using IUPAC 2.205 (Hanus method) involving the reaction of double bonds with an excess of iodobromine.
- Viscosity was determined according to ASTM D5225 using AR 200 EX Rheometer at 25 °C, with cone/plate geometry (truncation height 55µm for the 40 mm diameter, 2° cone).
- Swelling ratio and soluble fraction were measured according to ASTM C1247, using toluene as solvent.

Instrumentation

Gel permeation chromatography was used to determine molecular weights and molecular weight distribution of polyester polyols. The GPC chromatograms were acquired on a Waters system consisting of a 510 pump and 410 differential refractometer and four Phenogel columns from Phenomenex, Torrance, CA, covering a MW range of 100 to 5×10^5. Tetrahydrofuran was used as the eluent at a flow rate of 1.00 mL/min at 30 °C.

FT-IR spectra were carried out by using a Perkin Elmer Spectrum 1000 Fourier transform spectrometer, between 4000 and 400 cm^{-1} wave numbers. ^{1}H NMR and ^{13}C NMR spectra were acquired on a Bruker DPX-300 NMR spectrometer. Differential scanning calorimeter, model Q100 from TA Instruments was used to determine melting points and glass transitions (T_g). X-ray diffraction (XRD) analysis was carried out on Shimadzu X-ray diffractometer XRD-600. Thermogravimetric analyzer (TGA), model Q50 from TA Instruments was used for assessing thermal stability. Thermomechanical analysis (TMA) was carried out on a TMA Q400 (TA Instruments). Dynamic mechanical analysis (DMA) was carried out on a DMA-2980 (TA Instruments). Dielectric properties of polyurethanes were followed on dielectric analyzer DEA 2970 (TA Instruments). Stress-strain behavior (tensile stress and elongation) was studied on a Q-Test 2 tensile tester from MTS at gauge lengths of 50 mm and extension rates of 50 mm/min. Hardness was determined using ASTM D785 with a Shore A durometer (PTC Instruments).

Synthesis of Hybrid Biobased-Petrochemical Polyester Polyols

Hybrid biobased-petrochemical polyester polyols were prepared by polyesterification of organic diacids (adipic acid, azelaic acid or sebacic acid) and diols (diethylene glycol, 1,2 propane diol, 1,3 propane diol) and a vegetable oil polyol (castor oil, soy polyol X-173, hydroformylation polyol) as starter. The polycondensation was catalyzed by 0.5% titanium (IV) isopropoxide as a catalyst. The main products of the reaction were a polyester polyol and water as a byproduct. The polyesterification reaction is an equilibrium reaction and the equilibrium is shifted to the desired product, the polyester polyol, by continuous removal of water from the reaction system by a stream of nitrogen. The esterification temperature was 160-210 °C. The first part of the reaction was carried out at 160-180 °C, when a major part of water was collected (~80% from the total water). When the distillation of water became very slow the temperature was increased to 190-200 °C and finally to 210 °C. The polyesterification was stopped when the acid value of the reaction mass was lower than 2 mg KOH/g.

Preparation of Cast Polyurethanes

Polyurethanes were prepared by reacting dry polyester polyol with Mondur CD. The mixture was poured in a mold and held at 110 °C for about 22 hours to complete curing of 1 mm thick films.

Preparation of Flexible Polyurethane Foams

Toluene diisocyanate (TDI 80/20) was added quickly to a homogeneous mixture of a polyol containing silicone surfactants (Struksilon 8026 and DC-198), catalysts (Niax A1 and Niax A33) and water as a chemical blowing agent. The mixture was homogenized with a high speed stirrer (3000 rotations per minute) for 3-5 seconds. Cream time was 3-4 seconds and the rise time 25-30 seconds. The resulting foams were characterized by measuring density, indentation force at 25% and 65% deformation (IDF 25 and 65), support factor, resiliency air flow and open cell content.

Results and Discussion

Esterification of organic diacids and glycols initiated by castor oil is presented in Scheme I. The reaction is followed by measuring collected water and acid value at different reaction times. Acid values (see Fig.1) and the hydroxyl numbers of the reaction mass decreased during the polycondensation reaction. The reaction was stopped when the volume of water collected was constant and the acid value was below 2 mg KOH/g.
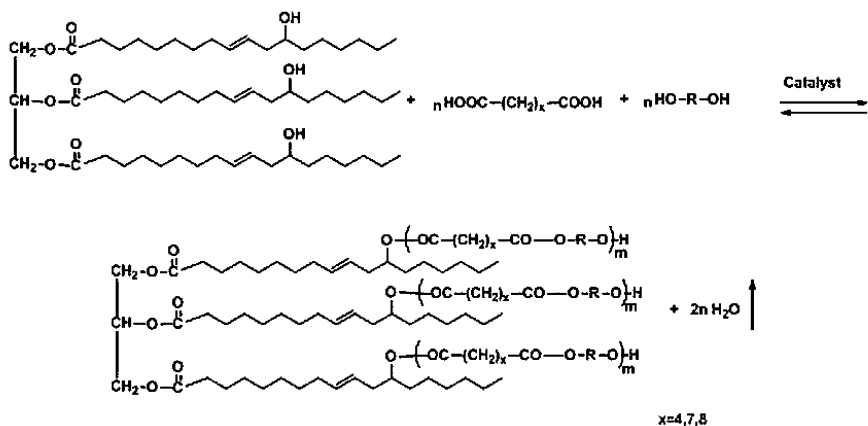
Scheme I. Synthesis and Structure of Hybrid Biobased-Petrochemical Polyester Polyols
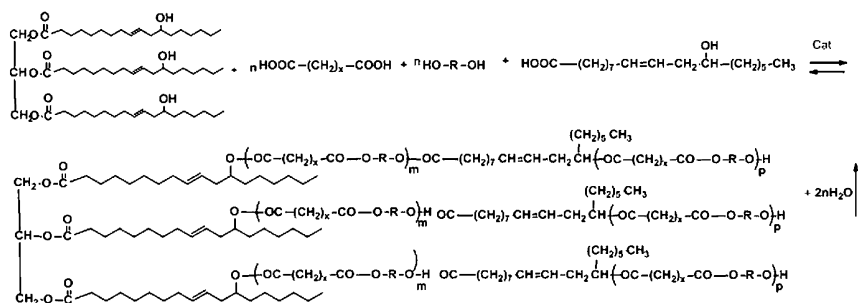
Scheme II. Synthesis and Structure of Polyester Polyols by Esterification of Diacids, Ricinoleic Acid and Glycols Initiated by Castor Oil

Scheme II shows the esterification reaction and the structure of synthesized polyester polyols when ricinoleic acid is used as a co-monomer with organic diacids, glycols and castor oil.

When soy-based polyols, such as X-173 polyol or hydroformylation polyol (HF-polyol), are used as starters, the reaction and structure of the resulting polyester polyols are similar to those presented in Scheme I. The polyester chains are initiated by hydroxyl groups from a vegetable polyol. Thus, Scheme III presents the general reaction scheme and structure of a hybrid polyol based on soybean polyol X-173 (reaction A) and HF-polyol (reaction B) (6), adipic acid and diethylene glycol.
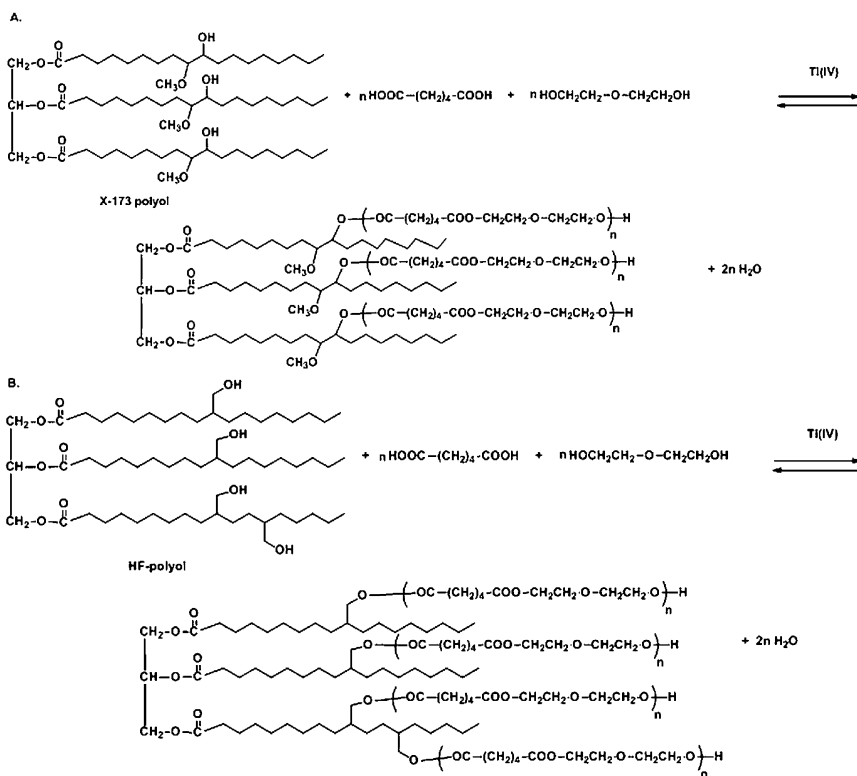
Scheme III. Synthesis and Structure of Polyols Based on Adipic Acid and Diethylene Glycol Initiated by Soy Polyol X-173 (Reaction A) and Hydroformylation Polyol (Reaction B)
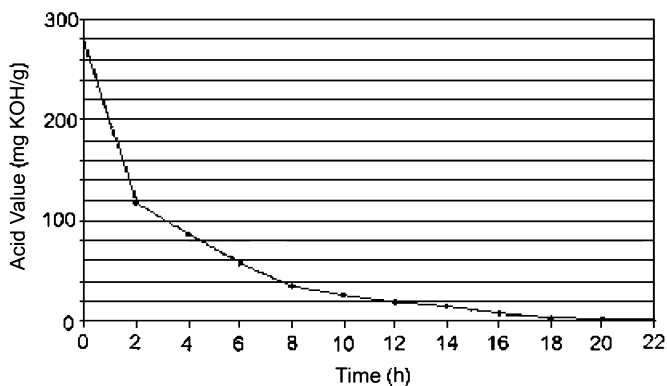
Figure 1. Decrease of acid value during polyesterification of adipic acid with diethylene glycol initiated by castor oil.

Figure 1 shows the decrease of acid value of the reaction mass during polycondensation of adipic acid with diethylene glycol initiated by castor oil. It shows that an acid value lower than 2 mg KOH/g was obtained after 20-22 hours.

Adipic acid, diethylene glycol and 1,4-butanediol are petrochemical raw materials. Vegetable oil polyols (castor oil, polyol X-173, HF-polyol), azelaic acid, sebacic acid, 1,2-propanediol and 1,3-propanediol are bio-based compounds. Azelaic acid is produced by ozonolysis of vegetable oils (7), sebacic acid is the product of alkaline oxidation of castor oil (8), 1,2-propanediol is a product of glycerol hydrogenation (9) and 1,3-propanediol is produced by glucose fermentation in the presence of specific microorganisms (10). GPC values for molecular weights were indicative but not correct since no good calibration standard for branched polyols is available, but the distribution width (M_w/M_n) is reasonably good. Characteristics of synthesized hybrid bio-based polyester polyols presented in this work are listed in Table 1.

Table 1. Properties of Hybrid Biobased-Petrochemical Polyester Polyols

Polyol	Compo-sition	OH# mgKOH/g	Acid# mgKOH/g	Vis-cosity 25 °C Pa.s	Mn (GPC)	Mw (GPC)	Bio Content %
PE-SOY-1	X-173 Adipic acid DEG	61.0	2.0	54	2350	11460	38
PE-SOY-2	X-173 Adipc acid 1,4 BD	58.0	1.5	8.3 (50 °C) solid @RT	2590	8730	65
PE-CO-1	Castor oil Azelaic acid 1,3 PD	74.2	1.2	5.1 (50 °C) solid @RT	2030	4620	100
PE-CO-2	Castor oil Adipic acid DEG	67.0	1.3	37.1	2920	10950	30
PE-CO-5	Castor Oil Adipic acid DEG	73.8	1.1	2.6	1510	3670	39

Continued on next page.

Table 1. (Continued). Properties of Hybrid Biobased-Petrochemical Polyester Polyols

Polyol	Compo-sition	OH# mgKOH/g	Acid# mgKOH/g	Vis-cosity 25 °C Pa.s	Mn (GPC)	Mw (GPC)	Bio Content %
PE-CO-6	Castor Oil Adipic acid DEG Ricinoleic A	94.4	2.0	4.0	1790	4600	39
PE-CO-7	Castor Oil Adipic acid DEG Ricinoleic A	86.8	1.6	6.0	2140	5760	52
PE-CO-10	Castor oil Adipic acid, 1,3 PD	59.8	1.6	3.7	-	-	56
PE-CO-11	Castor Oil Adipic acid 1,2 propane diol	26.2	1.9	2.4	-	-	51
PE-CO-12	Castor Oil Adipic acid 1,2 PD	30.9	1.5	10.8	-	-	55
PE-HF-1	HF-polyol Adipic acid DEG	88.5	1.4	7.1	1430	7300	37

Figures 2, 3, 4 and 5 display GPC chromatograms of some representative polyester polyols together with starting components. It is observed that a small quantity of unreacted monomers remains in the final product.
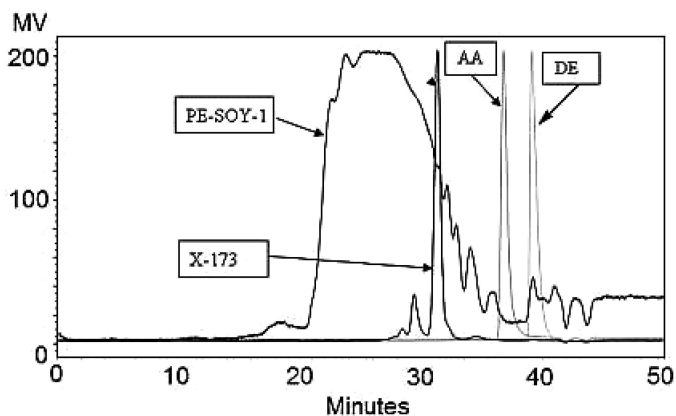
Figure 2. GPC chromatogram of PE-SOY-1 based on X-173 polyol, adipic acid and diethylene glycol.
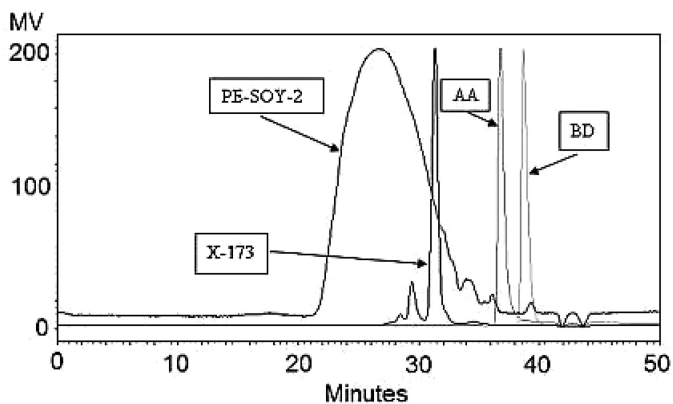
Figure 3. GPC chromatogram of PE-SOY-2 based on X-173 polyol, adipic acid and 1,4-butanediol.
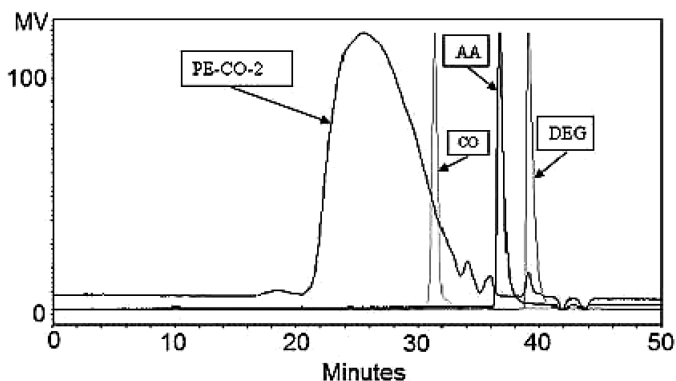
Figure 4. GPC chromatogram of PE-CO-2 based on castor oil, adipic acid and diethylene glycol.
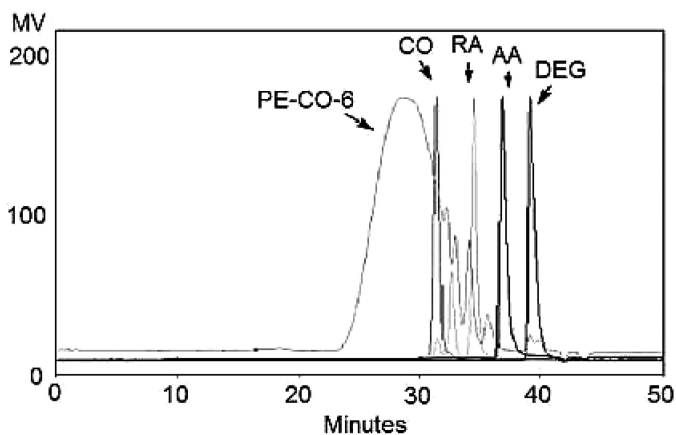
Figure 5. GPC chromatogram of PE-CO-6 based on castor oil, adipic acid, ricinoleic acid and diethylene glycol.
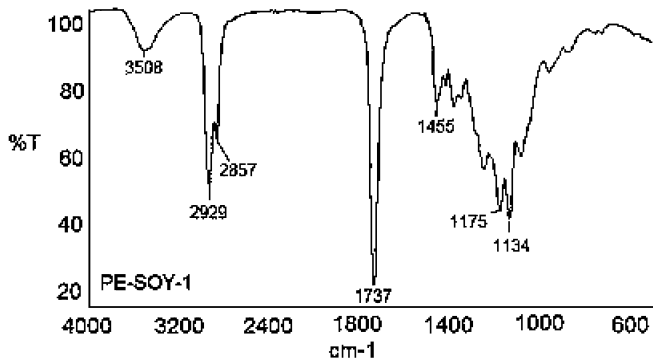
Figure 6. FT-IR spectrum of PE-SOY-1 based on X-173 soy polyol, adipic acid and diethylene glycol.
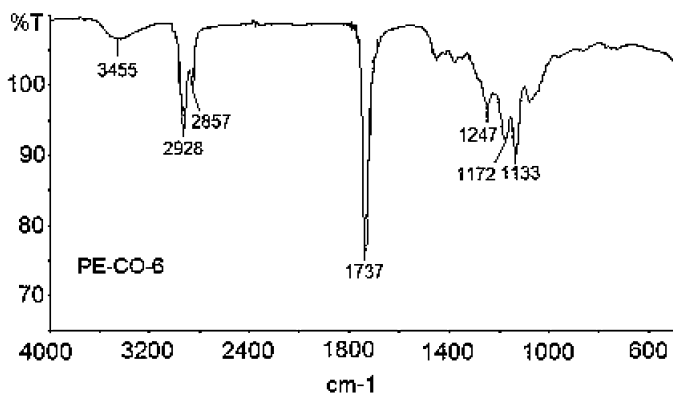
Figure 7. FT-IR spectrum of PE-CO-6 based on castor oil, adipic acid, ricinoleic acid and diethylene glycol.
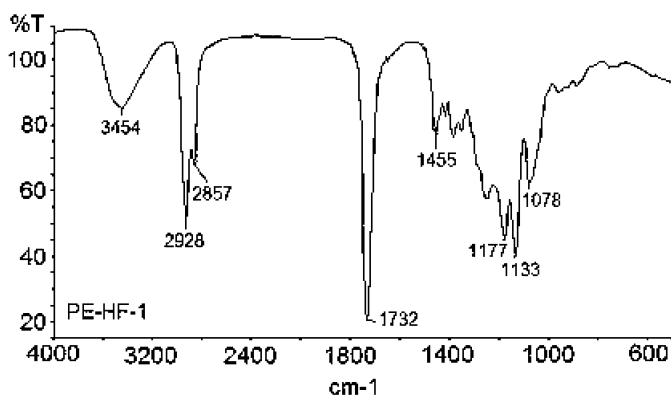
Figure 8. FT-IR spectrum of PE-HF-1 based on hydroformylation polyol, adipic acid and diethylene glycol.

Vegetable oil polyols used as starters are polyfunctional compounds, castor oil having a functionality of f=2.67, soy polyol X-173 has f=3.3 and HF-polyol has f=4 OH groups/mol. These polyols after esterification generate polyester polyols with the same functionality. Formation of some linear polyesters is also possible but less probable at very low acid values. Figure 6 displays the FT-IR spectrum of a polyester based on X-173 polyol and Figure 7 the spectrum of a polyester based on castor oil. The FT-IR spectrum of a polyester based on HF-polyol is presented in Figure 8.

The FT-IR spectra confirm the presence of expected functional groups existing in the synthesized polyester polyols. The broad peak at 3454-3500 cm^{-1} is assigned to hydroxyl groups, while the bands at 2928 cm^{-1} and 2857 cm^{-1} are assigned to C-H in-phase symmetric stretch and out-of-phase asymmetric stretching vibrations of methylene groups. The strong and sharp peak at 1733 cm^{-1} is characteristic of the ester carbonyl. The peak at 1455 cm^{-1} is assigned to asymmetric C-H bending and the peaks at 1078 cm^{-1}, 1177 cm^{-1} and at 1133 cm^{-1} to C-O-C symmetric and asymmetric stretching.

Figure 9 illustrates the ^{1}H NMR spectrum of the polyol PE-CO-2 based on castor oil, adipic acid and diethylene glycol and Figure 10 shows the ^{13}C NMR spectrum of the same polyol. The NMR spectra are consistent with the expected structure of the synthesized hybrid polyester polyol. The peaks at 5.4-5.5 ppm in the ^{1}H NMR correspond to protons linked to the carbon atoms of double bonds from castor oil, the peaks at 3.6 and 4.2 ppm are assigned to methylene groups near oxygen atoms while the peak at 2.34 ppm comes from methylene groups next to the carbon of the ester groups. The peaks between 1 and 2.5 ppm correspond to various methylene groups present in fatty acid chains of castor oil and adipic acid. The peak at 0.88 ppm corresponds to terminal methyl groups of the castor oil. The ^{13}C resonances in Figure 10 are identified as follows: C=O, 172 ppm; C=C, 125-132 ppm (4 peaks); CH at the esterified hydroxyl group from the castor oil portion, 72-73 ppm (2 peaks); CH$_2$ from the diethylene glycol portion, 69 and 62 ppm; glyceryl carbons from the castor oil portion, 69 and 62 ppm; CH$_2$ from adipic acid and castor oil portions, 22 to 39 ppm; CH$_3$ from the castor oil portion,

14 ppm; DMSO, 39 ppm. The ^{13}C NMR spectrum gives evidence that most of the castor oil hydroxyls have reacted with the adipic acid since the peaks at 130 ppm and at 72-73 are not at the positions found for these carbons in the NMR spectrum of pure castor oil.

Incorporation of ricinoleic acid introduced six carbon long "dangling chains" which have a plasticizing effect. Polyester segments in the polyols may be in some cases incompatible with the triglyceride part creating cloudy products (PE-CO-1 and PE-CO-10) and eventually solid upon standing at room temperature. PE-SOY-1 and PE-CO-6 are clear liquids all the time, because DEG and ricinoleic acid with dangling chains do not allow crystallization.

Figure 11 shows the DSC diagram of four hybrid polyester polyols PE-SOY-1, PE-CO-1, PE-CO6 and PE-CO-10. Glass transitions of all polyols are at very low temperatures, between -50 °C and -65 °C, which is a necessary condition for the preparation of elastic polyurethanes. The DSC curve of the polyol PE-CO-1 based on castor oil-azelaic acid and 1,3 propane diol shows crystallinity and a clear melting point at around 29 °C.
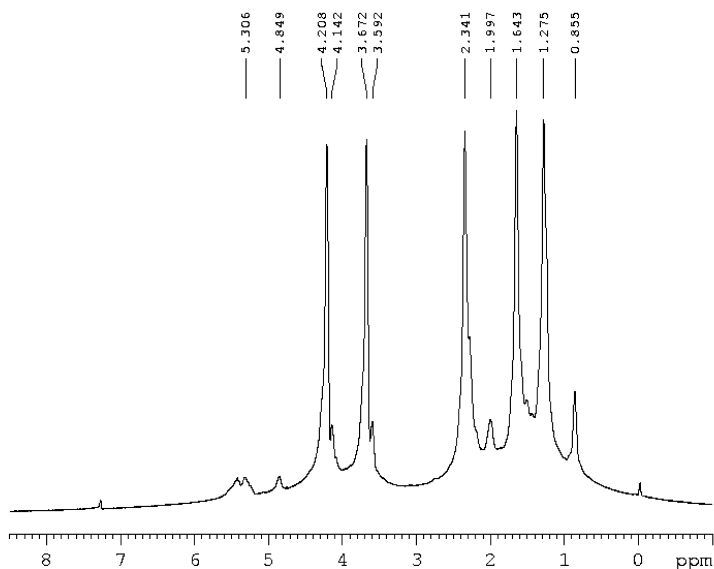
Figure 9. ^{1}H NMR spectrum of the polyester polyol PE-CO-2 based on castor oil, adipic acid and diethlyene glycol in deuterated chloroform.
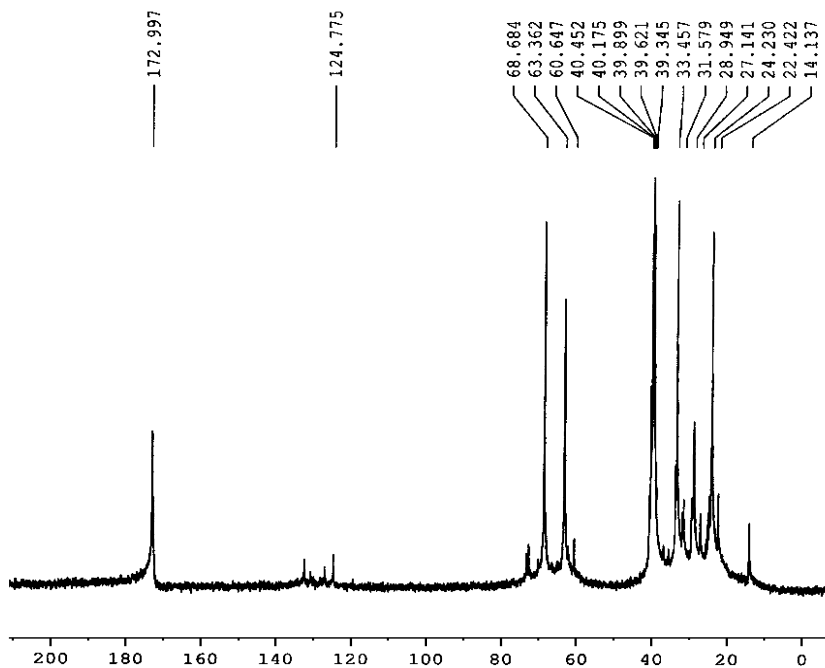
Figure 10. ¹³C NMR spectrum of the polyester polyol PE-CO-2 based on castor oil, adipic acid and diethylene glycol in deuterated DMSO.
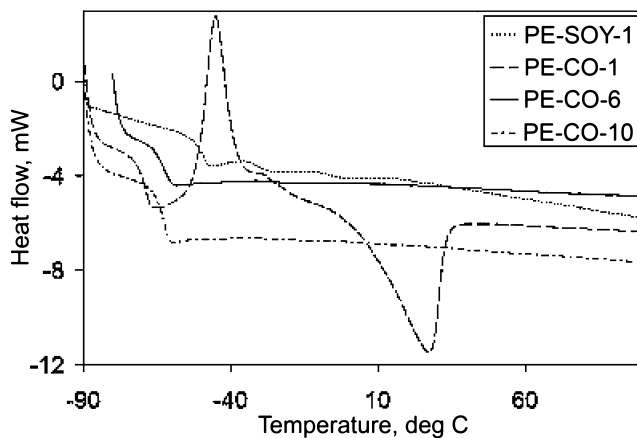
Figure 11. DSC diagrams of four hybrid polyester polyols (PE-SOY-1, PE-CO-1, PE-CO-6 and PE-CO-10).

Properties of Cast Polyurethanes Based on the Synthesized Hybrid Polyester Polyols

Although some polyols are cloudy all polyurethanes were clear and transparent as shown in Figure 12. As will be shown later, none of the polymers displayed a significant degree of crystallinity. Properties of polyurethanes are controlled by several factors: chemical structure, OH content, molecular weight and functionality. Table 2 presents the characteristics of polyurethane networks based on the synthesized hybrid polyester polyols and Mondur CD. Glass transitions of these networks were influenced by chemical composition, functionality of polyols and hydroxyl number, since at higher OH numbers more isocyanate is used.

DSC traces of polyurethanes based on Mondur CD and four representative hybrid polyester polyols: PU-SOY-1, PU-CO-1, PU-CO-6 and PU-CO-10 are displayed in Figure 13. Three polyurethanes of different structures and OH numbers had T_g's in the -30 °C range while one with adipic acid and 1,3-propanediol displayed T_g at -52 °C (PE-CO-10). All polyurethanes are amorphous with T_g values in the range -32 to -52 °C. Shore A hardness, which is another expression of modulus, was in the 50 units range, characteristic of moderately soft polymers.

Polyurethane elastomers with polyester chains display relatively low tensile strength but those from cloudy polyols containing azelaic acid\1.3-propanediol (PU-CO-1) and adipic acid/1,3-propanediol (PU-CO-10) are stronger. They also display higher elongations at break. Particularly instructive is the case of polyurethanes from castor oil with adipic acid/propylene glycol chains, which display the lowest T_g and the highest strength and elongation, possibly due to a better molecular organization, higher chain interaction and higher ester content.

Table 2. Properties of Polyurethane Networks

Polyurethane	Tg oC	Hard-ness Shore A	Swelling ratio	Soluble Fraction, %	Tensile strength MPa	Elon-gation %
PU-SOY-1	-32	50	1.98	5.7	0.94	83
PU-SOY-2	-36	49	2.25	5.3	0.83	77
PU-CO-1	-38	56	2.23	1.9	1.68	141
PU-CO-2	-36	55	1.97	5.0	1.27	87
PU-CO-5	-35	41	2.28	7.0	0.63	90
PU-CO-6	-32	50	2.05	3.1	0.64	109
PU-CO-10	-52	54	2.21	4.5	1.76	165
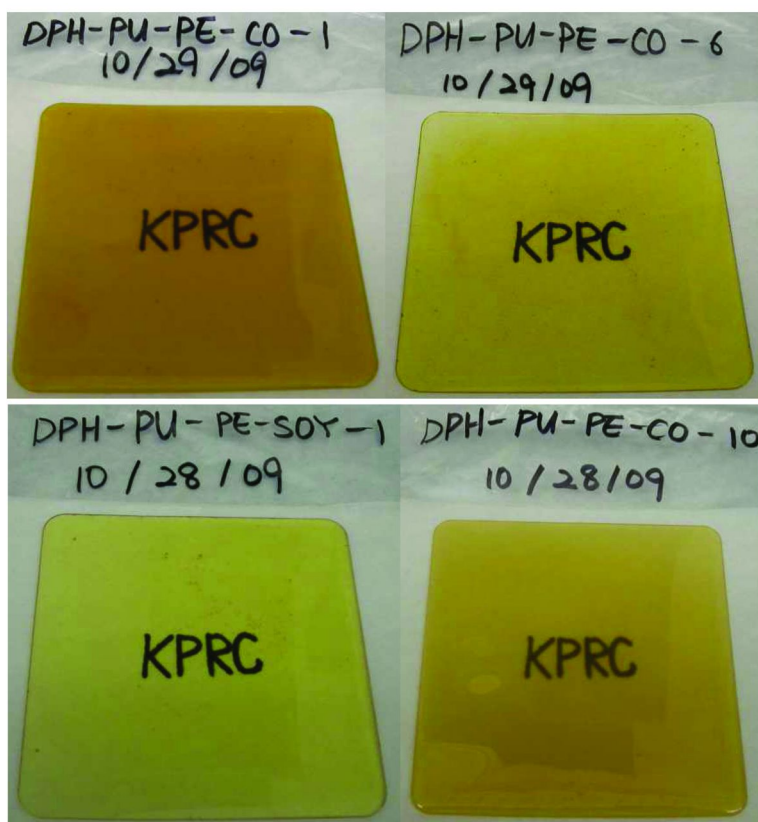
Figure 12. The appearance of cast polyurethane elastomers. The text below the 1 mm thick samples can be read easily.
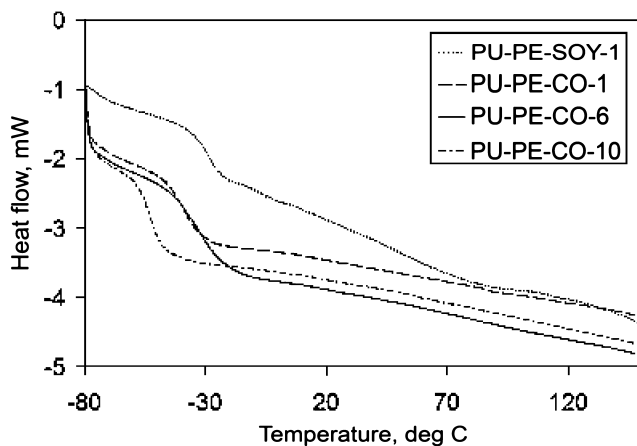
Figure 13. DSC of polyurethanes based on MONDUR CD and hybrid polyester polyols.
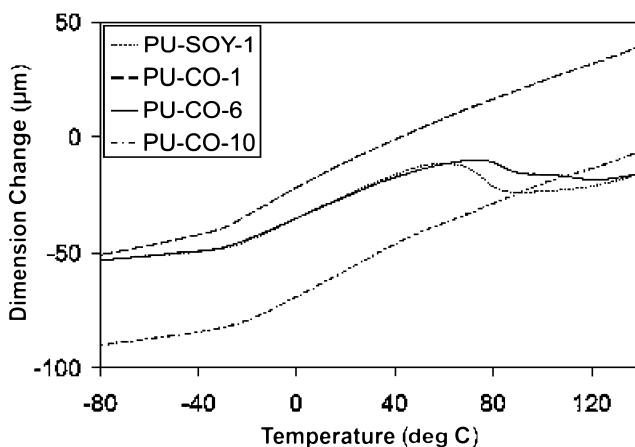
Figure 14. Thermomechanical curves for four cast polyurethanes based on Mondur CD and hybrid polyester polyols.

X-ray difraction of polyurethanes PU-SOY-1, PU-CO-6 and PU-CO-10 reveals that all are amorphous and only polyurethane PU-CO-1 has a very small crystalline fraction, although is mainly amorphous.

Thermomechanical curves for the same cast polyurethanes PU-SOY-1, PU-CO-1, PU-CO-6 and PU-CO-10 are displayed on Figure 14. The T_g values from TMA are very close to those from DSC (see Figure 13).

Dynamic mechanical curves for the four selected polyurethanes are fairly similar, but PU-CO-6 displays a somewhat lower rubbery plateau storage modulus and lower T_g (maximum on the loss modulus-temperature curve), Figure 15. Rubbery plateau moduli for the other three networks are similar, indicating similar crosslinking density. The variation of tan δ as function of temperature for the four selected cast polyurethanes based on Mondur CD and hybrid polyester polyols is shown in Figure 16. Tan δ is a measure of relative viscosity losses in the materials during cyclic deformation. Maxima of tan δ curves are related to glass transitions. High absolute values over 1, suggest that these materials have fairly good damping properties at room temperature.

Dielectric Properties of Cast Polyurethanes

The complex nature of bio-based polyurethanes is a result of a blend of polar polyesters and non-polar triglyceride molecules. Glassy polyurethanes have permittivity below 4, while their values in the rubbery region jump to 10 or higher, as shown in Figure 17 for the cast polyurethane PU-SOY-1. Figure 18 presents the dependence of loss factor on temperature for the same polyurethane. Activation energies for the α-transition of three cast polyurethanes, calculated from the shift of the αtransition with frequency from the loss factor-temperature curves, were about 134-137 kJ/mol but PU-CO-1 had E_a=113 kJ/mol. Lower activation energy is associated with higher mobility of chains.
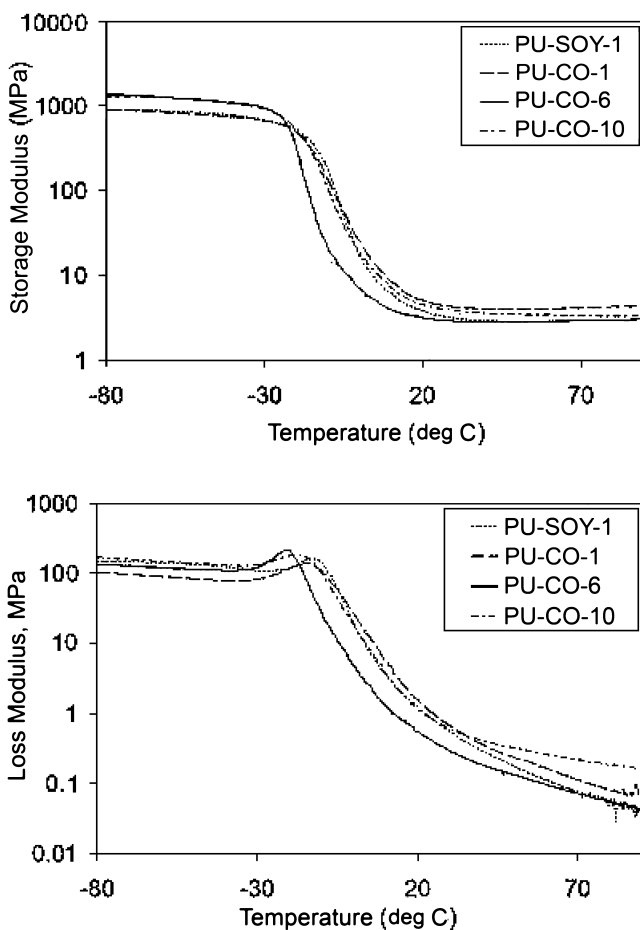
Figure 15. Dynamic Mechanical curves of hybrid polyesters based cast polyurethanes. Storage modulus and loss modulus as a function of temperature.

Thermal Stability of Polyester Urethanes

Thermogravimetric curves of polyester urethanes PU-SOY-1, PU-CO-1, PU-CO-6 and PU-CO-10 in nitrogen are presented in Figure 19. The onset of degradation for all samples appears to be the same at about 300 °C. The slowest weight loss appears to be in PU-CO-1 and the fastest in PU-CO-10. Azelaic acid gives more thermally stable polyesters than adipic acid.
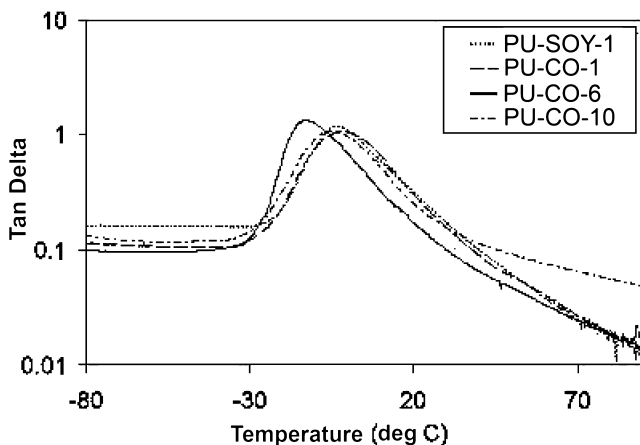
Figure 16. Mechanical tan δ as a function of temperature for cast polyurethanes based on four hybrid polyester polyols and Mondur CD.
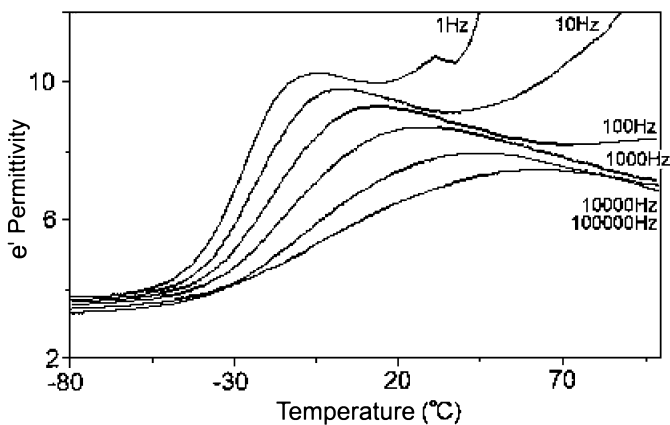
Figure 17. Permittivity dependence on temperature at six frequencies for PU-SOY-1.

Flexible Polyurethane Foams Based on Hybrid Polyester Polyols

One of the most important applications of branched petrochemical polyols is in flexible polyurethane foams. The foams based on polyester polyols have a specific property called "clickability". This means that the foam can be cut to very thin layers necessary for the textile industry. Polyurethane foams based on polyether polyols cannot be cut to such thin layers. The main problem in the preparation of foams from hydrophobic polyols based on vegetable oils is to find a silicone surfactant able to stabilize the foam during rising and to generate the uniform cellular structure. We tested unsuccessfully various surfactants used currently in the production of flexible polyurethane foams. Only Struksilon 8026 silicone surfactant gave suitable foams from hybrid polyester polyols. A mixture

of Struksilon 8026 and DC-198, which is a standard surfactant for flexible foams, at a ratio 2.5/1 (w/w) was efficient too. Two hybrid polyester polyols, PE-CO-5 and PE-CO-11 gave good foams. They were selected because of their low viscosities (2.6 Pa.s and 2.4 Pa.s at 25 °C, respectively). The formulation used contained 4% water. The homogenized polyol with all components was mixed with TDI 80/20, at an isocyanate index of 105, using a high speed stirrer (3000 rot/minute). The resulting flexible foams had uniform cellular structure typical for good flexible polyurethane foams. The characteristics of flexible polyurethane foams based on polyol PE-CO-11 are presented in Table 3.
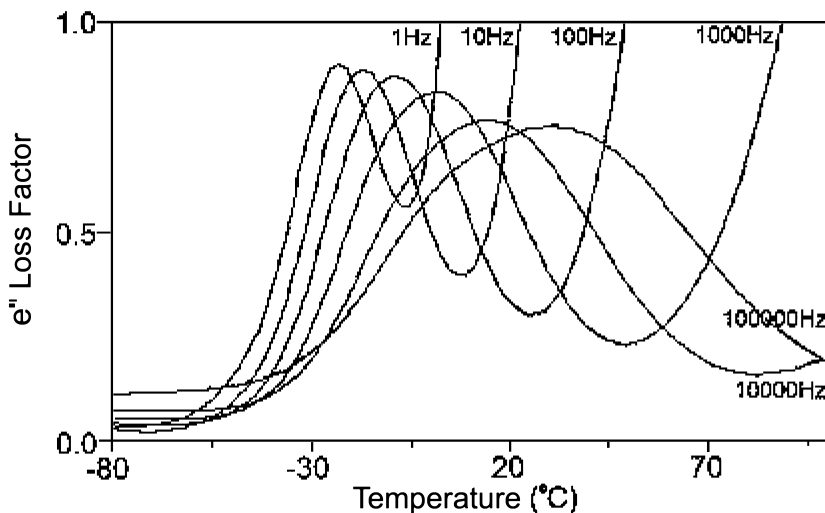
Figure 18. Dependence of loss factor on temperature at six frequencies for PU-SOY-1.
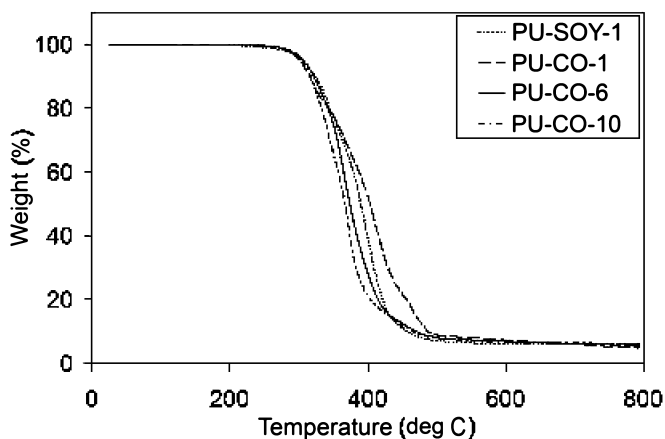
Figure 19. Thermogravimetric curves of polyester urethanes PU-SOY-1, PU-CO-1, PU-CO-6 and PU-CO-10. TGA in nitrogen at 10 °C/min.

Table 3. Some Physical-Mechanical Characteristics of Flexible Pu Foams Made with the Polyester Polyol PE-CO-11

Property	*Unit*	*PE-CO-11*
Density	Kg/m^3	26.6
Compression strength, 25%	KPa	4.3
Compression Strength, 65%	KPa	8.5
Support factor (SAG)	-	1.97
Resiliency,	%	~42
Open cell content	%	98
Air Flow	CFM*	1.6

* CFM- cubic foot/minute=28.3 L/min

Flexible polyurethane foams from these polyols were not optimized and the properties could be improved. The experiments demonstrated the feasibility of making flexible polyurethane foams with good properties from the synthesized hybrid bio-based/petrochemical polyester polyols with an adequate silicon surfactant.

Conclusions

A new group of hybrid biobased-petrochemical polyester polyols, with a bio content varying from 30-100% were prepared by esterification of castor oil or a soy polyol with biobased acids and diols or petrochemical analogs. Chain extension by esterification is a viable and flexible method for modifying the structure of oil based polyols. The synthesized hybrid polyester polyols were used to make elastic polyurethanes (cast elastomers and flexible foams). The prepared cast polyurethanes were crosslinked, amorphous and relatively soft rubbers. We obtained good flexible polyurethane foams from the hybrid polyols when a proper silicone surfactant was employed. The synthesized new hybrid vegetable oil/petrochemical polyester polyols are also suitable for other applications of elastic polyurethanes such as coatings adhesives and sealants.

References

1. Bauer, S.; Ruppel, R.; Baum, E.; Winkler, J.; Bohres, E. Patent WO 20040203497, 2004.
2. Ionescu, M.; Petrović, Z.; Javni, I.; Stojadinov, J. In 96th AOCS Annual Meeting and Expo, Salt Lake City, 2005.
3. Penczek, P.; Ostrysz, R.; Wieczorek, D.; Tomaszewski, Z. B.; Udeshi, S. V. In Polyurethane Expo 2001, Columbus, Ohio, 2001; Vol. Conference Proceedings, pp 565−568.
4. Xu, Y.; Petrovic, Z. S.; Das, S.; Wilkes, G. L. *Polymer* **2008**, *49*, 4248–4538.

5. Petrovic, Z. S.; Cvetkovic, I.; Hong, D.; Wan, X.; Zhang, W.; Abraham, T. W.; Malsam, J. *Eur. J. Lipid Sci. Technol.* **2010**, *112*, 97–102.

6. Guo, A.; Cho, Y.-J.; Petrovic, Z. S. *J. Polym. Sci., Part A: Polym. Chem.* **2000**, *38*, 3900–3910.

7. Hill, K. *Pure Appl.Chem.* **2000**, *72*, 1255–1264.

8. Mutlu, H.; Meier, M. A. R. *Eur. J. Lipid Sci. Technol.* **2010**, *112*, 10–30.

9. Dasari, M. A.; Kiatsimkul, P. K.; Sutterlin, W. R.; Suppes, G. J. *Appl. Catal., A* **2005**, *281*, 225–231.

10. Corma, A.; Iborra, S.; Velty, A. *Chem. Rev.* **2007**, *107*, 2411–2502.

Chapter 6

Revitalizing Chemurgy: Chemicals from Agricultural Resources

Patrick B. Smith*

**Archer Daniels Midland Research, James R. Randall Research Center,
1001 N. Brush College Road, Decatur, IL 62521**
***smith@mmi.org**

The global chemical industry is undergoing a transformation driven by price volatility and geographical location of petrochemical feedstocks. In part, this pressure on petro-feedstocks has led to a resurgence of interest in renewable feedstocks. Even though renewable chemistry is receiving considerable interest today, it is by no means a new idea. In fact, it developed along with the early chemical industry and its proponents even coined a name for it, chemurgy. A number of leading global chemical and agricultural companies have shown renewed interest in chemurgy. This is primarily due to the cost competitiveness and abundance of renewable feedstocks as a result of significant improvements in agriculture over the past several decades. Major initiatives in the chemical industry have focused on both direct chemical replacements and bio-advantaged molecules. Direct chemical replacements use agricultural feedstocks to produce an existing petrochemical product. Bio-advantaged molecules are not readily accessible from petrochemical sources. Several examples of each will be discussed.

Introduction

Chemurgy

Bio-based chemicals and advanced biofuels have experienced a resurgence over the past decade. Driving this movement is the need for more energy, enhanced energy security and for a greater portion of our energy to come

from environmentally favorable sources. In particular, there has been focus on alternatives to products derived from petroleum. In spite of this recent emphasis, bio-based chemicals have been around for a very long time. Many of the research ideas being discussed today were introduced through the chemurgy movement in the 1920s or earlier (*1*). Chemurgy is a combination of "chem" for chemistry and "urgy" from the Greek word to work. The chemurgy movement was determined to put chemistry to work by developing industrial products from agricultural feedstocks.

There are many notable examples of early 20th century Chemurgy. Prior to World War II, *n*-butanol was primarily derived from acetone/butanol/ethanol fermentation. Furfural, furan and tetrahydrofuran were traditionally bioderived molecules from cellulosic feedstocks (corn cobs). Conversions of glycerol to allyl alcohol and acrolein, the precursor for acrylic acid, were well documented from the 1880s (*2*). Hydrogenolysis chemistry of carbohydrates to produce, for example, 1,2-propylene glycol was reported in 1933 (*3*). Ethanol dehydration to ethylene was documented as early as 1932 (*4*). With all of this innovation at such an early stage of our industrial chemical history, there was one obstacle to the continued development of Chemurgy. During the time period of the early chemurgic movement, between 1920 and 1969, the price of petroleum never exceeded $3.10 per barrel, and it was in abundant supply relative to other feedstocks (*5*).

Agricultural Feedstocks

While crude oil pricing remained low through the early 1970s, more recent price volatility and environmental concerns have resulted in resurgence in alternative energy and materials research efforts. However, advances in agriculture over the past several decades should receive the majority of the credit for enabling Chemurgy to proceed. For example, from 1980 to 2008 there was an approximate 2% increase in the number of acres of corn planted in the United States. The total number of acres planted in 2008 was just shy of 86 million acres. While the number of acres planted was nearly constant, the average yield of corn was 91 bushel/acre in 1980 and 154 bushel/acre in 2008. This 69% increase in yield on approximately the same number of acres was a major achievement. Furthermore, these improvements in productivity have not come at the expense of higher farm inputs such as chemicals, additional machinery, etc. The United States Department of Agriculture, Economic Research Service has compiled data on U.S. agricultural output, input and productivity since 1948. The comparisons made by the USDA take into account all outputs and inputs to develop a total productivity number. A clear trend of sustainable improvement in output and productivity has been demonstrated with essentially the same inputs used in 1948 and 2006 (*6*).

Looking ahead, industry leaders expect these trends of increased productivity to continue into the future. Monsanto projects that by 2030, corn yields could reach an average 300 bushels per acre with advances in biotechnology (*7*). This would represent another doubling of output from existing acres. With increased yields, it is not just more corn that will be produced. Additional corn stover

(stalks, leaves, cobs), collected using sustainable practices under development today, will be available as additional raw material base for new feed, fuel and industrial chemical initiatives.

Archer Daniels Midland

Archer Daniels Midland Company traces its early history to 1902 when George A. Archer and John W. Daniels founded a linseed crushing business, the Archer-Daniels Linseed Company. In 1923, it acquired Midland Linseed Products Company, and the Archer Daniels Midland Company was formed (*8*, *9*). ADM's early history was associated with this nascent chemurgy movement, as primarily a chemical company supplying linseed oil and derivatives to alkyd paint makers, foundry products and for other industrial applications. However, in 1967, ADM sold its chemicals business to Ashland Oil in order to focus on agricultural processing. Today, ADM has increased focus on the chemurgy arena with its efforts to commercialize propylene glycol, isosorbide and poly(hydroxyalkanoates), the latter through the Telles joint venture between ADM and Metabolix. In addition, ADM was awarded a U.S. DOE grant to pilot cellulosic ethanol and biomass derived ethyl acrylate as part of an integrated biorefinery pilot plant project under the American Recovery and Reinvestment Act (*10*).

ADM is one of the largest diversified global agricultural processors participating in four main businesses; food, feed, fuels and industrial chemicals. Headquartered in Decatur, Illinois, ADM has over 28,000 employees, more than 230 processing plants in over 60 countries, with net sales for the fiscal year ended June 30, 2009 of $69 billion.

Bio-Based Chemicals

There is significant value in the chemicals sector as pointed out by Figure 1 (*11–13*). The chemicals sector accounted for about 3.4% of the roughly 300 billion gallon US petroleum consumption in 2007. In comparison, the liquid transportation fuel sector comprised over 70% of the consumption, but had a similar pre-tax value as the chemicals sector, excluding pharmaceuticals. Renewable chemicals are finding acceptance in traditional petrochemical markets as they are becoming economically competitive. In addition, there is value for a product being from a renewable source, as well as some value for being biodegradable, but they still must compete primarily on a cost/performance basis.

There are two main approaches for the commercialization of a new renewable chemical: direct replacements and bio-advantaged molecules. In the first case a renewable route can be developed for an existing chemical such as propylene glycol or epichlorohydrin from glycerol, of which more will be said.

US Petroleum Consumption by End Use (%)
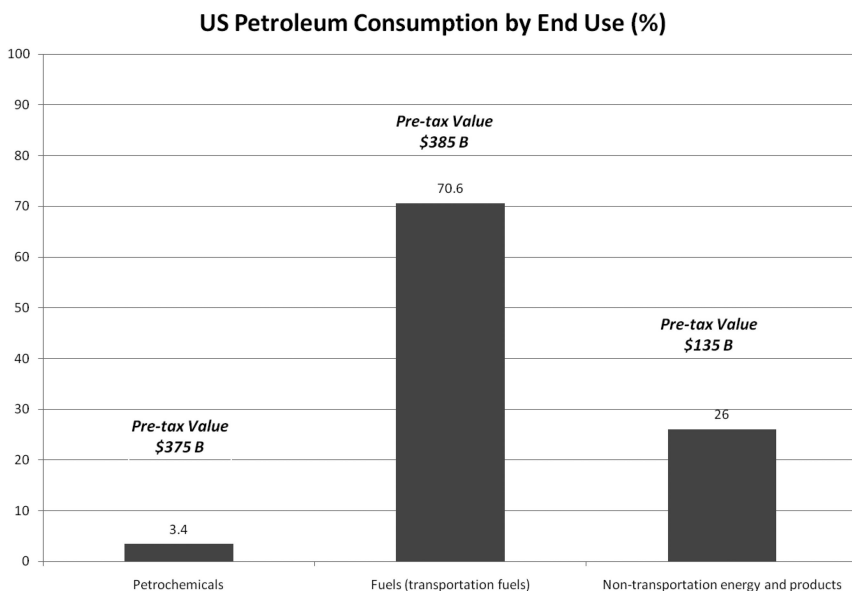
Figure 1. 2007 US Petrochemical Consumption and Value for Liquid Fuel, Non-transportation Energy and Chemicals Sectors (Total U.S. Consumption = 300 Billion Gallons).
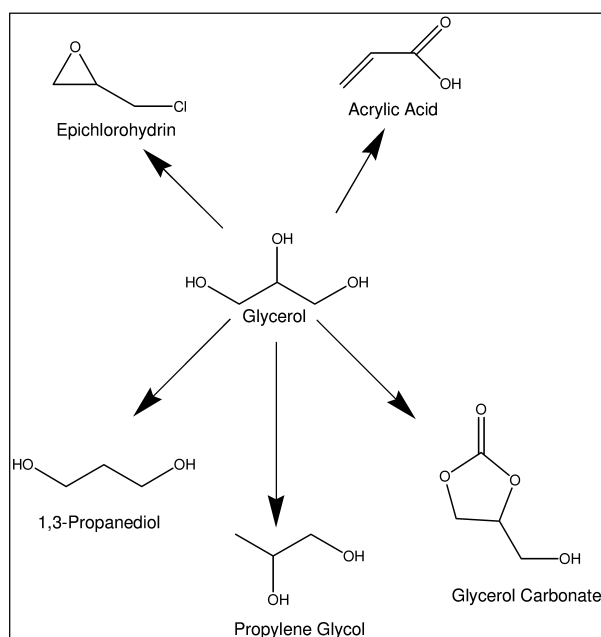
Figure 2. Glycerol Derivatives.

98

The other route is to develop a biobased chemical not currently in widespread commercial use in a new market space to compete against traditional petrochemical compounds. Some examples of this approach include Cargill Dow's launch of poly(lactic acid), introduction of levulinate ketals by Segetis and multiple efforts around commercialization of isosorbide and derivatives by companies including Roquette, DuPont and ADM.

Direct Replacements

The first approach, commercializing direct replacements, has well defined targets. Production of a direct replacement requires that it possess an equivalent quality and have competitive economics to the incumbent petrochemical product. Depending on the technology used, these biobased products may possess other advantages such as a more favorable life cycle analysis (LCA), lower greenhouse gas (GHG) emissions and the ability to track final bio-content of end products with test methods such as ASTM D6866.

Glycerol has emerged as a key feedstock for direct replacement of platform chemicals. Glycerol can be used to produce many core industrial monomers due to its low cost and large availability as a by-product from biodiesel production. It is clear that glycerol is an attractive platform chemical as can be seen from Figure 2 adapted from the Department of Energy's publication "Top Value Added Chemicals from Biomass" (*14*).

There have been a number of announcements over the past five years with regard to glycerol as a feedstock for industrial chemicals, as given in Table 1 (*15*). ADM, Cargill/Ashland, Dow and Synergy announced their intent to commercialize propylene glycol from glycerol (*16–18*). In all the glycol cases, glycerol is converted to propylene glycol via thermochemical transformations.

Dow and Solvay announced the production of epichlorohydrin from glycerol (*19*, *20*), which itself is the common synthetic precursor to glycerol. Solvay reported a process to first convert glycerol into a dichloropropanol intermediate using anhydrous HCl and an optional catalyst as shown in Figure 3. The resulting 1,3-dichloro-2-propanol is then treated with NaOH to promote S_N2 displacement of chloride to yield epichlorohydrin (*21*). Solvay recently announced that Vinylthai, which is half owned by Solvay, will be taking over the project in Thailand with a projected start-up in 2012 (*22*).

Huntsman announced plans to commercialize glycerol carbonate which is a building block for polyesters, polycarbonates and polyurethanes as well as having applications as a solvent in cosmetic and personal care applications. Other announcements include Arkema's, which is exploring technology to produce acrolein and acrylic acid from glycerol (*23*) and Linde's intention to reform glycerol to hydrogen (*24*). An excellent review of the conversion technology for acrolein from glycerol has recently been published (*25*). Many of these ventures have been delayed due to the recent downturn in the economy and some have been discontinued.

Table 1. Glycerol Feedstock Announcements

Company	Product	Volume	Location
ADM	Propylene Glycol	100,000 mt	Decatur, IL
Cargill/Ashland	Propylene Glycol	65,000 mt	Europe
Dow	Propylene Glycol	NA	Texas
Dow	Epichlorohydrin	150,000 mt	China
Huntsman	Glycerol Carbonate	NA	Texas
Solvay/Vinythai	Epichlorohydrin	100,000 mt	Thailand
Arkema	Acrylic Acid	NA	France
Synergy	Propylene Glycol	NA	NA
Linde	Hydrogen Reformation	Demonstration Plant	Germany
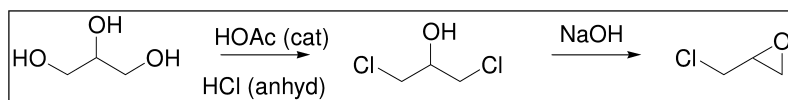
Figure 3. The Conversion of Glycerol to Epichlorohydrin.

While glycerol is an attractive feedstock, availability from biodiesel or fat splitting offers a unique, but limited opportunity as a feedstock for large chemical markets like epichlorohydrin, propylene glycol and acrylic acid. For example, roughly 11 million metric tons of biodiesel were produced globally in 2008 from which about 1.1 million metric tons of crude glycerol was produced (*26*). The total market for refined glycerol was about 900,000 metric tons in 2005 (*27*). Again, in comparison to the multi-million metric ton per year target chemicals that can be made from glycerol, these numbers are relatively small. However, supply of glycerol is not limited to oilseed sourcing. Glycerol can also be produced on demand via fermentation or by other thermochemical processing of carbohydrates.

ADM is currently commissioning its production facility in Decatur, IL to produce propylene glycol from the hydrogenolysis of glycerol and carbohydrates. In addition to ADM, Global Biochem is producing glycols via hydrogenolysis in China using sorbitol as the feedstock (*28*). Hydrogenolysis catalysts have been developed that are very selective for conversion of glycerol to propylene glycol with water as the main co-product. Hydrogenolysis chemistry also offers feedstock flexibility, not being limited to glycerol, but can also accept other carbohydrate feedstocks as shown in Figure 4. The other main co-product typically produced from hydrogenolysis of glycerol and sorbitol is ethylene glycol, which has large demand in polymers like poly(ethyleneterephthalate).
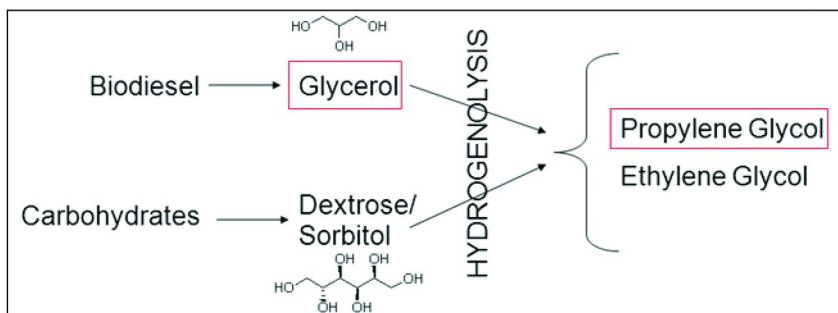
Figure 4. Hydrogenolysis pathway to glycols. ADM has developed very selective catalysts for the production of propylene glycol from glycerol in conjunction with Pacific Northwest National Laboratory.
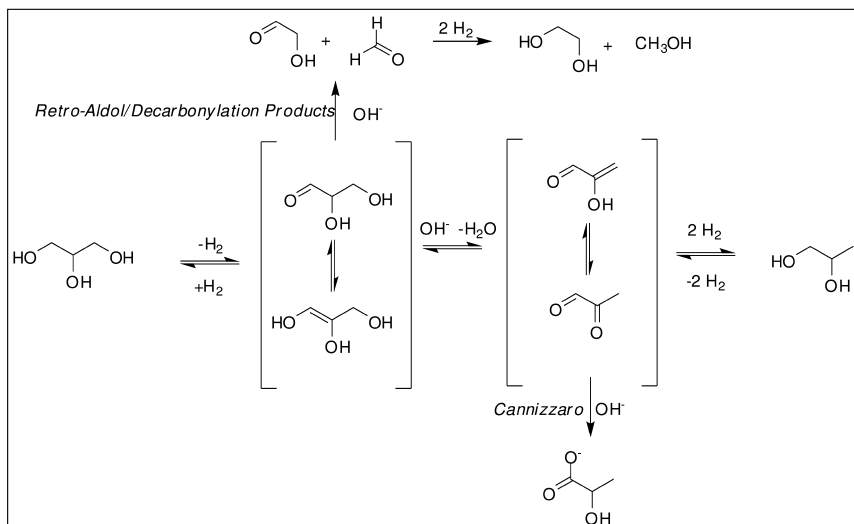
Figure 5. Proposed Pathway for Glycerol Hydrogenolysis

In comparison to hydrogenolysis, the traditional petrochemical route to propylene glycol consists of propylene oxidation to propylene oxide followed by ring opening of the oxirane to form 1,2-propylene glycol. Co-products include either styrene or t-butanol (typically converted to MTBE) derived from ethylbenzene hydroperoxide and t-butyl hydroperoxide, respectively. However, new hydrogen peroxide technology used for propylene epoxidation also only produces water as co-product.

The hydrogenolysis of glycerol is thought to proceed by the dehydrogenation of glycerol to glyceraldehyde, followed by dehydration to 2-hydroxyacolein which is then hydrogenated to propylene glycol, as shown in Figure 5 (*29*, *30*). Several side reactions can also take place via retro-aldol or decarbonylation reactions to give formaldehyde and 2-hydroxyacetaldehyde which when hydrogenated, yield

101

methanol and ethylene glycol, respectively. Lactic acid (d,l) can also be produced by the Cannizzaro reaction of the keto isomer of 2-hydroxyacolein.

While the same end propylene glycol specifications are met by both the petrochemical and biobased routes, other advantages to the direct replacement route are present. As previously mentioned, biobased propylene glycol produced by hydrogenolysis can be tested by ASTM D6866 to show it contains only biobased carbon. This allows consumers for major markets such as unsaturated polyester resins to continue to produce the same end products and easily convert a measurable and auditable amount of their end product to a renewable source. Furthermore, life cycle assessment of the new propylene glycol route was very favorable for greenhouse gas emission (GHG) reduction (*31*). ADM has estimated the life cycle GHG impacts for production of bio-based propylene glycol (bio-PG) from soybean derived glycerol was approximately 80% lower than that of petro-PG. The GHG emissions evaluated in the study were CO_2, CH_4 and N_2O. The overall lifecycle GHG emissions for biobased PG were 1.72 kg CO_2eq per kg PG using energy content allocation. The environmental performance of biobased PG was benchmarked against the petroleum process which was provided by GaBi lifecycle software database and has an overall lifecycle GHG emission of 8.61 kg CO_2eq per kg PG. Therefore, the bio-PG offers better environmental performance than petroleum based PG in terms of global warming impact. Professors Bruce E. Dale and Seungdo Kim of Michigan State University reviewed the LCA study which ADM performed and endorsed the results and conclusions.

Bio-Advantaged Molecules

A prime example of a bio-advantaged molecule under development for the polymer industry is isosorbide which is produced in a two step process as shown in Figure 6. Initially, dextrose is hydrogenated to sorbitol and then sorbitol undergoes two dehydrations to give the dianhydrohexitol, isosorbide (*32*).

Figure 7 shows a schematic of a proposed process for the production of isosorbide from sorbitol. In this process, two grades of isosorbide can be produced, one of very high purity for polymer applications and a technical grade of greater than 95% purity for other potential applications such as plasticizers and personal care applications. The overall yield based on sorbitol was reported to be 77.5 mol%.

Isosorbide has seen only limited industrial use but imparts an interesting set of properties when used in polymeric materials (*33*). Like most biobased molecules, isosorbide has a rich history that spans over 100 years of development. Until recently cost competitive feedstocks relative to petroleum derivatives such as bisphenol-A (BPA) which is derived from phenol and acetone, were not available to help enable its development. Nevertheless, isosorbide has been evaluated as a building block for polyesters (*34–38*) and has potential for replacing BPA in polycarbonates and epoxy resins (*39, 40*) in that its polymers possess similar glass transition temperatures as BPA copolymers but with enhanced UV stablility (*41*).
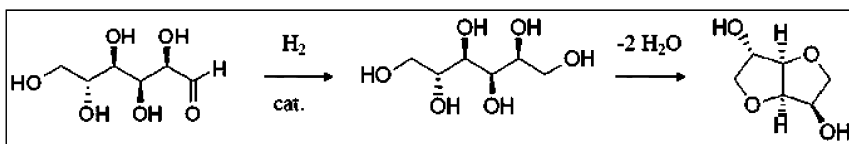
Figure 6. The Dehydration of Sorbitol to Isosorbide.
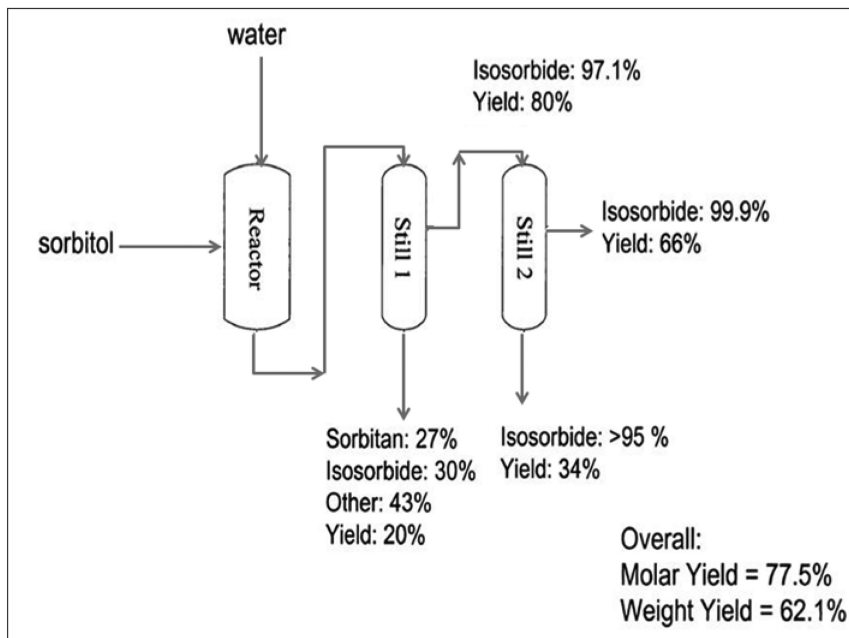
Figure 7. A Proposed Process for the Production of Isosorbide from Sorbitol.

Epoxy resins have been a major R&D area for isosorbide for many years. However, with the concerns around Bis-A, efforts to develop this molecule as a viable alternate in this space have gained momentum. Figure 8 illustrates the synthetic methods evaluated to develop isosorbide-based epoxy resins, showing continued efforts from the early 1960s through today. The properties of the epoxy resins of Figure 8 cured with various agents are listed in the Table 2.

A strong body of literature also exists on the utilization of isosorbide in polyesters to enhance glass transition temperatures. Isosorbide was evaluated as a comonomer with terephthalic acid and ethylene glycol for PEIT terpolymer polyester resins (*42*). The Tg of the resin increased markedly with increasing isosorbide content (Figure 9). This enhanced thermal performance of PEIT resins affords engineering polymer performance at nearly the cost of PET.

In addition to isosorbide, six carbon sugars such as glucose, dextrose and fructose, can be chemically converted to hydroxymethyl furfural (HMF) which can then be oxidized to 2,5-furandicarboxylic acid (FDCA) as shown in Figure 10 (*43*). The chemistry used for this transformation is very similar to that used

103

for conversion of p-xylene to terephthalic acid. Not surprising, FDCA is of interest as a potential replacement for terephthalic acid in polyesters and polymer additives. Diols and diamines from FDCA also have potential applications as polymer building blocks for polyesters and polyamides. FDCA is also a potential direct replacement option to produce terephthalic acid via Diels Alder addition of ethylene, followed by dehydration (*44*).

Perhaps one of the most interesting high performance bio-advantaged polymers was demonstrated by Storbeck and Ballauff in 1993 (*37*). They produced a series of polyesters from dianhydrohexitols including isosorbide and 2,5-furandicarboxylic acid. The polymers exhibited very high glass transition temperatures and had no reported crystallinity as shown in Table 3.

US 3,041,300 (1962): Claims water soluble polyglycidyl ethers

US 3,272,845 (1966): Claims bisglycidyl ether of isosorbide

Biomass **1986** 9, 247: shows enhanced bisglycidyl molar yields of 85%

US 7,619,056 and US 2008/0021209: Incorporated US 3,041,300 by reference, claims diamines derived from isosorbide as curing agents and claims modified process for other ether derivatives.

Figure 8. The Epoxy Resins Based on Isosorbide.

Table 2. The Properties of Isosorbide-Based Epoxy Resins Cured with Various Curing Agents

Curing agent	T_g (°C)	Modulus (MPa)	Izod (rev. notch, MPa)
Nadic Methyl Anhydride	113	--	--
Aliphatic Polyether Triamine	48	2900	69
4,4'-Methylenedianiline	89	--	--
4,4'-(Hexafluoro-isopropylidene)diphthalic anhydride	200	--	--
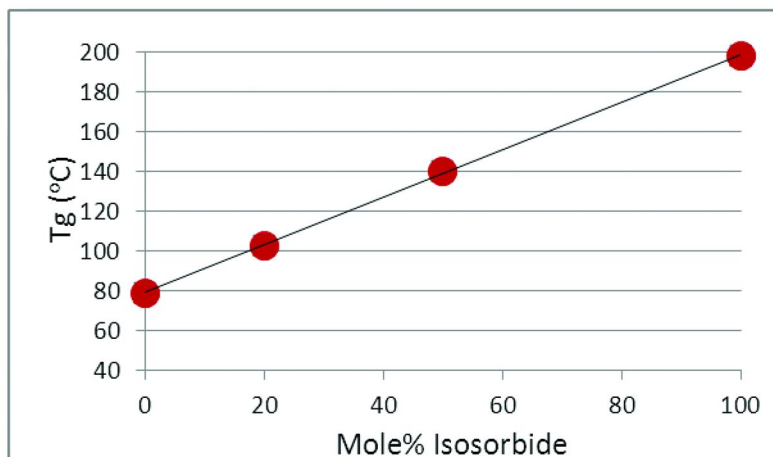
Figure 9. The Glass Transition Temperature of the PEIT Resin as a Function of Isosorbide Incorporation in the Copolymer.

ADM and Metabolix have formed a joint venture named Telles to commercialize poly(hydroxyalkanoates) or PHAs, a renewable, biodegradable plastic. PHAs are naturally accumulated in a variety of microorganisms as an energy storage medium (*45*). In the case of the Metabolix process, the PHAs are produced by a fermentation using an engineered bacterium. The polymer grows to very high molecular weight within the cell. When the fermentation is complete, PHA is recovered from the cell mass, purified and pelletized. The PHA being commercialized is a copolymer of 3-hydroxybutyrate (3HB) whose comonomer level can be adjusted to obtain a diverse property space. 3HB itself is not as interesting from a commercial standpoint because it has a high degree of crystallinity (very stereoregular), possesses a melting point near its degradation temperature, and hence degrades by thermolysis at melt processing temperatures (*46*). It is also very brittle and ages considerably. Copolymerization, with a variety of comonomers, both reduces its level of crystallinity and melting point such that it can be melt processed without incurring significant thermal degradation. Copolymers age to a much lesser extent than the homopolymer and possess

improved ductility. Copolymers have been produced from 3-hydroxyvalerate, 3-hydroxyheptanoate, 3- hydroxyoctanoate, 4-hydroxybutyrate and many others using a variety of organisms (*45*, *47*). The level of crystallinity and the crystalline melting point ranges from roughly 60% and 177°C, respectively, for the 3HB homopolymer to non-crystalline rubbers at high comonomer levels possessing glass transition temperatures ranging from about 10°C for 3HB homopolymer to below -20°C for certain copolymers. The Telles joint venture has constructed a 110 million pound per year plant collocated with ADM's processing facility in Clinton, Iowa.

EnviroStrip® is a specialty starch-based abrasive blasting medium for paint stripping and other applications. In particular, it has found broad acceptance for stripping aircraft coatings because it combines an effective paint stripping capability with minimal erosion of the fragile substrates. Historically, methylene chloride chemical stripping was the primary mode to remove paint from aircraft. Other paint stripping technologies have evolved to compete with this traditional method. These included chemical, mechanical, thermal, and hybrid combinations. These stripping methods must not compromise the integrity of the aircraft's substrates and components below the surface of the coating. One of the more interesting applications of EnviroStrip is for the removal of the Radar-absorbing coating of the B2 Stealth Bomber (*48*).

Finally, BioSAP® is a starch-based superabsorbent polymer being commercialized by ADM. It is a derivatized starch that has properties similar to those of conventional polyacrylate superabsorbent materials but has a renewable origin. Applications include baby diapers, feminine hygiene products and adult incontinent products.
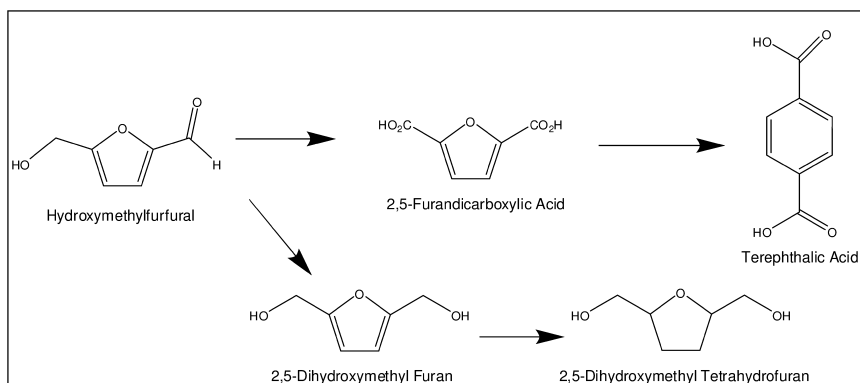
Figure 10. Furanic Derivatives from Hydroxymethylfurfural.

Table 3. The Properties of Isosorbide, Furandicarboxylic Acid Copolymers as a Function of the Degree of Polymerization
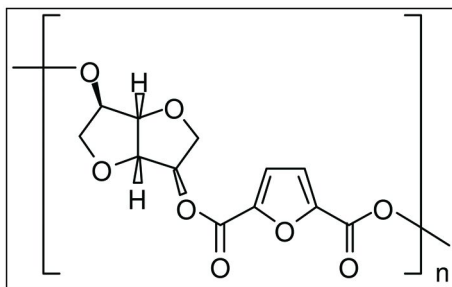
Sample	M_n (g/mol)	DP	$[\eta]$ (dL/g)	T_g (°C)	TGA (°C) (air/N_2)
A	9000	34	0.11	173	--
B	22500	85	0.35	190	--
C	25000	94	0.38	194	320/340

Summary

This "new" field of renewable chemistry is not as new as many believe. It has its roots in the early 20th century right along with the emergence of the modern petrochemical industry. Chemurgy has had support from major industrialists from its beginnings. Increases in productivity over the past 60 years have enabled agricultural-derived feedstocks to be competitive with those derived from petroleum. Biobased direct replacement compounds have clear potential benefits from the LCA perspective and can be tracked in final products by recognized ASTM test methods. As regulatory pressure on certain petrochemicals, including Bisphenol-A and certain phthalates, continues, new opportunities for bio-advantaged alternatives including isosorbide, furandicarboxylic acid and other new bioplasticizers will continue to expand. Like agriculture, the future for chemurgy is full of opportunities for new growth.

Acknowledgments

References

1. Finlay, M. R. *J. Ind. Ecol.* **2004**, *7* (3−4), 33–46.
2. Leeds, A. R. *J. Am. Chem. Soc.* **1882**, *4* (5), 58–61.
3. Zartman, W. H.; Adkins, H. *J. Am. Chem. Soc.* **1933**, *55* (11), 4559–4563.
4. Lazier, W. A.; Vaughen, J. V. *J. Am. Chem. Soc.* **1932**, *54* (8), 3080–3095.
5. http://tonto.eia.doe.gov/dnav/pet/hist/LeafHandler.ashx?n=PET&s=F000000__3&f=A.
6. http://www.ers.usda.gov/Data/AgProductivity/.
7. Begemann, B., Monsanto presentation at Goldman Sachs Fourteenth Annual Agricultural Biotech Forum, February 10, 2010. http://www.monsanto.com/investors/documents/2010/02_10_10.pdf.
8. *The Nature of What's To Come: A Century of Innovation*; Archer Daniels Midland: Decatur, IL, 2002.
9. *C&EN* **2006**, *84* (2), 32−33.
10. http://www1.eere.energy.gov/biomass/pdfs/ibr_arra_adm.pdf.
11. Frost, J. *Ind. Biotechnol.* **2005**, *1* (Spring), 23–25.
12. Marshall, J. *New Sci.* **2007**, *2611* (July 4), 28–31.
13. http://www.eia.doe.gov/oil_gas/petroleum/info_glance/petroleum.html.
14. Werpy, T.; Petersen, G. DOE Top Value-Added Chemicals from Biomass, 2004. http://www1.eere.energy.gov/biomass/pdfs/35523.pdf.
15. *C&EN* **2009**, *87* (22), 16−17.
16. Bloom, P. D. World Patent Application 2008051540A3, 2008.
17. Zacher, A. H.; Werpy, T. A.; Miller, D. J.; Frye, J. G., Jr. World Patent Application 2003035593A1, 2003.
18. Dasari, M.; Sutterlin, W. R.; Suppes, G. J. U.S. Patent Application 2008315151A1, 2008.
19. Alvarado, R. M.; Basile, P. S.; Briggs, J. R.; Hook, B. D.; Kruper, W. J.; Mehta, A. J.; Noormann, S. World Patent Application 2008128011A2, 2008.
20. Gilbeau, P.; Krafft, P. U.S. Patent Application 20080194847A1, 2008.
21. Krafft, P.; Gosselin, B.; Gilbeau, P.; Claessens, S. U.S. Patent Application 20090275726, 2009.
22. *C&EN* **2009**, *87* (40), 20.
23. Dubois, J. L. World Patent Application 2009044081, 2009.
24. Behrens, A.; Boelt, H.; Fritz, P. M; Korn, W. U.S. Patent Application 20080283798A1, 2008.
25. Katryniok, B.; Paul, S.; Capron, M.; Dumeignil, F. *ChemSusChem.* **2009**, *2*, 719–730.
26. Biodiesel 2020, Introduction and Executive Summary, Multi-Client Study, 2nd ed., 2008, Emerging Markets Online. http://www.emerging-markets.com/PDF/Biodiesel2020Study.pdf.
27. Impact of Biodiesel Production on the Glycerol Market, 2006. http://www.ruralsementes.com.br/produtos/Impact_of_Biodiesel_Production_on_the_Glycerol_Market.pdf.
28. http://www.globalbiochemna.com/Glycol_Products.html.
29. Kovacs, D. G.; Jackson, J. E.; Miller, D. J Abstracts of Papers, 221st ACS National Meeting, April 1−5, 2001, or Sinha, N. K.; Neurock, M. Abstracts

of Papers, 21st North American Catalysis Society Meeting, San Franscisco, California, June 7−12, 2009, P-M-88, paper 2162. http://www.nacatsoc.org/21nam/data/papers/Paper2162.pdf#page=1.

30. Alhanash, A.; Kozhevnikova, E.; Kozhevnikova, I. *Catal. Lett.* **2008**, *120*, 307–311.

31. http://www.adm.com/en-US/products/evolution/Propylene-Glycol/Pages/Life_Cycle_Analysis.aspx.

32. Moore, K. M.; Sanborn, A. J.; Bloom, P. U.S. Patent 7,439,352, 2008.

33. Stoss, P.; Hemmer, R. *Adv. Carb. Chem. Biochem.* **1992**, *49*, 93–173.

34. Noordover, B. A. J.; van Staalduinen, Vi. G.; Duchateau, R.; Koning, C. E.; van Benthem, R. A. T. M.; Mak, M.; Heise, A.; Frissen, A. E.; van Haveren, J. *Biomacromolecules* **2006**, *7*, 3406–3416.

35. Sablong, R.; Duchateau, R.; Koning, C. E.; de Wit, G.; van Es, D.; Koelewijn, R.; van Haveren, J. *Biomacromolecules* **2008**, *9*, 3090–3097.

36. Bachmann, F.; Reimer, J.; Ruppenstein, M.; Thiem, J. *Macromol. Chem. Phys.* **2001**, *202*, 3410–3419.

37. Storbeck, R.; Ballauff, M. *Polymer* **1993**, *34*, 5003–5006.

38. Kricheldorf, H. R.; Behnken, G.; Sell, M. *J. Macromol. Sci., Part A: Pure Appl. Chem.* **2007**, *44*, 679–684.

39. Chatti, S.; Kricheldorf, H. R.; Schwarz, G. *J. Poly. Sci., Part A: Polym. Chem.* **2006**, *44*, 3616–3628.

40. Kricheldorf, H. R. *J. Macromol. Sci., Rev. Macromol. Chem. Phys.* **1997**, *C37*, 599–631.

41. East, A.; Jaffe, Mi.; Zhang, Y.; Catalani, L. H. U.S. Patent Application 2008009599, 2008.

42. Roquette Presentation, BREW Symposium, Wiesbaden, Germany, 2005.

43. Kroger, M.; Prusse, U.; Vorlop, K.-D. *Top. Catal.* **2000**, *13*, 237–242.

44. Gong, W. H. World Patent Application 2009064515, 2009.

45. Doi, Y. *Microbial Polyesters*; VCH Publishers, Inc,: New York, 1990.

46. Kunioka, M.; Doi, Y. *Macromolecules* **1990**, *23*, 1933−1936.

47. Lu, J.; Tappel, R. C.; Nomura, C. T. *J. Macromol. Sci., Part C: Polym. Rev.* **2009**, *49*, 226–248.

48. http://www.adm.com/en-US/products/brands/envirostrip/Documents/Evolution_Biobased_Media.pdf.

Chapter 7

Cellulosic-Derived Levulinic Ketal Esters: A New Building Block

Cora Leibig,[*] **Brian Mullen, Tara Mullen, Lee Rieth, and Vivek Badarinarayana**

Segetis, Inc., 680 Mendelssohn Ave. N., Golden Valley, MN 55427
[*]cora_leibig@segetis.com

Levulinic acid and levulinate esters are a class of compounds readily derived from cellulose, hemi-cellulose, or starch feedstocks. The discovery of highly selective ketalization of alkyl levulinates is enabling the development of novel bio-derived monomers and derivatives with applications ranging from solvents, lubricants and plasticizers to polyols, thermosets, and thermoplastics. Levulinic ketal esters bring many unique and desirable traits to polymer-based products: for example, when compounded in PVC, they bring efficient plasticization with low migration; incorporated in liquid formulations, they bring broad solvency and excellent solvent coupling. Levulinic ketals have cost-effective compositional breadth, can be readily functionalized, and are thermally and chemically stable. These characteristics make levulinic ketals important building blocks for a future of sustainable materials.

Synthesis of Levulinic Ketals

Levulinic acid esters (LAE's) are a versatile class of chemical compounds derived from renewable feedstocks (*1*). LAE's contain two carbonyl functionalities, a carboxylate ester moiety and a ketone group. Reaction of 2 moles of alcohol or a diol with the ketone leads to ketal formation; and reaction of an alcohol with the carboxylate ester leads to trans-esterification. Figure 1 shows the formation of ketals or transesterification products of LAE's.
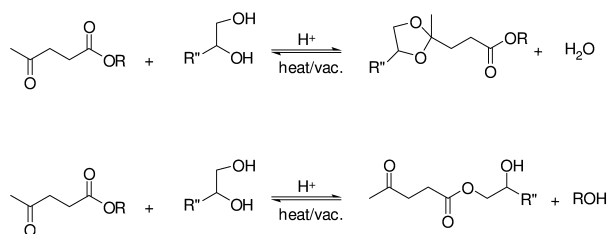
*Figure 1. Condensation of LAE by ketalization (top scheme) and
trans-esterification (bottom scheme).*

Table I. Reaction Data from Acid Catalyzed Ketalization of Keto-Esters

Catalyst	Moles of H⁺/Moles of limiting reagent	Conversion (%)	% Selectivity to Ketal
H_2SO_4	3×10^{-5}	> 99	100
H_2SO_4	3×10^{-3}	> 99	96.8
HCl	2.5×10^{-5}	> 99	100
Amberlyst® 15	2.5×10^{-5}	> 99	92.3
$NH_3^+SO_3^-$	2.5×10^{-5}	> 99	100

The condensation reactions of alcohols with ketones or esters typically use the same type and concentration of strong acid catalyst to complete the transformation. In this work, it was found that by using a substantially lower concentration of acid catalyst resulted in an unexpectedly selective reaction of the desired ketal versus the transesterified product. The selectivity of the formation of ketal was usually > 98%, and the reaction conversion reached > 99% in less than 1h of reaction time (*2*). A variety of acid catalysts, alcohols, and keto-esters were employed in this study to show the versatility of the method. The reaction was driven by the removal of water under vacuum at reaction temperatures ranging from 80-120 °C. The data in in Table I shows the selectivity and high reaction conversion for the ketalization of ethyl levulinate with glycerol. Consistent results were also observed with alcohols such as trimethylol propane and ethylene glycol and with keto-esters such as methyl-aceto acetate.

At low catalyst loadings, the reactions were very selective to ketal formations compared to trans-esterified by-products.   The use of the heterogeneous sulfonic acid catalyst, Amberlyst® 15, showed less selectivity compared to the homogeneous strong acid catalysts. Using weak acid catalysts, like sulfamic acid ($NH_3^+SO_3^-$), also resulted in high selectivity of ketalization compared to trans-esterification.

Physical Properties of Levulinic Ketals

Generally, levulinic ketal esters exhibit very low freeze points, high boiling points, and strong thermal stability. For example, EtLGK, the ketal product of glycerol and ethyl levulinate, has a freeze point below -60C, a viscosity of 37-40cP at 25C, a boiling point of 286C at 1atm, and does not thermally degrade significantly until it reaches temperatures of 300C. The ketal monomers are transparent and colorless liquids.

The chemical structures of levulinic ketals are unique in their diversity of functional groups. The presence of ester, ether, and (in some cases) hydroxyl functionality in the levulinic ketal brings about a "balanced hydrophilicity" that manifests itself in a broad solubility profile. EtLGK is miscible with water as well as aromatic hydrocarbons and some oils (e.g. castor oil). This broad solubility makes alkyl levulinic ketals outstanding solvents in a variety of oil- and water-based formulations such as cleaners, lotions, and paints.

This broad solubility characteristic carries over to polymer resins as well – levulinic ketals are excellent candidates to replace traditional solvents in coatings and adhesive applications. Segetis solvents have shown particular promise as coalescing solvents in water-borne latexes, with performance equivalent to incumbent fossil-based technologies and low VOC characteristics required in today's regulatory environment.

Derivatives of Levulinic Ketals via Trans-Esterification

Levulinic ketals can be used as building blocks for the synthesis of plasticizers, polyols and polymers. The derivatives of levulinic ketals can be synthesized via trans-esterification either at a hydroxyl pendant to the ketal or at the carboxylate end. Plasticizers have been synthesized by trans-esterification with commercially available ester and hydroxyl-functionalized products. Polyols with a range of functionalities and equivalent weights have been synthesized by trans-esterification with commercially available diols, triols and other multi-functional polyols. The trans-esterification may be carried out using traditional commercially available polycondensation catalysts at temperatures between 200 and 230C. These reactions may be carried out to high conversion and usually do not require subsequent purification to isolate the final product.

Plasticizers

Broad solubility of the levulinic ketals enables compatibility of extended levulinic ketals in a range of non-olefinic resins and thermoplastics. Over 25 levulinic ketal derivatives have been evaluated for plasticizer performance in PVC. Plasticizer efficiency, mechanical properties, resistance to extraction and migration, and processing were evaluated. A number of levulinic ketal candidates offer superior performance compared to the commercial phthalate plasticizers. The family of levulinic ketal plasticizers can access a wide range of properties. Overall, the levulinic ketal based plasticizers offer improved efficiency (Figure 2), superior resistance to non-polar extraction, equivalent resistance to polar

extraction (Table II), superior plastisol processing and viscosity stability, and equivalent dryblend processing when compared to benchmark phthalates. All levulinic ketal plasticizers offer extremely low vapor pressure, renewable carbon, broad miscibility, high efficiency with low extractables, and low migration in PVC across a wide molecular weight range.
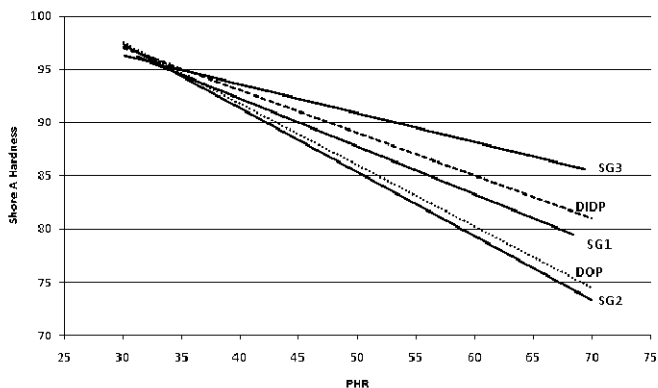
Figure 2. 15-second Shore A Hardness versus loading in parts per hundred resin (PHR) for di-octyl phthalate (DOP), di-isodecyl phthalate (DIDP), and three Segetis proprietary levulinic ketal plasticizers (SG1, SG2, SG3).

Table II. Extraction Weight Loss from a Controlled Geometry after 24h Immersion in Extraction Media with 70 phr Plasticizer Loading

	% Weight Loss		
	Hexane	*1% Soap in Water*	*Mineral Oil*
SG1	<1%	<1%	<1%
SG2	<1%	<1%	<1%
SG3	<1%	<1%	<1%
DOP	13%	<1%	<1%
Hexamoll® DINCH	27%	<1%	2%
Citroflex® A4	<1%	<1%	<1%

Rigid Insulation Foams	Must Have		Value-added	
	Insulation	Mechanical Properties	Versatile Chemistry	Bio-Based
Incumbent	+	+	+	--
Bio-alternative	-	--	-	+
Segetis	+	+	+	++

Figure 3. Relative performance of Segetis polyols in rigid insulation foam applications, compared to traditional polyol technology (polypropylene oxide based polyether polyol) and other natural oil bio-based alternatives.

Polyols

Segetis has produced a variety of ketal-based polyols for use in polyurethane foams and coating applications. Ketal-based polyols have ester linkages, however, their solubility characteristics are much more similar to polyether polyols than polyester polyols. The ketal polyol chains are amorphous, but more rigid than polyether polyols.

Segetis polyol technology allows foam producers to integrate high levels of bio-based content without sacrificing performance, particularly in applications requiring polyol stiffness. For example, efforts to incorporate natural oil-based polyols into polyurethane and polyisocyanurate foam insulation applications have been limited by loss of performance when more than a small percentage of natural polyols are used (*3*, *4*). Segetis polyol technology allows incorporation of higher levels of bio-based content in rigid insulation foams without loss of physical and thermal properties (Figure 3).

Conclusions

Levulinic ketals, enabled by the development of selective ketalization of levulinic acid esters, are a broad family of bio-based compositions with performance advantages in many applications. These compounds have broad solubility enabling their use as cleaning solvents or coupling agents in liquid formulations. When extended by trans-esterification, levulinic ketals can make effective plasticizers for a range of plastic compounds including PVC; can make polyols for polyurethane materials; and can be extended for use in polyester thermosets or thermoplastics.

Acknowledgments

References

1. *Top Value Added Chemicals from Biomass*, Volume I, U.S. Dept. of Energy Report; Werpy, T., Petersen, J., Eds.; Contributions from NREL, PNNL, and EERE, 1994.
2. Selifonov, S.; Rothstein, S.; Mullen, B. Method of Making Ketals and Acetals. Patent WO/2009/048874, 2009.
3. Singh, S. N.; Dubs, S.; Pilgrim, J. New Developments in Polyisocyanurate Laminate Foam Formulation and Processing. In *Proceedings of the Polyurethanes 2008 Technical Conference*, 2008.
4. Lambert, T.; Yao, J.; Lipske, G.; Hill, L. Effects of Natural Oil Polyols on Properties of Polyisocyanurate Foams. In *Proceedings of the Polyurethanes 2008 Technical Conference*, 2008.

Chapter 8

Biopolymers, Processing, and Biodegradation

Bo Shi,* Vasily Topolkaraev, and James Wang

**Corporate Research & Engineering, Kimberly-Clark Corporation,
2100 Winchester Road, Neenah, WI 54956
*bshi@kcc.com**

The recent advance in converting natural polymers such as starch, protein, and cellulose for melt processing is briefly reviewed. The technical challenges for using natural polymers for thermoplastic applications and recent innovation in extrusion plasticization of starch enabling rapid expansion of starch for high valued polymer applications are summarized. Synthetic biopolyesters including polylactic acid (PLA), terpolymer of terephthalic acid, adipic acid, and butandiol (Ecoflex polymer), and polybutylene succinate (PBS) are also briefly reviewed and provided with a special focus on inherent properties relevant to fiber and nonwoven applications. Technical approaches are discussed to enable high performance biopolyester melt spun webs. The effects on crystallization kinetics of heterogeneous nucleation with various nucleating agents are explored by using Avrami model. Process modifications are discussed including heated quench and heated fiber draw to maximize fibrous web crystallinity. Some biopolymers such as starch, protein, algae, and spunbond PLA are selected for anaerobic biodegradation in order to understand how they behave in the waste disposal environment. The results indicate that starch can achieve a complete biodegradation within about one month timeframe, whereas protein and algae can achieve 62 to 70% biodegradation. PLA biodegradation in anaerobic conditions is highly affected by degrading temperatures relative to its glass transition temperature.

Introduction

Natural Polymers

From prehistoric times, natural polymers played a critical role to the survival and civilization of human beings, providing the essential food, clothing, and sheltering. However, the natural polymers used for most of the time were natural polymers in their native forms such as cotton fiber, pulp fibers, silk fabric, tanned leather, and native starches.

The most utilized natural polymers are polysaccharides including cellulose, starches, etc. Among natural polymers, cellulose is the most abundant biomass produced annually, it is present in a broad range of plant species such as trees, grasses, and agricultural crops. Cellulose is a completely linear, semi-crystalline homopolymer of β-D-glucopyranose units linked by 1-4 glycosidic bonds. Cellulose molecules are organized into crystalline regions and amorphous regions, further organized into cellulose fibers (*1*). Cellulose is the main component of woods which are used in a wide range of structural materials for buildings and furniture. Pure cellulose is commonly separated from plants using various pulping processes, pulp fibers are utilized in writing and printing papers, industrial papers, consumer products such as facial tissue, bath tissue, and disposable personal care products, etc.

Modified cellulose was the first plastic material human made prior to the development of modern synthetic polymer industry. Celluloid was the first thermoplastic material invented in 19th century, it was made from nitrocellulose, camphor, dye and additives. Celluloid was used as an ivory and horn replacement material in billiard balls, jewelry, boxes, buttons, handles, frames, etc. (*2*)

Modified cellulose includes cellulose esters with either inorganic acids (cellulose nitrate, cellulose sulfate, cellulose phosphate) or organic acids (cellulose acetate, cellulose propionate, cellulose butyrate, cellulose salicylate, etc.). The applications of nitrocellulose include plastic, lacquers, photographic films, explosives, etc. Cellulose acetate was used as a safe photographic film material in large volume for many decades prior to age of digital photography. Cellulose ethers including alkyl cellulose (e.g. methyl cellulose, ethyl cellulose, hydroxyalkyl cellulose such as hydroxyethyl cellulose and hydroxylpropyl cellulose) are useful as thickeners, dispersing agents, stabilizers, additives for pharmaceutical products.

Regenerated cellulose is made from the extrusion or spinning of soluble cellulose xanthate into coagulation baths containing sulfuric acid, sodium sulfate, etc. Important regenerated cellulose includes cellophane film and rayon fiber. Cellophane is a transparent film recently promoted as biodegradable and renewable film with a low permeability to air, oil, and grease, however, it is semi-permeable to moisture. Cellophane was extensively used as food packaging films prior to the arrival of low-cost, large-volume packaging films synthesized from petroleum derived olefins, it is still used today in some specialty packaging films such as candy wraps, industrial films as base film for tapes, etc.

Rayon is semi-synthetic regenerated cellulose fiber made from a variety of cellulose raw materials such as wood, cotton, hemp, bamboo, etc. (*3*) Rayon fiber is used broadly in apparels, bedding products, disposable person hygiene

products including feminine pads and liners, furnishings, window treatment, medical products, tire cords, lighter fillings, etc.

Native cellulose, a majority of modified cellulose, as well as regenerated cellulose is not thermoplastic. Continuous cellulose films and fibers were typically made from solution-based film extrusion and spinning processes, only selected cellulose derivatives could be made into thermoplastic via plasticization.

Starch is another major type of polysaccharides used mostly in food products and to a less degree in industrial products. Starch is also a polysaccharide biosynthesized from α-glucose monomer units via glycolic bond formation. Starch is composed of a mixture of a linear, helical amylose and a highly branched amylopectin; the ratio of the two starch moieties depends on the plant sepecies, typically, amylose content is from 20 to 30% and amylopectin ranges from 70 to 80% (*4*).

Besides food applications, starch is used extensively as sizing agents in paper industry, as adhesive in corrugated board industry. Other applications include laundry starch, textile industry, baby powders, oil production, and bioplastics (*5*).

Lignin is yet another major natural polymer. In nature, lignin is the second most abundant natural polymer exceeded only by cellulose. Native lignin provides a key functional role in plants by creating hydrophobic polymer to protect highly hydrophilic cellulose and hemi-cellulose components. The chemical structure of lignin is significantly more complex than cellulose, hemicellulose, or starch. It has a three-dimensional crosslinked structure derived from various substituted phenylpropane structure units (*1*). In pulp and paper industry, lignin only remains in high yield pulp such as newsprint pulp. In most pulping processes, lignin is removed by chemical deligninification process during cooking step and becomes the major organic component of spent liquors. In Kraft process, lignin in black liquor is mostly burned as fuel to recover the latent energy of lignin. In sulfite process, lignin sulfonates are used as dispersants in high performance cement, as raw material for production of such chemicals as vanillin, xylitol, dimethyl sulfoxide (DMSO), textile dyes, and oil field applications.

Protein is yet another major natural polymer. Most animal proteins are used for food consumption for human and pets. While the majority of plant proteins are in harvested grains such as soybeans, wheat, corn, etc., they are used as animal feed. Recently, plant proteins were explored as a bioplastic component for polymer blends, composites, and environmentally friendly adhesives without releasing harmful formaldehyde.

Synthetic Biodegradable Polymers

Synthetic biopolymers include biodegradable, compostable resins that are derived using synthetic chemistry routes. These polymers include resins produced from renewable feedstock, as well as hundred percent petro-based polymers. Typically synthetic biopolymers are polyesters such as aliphatic polyesters and aliphatic aromatic polyesters.

Aliphatic polyesters can be synthesized from the polymerization of a polyol with an aliphatic carboxylic acid or anhydride. Examples of aliphatic polyesters include polybutylene succinate (PBS), polyethylene succinate (PES),

polypropylene succinate (PPS) and their copolymers. Specific commercially available examples of polybutylene succinate and polyethylene succinate biopolymers are ENPOL™ resins produced by Ire Chemical, South Korea and Bionolle® resins from Showa Highpolymer of Japan. Besides being primary aliphatic, biopolyesters can contain aromatic monomers. Aliphatic-aromatic bio-copolyesters can be synthesized by polymerization of polyol in conjunction with aliphatic and aromatic dicarboxylic acids. One example of such copolyesters is polybutylene adipate thereptthalate (PBAT) which is commercially available from BASF under designation ECOFLEX® resin. All these resins are biodegradable, but derived from petro based monomers. Fiber spinning and nonwovens fabrication from these resins can be challenging due to slow crystallization rate during fiber spinning, high tack, and limited draw ability to achieve desired molecular orientation in fiber structure.

Polylactic acid, a renewable feedstock polymer also belongs to the family of aliphatic polyesters commonly made from α-hydroxyl acids, which include polyglycolic acid or polymandelic acid. Polylactic acid (PLA) can generally be derived from monomer units of any isomer of lactic acid, such as levorotory-lactic acid (L-lactic acid), dextrotatory-lactic acid (D-lactic acid), meso-lactic acid, or mixtures of L-, D-, and meso-lactic acids. Homopolymers and copolymers of both lactic and glycolic acid have been a subject of many publications in literature (*6*). Specific examples of commercially available PLA polymers include Natureworks LLC Ingeo® PLA resin and LACEA™ PLA of Mitsui Chemical.

Environmental Testing Standards

Biodegradable products appear to be a good alternative to conventional plastics. Bioeconomy Institute at Iowa State University is one of examples to work on biobased products using renewable resources. Biodegradable plastic industry is fundamentally important to prosperity in biobased economy and needs environmental testing standards to help guide research and development of various plastic materials. In recent years, acceptable standards were outlined in American Society for Testing and Materials (ASTM) (*7*, *8*). Many natural biodegradable polymers such as starch and protein cannot fulfill the performance requirements alone as plastics material, therefore, they are normally blended with synthetic polymers to produce plastics which meet functional requirements. However, most synthetic polymers such as polyethylene are not biodegradable. The first generation of degradable plastics, polyolefin-starch based materials, didn't degrade as claimed (*9*).

Plastics can undergo a variety of degradation mechanisms that are normally classified as degradable, biodegradable, photodegradable, oxidatively degradable, hydrolytically degradable, and compostable. Each of these modes of degradation was defined together with an outline of standard testing protocols (*7*). In this chapter, we will focus on aerobic and anaerobic biodegradation because they are frequently used in assessing the fate and effect of environmental polymers.

Aerobic biodegradation refers to microbial activities in the presence of oxygen to convert organic carbon into simple water, carbon dioxide, and biomass. Standard testing methods for aerobic biodegradation comprise plastics

degradation through composting (D5338, D5509, D5988, and D5521) or activated sludge (D5209, D5271, and D5247). The specifications for passing criteria were defined in D6400. During anaerobic biodegradation, microbial activities don't need the presence of oxygen. Standard testing methods are those of D5210, D5511, and D5526. International Standard Organization (ISO) issued three sets of the criteria by which European biodegradable plastics are currently assessed. They are ISO 14855 for a controlled aerobic composting test, ISO 14852 for aerobic biodegradation in aqueous environment , and ISO 15985 for anaerobic biodegradation in a high solids environment (*10*). ASTM and ISO methods are complementary.

There are several other testing methods developed by other entities such as European Committee for Normalisation (CEN). However, we will not discuss them here since they are more or less similar to those developed and issued by ASTM or ISO. In particular, we will not discuss testing standards for oxo-degradable polymers (*11*, *12*) because they are not biopolymers (*13–16*).

In recent years, there are many examples about false environmental sustainability claims about plastic products in the marketplace. Federal Trade Commission (FTC) has issued environmental marketing guidelines, which states that an unqualified claim that a product or package is degradable, biodegradable or photodegradable should be 1) substantiated by competent and reliable scientific evidence; 2) show that the entire product or package will completely break down and return to nature, i.e., decompose into elements found in nature; 3) within a reasonably short period of time; and 4) after customary disposal (*17*, *18*).

The FTC's Guides for the Use of Environmental Marketing Claims explain how the FTC Act is enforced when it comes to environmental claims. The Guides provide a framework for the use of environmental advertising and labeling claims in the marketplace: they reduce consumer confusion, help establish a level playing field for competition, and reduce the legal risk for marketers. That's important because increasingly, local and state jurisdictions are relying on the Guides for direction on enforcement.

It should be pointed out that FTC dominates US market practices. Other regions or countries should consult their respective legal entities for specific information on claims and labeling, etc. For example, Canadian Plastic Industry Association advocates that claims of degradability be made in accordance with Industry Canada No. 11368 94-03 – "*Principle and Guideline for Environmental Labeling and Advertising*.

Biopolymer Processing and Modification

Converting Non-Thermoplastic Natural Polymers to Thermoplastic Polymers

Native cellulose is not thermoplastic, the melting temperature of cellulose is higher than its decomposition temperature. Only certain cellulose derivatives such as cellulose ethers (e.g. methyl cellulose, ethyl cellulose, hydroxyl ethyl cellulose, hydroxylpropyl cellulose, etc.) and cellulose esters such as cellulose alkanoates and mixed cellulose esters showed limited thermoplastic processability. By using

appropriate plasticizers, thermoplastic cellulose can be melt extruded into films, molded articles, etc.

Similar to cellulose, native starch is also not thermoplastic. Recently, a number approaches were developed to convert native starch into thermoplastic starch (*19*, *20*). In general, native starch is mixed with one or more plasticizers such as a polyhydric alcohol, water, or a polymer (*21*) under heat and shear of an extruder, native starch is converted into thermoplastic starch (TPS) or plasticized starch materials (PSM). However, the thermoplastic starch has only limited utility due to the high water sensitivity and high stiffness.

For practical applications, useful polymer blends are prepared from TPS with biodegradable polymers such as aliphatic polyesters [e.g. polybutylene succinate (PBS), polylactide (PLA), polyhydroxy alkanoate (PHA), aliphatic-aromatic copolyesters, etc.]. The resulting blends can be made into thin films for biodegradable and compostable applications. Applications include packaging films for both food and non-food items, shopping bags, compostable garbage bags, mulching films for agricultural and nursery applications, injection molded articles for personal care, apparel, household applications, etc.

Recent work on utilizing low-cost renewable polysaccharide materials for thermoplastic, water dispersible film applications was reported (*22*, *23*). Water-dispersible films are typically made from expensive synthetic polymers such as plasticized polyvinyl alcohol, polyethylene oxide, etc. These synthetic polymers are not sustainable and also have a high carbon footprint. Therefore, there is an interest in developing alternative water-dispersible thin films from renewable resources.

Starch and thermoplastic native starch are not water dispersible. In order to develop water-dispersible films, the work was focused on exploring modified starches. Modified starches investigated include starch esters, starch ethers, pregelatinized Tapioca dextrin, and hydroxyalkyl starch.

The conversion from non-thermoplastic modified starch into thermoplastic starch was accomplished by plasticization inside a twin screw extruder. Subsequently, the melt rheology and water-dispersibility of the converted thermoplastic modified starch (TPMS) were characterized. Among the modified starches, three modified starch: Tapon ND (starch ester), Instant-n-Oil (pregelatinized Tapioca dextrin), and Glucosol 800 (a hydroxypropyl starch) were found to be water-dispersible. The rheological data of the three thermoplastic modified starches (TPMS) are shown in Figure 1.

The tensile properties for starch ether and the copolyester blend film were a little better than the films made from blend starch esters and copolyester. The peak stress of thermoplastic hydroxypropyl starch and copolyester film is shown in Figure 2.

In Figure 2, the film MD stands for machine direction when the film is cast, and the film CD stands for cross direction which is perpendicular to the machine direction. The peak stress is defined as film peak value on stress-strain curve.

The resulting films of TPMS with the biodegradable copolyester were dispersible in water at low level of copolyester. As copolyester content increases, the water dispersibility of the films decreases, showing the tailorability of the water dispersity to meet specific application needs.

Melt Rheology Comparison of TPS at 150°C
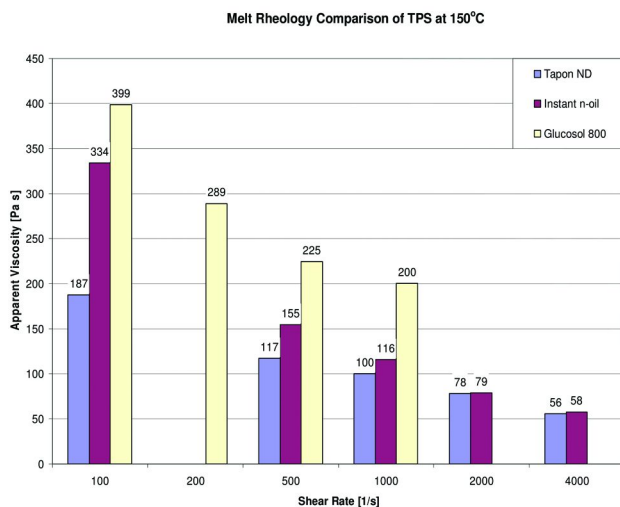
Figure 1. Melt Rheology of Thermoplastic Modified Starch at 150°C.

Peak Stress Comparison of Glucosol 800 TPS/Ecoflex Blends
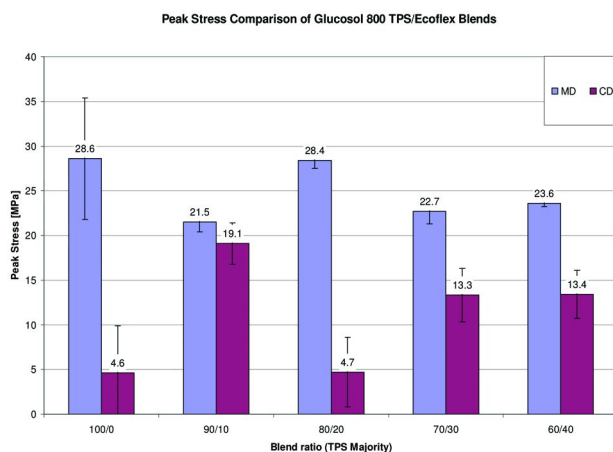
Figure 2. Peak Stress of A Thermoplastic Hydroxypropyl Starch and Copolyester Binary Polymer Blend Films.

The study has demonstrated that it is possible to develop renewable resource-based thermoplastic, water-dispersible thin films.

PLA Fiber Processing

Assessing fiber melt spinning of synthetic biopolymers is important to guide on development of fibrous structures such as nonwoven webs including spunbond and melt blown webs. Key parameters to be considered include molecular weight and melt flow rates, moisture sensitivity, crystallization rate and resin crystallinity, melt strength and fiber draw ability, melting profiles. Let us consider example of PLA resin.

PLA with a number average (Mn) molecular weight in the range 50,000 grams per mole and up to 120,000 grams per mole is used for melt spinning. The ratio of the weight average molecular weight to number average molecular weight is typically low and is in the range of 1.2 to 1.8. The melt extrusion is usually carried out at temperatures at least 20°C higher than melting temperature and typically is in the range of 190°C to 240°C. PLA extrusion and melt spinning is very sensitive to moisture. Water is capable of hydrolytically degrading the polylactic acid thus reducing molecular weight below desirable level. Hydroxyl groups of water can attack the ester linkages of PLA chain, thereby leading to chain scission or "depolymerization" of the polylactic acid molecule into shorter chains, oligomeric structures, and even monomers. High temperature and shear can accelerate this depolymerization process significantly making polymer unsuitable for spinning. Water content below 100 parts per million (ppm) is recommended for PLA melt spinning.

Polylactic acid is slow crystallizable polymer with high glass transition. The slow crystallization rates can arise when crystallization is hindered by slow nucleation. Slow crystallization rate might relate also to molecular mobility constrains when crystallization temperatures are close to PLA glass transition temperature of 60°C.

To achieve high fiber crystallinity during melt spinning and quenching process, PLA filaments typically spun at high speed take-up velocities of 4000 m/min and up to 6000 m/min with draw down ratio of up to 4000 or more (24–27). However, very high take-up fiber velocities are not always desirable as they might produce a fiber orientation during the formation of a fibrous web that is excessively biased along machine direction of the production process. Also, excessively high draw down ration can result in very high molecular orientation that can negatively affect fiber ductility and elongations at break.

To accelerate crystallization process, nucleation and molecular mobility constrains can be reduced by addition of plasticizers and nucleating agents (25, 28). Avramy equation can be used to evaluate effects of additives on isothermal crystallization kinetics (Crystallization Kinetics, Encyclopedia of Polymer Science and Engineering, John Wiley & Sons, pp. 231-241):

$$\theta = 1 - \exp\left(- kt^n\right) \qquad (1)$$

where

- Θ - percent total crystallinity
- t - crystallization time
- n - morphological factor related to crystal growth geometry
- K - rate parameter of a crystal growth

Table 1 illustrates results of isothermal crystallization kinetics study where Avramy model was used to determine crystallization kinetics parameters for the synthetic aliphatic polyesters, PLA and PBS (Bionolle®), and PLA blends with inorganic talc, and organic 4-biphenylcarboxylic acid (4-BP) nucleating agents, and a polyethylene glycol, Carbowax 8000 plasticizer. The Avramy parameters

K, which can be normalized as $K^{1/n}$, and n were determined using differential scanning calorimetry method described in (29). Temperature column represents isothermal crystallization temperatures representing temperatures at which material most rapidly crystallizes. $T_{1/2}$ illustrates crystallization half time of the material, that is the time required for the crystallinity of the selected materials to reach 50% of its equilibrium crystallinity. The equilibrium crystallinity is the maximum crystallinity level attainable by a material during isothermal crystallization.

The Avrami constant, K can be graphically plotted as a function of temperature. For the PLA polymer, this plot has a bell shape with the maximum corresponding to the temperature at which material most rapidly crystallizes.

As can be seen from Table 1, the PLA crystallization half times are in the range of 600 seconds as compared to polypropylene 140 seconds and Bionolle® 1020 polyester of 68 seconds. Addition of talc nucleating agent significantly accelerates crystallization process with crystallization half time of 44 seconds. Blending of a polyethylene glycol plasticizer, PEG8000 at 5% addition by weight also significantly reduces crystallization half times. Data illustrated in Table 1 suggests that nucleation and plasticization additive formulations can be developed for biopolyester fiber process to reduce nucleation and mobility constraints during crystallization. When using this approach, attention should be paid to fiber spinning and drawing process, as addition of low molecular weight plasticizers and additives can potentially negatively affect polymer melt strength and fiber draw ability during spinning.

Alternative approach to enhance fiber crystallinity at moderate fiber velocities and draw down ratios is to use anneal-quench temperatures during fiber quenching stage approximating a prime-temperature range of most rapid crystallization rate of PLA polymer. During fiber spinning, it is desirable to maximize crystallization rate to achieve a maximum amount of crystallinity in the fiber material during short residence time when fiber is being spun. The maximum crystallization rate temperature for PLA polymer is in the range of 100°C. The anneal-quench temperature during fiber spinning can be in the range from 20°C above PLA glass transition temperature (PLA Tg =~ 60°C) and up to 110°C to maximize crystallization rate during fiber spinning. Using anneal-quench approach fiber crystallinity can be maximized at moderate fiber velocities and fiber uptake speeds. Figure 3 illustrates dependence of PLA fiber crystallinity by x-ray diffraction method and fiber size produced using anneal quench (hot quench) and cold quench conditions in dependence of fiber draw pressure. As illustrated in Figure 3, at moderate draw pressures higher fiber crystallinity can be achieved using hot quench conditions. Fiber size produced with hot quench is typically larger across draw pressures, as more crystalline fibers are not being drawn to finer diameter as compared to less crystalline fibers. (28).

At moderate draw pressures in the range of 50kPa to 60kPa up to 50% increase in fiber crystallinity can be achieved by using heated quench conditions approximating temperatures that maximize crystallization rate of biopolymer. In addition, fibers can be drawn at higher draw pressures maximizing overall fiber crystallinity (28). The heated quench process can be applied during spunbond

nonwoven manufacturing resulting in webs with high strength and more balanced machine direction to cross direction web properties (*28*, *30*).

Polymer Biodegradability

Materials

Some plant polymers such as starch and protein and synthetic biopolymers such as PLA are examples of biopolymer degradation in the anaerobic environment. Native corn starch, Cargill Gum™ 03460, was purchased from Cargill, Inc. (Minneapolis, MN). Soy protein isolate, PC4200, was purchased from DuPont Soy Polymers (Louisville, KY), containing a minimum of 90% proteins.

Table 1. Isothermal Crystallization Avramy Parameters

Material	Temperature °C	n	$K^{1/n}x1000$	$T_{1/2}$, sec
PLA6200	105	2.1	1.3	645
Bionolle® 1020	80	2.79	12.9	68
PP PF-305	120	2.67	6.23	140
PLA/Talc	115	3.2	20.35	44
PLA6200+4-BP1%	100	2.55	11.4	76
PLA6200+PEG5%	110	2.23	6.2	100
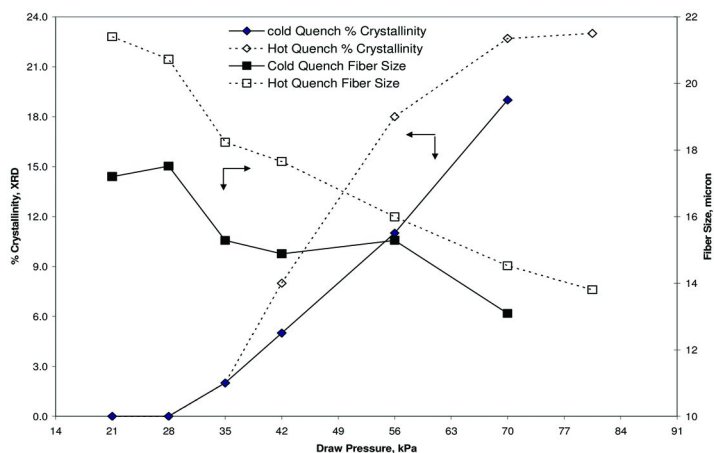
Figure 3. PLA fiber crystallinity and size versus draw pressure for heated and cold quench conditions.

Spirulina were obtained from Earthrise (Calipatria, CA). This type of algae bimass grows in warm, alkaline fresh-water bodies. It is a member of the class Eustigmatophyceae. The algae have both chlorophyll (green) and phycocyanin (blue) pigments in their cellular structure. Once harvested, they are in a form of fine powder with particle size at about 0.25 mm and a bulk density is 0.35 - 0.6 kg/liter.

The PLA samples were prepared using the neat PLA purchased from NatureWorks LLC (Minnetonka, MN) and used for anaerobic sludge digestion under 35, 50, and 65 °C, respectively. The weight averaged molecular weight of the PLA sample ranges from 110,000 to 160,000 grams per mole.

The digested sludge was collected from the Neenah-Menasha Regional Wastewater Treatment Facility, which operates single-stage digestion with sludge residence time estimated about 14 days. Solids content in the digested sludge was 2.5% and the pH of the digested sludge was within a range of 7.4-7.8. The digested sludge color is black because of the presence of organic matter.

Methods

Anaerobic sludge digestion was carried out according to D5210 except for PLA study where two sets of data obtained under the digestion temperatures of 50 and 65 °C. The high temperature at 50 and 65 °C served as a selector for a consortium of microorganisms from the mesophilic (25-40 °C) to thermophilic (55-65 °C) bacteria population (*31*).

Biodegradability Calculations

In chemical terms, a PLA monomer can be expressed as $[-C_3H_4O_2-]$. Therefore, its total conversion to methane and carbon dioxide can be estimated from the following equation (2):

$$[-C_3H_4O_2-]_n + H_2O = n\frac{3}{2}CH_4 + n\frac{3}{2}CO_2 \tag{2}$$
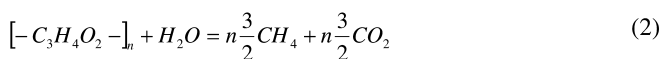
where "n" represents the number of repeating units in the polymer and can be as large as many thousands. As indicated in Equation (2), one mole of PLA monomer can, in theory, generate a total three moles of methane and carbon dioxide under standard conditions. For example, about 0.2 grams of the PLA material was used for each anaerobic sludge digestion experiment reported in this paper. Thus, $V_{Theoretical}$, potential total gas production from PLA sample is 186 mL, based on about 50% carbon composition in PLA material and one mole of gaseous carbon occupying 22.4 L under standard conditions. For experiments other than standard conditions, a correction factor has been considered in calculations for a percentage of PLA biodegradation, as shown in D5210.

The accumulated net CO_2 and CH_4 gas generation, $\sum V_{Sample}$ was obtained from an average of three samples after the accumulated CO_2 and CH_4 gases, generated from three blanks that are just anaerobically digested sludge without

PLA sample, $\sum V_{Sample}$, are subtracted. The equation (3) is then used to estimate PLA biodegradability.

$$Bio\deg radability = \frac{\sum V_{Sample} - \sum V_{Blank}}{V_{Theoretical}} \times 100\% \tag{3}$$

Cellulose is normally used as a reference material so that biodegradation of carbohydrate samples can be compared. The evolved gas (CO_2 + CH_4) volume is dependent on only the carbon amount regardless of the CO_2 and CH_4 ratio (*32*). For samples with the T_g modification, actual carbon content (%) is analytically determined and used for $V_{Theoretical}$ estimates.

Statistical Analysis

All data represented the mean of three independent experiments. Error bars shown in figures are standard deviations calculated using a method outlined by Young (*33*).

Plant Polymers

Anaerobic sludge digestion experiments were carried out to test plant polymer anaerobic biodegradation at a constant temperature of 35 °C with cellulose powder as the reference for the study. Figure 4 presents the results for starch, protein, and algae samples with a percentage of biodegradation calculated using Equation (3). In all sample data, a net amount of carbon dioxide and methane was obtained after subtraction of those from blanks that contained only the digested sludge without the presence of polymer samples. The blank sample is defined as digested sludge without the presence of the carbohydrate polymer samples. Although it is not shown in Figure 4, cellulose biodegradation under the same conditions achieved more than 75% biodegradation, indicating reliability of testing protocol for data collection.

The degree and rate of native corn starch biodegradation are faster and more complete than soy protein and algae. Soy protein isolate only achieved about 62-65% mineralization within 72 days of anaerobic digestion. The results seem to indicate that the protein aggregates are less accessible by microorganisms. Spirulina achieved about 70% biodegradation, which is slightly better than soy protein. Kinetically, both soy protein and algae biodegradation are slower than starch and cellulose material (*34*). The study of algae biodegradation is important because algae biomass can be processed into thermoplastic materials (*35*).

Polylactic Acid

Anaerobic sludge digestion experiments were arranged to test the neat PLA biodegradation at constant temperatures of 35, 50, and 65 °C, respectively, where the biodegrading temperature at 65 °C was slightly above the glass transition temperature of the neat PLA samples. Figure 5 presents the consolidated results for three sets of the neat PLA samples under experimental conditions specified

above. The y-axis in Figure 5 presents a percentage of biodegradation for each set of the sample calculated according to Equation (3). The x-axis shows the time for sample sludge digestion. In about three months, the PLA sample degraded at 65 °C achieved about 89% mineralization. However, it took about nine months for PLA sample to achieve the similar level of biodegradation when the degrading temperature was fixed at 50 °C, which was below PLA T_g. Further, it took about a year for PLA sample to achieve only 30% biodegradation at 35 °C, which echoes to the earlier observations reported by Shin et al. (*36*).

Additional study includes PLA biodegradation affected by altering its glass transition temperature. When the temperature is higher than PLA glass transition temperature, anaerobic biodegradation is accelerated (*37*). The information on PLA temperature-dependent biodegradation is important to waste management.
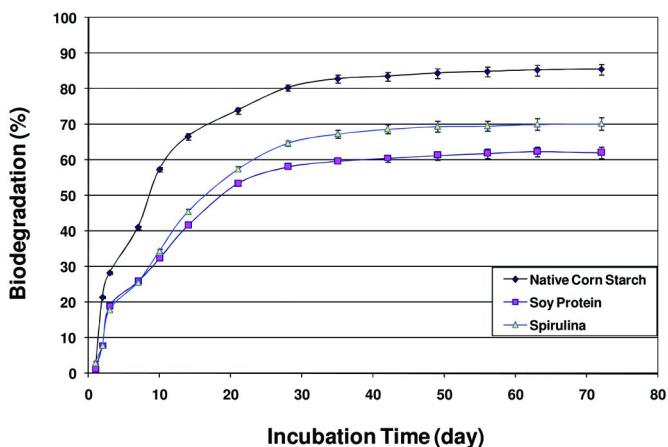
Figure 4. Plant Polymer Anaerobic Biodegradation at 35 °C
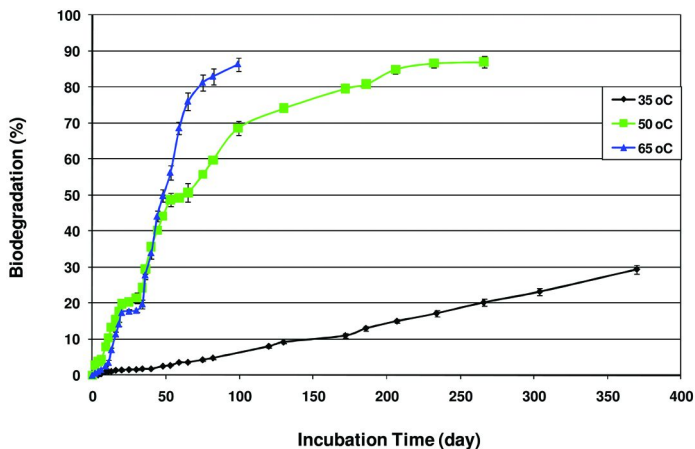
Figure 5. PLA Anaerobic Biodegradation at Different Temperatures

129

Conclusions

Before the dawn of the polymer age in the 20th century, human relies on naturally occurring biopolymers to meet their essential needs. Modification chemistry was developed to overcome the deficiencies of natural polymers for plastic applications. Among the modified natural polymers, modified cellulosics were the first artificial biopolymers for making packaging films, fibers, and molded articles. Other natural biopolymers explored extensively include starch, proteins, alginate, lignin, and hemicellulose.

Technical success in blending thermoplastic starch with other biodegradable polymers allowed the entrance of starch-based materials for highly demanding thin film applications. Examples of such applications in packaging films and flushable films applications are illustrated.

Research in meltspun fibrous structures produced from bio-polyesters has received increased attention in recent years. Melt spinning of polylactic acid (PLA) biopolyester has been of a special focus because PLA origination from renewable feedstock and its potentially low environmental footprint. (*38*). PLA can be processed using existing fiber spinning and nonwoven lines and has processing advantages such as high melt strength and good draw ability, reduced processing temperatures that are in a range of polypropylene processing, as compared to high process temperature requirements for polyethylene therepthalate. However, many challenges still exist in melt spinning and bonding of PLA webs, as well as in achieving desired processing and mechanical performance for PLA nonwovens. Among these challenges are PLA slow crystallization rate, high glass transition temperature, narrow melting profiles and low ductility.

The new trend in plastic industry demands the use of more natural biopolymers because they are viewed as sustainable, renewable and biodegradable.

Assessment of polymer biodegradability is a very important step to guide sustainable and renewable material development activities. It would be difficult to judge environmental footprint of biopolymers and product claims substantiation without such vigorous evaluations.

Anaerobic biodegradation assessments of natural biopolymers such as starch, protein, and algae as well as synthetic biopolymers such as polyatic acid indicate they can be assimilated and converted into water, methane, and carbon dioxide by microbials. The environmental factors such as temperature and the pH would have a significant effect on the rate of biopolymer degradation. Under composting environment, PLA degrades easily. However, its biodegradation is temperature-dependant in the anaerobic environment.

References

1. Sjöström, E. *Wood Chemistry: Fundamentals and Applications*; Academic Press: New York, 1981.
2. Fenichell, S. *Plastic: The Making of a Synthetic Century*; Harper Business: New York, 1996; p 17.
3. Kaufman, G. B. *J. Chem. Ed.* **1993**, *70*, 887.

4. Panda, H. *The Complete Technology Book on Starch and Its Derivatives*; NIIR Consultancy Project Services, 2004.
5. Radley, R. A. *Industrial Uses of Starch and Its Derivatives*: Applied Science Publishers: London, 1976.
6. Garlotta, D. J. *Polym. Environ.* **2001**, *9*, 63–84.
7. Narayan, R.; Pettigrew, C. ASTM Standards Define and Grow Biodegradable Plastics. ASTM Standards News, 1999.
8. Steven, E. S. *Green Plastics: An Introduction to the New Science of Biodegradable Plastics*; Princeton University Press: Princeton, NJ, 2001.
9. Greene, J. P. Biodegradable, Compostable, and Synthetic Plastics Biodegradation Testing in Compost, Marine, and Anaerobic Environments. Oregon Recyclers Conference, Salem, OR, 2008.
10. NIIR Board. *The Complete Book on Biodegradable Plastics and Polymers (Recent Developments, Properties, Analysis, Materials & Processes)*; Asia Pacific Business Press, Inc.: Delhi, India, 2006.
11. Scott. G. Science and Standards. In *Biodegradable Polymers and Plastics*; Chiellini, E., Solaro, R., Eds.; Kluwer Academic/Plenum Publishers: New York, 2003.
12. BSI 8472 (Draft). Packaging – Determination of the Compostability (Including Biodegradability and Ecotoxicity) of Packaging Materials Based on Oxo-degradable Plastics; British Standard Institute, 2004.
13. Billingham, N. C.; Bonora, M.; De Corte, D. Environmentally Degradable Plastics Based on Oxo-biodegradation of Conventional Polyolefins. In *Biodegradable Polymers and Plastics*; Chiellini, E., Solaro, R., Eds.; Kluwer Academic/Plenum Publishers: New York, 2003.
14. Chiellini, E.; Corti, A.; Swift, G. *Polym. Degrad. Stab.* **2003**, *81*, 341.
15. Chiellini, E.; Corti, A.; D'Antone, S.; Baciu, R. *Polym. Degrad. Stab.* **2006**, *91*, 2739.
16. Chiellini, E.; Corti, A.; D'Antone, S. *Polym. Degrad. Stab.* **2007**, *92*, 1378.
17. Federal Trade Commision. 16 CFR Part 260 Guides for the Use of Environmental Marketing Claims, 1998. http://www.ftc.gov/os/1998/04/greengui.fr1.htm.
18. Federal Trade Commission. Guide to Environmental Marketing Claims, 1999. http://www.ftc.gov/bcp/conline/pubs/buspubs/epaclaims.shtm.
19. Bastioli, C.; Bellotti, V.; Lombi, R.; Perego, G. U.S. Patent, 6,506,824 B1, 2003.
20. Loercks, J.; Pommeranz, W.; Schmidt, H.; Timmermann, R.; Grigat, E.; Schulz, S. W. U.S. Patent, 6235815 B1, 2001
21. Loercks, J.; Pommeranz, W.; Schmidt, H.; Timmermann, R.; Grigat, E.; Schulz, S. W. U.S. Patent, 6472497 B2, 2002.
22. Wang, J. H.; Shi, B. Patent WO 2008/072114, 2008.
23. Wang, J. H.; Shi, B. Patent WO 2009/024876, 2009.
24. Ziabicki,A. *Fundamentals of Fiber Formation*; Wiley-Interscience: New York, 1976.
25. Lehermeier, H. J.; Dorgan, J. R. *Polym. Eng. Sci.* **2001**, *41*, 2172.
26. Agrawal, A. K.; Bhalla, R. *J. Macromol. Sci., Part C: Polym. Rev.* **2003**, *C43*, 479.

27. Lim, L. T.; Auras, R.; Rubino, M. *Prog. Polym. Sci.* **2008**, *33*, 820.
28. Topolkaraev, V.; Chakravarty, J.; Possell, K.; Hristov, H. U.S. Patent Publication, US20060273495A1, 2006.
29. Lin, C. C. *Polym. Eng. Sci.* **1983**, *23*, 113.
30. Topolkaraev, V.; McEneany, R.; He, A. Additive Formulations and Modification Chemistry for Meltspun Fibrous Structures from Biopolyesters, 239th American Chemical Society National Meeting, March 21−25, 2010.
31. Tchobanoglous, G.; Burton, F. L.; Stensel, H. D. *Wastewater Engineering: Treatment and Reuse*, 4th ed.; McGraw-Hill Higher Education: New York, 2002.
32. Itavaara, M.; Vikman, M. *J. Environ. Polym. Degrad.* **1996**, *4*, 29–36.
33. Young, H. D. *Statistical Treatment of Experimental Data: An Introduction to Statistical Methods*; Waveland Press: Long Grove, IL, 1996
34. Shi, B.; Bunyard, C.; Palfery, D. *Carbohydr. Polym.* **2010**, *82*, 401.
35. Shi, B; Wang, J. H. U.S. Patent 2010/0272940, 2010.
36. Shin, P. K.; Kim, M. H.; Kim, J. M. *J. Environ. Polym. Degrad.* **1997**, *5*, 33.
37. Shi, B.; Palfery, D. *J. Polym. Environ.* **2010**, *18*, 122.
38. Vink, E. T. H.; Rabago, K. R.; Glassner, D. A.; Gruber, P. R. *Polym. Degrad. Stab.* **2003**, *80*, 403.

Flame Retardants Based on Tartaric Acid: A Renewable By-Product of the Wine Industry

B. A. Howell,* K. E. Carter, and H. Dangalle

**Center for Applications in Polymer Science and Department of Chemistry,
Central Michigan University, Mt. Pleasant, MI 48859-0001**
*bob.a.howell@cmich.edu

Organohalogen flame retardants, particularly brominated aromatics, are popular, effective, low cost, and widely used in the plastics industry. However, an increasing concern about persistence in the environment and potential negative health effects of these materials has generated intense interest in the development of alternatives. Ideally, these should have all the positive attributes of the materials that will be replaced. In addition, it is desirable that the new materials be as "green" as possible, i.e., based on renewable resources and be degradable to nontoxic products in the environment. A series of new, non-halogenated flame retardants based on tartaric acid is being developed. Tartaric acid is a by-product of the wine industry and is readily available locally on an annual basis (Michigan is the thirteenth largest producer of wine in the U.S.). It can be readily converted to the corresponding diethyl ester. This ester may serve as the base for the development of a series of new, non-halogenated flame-retarding agents. The presence of the reactive hydroxyl groups allows the introduction of a variety of phosphorus-containing moieties. For example, treatment of diethyl tartrate with diphenylphosphinyl chloride generates diethyl 2,3-di(diphenylphosphinato)-1,4-butanedioate. This material may serve as a monomer for the preparation of various phosphorus-containing polymers and oligomers via step-growth transesterification.

Keywords: green flame retardants; bio-based polymer additives; renewables; degradation of phosphorus esters

Introduction

The development of polymeric materials over the past six decades has permitted a standard of living in most of the world unparalleled in history. These materials form critical components of everything from personal care items (creams, lotions, hair dressing, toothpaste, etc.), clothing, furniture, home contruction (vinyl siding, roofing material, insulation, particle board, plywood, floor tile, carpeting, paints, window blinds, etc.) to automobiles and aircraft.

Every individual is impacted multiple times daily by the presence of these materials. In general, polymeric materials are flammable and must be flame retarded for most applications. Flame retardance may be imparted in a number of ways. This is most often done by the introduction of an additive during polymer proccessing. For some applications the incorporation of an inorganic additive, usually metal oxides or hydrates, may provide an adequate level of flame retardancy. In general, large loadings (up to 40-50%) of these additives are required. Incorporation of high levels of additive may seriously alter the mechanical properties of the polymer. As a consequence, the use of these additives is limited to applications in which this deterioration in properties can be tolerated. Typically, organic additives are effective at much lower levels, impact the properties of the polymer matrix to a much smaller extent, and are widely used. The two most important classes of flame retardant additives are organohalogen and organophosphorus compounds. Organohalogen compounds are usually prefered on a cost basis. Brominated aromatics, particularly multiply brominated diphenyl ethers, have been among the most widely used compounds of this class (*1*). They are readily available at modest cost and are very effective gas-phase flame retardants. Although these compounds are highly effective as flame retardants, they tend to bioaccumulate when released into the environment (*2*). Because of concern about potential health risks that might be associated with these compounds their use has come under increasing regulatory pressure worldwide (*3–11*). Two of these, pentabromo- and octabromodiphenyl ether, have been voluntarily withdrawn from the market. A third, decabromodiphenyl ether, was thought to offer lower health risks and its position in the market was maintained. However, this compound is persistent in the environment–oxidative degradation is difficult. Now the manufacturers of this compound have reached an agreement with the US Environmental Protection Agency to phase out its use (*12*, *13*). Because of the projected lack of availability of the brominated diphenyl ethers, there is intense interest in finding suitable replacements for them. Organophosphorus compounds would seem to offer the greatest potential for the replacement of organohalogen flame retardants (*14–17*). Most organophosphorus compounds are solid-phase active. They promote char formation at the surface of the burning polymer which prevents heat feedback from the flame and pyrolytic decomposition of the polymer to generate volatile fuel fragments to feed the flame. These materials are most effective in oxygen-containing polymers. For flame-retarding polymers lacking oxygen in the structure an oxygen rich promoter (pentaerythritol, dipentaerythritol, etc.) may be used in conjunction with the organophosphorus compound. It is thought that during combustion phosphoric acid is generated which promotes crosslinking of the polymer and char formation.

Recently, some remarkably effective gas-phase active organophosphorus flame retardants have been developed to replace tetrabromobisphenol A in the production of epoxy resins. Much of this is based on the incorporation of 9,10-dihydro-9-oxa-10-phosphaphenathrene 10-oxide (DOPO) into either the epoxy component or the hardener (*18–24*). During polymer pyrolysis these compounds extrude PO radical to the gas phase where it may function as an efficient scavenger of flame propagating radicals. As a consequence, adequate flame retardance can be achieved at very low loading of these materials in the polymer matrix. Not only do organophosphorus compounds offer good potential for flame retardancy but when generated as monomers and incorporated, chemically, into the polymer lead to decreased mobility and diminished environmental concerns. The incorporation of phophorus-containing comonomer units into various polymers leads to enhanced flame retardancy as evidenced by significantly increased limiting oxygen index (LOI) and increased char yield upon thermal degradation (*25–47*). These may be incorporated as substituients in vinyl polymers (*25–31*), into poly(ester)s as pendants (*32–40*), into poly(siloxane)s as pendants (*43*), into poly(ester)s as an integral component of the mainchain (*44–46*) or into poly(ester)s as both pendant groups and components of the mainchain (*47*). Many of the poly(ester)s are based on the DOPO derivative of hydroquinone (*33, 35–37, 40, 41*).
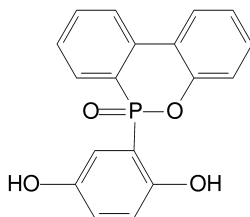
This monomer may be readily incorporated into a variety of poly(ester) structures. The DOPO derivative of itaconic acid has also been used for the generation of poly(ester) bearing phosphorus-containing pendant units (*34, 38*).

135
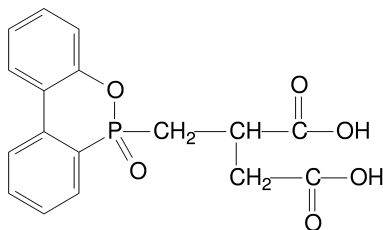
A phosphorus-containing derivative of pentaerythritol has been used for modifying cellulosic polymers (*42*).
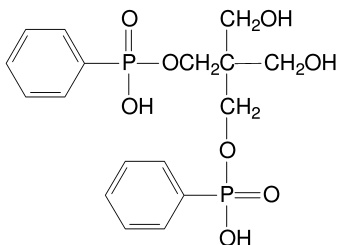
A polymeric silicon-phosphorus flame retardant for poly(carbonate) may be generated from the DOPO derivative of vinyltriethoxysilane (*43*).
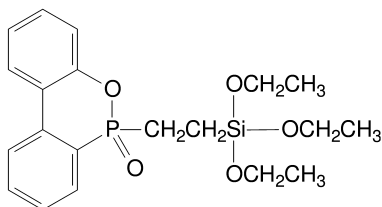
A polymeric flame retardant containing phosphorus in both pendant groups and the mainchain can be prepared from the DOPO-hydroquinone derivative and phenylphosphonic dichloride (*47*).
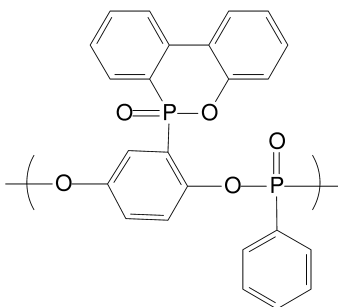
While a great variety of poly(ester)s, many containing the DOPO unit as the active component, has been prepared none have been based on a renewable bio-source. The wine industry offers an attractive compound from which flame-retarding poly(ester)s may be produced.

Tartaric acid, 2,3-dihydroxybutanedioic acid, is a principal by-product of the conversion of grape stock to wine by fermentation (*48*, *49*). This compound has a storied history. Crystals of a salt, potassium ammonium tartrate, were the object of the first resolution (by manual means) of a racemic mixture by Pasteur. This demonstrated the existence of enantiomeric compounds. Pasteur's interest in the formation of this compound led to the demonstration that the presence of yeast or bacteria is required for fermentation, i.e., that enzymes are required for the conversion of carbohydrates, primarily glucose and other simple

monosaccharides, to ethanol. He also was able to demonstrate that spoilage due to bacterial contamination could be avoided by heating the medium to 52-60° C for a short time, a process now known as pasteurization and which has been immensely useful for preservation by the food industry.

The United States ranks fourth behind Italy, France, and Spain in wine production accounting for about 10% of the total. Wine is widely produced in the United States but large-volume production is localized in a few regions (*50*, *51*). Michigan ranks fourth among the US states in acreage devoted to grape growing and thirteenth in the production of wine (*52*). Vineyards are located in southwest Michigan near Fennville and in the peninsular region near Traverse City. All are located within 25 miles of the Lake Michigan shore. The lake effect provides a favorable microclimate for grape production. The presence of this robust wine industry provides an annual, renewable source of tartaric acid. Tartrates occur naturally in winery pomace, in still slops from brandy distillation, in lees that settle in wine tanks, and in argols that separate as a crystalline coating of nearly pure cream of tartar (potassium bitartrate) on the walls and bottoms of wine storage tanks (*53–56*). Cream of tartar also crystallizes in tanks of filtered wine undergoing refrigeration (*56*).

Tartaric acid may be readily converted to the corresponding diethyl ester (*57*, *58*). This compound represents a useful starting point for the synthesis of "green" flame retardant materials based on a plentiful, inexpensive, and renewable by-product of the thriving Michigan wine industry (*59*, *60*).

Experimental

General

In general, reactions were carried out in a dry (all glassware was dried in a oven overnight at 120° C and allowed to cool under a stream of dry nitrogen prior to use) three-necked, round-bottomed flask fitted with Liebig condenser bearing a gas-inlet tube, a magnetic stirring bar (or Trubore stirrer), and a pressure-equalizing dropping funnel (or syringe port). Chromatography was accomplished using SilaFlash P60 (230-400 mesh silica; Silicycle) in a column of appropriate size and hexane/ethyl acetate as eluant. Silica-coated Mylar plates (ThermoFisher Scientific) were used for thin layer chromatography (TLC). Melting points were determined by differential scanning calorimetry (DSC) using a Perkin Elmer Pyris Diamond DSC. All samples were analyzed at a heating rate of 5°C/min in a constant nitrogen purge of 50 ml/min. Thermal decomposition temperatures were obtained using a TA Instruments 2950 Hi-Res TGA instrument interfaced with the Thermal Analyst 2100 control unit. Most generally, a heating rate of 5°C/min was used. TA Thermal Advantage software was used for data analysis. Samples (5-10 mg) were contained in a platinum pan. The sample compartment was purged with dry nitrogen at 50 ml/min during analysis. Nuclear magnetic resonance (NMR) spectra were obtained using a 10% to 25% solution in deuterochloroform or dimethyl sulfoxide-d_6 and a Varian Mercury 300 MHz spectrometer. Proton and carbon chemical shifts are reported in parts-per-million (δ) with respect to tetramethylsilane (TMS) as internal reference (δ = 0.00).

Phosphorus chemical shifts are in δ with respect to triethyl phosphate as internal reference (δ = -18.0). Infrared (IR) spectra were obtained using attenuated total reflectance, thin films between sodium chloride plates or solid solutions (1%) in anhydrous potassium bromide (as discs) and a Nicolet MAGNA-IR 560 spectrometer. Absorptions were recorded in wave numbers (cm^{-1}), and absorption intensities were classified in the usual fashion as very weak (vw), weak (w), and medium (m), strong (s), and very strong (vs) relative to the strongest band in the spectrum. Mass spectra were obtained using a Hewlett-Packard 5890A gas chromatograph/mass spectrometer (MSD) with an ionizing potential of 70 electron volts and temperature programmed elution into the spectrometer inlet (90-200°C).

Materials

Common solvents and reagents were obtained from ThermoFisher Scientific or the Aldrich Chemical Company. Tetrahydrofuran (THF) was distilled from lithium aluminum hydride prior to use; methylene chloride from calcium hydride. Diethyl tartrate and 1,4-dihydrobenzene were obtained from Aldrich Chemical Company and used as received. Diphenylphosphonic chloride was from Alfa Aesar.

Synthesis

Diethyl 2,3-Diphosphinato-1,4-butanedioate

To a stirred solution of 11.20 g (54.2 mmol) of diphenylphosphinic chloride in 80 ml of dry benzene was added, dropwise over a period of 0.5 hr., a solution of 5.12 g (24.8 mmol) of diethyl tartrate and 7.5 ml (5.30 g, 12.5 mmol) of triethylamine in 40 ml of benzene (*61*). The resulting mixture was allowed to stir for 36 hr at room temperature. The solution was washed, successively, with 50 ml of water, 50 ml of 10% aqueous hydrochloric acid solution, two 50-ml portions of saturated aqueous sodium bicarbonate solution and two 50-ml portions of saturated aqueous sodium chloride solution. The solution was dried over anhydrous sodium sulfate and the solvent was removed by rotary evaporation at reduced pressure. Recrystallization of the residual material from ethyl acetate afforded diethyl 2,3-diphosphinato-1,4-butanedioate (9.28 g, 63.8 % yield) as a white crystalline solid, mp 152° C (DSC); decomposition, T_{onset} = 242 °C; **IR** (thin film, cm^{-1}) 3061 (m), C_{sp2}–H; 2997 (m), 2982 (m), 2968 (m), 2937 (m), 2912 (m), C_{sp3}–H; 1766 (vs), ester C=O; 1592 (m), aromatic nucleus; 1265 (vs), P=O; 1230 (vs), 1112 (vs), 937 (m), P-O-C; **^{1}H-NMR** (δ, CDCl$_3$) 0.98 (t, J_{H-H} =6.9 Hz, 6H, methyl protons of ethyl group); 3.66 (m, 2H, methylene protons of ethyl group); 3.92 (m, 2H, methylene protons of ethyl group); 5.52 (dd, J_{P-H} = 10.1 Hz, J_{H-H} = 1.92 Hz, 2H, methine protons); 7.44(m), 7.52(m), 7.86(m) (20H, aromatic protons); **^{13}C-NMR** (δ, CDCl$_3$) 13.6 (carbon atoms of methyl groups); 62.2(carbon atoms of methylene groups); 73.2 (d, J_{P-C} = 5.7 Hz, methine carbon atoms); 128.2 (d, J_{P-C} = 23.0 Hz, aromatic carbon atom attached to phosphorus); 131.8 (d, J_{P-C} = 1.1 Hz, aromatic carbon atom *para* to phosphorus); 132.0 (d, J_{P-C}

= 7.4 Hz, aromatic carbon atom *meta* to phosphorus); 132.3 (d, J_{P-C} = 7.4 Hz, aromatic carbon atom *ortho* to phosphorus); 166.6 (s, carbonyl atom); **^{31}P-NMR** (δ, CDCl$_3$) 34.9.

1,4-(Diphenylphosphinato)benzene

To a stirred solution of 5.00 g (45.0 mmol) of hydroquinone and 21.30 g (90.0 mmol) of diphenylphosphonic chloride in a mixture of 50 ml of toluene and 25 ml of THF was added, dropwise over a period of 0.5 hr, a solution of 13.0 ml (9.10 g, 90.0 mmol) of triethylamine in 30 ml of toluene (*62*). The resulting mixture was allowed to stir 24 hr at room temperature. Water (120 ml) was added. The precipitate which formed was collected by filtration at reduced pressure, washed with water, and recrystallized from methanol to provide 17.5 g (76.2% yield) of 1,4-(diphenylphosphinato)benzene as a white solid, mp 213 °C (DSC); decomposition, T_{onset} = 285 °C; **IR** (thin film, cm^{-1}) 3104 (w), C$_{sp2}$ –H; 1494 (m), aromatic nucleus; 1235 (vs), P=O; 1130 (vs), 1112 (vs), 913 (m), P-O-C; **^{1}H-NMR** (δ, CDCl$_3$) 7.05 (s, protons of aromatic nucleus attached to oxygen); 7.48 (m), 7.83 (m) (20H, aromatic protons); **^{13}C-NMR** (δ, CDCl$_3$) 147.2 (carbon atoms of the aromatic nucleus attached to oxygen); 116.1 (m, aromatic carbon atoms *ortho* and *meta* to oxygen); 121.5 (d, aromatic carbon atom attached to phosphorus); 128.4 (d, aromatic carbon atom *ortho* to phosphorus); 131.4 (d, aromatic carbon atom *meta* to phosphorus); 132.4 (d, aromatic carbon atom *para* to phosphorus); **^{31}P-NMR** (δ, CDCl$_3$) 30.6.

Results and Discussion

Because of the concern about the potential negative environmental impacts of organohalogen flame retardants, particularly brominated aromatics, there is increasing effort being directed to the development of effective, nonpersistant, non-halogen flame retardant compounds. Ideally, they should be "green" materials-based on renewable resources with ease of manufacture requiring minimal use of corrosive reagents and generating no toxic waste and degradable in the natural environment to nontoxic materials. Organophosphorus compounds offer the greatest potential to replace organohalogen flame retardants. Properly constructed such compounds may function as very effective flame retardants. Tartaric acid is a renewable material generated annually in large quantity as a by-product of wine making. It is nontoxic and may be found as a constituent of many processed foods. It is tetrafunctional which provides ready access to a variety of derivatives including phosphorus flame retardants. It may be readily converted to the diethyl ester which can serve as a base for the generation of a variety of phosphorus compounds. For example, treatment of the diethyl ester with diphenylphosphonic chloride introduces phosphinato groups at the hydroxyl-bearing carbon atoms.
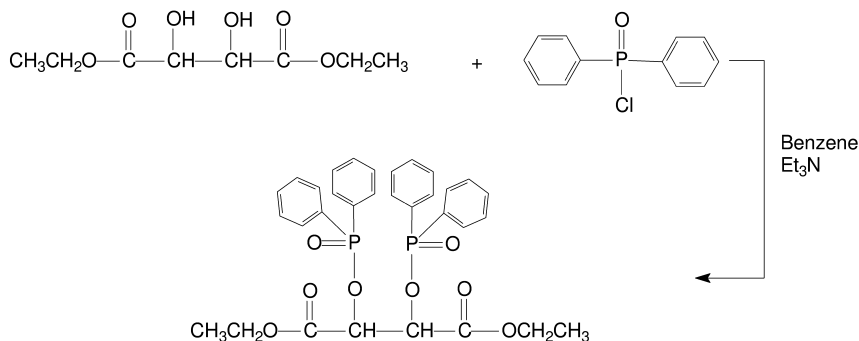
Scheme 1. Synthesis of diethyl 2,3-diphenylphosphinato-1,4-butanedioate
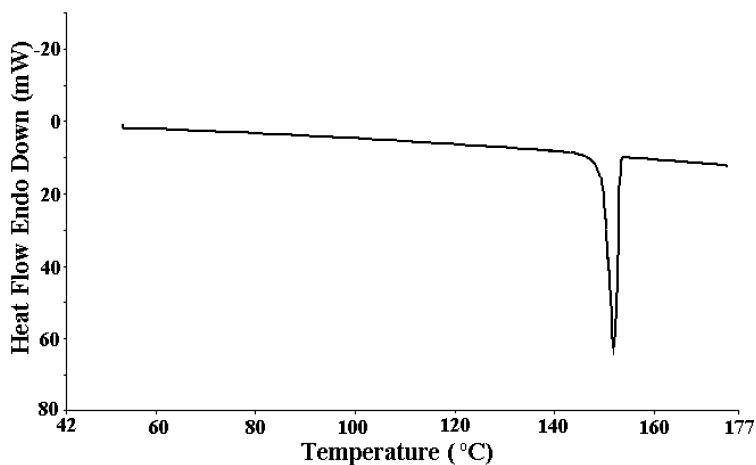
Figure 1. DSC thermogram for diethyl 2,3-diphenylphosphinato-1,4-butanedioate.

The product, diethyl 2,3-diphenylphosphinato-1,4-butanedioate is a white crystalline solid, mp 152 °C (see Figure 1).

This compound undergoes degradation in two stages (Figure 2). The first stage has an onset temperature of 176 °C and represents a 44.7 % loss of the initial sample mass, probably corresponding to the loss of diphenyl phosphonic acid. The second larger loss (55.4 % of the initial sample mass), occurs with an onset temperature of 216 °C.

The infrared spectrum of this compound (Figure 3) contains aromatic C-H absorption at 3061 cm^{-1}, absorption for aromatic nucleus at 1592 cm^{-1}, P=O absorption at 1265 cm^{-1} and P-O-C absorptions at 1230 cm^{-1}, 1112 cm^{-1} and 937 cm^{-1}.
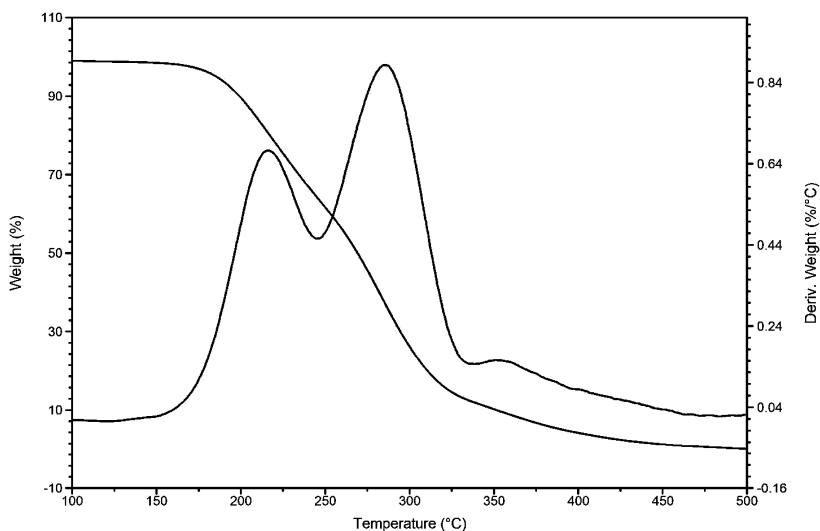
Figure 2. Thermal decomposition of diethyl 2,3-diphenylphosphinato-1,4-butanedioate.
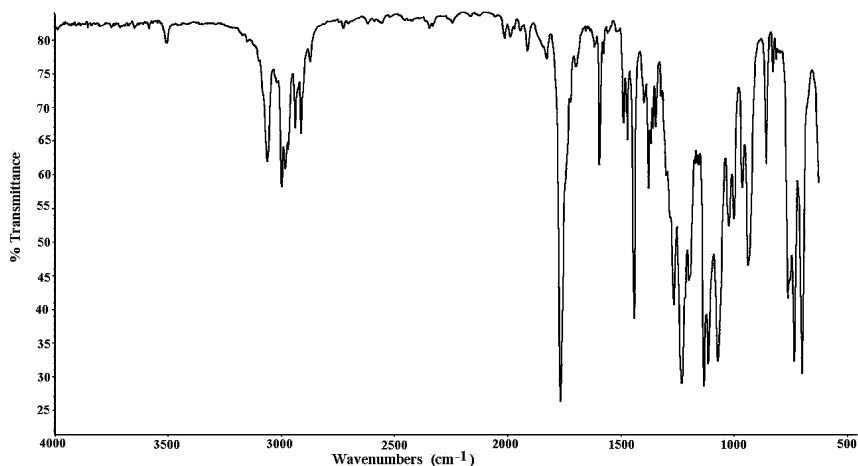
Figure 3. Infrared spectrum of diethyl 2,3-diphenylphosphinato-1,4-butanedioate.

The proton NMR spectrum of this material is shown in Figure 4. The stereochemistry of the compound is reflected in the two quartets of doublets for the methylene protons at δ 3.8.
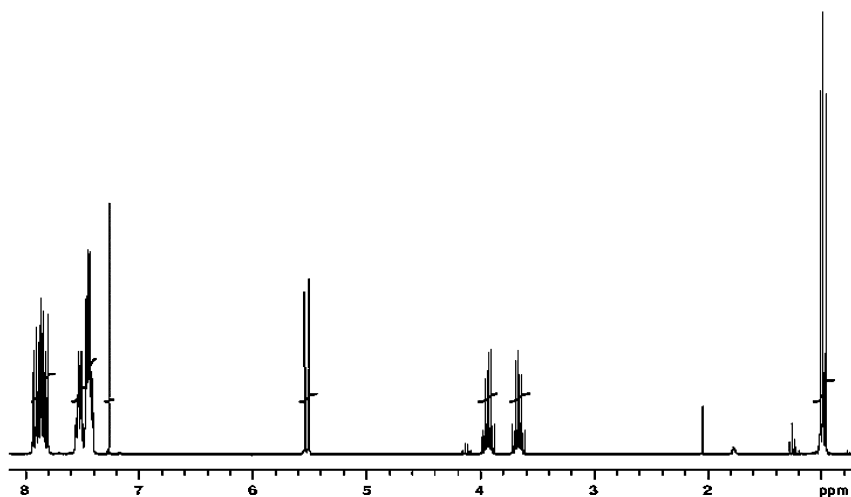
Figure 4. Proton NMR spectrum of diethyl 2,3-diphenylphosphinato-1,4-butanedioate.
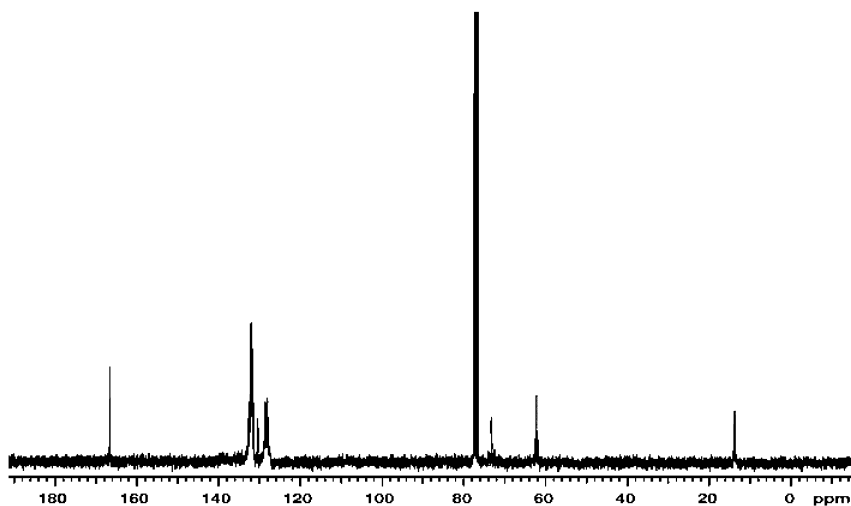
Figure 5. Carbon-13 NMR spectrum of diethyl 2,3-diphenylphosphinato-1,4-butanedioate.

The corresponding carbon-13 NMR spectrum is depicted in Figure 5. Absorption due to the carbon atom of the methyl group ($CH_2\underline{C}H_3$) appears at δ 13.6, absorption due to the carbon atoms of the methylene groups ($\underline{C}H_2CH_3$) at δ 62.2, those for methine carbon atoms at δ 73.2 and for the carbonyl carbon atoms at δ 166.6. Absorptions for the carbon atoms of the phenyl groups attached to phosphorus appear at δ 128.2, 131.8, 132.0 and 132.3.

The phosphorus-31 NMR spectrum is displayed in Figure 6. The peak corresponding to the phosphorus atoms present appears at δ 34.9.
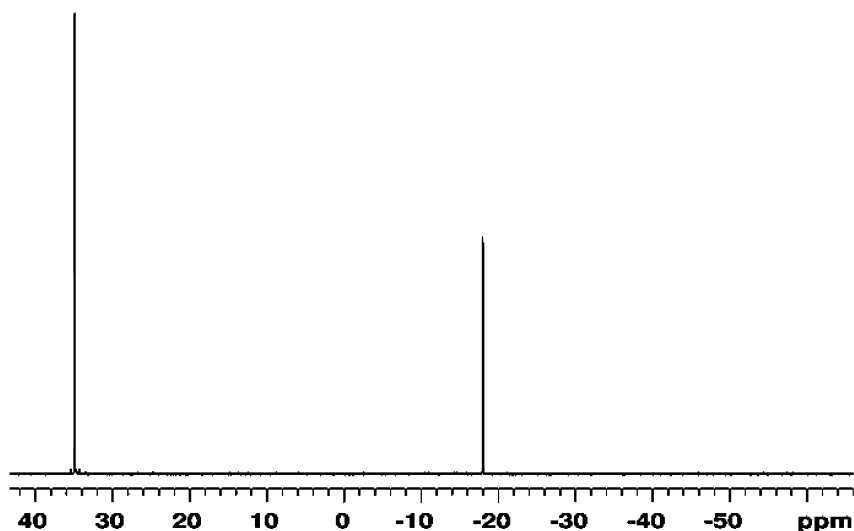
Figure 6. Phosphorous-31 NMR spectrum of diethyl 2,3-diphenylphosphinato-1,4-butanedioate.

The nature of this compound can be readily manipulated by varying the carboxyl ester functionality. In addition, it may be converted to high phosphorus-content oligomers by condensation with 2,5-(diphenylphosphonato)-1,4-dihydroxybenzene or 2,5-(diphenylphosphonato)-1,4-(2-hydroxyethoxy) benzene (structures shown below). The dihydroxy compound may be converted to the di(2-hydroxyethoxy) analog by treatment with ethylene carbonate (*33*, *35*).
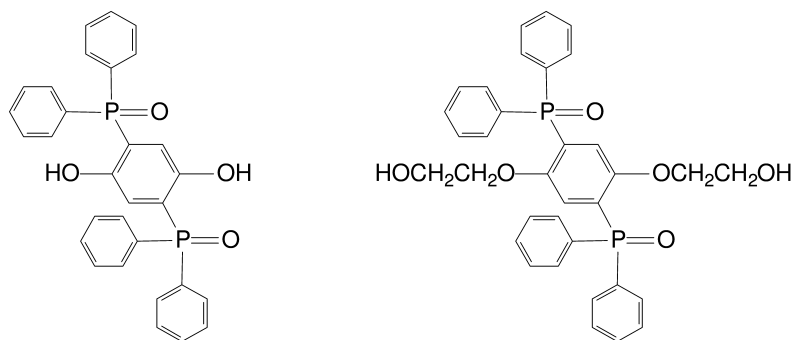
2,5-(Diphenylphosphonato)-1,4-dihydroxybenzene may be obtained by treating 1,4-(diphenylphosphonato)benzene with strong base. The synthesis of this precursor compound is outlined in Scheme 2. It has been isolated and thoroughly characterized spectroscopically.

This compound is a white solid, mp 213 °C (DSC) (Figure 7). It undergoes smooth thermal degradation with an onset of 285 °C (Figure 8).
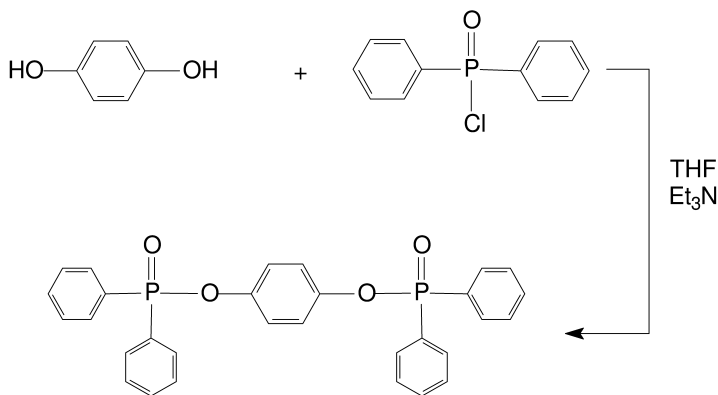
Scheme 2. Synthesis of 1,4-(Diphenylphosphinato)benzene
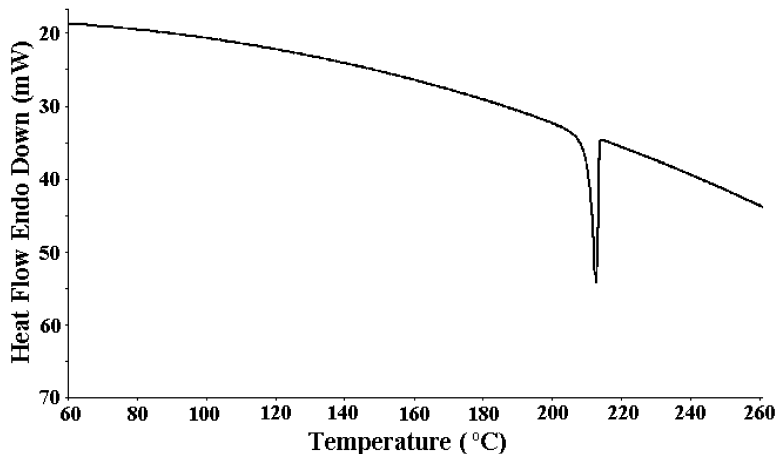
Figure 7. DSC thermogram for 1,4-(diphenylphosphinato)benzene.

The infrared spectrum of this compound (Figure 9) contains aromatic C-H absorptions at 3104 cm^{-1}, absorption for an aromatic nucleus at 1494 cm^{-1}, P=O absorption at 1235 cm^{-1} and P-O-C absorptions at 1130 cm^{-1}, 1112 cm^{-1} and 913 cm^{-1}.

The proton NMR spectrum of this compound is shown in Figure 10. It contains a singlet at δ 7.08 corresponding to the protons of the central aromatic nucleus. Absorptions for the protons of the aryl groups attached to phosphorus appear at δ 7.82 and 7.45 in a ratio of 2:3. The corresponding carbon-13 NMR spectrum is depicted in Figure 11. Absorption due to the aromatic carbon atoms attached to oxygen appears at δ 147.2. Absorptions due to aromatic carbon atoms *ortho* to oxygen appears at δ 116.1. Absorptions due to aromatic carbon atoms attached to phosphorus appears at δ 121.5. Absorptions for the other carbon atoms of the phenyl groups attached to phosphorous appear at δ 128.4, 131.4, and 132.4. The phosphorous-31 NMR spectrum is displayed in Figure 12. The peak corresponding to the phosphorous atoms present appears at δ 30.6.

The phosphinated tartrate ester and 1,4-(diphenylphosphinato)benzene (or a derivate) may be used as monomers for the generation of oligomers containing high levels of phosphorus (Scheme 3).
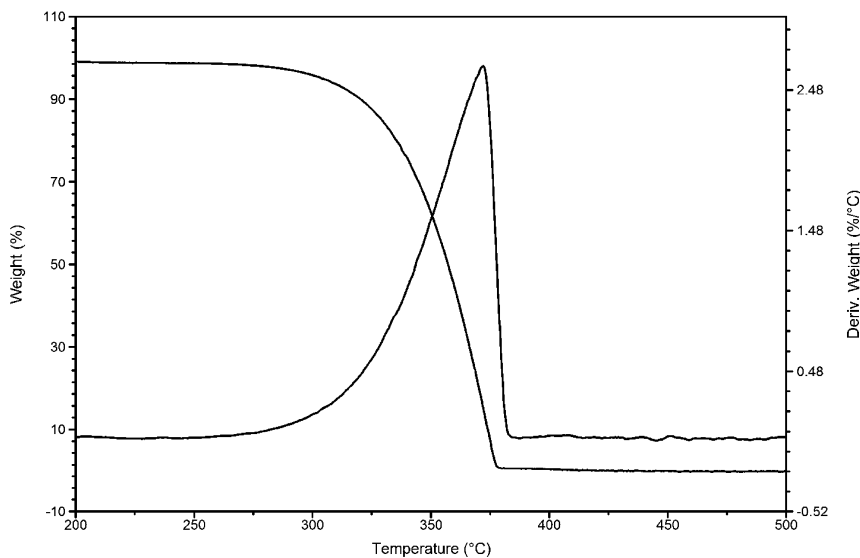
Figure 8. Thermal decomposition of 1,4-(diphenylphosphinato)benzene.
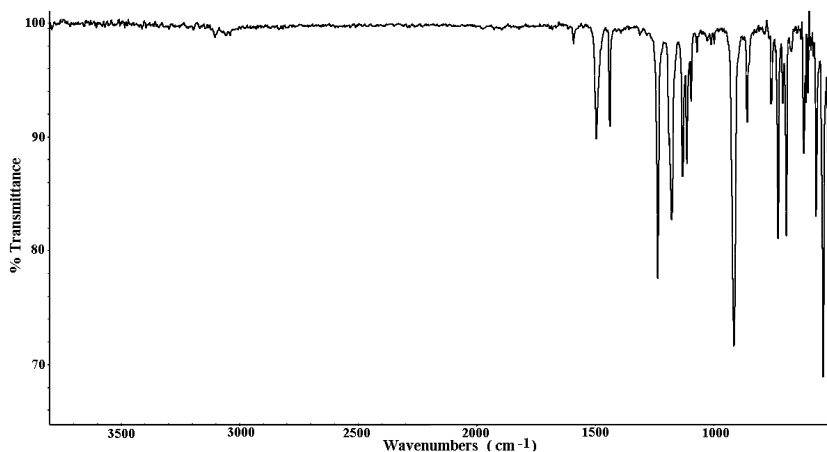
Figure 9. Infrared spectrum of 1,4-(diphenylphosphinato)benzene.
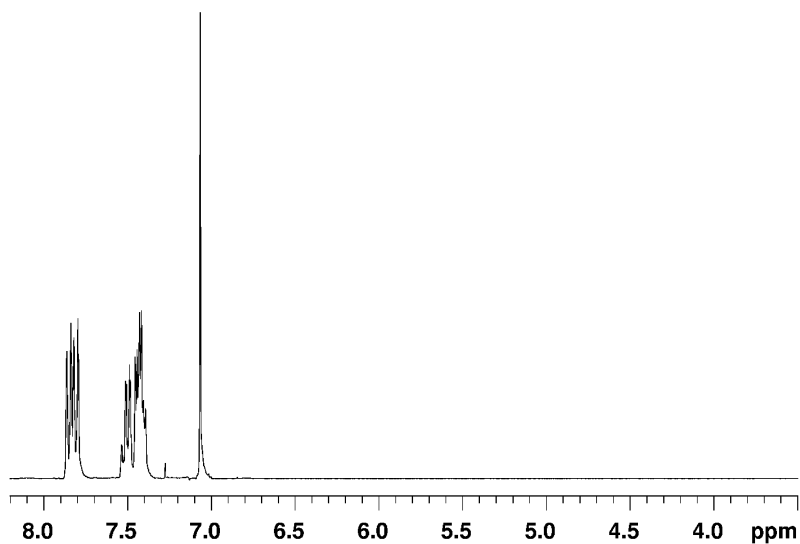
Figure 10. Proton NMR spectrum of 1,4-(diphenylphosphinato)benzene.
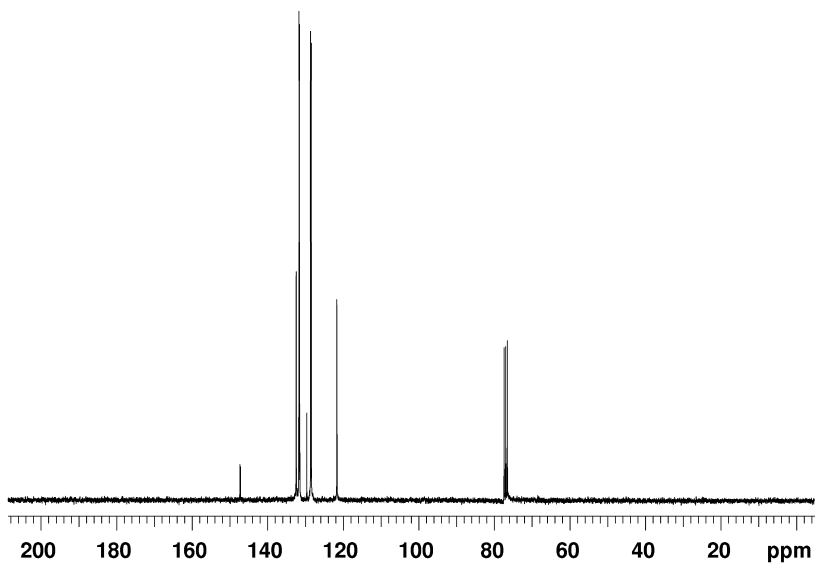
Figure 11. Carbon-13 NMR spectrum of 1,4-(diphenylphosphinato)benzene.
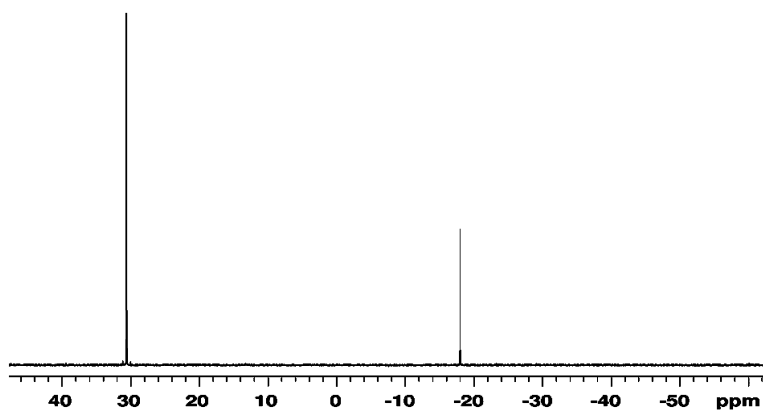
Figure 12. Phosphorous-31 NMR spectrum of 1,4-(diphenylphosphinato)benzene.
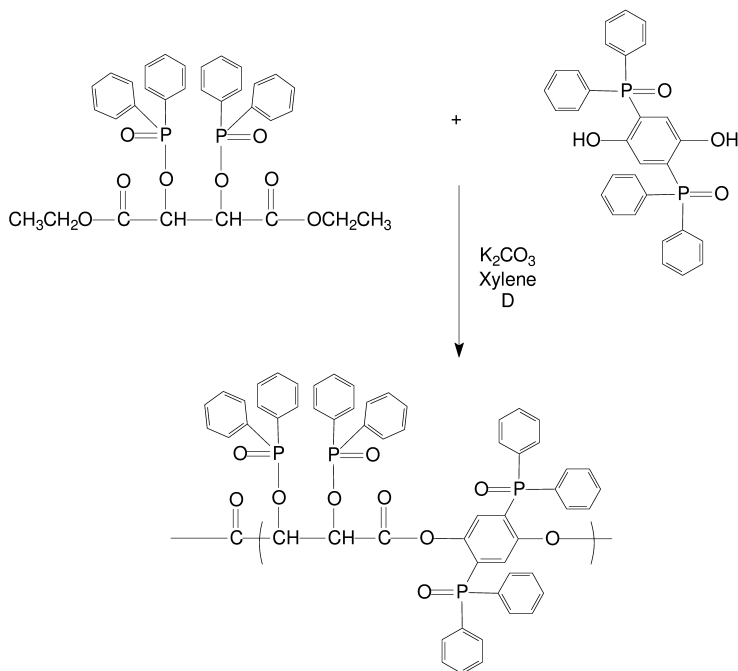
Scheme 3. Generation of Oligomers Containing High Levels of Phosphorus

147

Conclusions

The increasing concern about the potential negative health effects of organohalogen flame retardants has stimulated interest in the development of nontoxic, biodegradable but effective alternatives. Ideally, suitable replacements should be based on an inexpensive, nontoxic, renewable biomaterial. Tartaric acid may be obtained from naturally-occuring materials by fermentation and, in fact, is a by-product of wine production. It is readily available at modest cost and is nontoxic-it is an edible component of processed foods. It represents an excellent starting point for the development of a family of green organophosphorus flame retardants.

References

1. (a) Weil, E. D. Flame Retardancy. In *Encyclopedia of Polymer Science and Technology*, 3rd ed.; Mark, H. F., Ed.; John Wiley and Sons: New York, 2004; Vol. 10, pp 21−54. (b) Pettigrew, A. Halogenated Flame Retardants. In *Encyclopedia of Polymer Science and Technology*, 4th ed.; Kroschwitz, J. I., Howe-Grant, M., Eds.; John Wiley and Sons: New York, 1993; Vol. 10, pp 954−976.

2. Alace, M.; Wenning, R. J. The Significance of Brominated Flame Retardants in the Environment: Current Understanding, Issues and Challenges. *Chemosphere* **2002**, *46*, 579–582.

3. Pakalin, S.; Cole, T.; Steinkellner, J.; Nicoles, R.; Tissier, C.; Munn, S.; Eisenreich, S. *Review of Production Processes of Decabromodiphenyl Ether (Decabde) Used in Polymeric Applications in Electrical and Electronic Equipment and Assessment of Decabde*. European Chemicals Bureau, Institute for Health and Consumer Protection, Joint Research Center, European Commission, January 2007.

4. *European Union Risk Assesment Report: bis(Pentabromophenyl) Ether*. European Chemicals Bureau, Institute for Health and Consumer Protection, Joint Research Center, European Commission: CAS No. 1163-19-5; EINECS No. 214-604-9, 2002.

5. Hites, R. A. Polybrominated Diphenyl Ethers in the Environment and in People: A Meta-Analysis of Concentrations. *Environ. Sci. Technol.* **2004**, *38*, 945–956.

6. Alaee, M.; Arias, P.; Sjodin, A.; Bergmann, A. An Overview of Commercially Used Brominated Flame Retardants, Their Applications, Their Use Patterns in Different Countries/ Regions and Possible Modes of Release. *Environ. Int.* **2003**, *29*, 683–689.

7. Sjodin, A.; Wong, L.-Y.; Jones, R. S.; Park, A.; Zhang, Y.; Hodge, C.; Dipietro, E.; McClure, C.; Turner, W.; Needham, L. L.; Patterson, D. G., Jr. Serum Concentrations of Polybrominated Diphenyl Ethers (PBDEs) and Polybrominated Biphenyls (PBB) in the United States Population: 2003−2004. *Environ. Sci. Technol.* **2008**, *42*, 1377–1384.

8. Lorber, M. Exposure of Americans to Polybrominated Diphenyl Ethers. *J. Expo. Sci. Environ. Epidemiol.* **2008**, *18*, 2.

9. Darnerud, P. D. Brominated Flame Retardants as Possible Endocrine Disrupters. *Int. J. Androl.* **2008**, *31*, 152.

10. Bloom, M.; Spliethoff, H.; Vena, J.; Shaver, S.; Addink, R.; Eadon, G. Environmental Exposure to PBDEs and Thyroid Function among New York Anglers. *Environ. Toxicol. Pharm.* **2008**, *25*, 386–392.

11. Herbstman, J. B.; Sjodin, A.; Kurzon, M.; Lederman, S. A.; Jones, R. S.; Rauth, V.; Needham, L. L.; Tang, D.; Niedzwiecki, M.; Wang, R. Y.; Perera, F. Prenatal Exposure to PBDEs and Neurodevelopment. *Environ. Health Perspect.* **2010**, *118*, 712–719.

12. Hess, G. Industry to Phase Out DecaDBE. *Chem. Eng. News* **2009**, *87* (51), December 21, 2009.

13. Hess, G. Industry Drops Flame Retardant. *Chem. Eng. News* **2010**, *88* (1), 10, January 4, 2010.

14. Weil, E. D. Phosphorus-Based Flame Retardants.   In *Handbook of Organophosphorus Chemistry*; Engel, R. E., Ed.; Marcel Dekker: New York, 1992.

15. Weil, E. D.; Levchik, S. V.; Ravey, M.; Zhu, W. M. A Survey of Recent Progress in Phophorus-based Flame Retardants and Some Mode of Action Studies. *Phosphorus Sulfur Silicon Relat. Elem.* **1999**, *146*, 17–20.

16. Lu, S. Y.; Hamerton, I. Recent Developments in the Chemistry of Halogen-Free Flame Retardant Polymers. *Prog. Polym. Sci.* **2002**, *27*, 1661–1712.

17. Davis, J. The Technology of Halogen-Free Flame Retardant Additives for Polymeric Systems. *Eng. Plast.* **1996**, *9*, 403–419.

18. Artner, J.; Ciesielski, M.; Walter, O.; Doring, M. R.; Perez, M.; Sandler, J. K. W.; Altstadt, V.; Schartel, B. A Novel DOPO-Based Diamine as Hardener and Flame Retardant for Epoxy Resin Systems. *Macromol. Mater. Eng.* **2008**, *293*, 503–514.

19. Ciesielski, M.; Schafer, A.; Doring, M. Novel Efficient DOPO-Based Flame-Retardants for PWB Relevant Epoxy Resins With High Glass Transition Temperatures. *Polym. Adv. Technol.* **2008**, *19*, 507–515.

20. Schartel, B.; Balabanovich, A. I.; Braun, U.; Knoll, U.; Artner, J.; Ciesielski, M.; Doring, M.; Perez, R.; Sandler, J. K. W.; Altstadt, V.; Hoffman, T.; Pospiech, D. Pyrolysis of Epoxy Resins and Fire Behavior of Epoxy Resin Composites Flame-Retarded with 9,10-Dihydro-9-oxa-10-phosphaphenanthrene-10-oxide Additives. *J. Appl. Polym. Sci.* **2007**, *104*, 2260–2269.

21. Perez, R.; Sandler, J. K. W.; Altstadt, V.; Hoffman, T.; Pospiech, D.; Artner, J.; Ciesielski, M.; Doring, M; Balabanovich, A. I.; Knoll, U.; Braun, U.; Schartel, B. Novel Phophorus-Containing Hardeners with Tailored Chemical Structures for Epoxy Resins: Synthesis and Cured Resin Properties. *J. Appl. Polym. Sci.* **2007**, *105*, 2744–2759.

22. Perez, R.; Sandler, J. K. W.; Altstadt, V.; Hoffman, T.; Pospiech, D.; Artner, J.; Ciesielski, M.; Doring, M; Balabanovich, A. I.; Schartel, B. Effective Halogen-Free Flame Retardancy for a Monocomponent Polyfunctional Epoxy Using An Oligomeric Organophosphorus Compound. *J. Mater. Sci.* **2006**, *41*, 8347–8351.

23. Perez, R.; Sandler, J. K. W.; Altstadt, V.; Hoffman, T.; Pospiech, D.; Artner, J.; Ciesielski, M.; Doring, M; Braun, U.; Knoll, U.; Schartel, B. Effective Halogen-Free Flame Retardants for Carbon-Reinforced Epoxy Composites. *J. Mater. Sci.* **2006**, *41*, 4981–4984.

24. Perez, R.; Sandler, J. K. W.; Altstadt, V.; Hoffman, T.; Pospiech, D.; Ciesielski, M.; Doring, M. Effect of DOPO-Based Compounds on Fire Retardancy, Thermal Stability, and Mechanical Properties of DGEBA Cured with 4,4′-DDS. *J. Mater. Sci.* **2006**, *41*, 341–353.

25. Furukawa, J.; Kobayashi, E.; Wakui, T. Phosphorus-Containing Polystyrene Derivatives as Flame Resistance. *Polym. J.* **1980**, *12* (5), 277–285.

26. Yu, Z.; Zhu, W.-E. Synthesis and Polymerization of Vinylbenzylphosphonate Diethyl Ester. *J. Polym. Sci., Part A-1: Polym. Chem.* **1990**, *28*, 227–230.

27. Boutevin, B.; Hamoui, B.; Bessière, J.-M. M. Synthesis of a Phosphonated Styrene Monomer. Instability of the Diacidic Moiety and Polymerization. *Macromol. Chem. Phys.* **1995**, *196*, 1865–1873.

28. Ebdon, J. R. Flame Retardancy in Styrenic and Acrylic Polymers With Covalently Bound Phosphorus-Containing Groups. *Recent. Adv. Flame. Retard. Polym. Mat.* **1997**, *8*, 161–170.

29. Ebdon, J. R.; Price, D.; Hunt, B. J.; Joseph, P.; Gao, F.; Milnes, G. J.; Cunlife, L. K. Flame Retardance in Some Polystyrenes and Poly(methyl methacrylate)s with Covalently Bound Phosphorus-Containing Groups: Initial Screening Experiments and Some Laser Pyrolysis Mechanistic Studies. *Polym. Degrad. Stab.* **2000**, *69*, 267–277.

30. Dworak, C.; Koch, T.; Varga, F.; Liska, R. Photopolymerization of Biocompatible Phosphorus-Containing Vinyl Esters and Vinyl Carbamates. *J. Polym. Sci., Part A-1: Polym. Chem.* **2010**, *48*, 2916–2924.

31. Catel, Y.; LePluart, L.; Madec, P.-J.; Pham, T.-N. Synthesis and Photopolymerization of Phosphonic Acid Monomers for Applications in Compomer Materials. *J. Appl. Polym. Sci.* **2010**, *117*, 2676–2687.

32. Chang, S.-J.; Sheen, Y.-C.; Chang, R.-S.; Chang, F.-C. The Thermal Degradation of Phosphorus-Containing Polyesters. *Polym. Degrad. Stab.* **1996**, *54*, 365–367.

33. Wang, C. S.; Liu, C. H.; Chen, C. Y. Synthesis and Properties of Phosphorus-Containing Polyesters Derived From 2-(6-Oxido-6H-dibenz<e,e><1,2>oxaphosphorin-6-yl)-1,4-hydroxyethoxy phenylene. *J. Polym. Sci., Part A-1: Polym. Chem.* **1998**, *36*, 3051–3061.

34. Wang, C. S.; Shieh, J. Y.; Sun, Y. M. Synthesis and Properties of Phosphorus-Containing PET and PEN. *J. Appl. Polym. Sci.* **1988**, *70*, 1959–1964.

35. Wang, C. S.; Lin, C. H. Synthesis and Properties of Phosphorus-Containing PEN and PBN Copolyesters. *Polymer* **1999**, *40*, 747–757.

36. Wang, C. S.; Shieh, J. Y. Synthesis and Flame Retardancy of Phosphorus-Containing Polycarbonate. *J. Polym. Res.* **1999**, *6*, 149–154.

37. Wang, Y.-Z.; Chen, X.-T.; Tang, X.-D. Synthesis, Characterization and Thermal Properties of Phosphorus-Containing, Wholly Aromatic Thermotropic Copolyesters. *J. Appl. Polym. Sci.* **2002**, *86*, 1278–1284.

38. Park, J. M.; Park, Y. H. Synthesis and Properties of Novel Flame Retardant Poly(butylene terephtalate). *Macromol. Res.* **2005**, *13*, 128–134.

39. Hamciuc, C.; Vlad-Bubulac, T.; Sava, I.; Petreus, D. New Phosphorus-Containing Copolyesters. *J. Macromol. Sci., Part A: Pure Appl. Chem.* **2006**, *43*, 1355–1364.

40. Du, X.-H.; Zhao, C.-S.; Wang, Y.-Z.; Zhou, Q.; Deng, Y.; Qu, M.-H.; Yang, B. Thermal Oxidative Degradation Behaviours of Flame-Retardant Thermotropic Liquid Crystal Copolyester/PET Blends. *Mater. Chem. Phys.* **2006**, *98*, 172–177.

41. Balabanovich, A. I.; Pospiech, D.; Korwitz, A.; Hausler, L.; Harnisch, C. Pyrolysis Study of a Phosphorus-Containing Aliphatic-Aromatic Polyester and its Nanocomoposites with Layered Silicate. *Polym. Degrad. Stab.* **2009**, *94*, 355–364.

42. Li, Q.-L.; Wang, X.-L.; Wang, D.-Y.; Xiong, W.-C.; Zhong, G.-H.; Wang, Y.-Z. A Novel Organophosphorus Flame Retardant: Synthesis and Durable Finishing of Poly(ethylene terephtalate)/ Cotton Blends. *J. Appl. Polym. Sci.* **2010**, *117*, 3066–3074.

43. Hu, Z.; Chen, L.; Zhao, B.; Luo, Y.; Wang, D.-Y.; Wang, Y.-Z. A Novel Efficient Halogen-Free Flame Retardant System for Polycarbonate. *Polym. Degrad. Stab.* **2010**, *xxx*, 1–8.

44. Annakutty, K. S.; Kishore, K. Synthesis and Properties of Flame-Retardant Polyphosphate Esters: A Review. *J.Sci. Ind. Res.* **1989**, *48*, 479–493.

45. Ronganathan, T.; Zilbermann, J.; Farris, R. J.; Coughlin, E. B.; Emrick, T. Synthesis and Characterization of Halogen-Free Antiflammable Polyphosphonates Containing 4,4′-Bishydroxydeoxy benzoin. *Macromolecules* **2006**, *39*, 5974–5975.

46. Ranganathan, T.; Ku, B. C.; Zilbermann, J.; Beaulieu, M.; Farris, R. J.; Coughlin, E. B.; Emrick, T. Poly(arylate-phosphonate) Copolymers with Deoxybenzoin in the Backbone: Synthesis, Characterization and Properties. *J. Polym. Sci., Part A-1: Polym. Chem.* **2007**, *45*, 4573–4580.

47. Chang, Y.-L.; Wang, Y.-Z.; Ban, D.-M.; Yang, B.; Zhao, G.-M. A Novel Phosphorus-Containing Polymer as a Highly Effective Flame Retardant. *Macromol. Mater. Eng.* **2004**, *289*, 703–707.

48. Amerine, M. A.; Berg, H. W.; Cruess, W. V. *The Technology of Wine Making*; The Avi Publishing Company, Inc.: Westport, CT, 1972.

49. Austin, C. *The Science of Wine*; University of London Press Ltd.: London, 1968.

50. Pinney, T. *A History of Wine in America: From Prohibition to the Present*; University of California Press: Berkeley, 2005.

51. Wine Regions of the United States. http://www.wineforeveryone.com/wine_regions_united_states.html (accessed March 14, 2010).

52. Michigan Wine and Grape Council: http://www.michiganwines.com/page.php?menu=maps (accessed February 19, 2009).

53. Rivas, B.; Torrado, A.; Moldes, A. B.; Dominguez, J. M. Tartaric Acid Recovery From Distilled Lees and Use of the Residual Solid as an Economic Nutrient For *Lactobacillus*. *J. Agric. Food. Chem.* **2006**, *54* (20), 7904–7911.

54. Versari, A.; Castellari, M.; Spinabelli, U.; Galassi, S. Recovery of Tartaric Acid from Industrial Ecological Wastes. *J. Chem. Technol. Biotechnol.* **2001**, *76* (5), 485–488.

55. Brown, E. M.; Henriques, V. D. Vinification in California Wineries. *Ind. Eng. Chem.* **1935**, *27*, 1235–1240.

56. Marsh, G. L.; Joslyn, M. A. Effect of Temperature on the Precipitation Rate of Cream of Tartar from Wine. *Ind. Eng. Chem.* **1935**, *27*, 1252–1257.

57. Zhou, X.; Lin, W.-J.; Ye, J.-L.; Huang, P.-Q. A Versatile Approach to Pyrrolidine Azasugars and Homoazasugars Based on a Highly Diastereoselective Reductive Benzyloxymethylation of Protected Tartarimide. *Tetrahedron* **2007**, *63* (7), 6346–6357.

58. Lemieux, R. U.; Howard, J. The *O*-inside Conformation of 1,3:2,4-Di-*O*-methylene-*L*-threitol. *Can. J. Chem.* **1963**, *41*, 393–398.

59. Howell, B. A.; Carter, K. E. Thermal Stability of Phosphinated Diethyl Tartrate. *J. Therm. Anal. Cal.*, in press.

60. Howell, B. A.; Dangalle, H. *Thermal Properties of Phosphinated Derivatives of Tartaric Acid*. Proceedings of the 38th Annual Technical Meeting of the North America Thermal Analysis Society, 2010.

61. Tyssee, D. A.; Bausher, L. P.; Haake, P. Displacement at Phosphorus by a Mechanism with A1 Character. Acid-Catalyzed Hydrolysis of Phosphinanilides. *J. Am. Chem. Soc.* **1978**, *95* (24), 8066–8072.

62. Dhawan, B.; Redmore, D. *o*-Hydroxyaryl Diphosphonic Acids. *J. Org. Chem.* **1984**, *49* (21), 4018–4021.

Controlled Ring-Opening Polymerization of *L*-Lactide Triggered by Supramolecular Organocatalytic Systems

Joji Kadota,[a] Sylvain Koeller,[b] Dražen Pavlović,[a] Jean-Pierre Desvergne,[b] Brigitte Bibal,[b] Frédéric Peruch,*,[a] and Alain Deffieux[a]

[a]Laboratoire de Chimie des Polymères Organiques, UMR CNRS 5629, 16 Avenue Pey Berland, 33607 Pessac Cedex, France
[b]Université de Bordeaux, UMR CNRS 5255, 351 cours de la Libération, 33405 Talence Cedex, France
***peruch@enscbp.fr**

In this paper, we describe our last discoveries concerning new original organocatalytic systems that take advantages of supramolecular interactions to trigger the Ring-Opening Polymerization of *L*-lactide. (Thio)Amidoindoles and *N,N*-dimethylaminopyridine based systems proved to be efficient catalysts that allow an excellent control of the polymerization. In all cases, dual activation of the monomer and the polymer growing chain-end was demonstrated.

Introduction

Over the past decades, great efforts have been made to develop new synthetic methods for polymer synthesis, such as single site catalysts for olefin polymerization (*1–4*), metathesis polymerization (*5, 6*) or controlled free-radical polymerization (*7–10*). Most of them are based on transition metal catalysts, which are very hard to remove from the polymer and reveal to be undesirable for some applications (biomedical and microelectronics for example). As a consequence, it is of high interest to develop new alternatives based on non-metallic polymerization processes.

Enzyme-catalyzed polymerizations, which have been explored for quite a long time, constitute one alternative route for metal free polymerization (*11–13*).

Nevertheless, even if several kinds of polymer (polysaccharides, polyphenol, polyaniline, polyesters, polycarbonate, etc.) are now accessible through this route, enzyme availability is still limited and polymerizations are often not well controlled and appear as very slow processes.

Another promising alternative is the use of organic catalysts (*14–18*). Currently, organocatalyzed polymerization has been essentially developed for the Ring Opening Polymerization (ROP) of cyclic esters, diesters and carbonates (*19*, *20*). From a mechanistic point of view, it has been demonstrated that these ROP can be promoted by organocatalysts *via* the activation of the reagents, through temporary covalent bonds or weak interactions. The strategies have encompassed the activation of the monomer, *i.e.* the electrophile (using Brönsted acids (*21–25*), alcohols (*26*), DMAP derivatives (*18*), phosphines (*27*), *N*-heterocyclic carbenes (*28–31*)), the activation of the polymer growing chain, *i.e.* the nucleophile (using basic phosphazenes (*32*, *33*), biazabicycle DBU and triazabicycle MTBD (*34–36*)) or the dual activation of both monomer and chain end (thiourea derivatives (*37*, *38*) and triazabicyclodecene TBD (*39*)).

In this paper, we report the ring opening polymerization of lactide using original organocatalytic systems based on Hydrogen-Bonds (H-bonds) that control the activation of both monomer and growing chain.

Results and Discussion

Ring-Opening Polymerization of *L*-lactide Catalyzed by (Thio)Amidoindoles

Among the H-bonding organocatalysts, thioureas (*40–43*) have shown promising results in the access of polymers with controlled molar masses, operating under mild conditions (20 °C, loading of catalyst below 10 % mol). This remarkable catalytic activity relies on their ability to promote hydrogen bonds with the monomer and thus the smooth increase of its electrophilicity. Additionally, a H-bond acceptor cocatalyst partner, generally a tertiary amine, was required to increase the nucleophilicity of the initiator and the polymer growing chain. These catalytic systems can be a unique compound such as the Takemoto's catalyst **1** (*44*, *45*), or two independent molecules such as thiourea **2** + amine **3** (Scheme 1). Under drastic anhydrous conditions, at 20 °C in 24 h, catalyst **1** (5 % mol in dichloromethane, 5 % mol of initiator) allowed 97 % conversion of lactide into a poly(lactide) with a narrow polydispersity index and controlled molar masses, as the experimental degree of polymerization DP matches with the theoretical one. The ROP of lactide was also efficient in 24 h, in the presence of thiourea **2** and cocatalyst dimethylcyclohexylamine (Me$_2$NCy) **3a** or (−)-sparteine (Sp) **3b** (Scheme 1). Notably, due to better H-bonding properties of **3b** *vs* **3a**, the combination of **2** + **3b** allowed a complete polymerization reaction within 2 h whereas time reaction in the presence of the partners **2** + **3a** was 24 h (*37*).
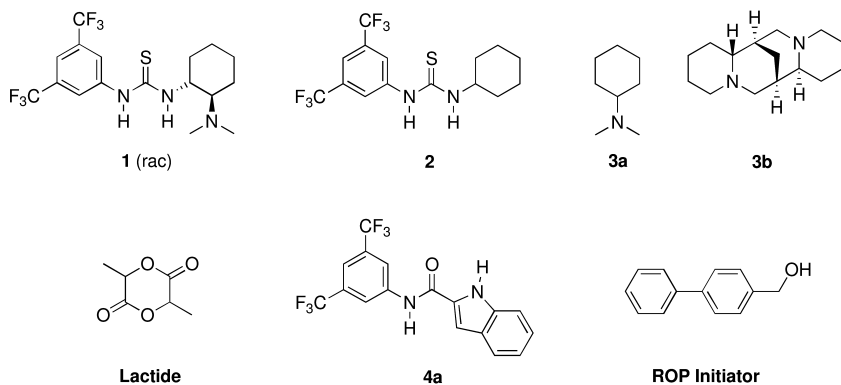
*Scheme 1. H-bonding organocatalysts designed for the dual activation of the reagents involved in the ROP of lactide, initiated by a primary alcohol: **1**, systems **2**+**3** and **4a** +**3***

To expand the scope of controlled ROP, new H-bonding organocatalysts are highly desirable, especially versatile ones. They should be available through a rapid synthesis and should be efficient at room temperature under easy-going conditions. Our interest in supramolecular chemistry (*46–48*) prompted us to design H-bonding catalysts for the ROP of lactide. In this context, amides, which are modular compounds of an easy synthetic access, were anticipated as polymerization promoters through H-bonding.

As part of our exploration of modular catalytic systems based upon separate dual functionalities (*49, 50*), we were interested in a donor + acceptor combination of two distinct hydrogen-bonding structures, that can promote polymerization, through the activation of both electrophile and nucleophile in the reaction medium.

We showed that, in the presence of (–)-sparteine **3b**, an activated amido-indole **4a** is an efficient organocatalyst (*49*). We did demonstrate that both NH groups from the amide and the indole moieties, participate to the H-bonding of lactide, thus allowing its total conversion in 2 h.

Moreover, an X-ray structure of a H-bonded complex between a ROP organocatalyst and the monomer was reported for the first time (Figure 1). In the crystal, the molecules are packed in layers (interlayer separation: *ca.* 3.2 Å). Molecules **4a** are arranged in head-to-tail dimers where the N-H of the indole moiety is tightly H-bonded with the carbonyl group of the amide linker. These H-bonds are not identical, and vary from 2.11 to 2.19 Å. Inspection of the molecular packing underlines that, within (**4a**)$_2$, each molecule **4a** forms a H-bonded complex with one *L*-lactide.

In order to deepen and broaden our investigation, we decided to explore the behaviour of a series of amides and related thioamides **4**, which bear an indole group, as a second H-bond donor (Scheme 2).
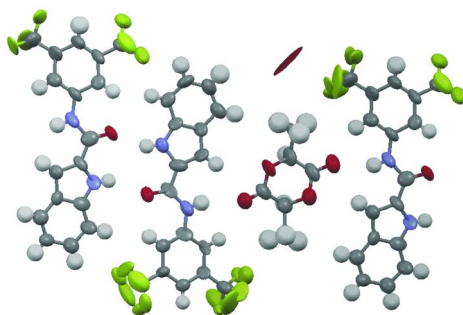
*Figure 1. Molecular packing of **4a** and L-lactide, showing the different H-bonded associations in one layer: Dimer (**4a**)₂ and complex **4a**: L-Lactide. Oxygen atoms are represented in red, nitrogen in blue and fluorine in green.*

4a: X = O
4b: X = S

4c: X = O
4d: X = S
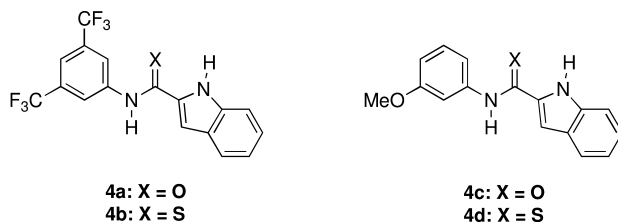
*Scheme 2. Molecular structures of H-bonding organocatalysts **4a-d***

In compounds **4a-d**, the global geometry of the H-bond donor subunits is identical and should not have an impact upon the catalytic properties. Besides, the strength of the H-donor properties of the NH-C=X group could also be modulated by two factors: (i) the nature of the X atom, oxygen (amide function) or sulfur (thioamide function), (ii) the electronic density on the phenyl group, from electron-deficient derivatives (**4a-b**) to electron-rich compounds (**4c-d**). Classically, thioamides are better H-bond donors and less subjected to self-aggregation. Electron-deficient substituents should increase the H-bond donor properties of the corresponding compounds. Finally, the effect of the cocatalyst in these ROP will also be evaluated using two tertiary amines **3a** or **3b**, as H-bond acceptors of a different strength (*34*).

The possible disadvantage of this approach is the potential formation of H-bonds between the partner activators, *i.e.* **4** and **3**, which could hamper the reaction efficiency. Consequently, a detailed supramolecular mechanism of ROP involving partner organocatalysts will be explored. Herein, we report the synthesis and the in-depth catalytic properties of new H-bonding organocatalysts for the polymerization of lactide, in connection with their aggregative properties.

Synthesis of the Catalysts

the straightforward preparation of new compounds **4** was achieved in one or two steps from commercial reagents, in high yields (*50*). Detailed descriptions of the X-ray structures were also reported for molecules **4a** and **4c**. All catalysts are found to be fairly soluble in dichloromethane. In the presence of lactide, this solubility is increased, which allows to undertake reactions under classical conditions (20 °C, 5 % mol with respect to monomer, *i.e.* 35 mM). This behavior is probably due to specific intermolecular interactions between the H-bonding catalysts and lactide as an H-bond acceptor. This is well supported by the weak interactions between reagents and catalysts (*vide infra*), unrevealed so far.

H-Bonding Properties in Solution

based on the observations in the solid state, we decided to investigate the propensity of the catalysts to self-aggregate in solution. Titrations monitored by ^{1}H NMR (CDCl$_3$) were conducted on compounds **2** (as a model) and **4** in the 0.5-35 mM concentration range. NMR spectra showed concentration dependent chemical shifts, except for compounds **4b** and **4d**. The variations mainly concern the amide NH groups and, to a lesser extent, some aromatic or aliphatic protons. These observations were interpreted as the formation of H-bonded complexes between complementary O=C-NH moieties. Experimental data were fitted with a model of dimerization (except compound **2** which oligomerizes).

Taken as a reference catalyst in ROP of lactide, thiourea **2** showed moderate aggregative properties (K$_{aggreg}$ = 6 M^{-1}) which were not reported before us (*50*). Amidoindoles **4a** and **4c** form dimers with a small association constant (K$_{dimer}$ = 4 and 5 M^{-1} respectively). Notably, thioamidoindoles **4b** and **4d** do not aggregate ($\Delta\delta_{Max}$ < 0.05 ppm). This behavior is expected for thiocarbonyles, because the latter are less efficient H-bond acceptors than their oxo-derivatives. Interestingly, even if the values of the self-association constants are weak (4-6 M^{-1}), *ca.* 15-20 % of dimer is present in solution, under the ROP conditions (concentration of catalyst = 35 mM). This data has obviously to be taken into account for the evaluation of the catalytic activity.

Catalytic Properties in ROP Reactions

Molecules **4** were tested as organocatalysts in the ROP of lactide, chosen as a model monomer. Classical conditions were employed: concentration of lactide at 0.7 M in dichloromethane, 20 °C, using biphenylmethanol as the initiator (5 % mol) and a cocatalyst **3a** or **3b** (5 % mol) as an activator of the initiator/polymer growing chain (Table 1). All experiments were conducted under anhydrous conditions (dry reagents and solvents) and in the presence of 4 Å molecular sieves to trap residual water, a competitor of the catalysts in the H-bonding process. An independent experiment proved that the activated or non activated molecular sieves had no catalytic effect upon reactions. Preliminary experiments showed

that each component alone (amide **4**, cocatalyst **3**, initiator) was not able to trigger the ROP of lactide (*49*), indicating the necessary presence of the three partners for the polymerization to proceed. Time reactions were programmed between 24 h and 72 h to evaluate the kinetics. When, in the presence of **3b**, the conversion of the monomer overcame 50 %, the crude polylactides were characterized by the average molar mass determined by ^{1}H NMR, ($M_{n\ NMR}$) and size exclusion chromatography ($M_{n\ SEC}$). The polydispersity index PDI was also determined from the SEC analysis.

Table 1 shows the conditions of the ROP experiments in the presence of different organocatalysts **1**, **2**, or **4** and a cocatalyst **3** and the characterization of the resulting polylactides. Molar masses determined by ^{1}H NMR ($M_{n\ NMR}$) are in good agreement with the theoretical value ($M_{n\ TH}$) whereas molar masses determined by SEC are overestimated, as they are calculated versus polystyrene standards.

Under our conditions, in the presence of molecular sieves, thioureas **1** and **2** allowed a very good conversion (85-100 %, entries 1-3), especially when the cocatalyst was **3b**, recognized as a better H-bond acceptor than **3a** (*34*). Moreover, the polylactides with a narrow polydispersity index and predictable molar mass were obtained in reasonable time (24 h). The catalytic efficiency of **1** and **2** under our conditions is thus identical to that previously reported (*37, 38*).

Each compound **4** was found to be active and allowed the conversion of lactide in 24 h with 43 % to 100 % yield. Notably, all polymers had a narrow polydispersity index (PDI = 1.05-1.07) coupled with experimental molar mass determined by ^{1}H NMR in agreement with theory ($M_{n\ TH}$) assuming the formation of one chain per initiator molecule (Table 1).

Compound **4a** with an electron-withdrawing group is the most active catalyst of the series (run 4, 72-100 % conv.). Its corresponding electron-donating derivative **4c** and its thioamide derivative **4b** are less active, allowing 53-74 % conv. (run 8) and 43-53 % conv. (run 6), respectively. These observations can be explained by two opposite phenomena: in the structure of **4c**, the amido NH is less acid than in **4a** and thus it is a worse H-bond donor than **4a** whereas, in compound **4b**, the acidity of NH is largely increased (in acetonitrile, pK_a (S=C-NH) = 11-13 and pK_a (O=C-NH) = 17) (*51, 52*) and thus might be partly inhibited by the basic species present in the solution, *i.e.* the cocatalyst **3** (*vide infra*). Interestingly, catalyst **4c** was as efficient as its thio-derivative **4d**. In this case, due to the electron-rich aromatic substituent, the NH group is a poorer H-bond donor whatever the nature of the C=X bond.

As expected, the ROP of lactide appeared to be strongly dependent upon the nature of the partner organocatalysts. Indeed, the catalytic activity of (thio)amides **4a-d** was slightly influenced by the H-bond acceptor character of amine **3** (runs 4, 6, 8 and 9). In the presence of the better H-bond activator **3b**, the percentage of conversion was higher in 24 h: 53-100 % compared to 43-72 % when **3a** was employed as a cocatalyst. Notably, quantitative conversion with **4a** was obtained in 2 h in the presence of **3b** (run 4 indicates the conversion after 2 h). These observations can be ascribed to the better H-bond donor character of amine **3b** (*34, 37, 38*). This assumption will be checked by the measurement of the corresponding association constants (*vide infra*). For partner catalysts **3a** + **4a** or

3a + **4b**, conversion was significantly increased when reaction time was extended to 48 h (runs 5 and 7), indicating that polymerization was still going on and that chain ends were not deactivated. This phenomenon was already observed with thiourea **2** (run 3). Kinetics of these ROP reactions were slow in some cases and were dependent upon the activation efficiency of both catalytic partners.

Variation of the [Monomer]/[Initiator] ratio from 20 to 50 and 100 led to narrowly dispersed polymers (PDI = 1.12 and 1.11 respectively), again with masses that match the theoretical ones (respectively, $M_{n\ SEC}$ = 8400 g/mol and 12000 g/mol, to be compared to their $M_{n\ TH}$ = 7384 g/mol and 14584 g/mol). Besides, ^{13}C NMR indicates that the polymers exhibit a fully isotactic structure suggesting the absence of side transesterification reactions. Additionally, a chain extension experiment was successfully realized: at first, the polymerization of lactide was conducted in standard conditions (run 4, 100 % conversion, $M_{n\ TH}$ = 3064 g/mol, $M_{n\ SEC}$ = 3470 g/mol and PDI = 1.08, after 24h) and, secondly, the same quantity of lactide was added. After 24h, the conversion was total and the resulting polylactide had similar characteristics ($M_{n\ TH}$ = 5944 g/mol, $M_{n\ SEC}$ = 7570 g/mol and PDI = 1.12). All this did support that a controlled process is occurring in these organocatalysed ROP reactions.

Table 1. ROP Conditions and Properties of the Poly(lactide)s

Run	Catalyst	Time	Conv.[a]		$M_{n\ TH}$[b]	$M_{n\ NMR}$[c]	$M_{n\ SEC}$[d]	PDI[d]
		(h)	**3a**	**3b**	(g/mol)	(g/mol)	(g/mol)	
1	**1**	24	95	100	3070	3210	5150	1.08
2	**2**	24	85	100	3070	2633	5420	1.10
3	**2**	48	95	-	2920	2778[e]	3970[e]	1.06
4	**4a**	24	72	100[f]	3070	3070	4460	1.07
5	**4a**	48	95	-	2920	3498[e]	4190[e]	1.06[e]
6	**4b**	24	43	53	1630	1480	1907	1.05
7	**4b**	48	63	59	1810	1769	2119	1.05
8	**4c**	24	53	74	2270	2489	2850	1.07
9	**4d**	24	54	71	2180	2489	3200	1.07

SOURCE: Reproduced with permission from reference (*49*). Copyright Wiley-VCH Verlag GmbH & Co. KGaA. Lactide 0.7 M in CH$_2$Cl$_2$; catalyst **4** (5 % mol); Tertiary amine **3** (5 % mol); biphenylmethanol as initiator (5 % mol); 4Å molecular sieves; 20 °C. [a] Monomer conversion determined by ^{1}H NMR. [b] Theoretical molar mass when conversion was 100 %. [c] Experimental molar mass determined by ^{1}H NMR. [d] Experimental molar mass determined by Size Exclusion Chromatography in THF at 40°C *versus* polystyrene standards. [e] Experiment achieved in the presence of amine **3a**. [f] Time: 2 h.

Supramolecular Insight into the ROP Reactions

Partner organocatalysts were poorly studied in the ROP reactions. In this field of research, to the best of our knowledge, only one binding constant of 39 M^{-1} was measured in C_6D_6 between thiourea **2** and valerolactone (*34*), which represents a rough model for the ROP of lactide in dichloromethane. In a first approach, we can speculate that these H-bonding compounds **4** and **3** respectively activate the monomer and the initiator/growing chain in a similar manner as the thiourea organocatalysts (Figure 2, framed equilibria). However, we already demonstrated that organocatalysts **4** can self-aggregate in a dimeric form. Thus an extra equilibrium K_{dimer} is present in the reaction medium and should be considered in the mechanism (Figure 2).

Additional titrations monitored by ^1H NMR were achieved in $CDCl_3$ to demonstrate intermolecular interactions between the multiple components of the reaction: (i) catalyst and lactide (equilibrium K_1), (ii) initiator and cocatalyst **3** (equilibrium K_2), (iii) catalyst and cocatalyst **3** (equilibrium K_3) (*50*).

Based upon the values of K_1-K_3 that range from 2 to 14 M^{-1}, we showed that partner catalysts can self-inhibit through undesired H-bonding. Nevertheless, as all supramolecular species are in equilibrium, the progress of the ROP reaction appeared mainly driven by the balance between the four equilibria present in solution (K_{dimer}, K_1-K_3). A remarkable value was noticed between organocatalyst **4b** and (−)-sparteine **3b** which bind much strongly ($K_3 \sim 57$ M^{-1}). This result can explain the poorer catalytic properties of thioamide **4b** in the presence of the basic amine **3b** compared to those obtained with the cocatalyst **3a** which is a weaker base.
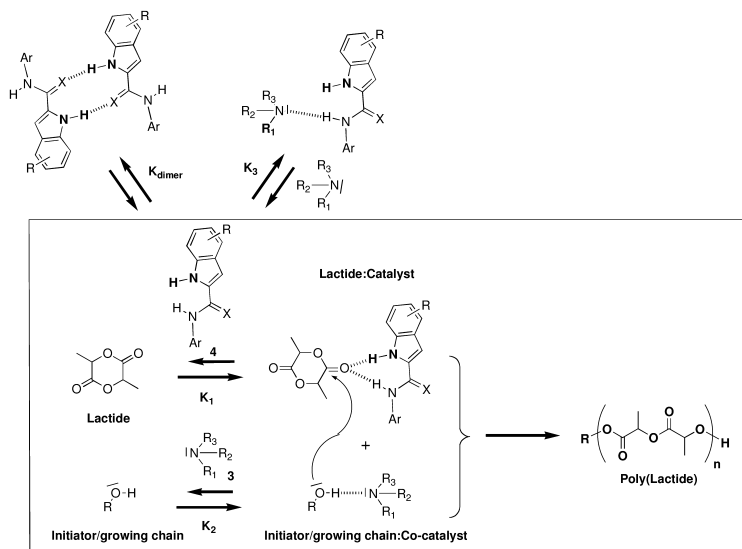
Figure 2. Multiple H-bonding equilibria involving reactants and catalysts 4 + 3 during the Ring Opening Polymerization of lactide. (Copyright Wiley-VCH Verlag GmbH & Co. KGaA. Reproduced with permission).

Intermolecular interactions do exist between the different H-bond donor and acceptors in solution. The dynamic equilibria are favourably shifted towards the formation of the polylactide in a controlled manner (predictable M_n and narrow PDI), especially when the organocatalyst poorly interact with itself or with its cocatalyst.

Ring-Opening Polymerization of L-lactide Catalyzed by DMAP/DMAP.HX

Catalysts for transesterification reactions are either acid-type or base-type. On one hand, acidic catalysts activate ester groups *via* protonation to increase its electrophilicity. On the other hand, basic catalysts activate alcohols through H-bond thus enhancing their nucleophilicity. Generally, acid-type and base-type catalysts cannot co-exist, as they will neutralize each other immediately. However, if these two catalytic systems could work together, the activity towards transesterification reactions should be strongly enhanced. So it was attempted to make co-exist a base and an acid form. To this end, the use of equivalent amounts of *N,N*-dimethylaminopyridine (DMAP), which has already revealed good catalytic activity for lactide polymerization (*18*), and protonated *N,N*-dimethylaminopyridine (DMAP.HX), as dual catalyst for *L*-lactide (*L*-LA) polymerization was investigated (Scheme 3).

Polymerizations were performed at room temperature in dichloromethane. *para*-Phenyl benzyl alcohol (*p*-PhBzOH) or 1-phenylethanol (PhEtOH) were used as initiators. A ratio initiator/DMAP/DMAP.HX of 1/1/1 was selected. The results are summarized in Table 2.

As already reported in the literature (*18*), DMAP alone is able to catalyze the ring-opening polymerization of *L*-lactide, but the conversion is low (runs 10 and 15, less than 20% after 24 h). On the other hand, DMAP.HX alone is unable to trigger the ROP of *L*-lactide, whatever the chemical nature of X. The combination of DMAP and DMAP.HX revealed to be more effective (runs 11 to 13 and 16 to 18). The nature of the counter anion had also a significant effect since for the same polymerization time, changing from Cl⁻ to $F_3CSO_3^-$ the yield increased significantly. When the triflic acid DMAP salt and DMAP were used, quantitative polymerization of *L*-lactide was achieved in 48 h (run 14). Furthermore, theoretical molar masses are in good agreement with experimental ones indicating a controlled polymerization. Besides, either primary or secondary alcohols can be used to initiate the polymerization, giving similar yields.

Kinetics of *L*-lactide polymerizations catalyzed by DMAP/DMAP.HX were also investigated. The conversions versus time curves are plotted on Figure 3. Results confirm reactivity order indicated in Table 1. DMAP/DMAP.HOTf is the most active catalytic system and activities decrease in the order: DMAP/DMAP.HOTf > DMAP/DMAP.HOMs, DMAP/DMAP.HCl > DMAP alone. Moreover, linear variation of ln([L-LA]$_0$/[L-LA]) versus time is in agreement with a first kinetic order with respect to monomer.

DMAP.HX

DMAP

X⁻ : Cl⁻, H₃CSO₂O⁻, F₃CSO₂O⁻
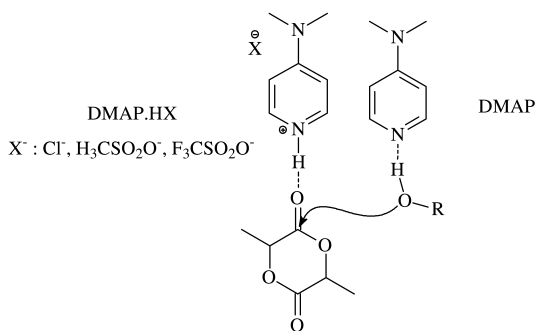
Scheme 3. Possible activation mechanism for the ring-opening polymerization of L-lactide with N,N-dimethylaminopyridine and its protonated form

Table 2. L-LA Polymerization by DMAP/DMAP.HX in Dichloromethane at Room Temperature

Run	Initiator	DMAP.HX X	Conv.[a] (%)	$M_{n\,TH}$[b] (g/mol)	$M_{n\,NMR}$[c] (g/mol)	$M_{n\,SEC}$[d] (g/mol)	PDI[d]
10	p-PhBzOH	-	16	650	690	660	1.12
11	p-PhBzOH	Cl	35	1200	1200	1300	1.12
12	p-PhBzOH	OSO₂CH₃	38	1300	1300	1300	1.12
13	p-PhBzOH	OSO₂CF₃	54	1700	1800	2000	1.13
14[e]	p-PhBzOH	OSO₂CF₃	100	3100	3000	3500	1.06
15	PhEtOH	-	21	900	570	770	1.12
16	PhEtOH	Cl	29	950	910	850	1.17
17	PhEtOH	OSO₂CH₃	37	1170	1250	930	1.12
18	PhEtOH	OSO₂CF₃	62	1980	1400	930	1.13

L-LA: 100 mg; CH₂Cl₂: 1 mL; Initiator/DMAP/DMAP.HX: 1/1/1 (5 %-mol); Temperature: 25°C; Time: 24 h. [a] Monomer conversion determined by ¹H NMR. [b] Theoretical molar mass. [c] Experimental molar mass determined by ¹H NMR. [d] Experimental molar mass determined by Size Exclusion Chromatography in THF at 40°C *versus* Polystyrene standards. [e] Time: 48 h.

Maldi-Tof spectrometry was also performed in order to characterize more precisely the polylactides. For those initiated by *p*-PhBzOH (Figure 4), one peak series corresponding to polylactide chains initiated by the alcohol is observed. No trace of chains resulting from side initiation is detected. Nevertheless, a second series shifted from 72 g/mol, corresponding to half lactide unit is also present and is due to transesterification reactions. For polylactide initiated by PhEtOH (Figure 5), a single peak series is observed with molar masses in agreement with polylactide chains initiated by the alcohol. This result has to be linked to the

observation made by Hedrick *et al.* in the case of polylactide depolymerization experiments, when DMAP was used as catalyst (*53*). Indeed, it was shown that secondary alcohols were not able to depolymerize polylactides in contrast to primary ones.
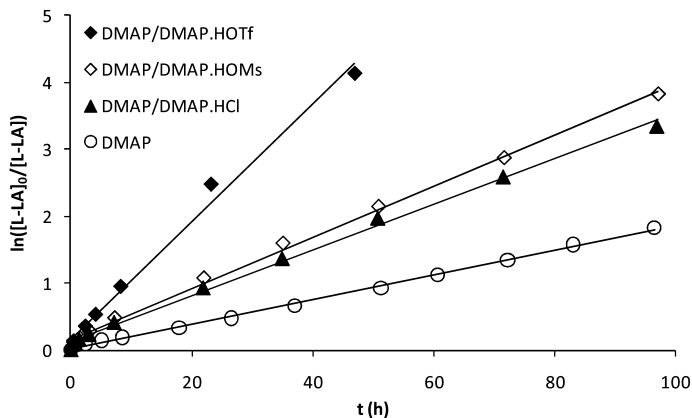
Figure 3. Kinetics of L-LA polymerization catalyzed by DMAP/DMAP.HX at 25°C in CD$_2$Cl$_2$.
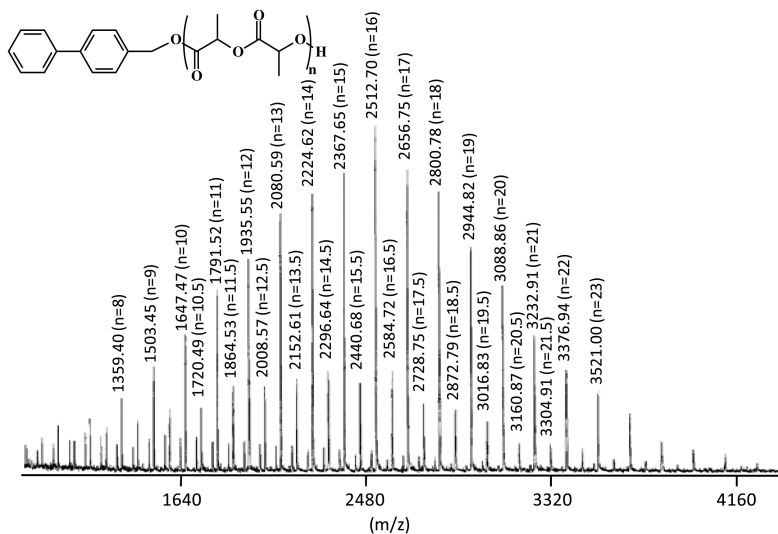
Figure 4. MALDI-TOF spectrum of poly(L-LA) initiated by p-PhBzOH and catalyzed by DMAP/DMAP.HOTf.
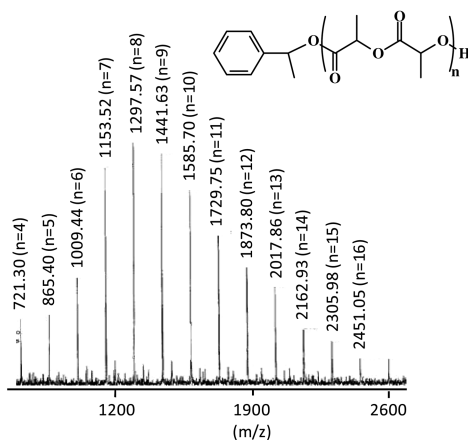
Figure 5. MALDI-TOF spectrum of poly(L-LA) initiated by PhEtOH and catalyzed by DMAP+DMAP.HOTf.
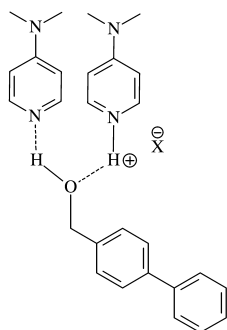
Scheme 4. Presumed complex of DMAP/DMAP.HX and initiator

Based on ^{1}H NMR experiments, strong interactions were observed between the catalytic system and the initiator (alcoholic proton highly shifted). When DMAP and DMAP.HX are combined, the same chemical shift is detected for the alcoholic proton and the acidic one, suggesting the complex shown in Scheme 4. Concerning the interaction between the monomer and the catalytic system, none to weak chemical shifts are observed, suggesting very weak interactions. During polymerization experiments followed by ^{1}H NMR, the complex showed on Scheme 4 is detected all along the polymerization process (Figure 6). A possible mechanism pathway could be as following: the complex shown on Scheme 4 could be a dormant species that could dissociate to yield the actual propagating species (initiator activated by DMAP and monomer activated by DMAP.HX) that will ring-open *L*-lactide.
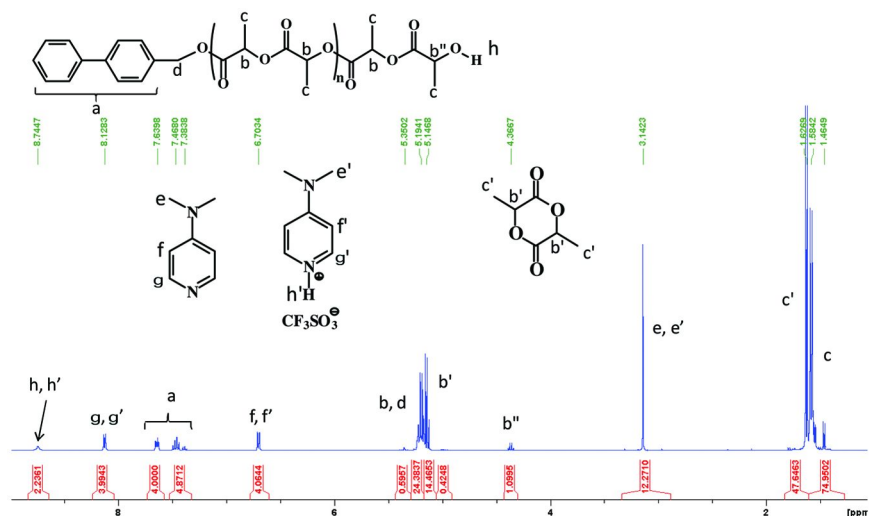
Figure 6. ¹H NMR spectrum of the ROP reaction medium.
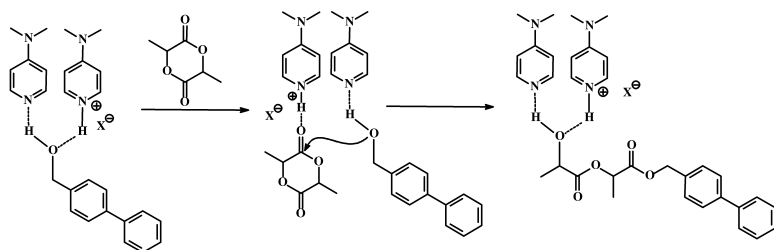
Scheme 5. Presumed polymerization mechanism with DMAP/DMAP.HX catalytic system

Conclusion

In conclusion, activated (thio)amides bearing a second H-bond donor group, **4** were straightforwardly synthesized and proved to be efficient organocatalysts for the controlled ROP of lactide. The catalytic power of the NH amide group was shown to be better when the aromatic substituent is electro-deficient and when NH is an amide *vs.* a thioamide. We also demonstrated that the H-bonding partner catalysts **4** + **3** do play their role by activating the monomer and the polymer growing chain, respectively. Notably, for the first time, undesirable H-bonds between the partner catalysts were highlighted. Some associations were strong and thus inhibit the catalytic power of the new (thio)amides. In a general manner, as H-bonding catalysts may be involved in multiple equilibria in the reaction medium, binding partners should be judiciously chosen to tune the outcome of the polymerization.

Fine controlled Ring-Opening Polymerization of *L*-lactide by new organic catalysts based on a concept of acid-base cooperative function was also performed.

DMAP and DMAP.HX act as acidic and basic catalysts at the same time and their combination is more active than DMAP alone, giving well-controlled polymers, provided that secondary alcohol is used as an initiator. It is believed that activation of both chain end and the monomer simultaneously occurs, explaining the reactivity increase. Moreover, these organic catalysts are easily accessible.

Acknowledgments

References

1. Böhm, L. L. *Angew. Chem., Int. Ed. Engl.* **2003**, *42*, 5010–5030.
2. Kaminsky, W.; Laban, A. *Appl. Catal., A* **2001**, *222*, 47–61.
3. Mülhaupt, R. *Macromol. Chem. Phys.* **2003**, *204*, 289–327.
4. Wilke, G. *Angew. Chem., Int. Ed. Engl.* **2003**, *42*, 5000–5008.
5. Bielawski, C. W.; Grubbs, R. H. *Prog. Polym. Sci.* **2007**, *32*, 1–29.
6. Grubbs, R. H. *Tetrahedron* **2004**, *60*, 7117–7140.
7. Braunecker, W. A.; Matyjaszewski, K. *Prog. Polym. Sci.* **2007**, *32*, 93–146.
8. Hawker, C. J.; Bosman, A. W.; Harth, E. *Chem. Rev.* **2001**, *101*, 3661–3688.
9. Kamigaito, M.; Ando, T.; Sawamoto, M. *Chem. Rev.* **2001**, *101*, 3689–3745.
10. Matyjaszewski, K.; Xia, J. *Chem. Rev.* **2001**, *101*, 2921–2990.
11. Gross, R. A.; Kumar, A.; Kalra, B. *Chem. Rev.* **2001**, *101*.
12. Kobayashi, S. *Macromol. Rapid Commun.* **2009**, *30*, 237–266.
13. Kobayashi, S.; Makino, A. *Chem. Rev.* **2009**, *109*, 5288–5353.
14. Kiesewetter, M. K.; Shin, E. J.; Hedrick, J. L.; Waymouth, R. M. *Macromolecules* **2010**, *43*, 2093–2107.
15. Bourissou, D.; Moebs-Sanchez, S.; Martin-Vaca, B. *C. R. Chim.* **2007**, *10*, 775–794.
16. Dove, A. P. *Chem. Commun.* **2008**, 6446–6470.
17. Kamber, N. E.; Jeong, W.; Waymouth, R. M.; Pratt, R. C.; Lohmeijer, B. G. G.; Hedrick, J. L. *Chem. Rev.* **2007**, *107*, 5813–5840.
18. Nederberg, F.; Connor, E. F.; Möller, M.; Glauser, T.; Hedrick, J. L. *Angew. Chem. Int. Ed. Engl.* **2001**, *40*, 2712–2715.
19. Nederberg, F.; Lohmeijer, B. G. G.; Leibfarth, F.; Pratt, R. C.; Choi, J.; Dove, A. P.; Waymouth, R. M.; Hedrick, J. L. *Biomacromolecules* **2007**, *8*, 153–160.
20. Pratt, R. C.; Nederberg, F.; Waymouth, R. M.; Hedrick, J. L. *Chem. Commun.* **2008**, 114–116.
21. Gazeau-Bureau, S.; Delcroix, D.; Martin-Vaca, B.; Bourissou, D.; Navarro, C.; Magnet, S. *Macromolecules* **2008**, *41*, 3782–3784.
22. Kricheldorf, H. R.; Kreiser, I. *Macromol. Chem. Phys.* **1987**, *188*, 1861–1873.
23. Lou, X. D.; Detrembleur, C.; Jerome, R. *Macromolecules* **2002**, *35*, 1190–1195.

24. Persson, P. V.; Schroder, J.; Wickholm, K.; Hedenstrom, E.; Iversen, T. *Macromolecules* **2004**, *37*, 5889–5893.

25. Sanda, F.; Sanada, H.; Shibasaki, Y.; Endo, T. *Macromolecules* **2002**, *35*, 680–683.

26. Coulembier, O.; Sanders, D. R.; Nelson, A.; Hollenbeck, A. N.; Horn, H. W.; Rice, J. E.; Fujiwara, M.; Dubois, P.; Hedrick, J. L. *Angew. Chem., Int. Ed.* **2009**, *48*, 5170–5173.

27. Myers, M.; Connor, E. F.; Glauser, T.; Möck, A.; Nyce, G. W.; Hedrick, J. L. *J. Polym. Sci., Part A-1: Polym. Chem.* **2002**, *40*, 844–851.

28. Connor, E. F.; Nyce, G. W.; Myers, M.; Mock, A.; Hedrick, J. L. *J. Am. Chem. Soc.* **2002**, *124*, 914–915.

29. Coulembier, O.; Lohmeijer, B. G. G.; Dove, A. P.; Pratt, R. C.; Mespouille, L.; Culkin, D. A.; Benight, S. J.; Dubois, P.; Waymouth, R. M.; Hedrick, J. L. *Macromolecules* **2006**, *39*, 5617–5628.

30. Dove, A. P.; Pratt, R. C.; Lohmeijer, B. G. G.; Culkin, D. A.; Hagberg, E. C.; Nyce, G. W.; Waymouth, R. M.; Hedrick, J. L. *Polymer* **2006**, *47*, 4018–4025.

31. Jeong, W.; Hedrick, J. L.; Waymouth, R. M. *J. Am. Chem. Soc.* **2007**, *129*, 8414–8415.

32. Zhang, L.; Nederberg, F.; Messman, J. M.; Pratt, R. C.; Hedrick, J. L.; Wade, C. G. *J. Am. Chem. Soc.* **2007**, *129*, 12610–12611.

33. Zhang, L.; Nederberg, F.; Pratt, R. C.; Waymouth, R. M.; Hedrick, J. L.; Wade, C. *Macromolecules* **2007**, *40*, 4154–4158.

34. Lohmeijer, B. G. G.; Pratt, R. C.; Leibfarth, F.; Logan, J. W.; Long, D. A.; Dove, A. P.; Nederberg, F.; Choi, J.; Wade, C.; Waymouth, R. M.; Hedrick, J. L. *Macromolecules* **2006**, *39*, 8574–8583.

35. Pratt, R. C.; Lohmeijer, B. G. G.; Long, D. A.; Waymouth, R. M.; Hedrick, J. L. *J. Am. Chem. Soc.* **2006**, *128*, 4556–4557.

36. Sun, X.; Gao, J. P.; Wang, Z. Y. *J. Am. Chem. Soc.* **2008**, *130*, 8130–8131.

37. Dove, A. P.; Pratt, R. C.; Lohmeijer, B. G. G.; Waymouth, R. M.; Hedrick, J. L. *J. Am. Chem. Soc.* **2005**, *127*, 13798–13799.

38. Pratt, R. C.; Lohmeijer, B. G. G.; Long, D. A.; Lundberg, P. N. P.; Dove, A. P.; Li, H.; Wade, C.; Waymouth, R. M.; Hedrick, J. L. *Macromolecules* **2006**, *39*, 7863–7871.

39. Chuma, A.; Horn, H. W.; Swope, W. C.; Pratt, R. C.; Zhang, L.; Lohmeijer, B. G. G.; Wade, C. G.; Waymouth, R. M.; Hedrick, J. L.; Rice, J. E. *J. Am. Chem. Soc.* **2008**, *128*, 6749–6754.

40. Berkessel, A.; Cleemann, F.; Mukherjee, S.; Muller, T. N.; Lex, J. *Angew. Chem., Int. Ed.* **2005**, *44*, 807–811.

41. Connon, S. J. *Chem. Eur. J.* **2006**, *12*, 5418–5427.

42. Takemoto, Y. *Org. Biomol. Chem.* **2005**, *3*, 4299–4306.

43. Taylor, M. S.; Jacobsen, E. N. *Angew. Chem., Int. Ed.* **2006**, *45*, 1520–1543.

44. Hoashi, Y.; Okino, T.; Takemoto, Y. *Angew. Chem., Int. Ed.* **2005**, *44*, 4032–4035.

45. Okino, T.; Hoashi, Y.; Takemoto, Y. *J. Am. Chem. Soc.* **2003**, *125*, 12672–12673.

46. Dumartin, M. L.; Givelet, C.; Meyrand, P.; Bibal, B.; Gosse, I. *Org. Biomol. Chem.* **2009**, *7*, 2725–2728.

47. Givelet, C.; Buffeteau, T.; Arnaud-Neu, F.; Hubscher-Bruder, V.; Bibal, B. *J. Org. Chem.* **2009**, *74*, 5059–5062.
48. Givelet, C.; Tinant, B.; Van Meervelt, L.; Buffeteau, T.; Marchand-Geneste, N.; Bibal, B. *J. Org. Chem.* **2009**, *74*, 652–659.
49. Koeller, S.; Kadota, J.; Deffieux, A.; Peruch, F.; Massip, S.; Léger, J.-M.; Desvergne, J.-P.; Bibal, B. *J. Am. Chem. Soc.* **2009**, *109*, 15088–15089.
50. Koeller, S.; Kadota, J.; Peruch, F.; Deffieux, A.; Pinaud, N.; Pianet, I.; Massip, S.; Léger, J.-M.; Desvergne, J.-P.; Bibal, B. *Chem. Eur. J.* **2010**, *16*, 4196–4205.
51. Frank, R.; Jakob, M.; Thunecke, F.; Fischer, G.; Schutkowski, M. *Angew. Chem., Int. Ed.* **2000**, *39*, 1120–1122.
52. Sifferlen, T.; Rueping, M.; Gademann, K.; Jaun, B.; Seebach, D. *Helv. Chim. Acta* **1999**, *82*, 2067–2093.
53. Nederberg, F.; Connor, E. F.; Glauser, T.; Hedrick, J. L. *Chem. Commun.* **2001**, 2066–2067.

Chapter 11

Zinc Complexes with Mono- and Polydentate Behaving Guanidine Ligands and Their Application in Lactide Polymerization

Janna Börner,[1] Ines dos Santos Vieira,[2] Ulrich Flörke,[1] Artjom Döring,[3] Dirk Kuckling,[3] and Sonja Herres-Pawlis*,[2]

**[1]Department of Chemistry, Inorganic Chemistry, Universität Paderborn Warburger Str. 100, 33098 Paderborn, Germany
[2]Department of Chemistry, Inorganic Chemistry II, Technische Universität Dortmund, Otto-Hahn-Str. 6, 44227 Dortmund, Germany
[3]Department of Chemistry, Organic Chemistry, Universität Paderborn Warburger Str. 100, 33098 Paderborn, Germany
* sonja.herres-pawlis@tu-dortmund.de**

Mono- and polydentate behaving guanidine ligands and their corresponding zinc complexes were prepared and investigated towards the influence of these special ligand classes on the molecular structures of the complexes as well as their performance in the ring-opening polymerization of lactide. All synthesized complexes exhibit polymerization activity and a correlation between ligand bite and denticity on the complex activity could be derived. In an integrated approach, these experimental results were accompanied by DFT calculations which evaluate the important role of the positive charge on the zinc center for the substrate activation. Further crucial influences on initiator design were identified.

Introduction

Polylactide or poly(lactic acid) (PLA) is an aliphatic polyester which can be produced by ring-opening polymerization (ROP) of lactide (LA), the cyclic diester of lactic acid. The monomer for PLA production is available from renewable raw materials like corn or sugar beets by a bacterial fermentation process. The

polylactide which is obtained by metal-catalyzed ROP can be either recycled or composted after use and therefore is CO_2 emission neutral. But also its unique physical properties qualify PLA to be a viable alternative to petrochemical-based plastics. Combined with its biocompatibility and its ability to degrade both in vivo and in vitro PLA has a great range of potential applications reaching from wide-spread use including coating, fibres, films and packages to special medical and pharmaceutical fields (*1*, *2*). PLAs have proven to be the most attractive and useful class of biodegradable polyesters among the numerous polyesters studied to date.

However, until now, PLA is still more expensive than petrochemical-based plastics and therefore it is merely used in biomedical applications and packaging of organic products. To change the polymer from a speciality material to a large-volume commodity plastic the development of new polymerisation catalysts is required. Most large-scale processes are based on the use of stannous compounds as initiators (*1*, *2*). For use in food packaging or similar applications, heavy metals are undesirable because of accumulation effects (*2*).
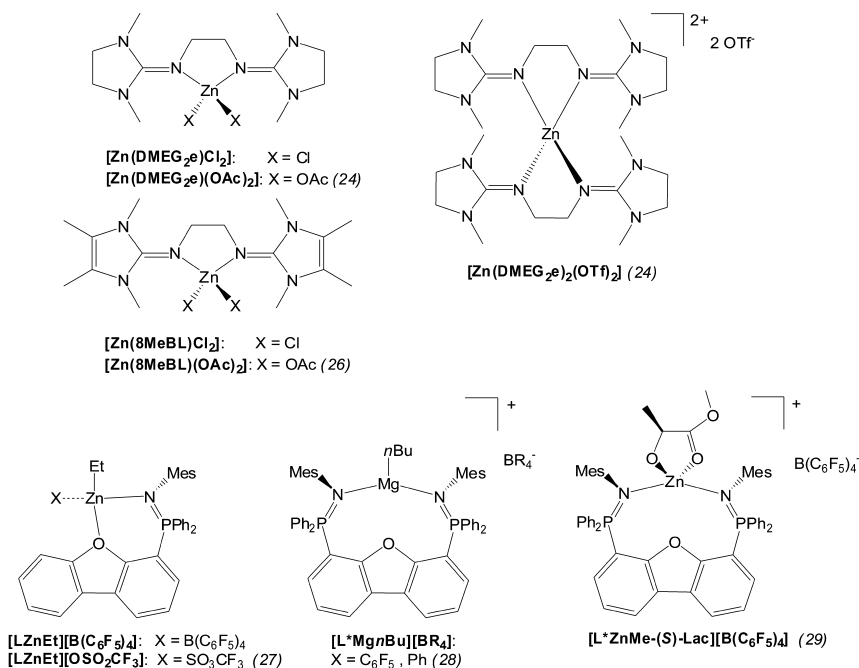
Scheme 1. Guanidine and phosphinimine complexes active in ROP of lactide or ε-caprolactone

Consequently, the development of new single-site metal catalysts for the ring-opening polymerization of lactide has seen tremendous growth over the past decade (*3–8*). A vast multitude of well-defined Lewis acid catalysts following a coordination-insertion mechanism has been developed for this reaction mainly based on tin (*9*), zinc (*10–13*), aluminium (*14*, *15*) and rare earth metals (*16–20*). Moreover, organocatalysts have been successfully used in the ROP (*21–23*).

However, the high polymerization activity of all these systems is often combined with high sensitivity towards air and moisture. For industrial purposes and especially the breakthrough of PLA in the competition with petrochemical based plastics, there is an exigent need for active initiators that tolerate air, moisture and small impurities in the monomer (*1*, *2*). The disadvantageous sensitivity can be ascribed to the anionic nature of the ligand systems stabilising almost all of these complexes. Up to now, only few ROP active systems using neutral ligands in single-site metal catalysts have been described. They make use of strong donors such as guanidines (*24–26*) and phosphinimines (*27–29*) for the ROP of lactide and ε-caprolactone (Scheme 1).

Guanidine systems gain their unique properties from the ability to effectively delocalise a positive charge over the CN_3 moiety (*25*, *26*, *30–32*). The guanidine ligands represent strong donors comparable to β-ketiminates but the resulting zinc complexes possess a considerably higher stability towards moisture and lactide impurities (*24*, *25*). Up to now, the anionic congeners of the guanidines, the guanidinates, have found great attention as stabilising ligands for ROP active catalysts with a variety of metals (*20*, *33–35*).

Previous studies have demonstrated that the mono- and bis-chelate guanidine systems exhibit great robustness and high catalytic activity at the same time (*24*, *25*). We found that the ROP activity depends on the amount of positive partial charge on the zinc center and the corresponding negative charge on the guanidine N_{imine} atoms (*25*). We relate this to a coordination-insertion-mechanism as working principle of our catalyst class (*26*). Our hypothesis implies the coordination of the lactide to the zinc center followed by nucleophilic attack of the guanidine on the carbonyl C atom of the lactide molecule (transition state TS1). The guanidine N_{imine} donor function is basic and nucleophilic enough to conduct the ring-opening of the lactide as first step of the polymerization. Prior to this step, the guanidine has to stride away from the zinc center (TS0) in order to allow the close substrate coordination. After the nucleophilic attack, we propose the formation of tetrahedral intermediates (INT1 and INT2) and the subsequent C-O bond breaking in accordance to other systems (*9*). The mechanism is detailed in Scheme 2. DFT calculations on this mechanism are presently carried out.

In the present contribution, we extend the former study by using NBO charges for the described systems and we present five new guanidine ligands with different binding motifs and seven new zinc guanidine complexes which show good ROP activity. Additionally, we provide with the NBO charges for the new complexes in order to evaluate the described correlation.
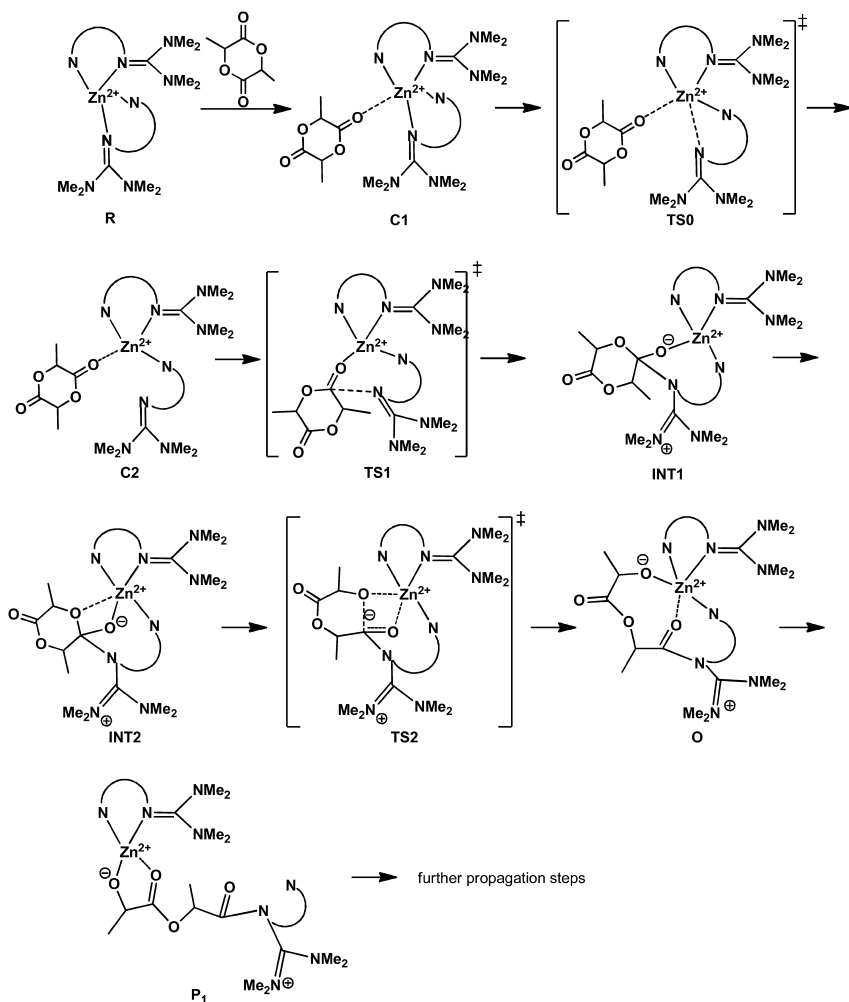
Scheme 2. Coordination-insertion mechanism for the ROP of lactide with a bis-chelate guanidine complex (R = reactants, C = zinc coordinated lactide, TS = transition state, INT = tetrahedral intermediate, P = propagating species).

Results and Discussion

Guanidine-Pyridine Chelate Zinc Complexes

As we recently reported (*25*), guanidine-pyridine chelate zinc complexes display excellent activity in the ROP of lactide. We were able to correlate the catalytic activity with the positive charge on the zinc atom which is crucial for the coordination and activation of the substrate lactide and the negative partial charge on the coordinating guanidine N_{imine} atoms. At that point in time, we calculated Mulliken charges by using density functional theory on B3LYP/6-31G(d) level. We chose B3LYP density functional theory and the 6-31G(d) basis sets because previous studies (*25*, *26*, *35–39*) have demonstrated that gas phase DFT calculations using this combination of functional and basis set are able to describe zinc N-donor complexes reasonably and it has been used successfully for DFT studies on ring-opening polymerization before (*9*, *40–43*) As natural bond orbital (NBO) charges are more trustful towards basis set change and comparison between substance classes (*44*, *45*), we herein provide with the corresponding NBO charges at B3LYP/6-31G(d) level for the complexes **1**-**10** (Figure 1, Table I).
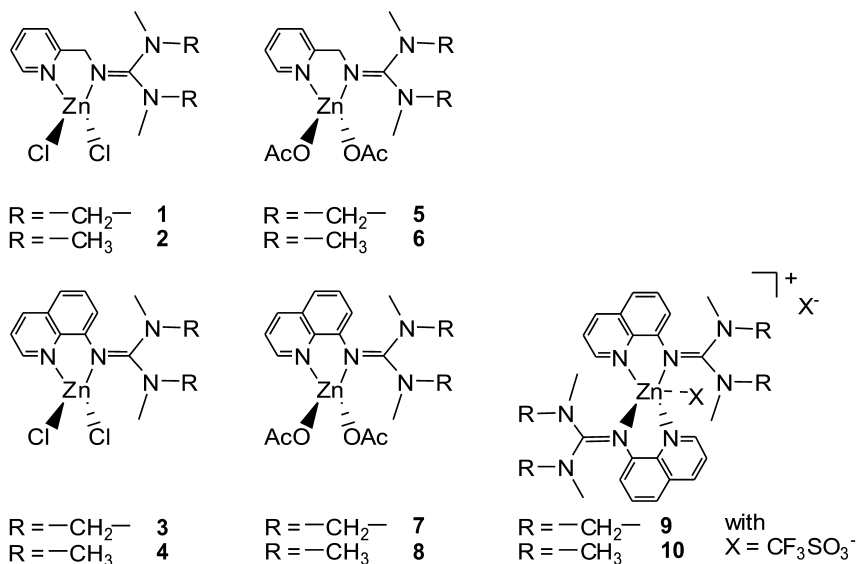
*Figure 1. Schematic depiction of complexes **1-10**.*

In Renewable and Sustainable Polymers; Payne, G., et al.;
ACS Symposium Series; American Chemical Society: Washington, DC, 2011.

Table I. NBO charges in electron units (charge of electron is equal to 1) of complex 1 - 10 (RB3LYP/6-31G(d))

	1	*2*	*5*	*6*
Zn	1.012	1.006	1.254	1.262
N_{py}	-0.548	-0.541	-0.553	-0.555
N_{gua}	-0.734	-0.718	-0.725	-0.716
C_{gua}	0.699	0.693	0.692	0.689
N_{amine}	-0.447	-0.450	-0.445	-0.457
	-0.484	-0.492	-0.490	-0.492
X=Cl,	-0.625	-0.622	-0.829	-0.828
OAc	-0.638	-0.637	-0.781	-0.785
	3	*4*	*7*	*8*
Zn	1.018	1.020	1.261	1.265
N_{py}	-0.536	-0.536	-0.547	-0.545
N_{gua}	-0.718	-0.711	-0.732	-0.726
C_{gua}	0.715	0.704	0.729	0.718
N_{amine}	-0.459	-0.442	-0.405	-0.435
	-0.420	-0.458	-0.455	-0.447
X=Cl,	-0.618	-0.620	-0.796	-0.802
OAc	-0.638	-0.641	-0.812	-0.816
	9		*10*	
Zn	1.320		1.333	
N_{py}	-0.574, -0.578		-0.604, -0.554	
N_{gua}	-0.777, -0.796		-0.752, -0.784	
C_{gua}	0.724, 0.709		0.694, 0.695	
$>N_{amine}$	-0.428, -0.440		-0.441, -0.460	
	-0.414, -0.431		-0.405, -0.456	
O	-1.003, -0.996		-1.038, -0.979	

Summarising the NBO results, the same trend can be deduced as found for the Mulliken charges (*25*): complexes with higher positive partial charge on the zinc center exhibit higher polymerization activity. Especially the bis-chelate complexes **9** and **10** are the most active complexes and they display the highest positive partial charge on the zinc and the most negative charge on the guanidine N_{imine} atom. Our further studies will use NBO partial charges for reasons of comparability.

Zinc Complexes with Monodentate Behaving Guanidine-Pyridine Ligands

In order to investigate the influence of different spacer units on the molecular structures and the properties of the corresponding complexes, the ligands N-(1,3-dimethylimidazolidin-2-ylidene)-3-methylpyridin-2-amine (DMEGpico) and 1,1,3,3-tetramethyl-2-(3-methylpyridin-2-yl)guanidine (TMGpico) as well as their chlorido and acetato complexes were synthesized and completely characterized. The amine 2-amino-3-picoline which possesses only one C building block between the N-donor functions was chosen as spacer-amine component due to its high structural similarity to 2-picolylamine (py) which offers a C_2 spacer and was used to prepare the ligands DMEGpy and TMGpy and their zinc complexes (*25*). The obtained chlorido complexes were tested for their ability to act as initiators in the ROP of lactide and their activity is compared to those of the chlorido complexes stabilised by the similar ligands, DMEGpy and TMGpy, which possess longer spacer units.

The syntheses of the guanidine-pyridine hybrid ligands DMEGpico and TMGpico were carried out by the condensation of 2-amino-3-picoline with the corresponding Vilsmeier salts (dimethylethylenechloroformamidinium chloride and tetramethyl chloroformamidinium chloride, respectively) in analogy to already reported guanidine syntheses (*30–32*, *46*, *47*). Figure 2 depicts the schematic structure of DMEGpico and TMGpico. Their reaction with equimolar amounts of zinc salts (ZnCl$_2$, Zn(CH$_3$COO)$_2$) in a dry, aprotic solvent (MeCN, THF) resulted in straightforward formation of the zinc complexes [Zn(DMEGpico)$_2$Cl$_2$] (**11**), [Zn(TMGpico)$_2$Cl$_2$] (**12**) and [(TMGpico)$_2$Zn$_3$(CH$_3$COO)$_6$] (**13**) in yields of 67-98%. Colorless single crystals of the complexes were obtained by slow diffusion of diethyl ether in a saturated solution.

The molecular structures of **11**, **12** and **13** were determined by single crystal X-ray analysis (Figures 3 and 4). The molecular structures of **12** exhibit two molecules per asymmetric unit. Due to their high similarity in the following only one structure is discussed as **12**.

In all three complexes, the ligands DMEGpico and TMGpico which both possess guanidine as well as pyridine N-donor atoms, coordinate the zinc atom only by the pyridine donor and thus act as monodentate ligands. The N$_{gua}$ with an average value of 2.854 Å is too far away from the zinc center to support interaction. This coordination behaviour is affected by the close distance of the N-donor atoms generating a very small bite.
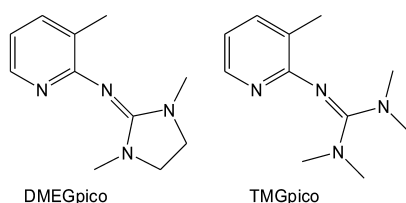
DMEGpico   TMGpico

Figure 2. Schematic structure of DMEGpico and of TMGpico.
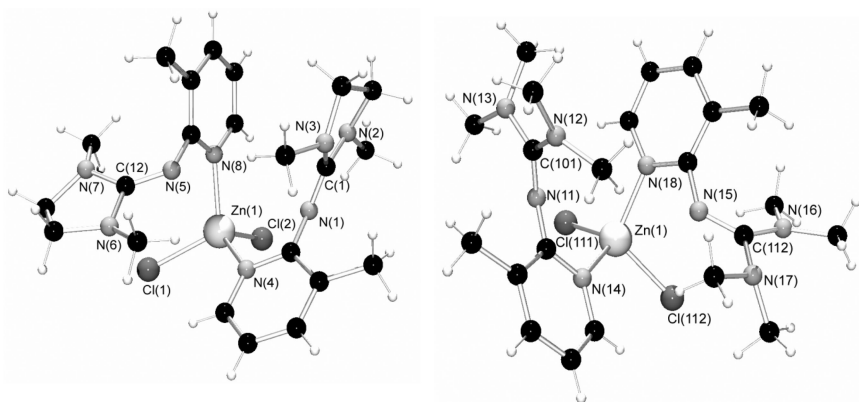
*Figure 3. Crystal structure of [Zn(DMEGpico)$_2$Cl$_2$] (**11**, left) and of [Zn(TMGpico)$_2$Cl$_2$] (**12**, right) as determined at 120 K.*
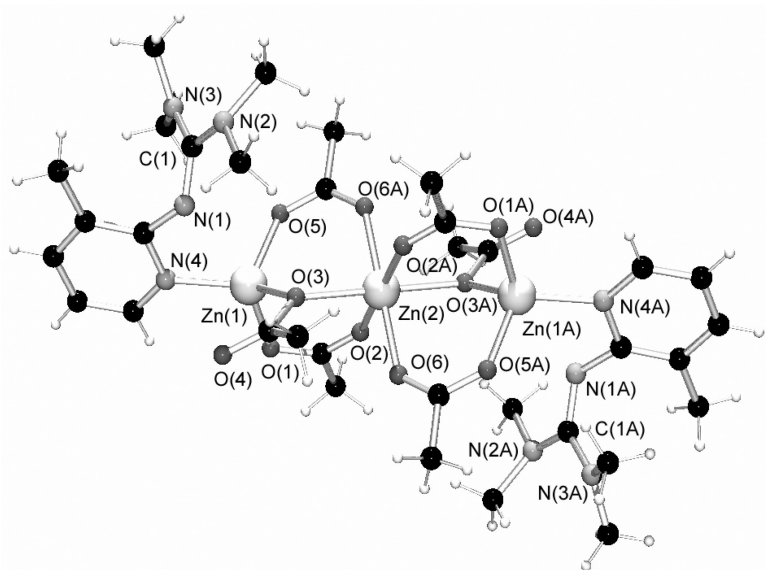
*Figure 4. Molecular structure of [Zn$_3$(TMGpico)$_2$(CH$_3$COO)$_6$] (**13**) as determined at 120 K.*

Table II. Selected bond lengths (Å) and bond angles (°) of 11 and 12

	11	*12*
Zn-N$_{py}$	2.039(3), 2.055(3)	2.036(2), 2.049(2)
Zn-Cl	2.285(1), 2.286(1)	2.277(1), 2.278(1)
C$_{gua}$-N$_{gua}$	1.294(4), 1.292(5)	1.301(2), 1.299(2)
C$_{gua}$-N	1.376(5), 1.375(5),	1.363(2), 1.370(2),
	1.374(5), 1.369(5)	1.362(2), 1.381(2)
N-Zn-N	112.9(1)	115.3(1)
Cl-Zn-Cl	108.4(1)	107.5(2)
Đ (ZnCl$_2$, ZnN$_{py2}$)	82.4	83.2
Structural parameter ρ	0.94, 0.94	0.95, 0.95

In the chlorido complexes [Zn(DMEGpico)$_2$Cl$_2$] (**11**) and [Zn(TMGpico)$_2$Cl$_2$] (**12**) the zinc center is twofold coordinated by two N$_{py}$ atoms of two guanidine-pyridine ligands and the remaining coordination sites are occupied by two chlorido ions resulting in a distorted tetrahedral coordination (Figure 3 and Table II). The Zn-N$_{py}$ bond lengths of the two coordinated ligands differ slightly from each other (**11**: 2.039(3), 2.055(3); **12**: 2.036(2), 2.049(2) Å) whereas the Zn-Cl bonds are equal in length (**11**: 2.285(1), 2.286(1); **12**: 2.277(1), 2.278(1) Å). In the guanidine moiety of DMEGpico and TMGpico the C$_{gua}$-N$_{gua}$ bond is with a difference of av. 0.08 (**11**) or av. 0.07 Å (**12**) significantly shorter than the C$_{gua}$-N bonds compared to similar complexes like [Zn(DMEGpy)Cl$_2$] (**1**) and [Zn(TMGpico)Cl$_2$] (**2**) in which the ligands coordinate the zinc atom also by the guanidine donor atom. In the latter case, the charge transfer generated by the coordination leads to the delocalisation of electron density over the guanidine function and to the levelling of bond length. For the evaluation of the levelling of intra-guanidine bond lengths, the structural parameter ρ was introduced by Sundermeyer et al. (*30*). In the case of a symmetrical CN$_3$ unit ρ is equal to 1. In the complexes **11** and **12**, ρ indicates with 0.94 and 0.95 a localized C=N bond. Remarkably, this value is slightly higher than in "free" guanidine-pyridine ligands with 0.93 (*48*).

The same effect was also observed for the guanidine moieties in the zinc acetato complex [Zn$_3$(TMGpico)$_2$(CH$_3$COO)$_6$] (**13**, Figure 4). This complex possesses a trinuclear solid-state structure in which two Zn atoms are coordinated each by the pyridine N-donor atom of the ligand TMGpico and three oxygen atoms of three acetato bridging ligands resulting in a distorted tetrahedral coordination environment. Each of the bridging ligands connects each Zn atom with a third Zn atom located between them. Consequently, the latter shows an octahedral coordination environment where each corner is occupied by an acetato oxygen atom. Interestingly, in each case two acetato ligands bridge the Zn atoms via two oxygen functions but the third acetato ligand connects the metal atoms via only one oxygen atom of the acetate group. This structure motif is very similar to that found for [Zn$_3$(bipy)$_2$(CH$_3$COO)$_6$] (*49*). The values for the Zn-O bonds in **13** depend on the coordination mode of the acetato ligands. The Zn-O bonds

at the terminal zinc atoms are in average with 1.978 Å generally shorter than those belonging to the ZnO_6 octahedron (av. 2.090 Å). Selected bond lengths and angles are summarised in Table III.

Table III. Selected bond lengths (Å) and bond angles (°) of 13

	13
Zn-N$_{py}$	2.016(3)
Zn-O	1.962(2), 1.983(2), 1.989(2), 2.062(2), 2.082(3), 2.126(2)
C$_{gua}$-N$_{gua}$	1.307(5)
C$_{gua}$-N	1.350(5), 1.365(5)
O-Zn-O	104.2(1), 105.5(1), 102.5(1), 180.0, 87.8(1), 92.2(1), 180.0, 91.1(1), 89.0(1), 88.2(1), 91.8(1), 180.0
Structural parameter ρ	0.96

Table IV. Polymerization of D,L-lactide initiated by 11 and 12

Initiator		Time[a] [h]	Yield [%]	M_w [g/mol]	PD[b]	P_r[c]
[Zn(DMEGpico)$_2$Cl$_2$]	**11**	24	79	37300	1.9	
[Zn(DMEGpico)$_2$Cl$_2$]	**11**	48	84	34200	1.9	
[Zn(TMGpico)$_2$Cl$_2$]	**12**	24	78	35600	1.7	0.52
[Zn(TMGpico)$_2$Cl$_2$]	**12**	48	82	34500	1.7	

Reaction conditions: Catalyst (0.2 mol%), 150 °C. [a] reaction times were not necessarily optimised. [b] PD = M_w/M_n where M_n is the number-average molar mass. [c] From analysis of the ^{1}H homonuclear decoupled NMR spectrum using the equation $P_r^2 = 2$ [sis] (*11*).

Based on mechanistic proposals on the ring-opening polymerization of lactide mediated by guanidine-pyridine zinc complexes (*25*, *26*) it is proposed that the guanidine function of the coordinated ligand plays a key role during the first ring-opening step. Possibly the uncoordinated guanidine functions close to the reaction center in **11** and **12** support the polymerization reaction and enhance the catalytic activity. Therefore, the chlorido complexes **11** and **12** were tested for their ability to initiate the ring-opening polymerization of D,L-lactide according to the standard procedure (0.2 mol% catalyst, 150°C). In order to rate the catalytic activity of the complexes, the polymer yield, the molecular weights as well as

the polydispersity of the PLA were determined (see Table IV). The tacticity was analysed by homonuclear decoupled ^{1}H NMR spectroscopy (*11*).

11 and **12** show independently of the coordinated ligand almost the same catalytic activity. Only the width of the molecular weight distribution is for **11** slightly higher. Their yields are quite high, but the experimental observed M_w values are smaller than the calculated ones (e.g. $M_{w,exp.} = 37,000$; $M_{w,theor.} = 57,000$ g/mol). Compared to the chlorido complexes containing the ligands DMEGpy and TMGpy, complexes **1** and **2** (*25*), which possess a spacer one CH_2 unit longer than in DMEGpico and TMGpico, their catalytic performance lies in the same range. Just complex **2** shows higher activity. Hence, it could not be demonstrated that the uncoordinated guanidine function near the reaction center supports the polymerization reaction.

In order to evaluate the hypothesis that high positive partial charge on the zinc center and more negative charge on the guanidine N_{imine} atom promotes the activity in ROP, we analysed complexes **11** – **13** by DFT. Tables V and VI summarize the most important geometrical parameters of these complexes. These tables show that the DFT methodology reproduces the experimental structures reasonably. The coordinational environment is in good agreement with the solid-state structure and the ligand structure within the complexes is reproduced excellently as well. Table VII collects the NBO charges for complexes **11**-**13**.

Table V. Key geometrical parameters of complex 11 and 12 calculated by DFT (RB3LYP/6-31G(d))

	11	*12*
Zn-N$_{py}$	2.060, 2.081	2.063, 2.083
Zn-Cl	2.273, 2.301	2.273, 2.303
C$_{gua}$-N$_{gua}$	1.287, 1.296	1.303, 1.299
C$_{gua}$-N	1.386, 1.377, 1.395, 1.377	1.379, 1.389, 1.384, 1.384
N-Zn-N	114.3	116.0
Cl-Zn-Cl	115.6	115.8
Ð (ZnCl$_2$, ZnN$_{py2}$)	85.4	85.6
Structural parameter ρ	0.93, 0.94	0.94, 0.94

Table VI. Key geometrical parameters of complex 13 calculated by DFT (RB3LYP/6-31G(d))

	13
Zn-N$_{py}$	2.034
Zn-O	1.969, 1.969, 1.990,
	1.990, 2.088, 2.112
C$_{gua}$-N$_{gua}$	1.301
C$_{gua}$-N	1.384, 1.383
Structural parameter ρ	0.93

Table VII. NBO charges in electron units (charge of electron is equal to 1) of complex 11 - 13 (RB3LYP/6-31G(d))

	11	*12*	*13*
Zn	1.064	1.058	1.286, 1.286, 1.298
N$_{py}$	-0.588, -0.591	-0.588, -0.585	-0.596, 0.596
N$_{gua}$	-0.620, -0.578	-0.577, -0.601	-0.588, -0.588
C$_{gua}$	0.684, -0.671	0.669, 0.684	0.676, 0.676
N$_{amine}$	-0.459, -0.456 -0.481, -0.489	-0.476, 0.477 0,484, -0.483	-0.474, -0.474 -0.485, 0.485
X=Cl, OAc	-0.652, -0.671	-0.654, 0.672	-0,794, -0,803, -0,861, -0,794, -0,803, -0,861, -0,718, -0,728, -0,861

The NBO analysis reveals that the positive partial charge on the zinc center is similar to those in the chlorido complexes **1 – 4**. The negative partial charge on the guanidine N$_{imine}$ atoms is not so distinct. As we propose that the guanidine function might help the ring-opening event (*25*, *26*), this finding is important for the understanding of the diminished reactivity of **11** and **12** in comparison to **1 – 4**. Addtionally, the unfavourable ligand bite might decrease the stability of the complexes and thus decrease the resulting polylactide chain length.

In summary, the guanidine-pyridine ligands DMEGpico and TMGpico as well as their chlorido and acetato complexes [Zn(DMEGpico)$_2$Cl$_2$] (**11**), [Zn(TMGpico)$_2$Cl$_2$] (**12**) and [Zn$_3$(TMGpico)$_2$(CH$_3$COO)$_6$] (**13**) were synthesized and characterized. Due to their short spacer unit, **11** and **12** act as monodentate ligands by coordinating the zinc atoms via the pyridine N-donor atom. The chlorido complexes were proven to be active initiators in the ROP of lactide. An impact of the ligand spacer on the complex properties could be observed: i) the ligand bite prevents the guanidine function from coordination to the zinc center, ii) the uncoordinated guanidine function next to the reaction center neither promotes

the initiation of lactide polymerization nor increases the catalytic activity in case of **11** and **12.**

Zinc Complexes with Polydentate Tris- and Tetraguanidine Ligands

Polydentate ligands like scorpionates are well suited to stabilise complexes which are active in lactide ROP (*50*). In this context, the novel neutral tetradentate guanidine ligands 2,6-bis{[bis(2-aminoethyl)1,3-dimethylimidazo-lidin-2-ylidene]methyl}benzol (DMEG$_4$(baem)$_2$b) and 2,6-bis{[bis(2-aminoethyl)tetramethyl-guanidino]methyl}benzol (TMG$_4$(baem)$_2$b) as well as the tridentate ligands 1,1,1-tris{2-[2N-(1,3-dimethylethylene guanidino)]ethyl}-amine (DMEG$_3$tren) (*51*) and 1,1,1-tris{2-[N^2-(1,1,3,3-tetramethylguanidino)]-ethyl}amine (TMG$_3$tren) (*52*), first described by Sundermeyer et al., were synthesized. In order to create a tridentate ligand that possesses a very high steric demand, the ligand 2',2',2''-(2,2',2''-nitrilotris(ethane-2,1-diyl))tris(1,1,3,3-tetraethyl-guanidine) (TEG$_3$tren) was developed by us. Their reaction with zinc chloride gave the corresponding zinc complexes which were investigated towards their catalytic activity in the ROP of lactide.

The tetradentate ligands DMEG$_4$(baem)$_2$b and TMG$_4$(baem)$_2$b were prepared by the reaction of four equivalents of chloroformamidinium chloride with the tetramine 2,6-bis{[bis(2-aminoethyl)amino]methyl}benzene. The latter is accessible in a three step synthesis starting with the protection of the amine functions of 1,5-diamino-3-azapentane as phthalimids according to Miranda et al. (*53*). In the next step two equivalents of the 1,5-phthalimido-3-azapentane were added to 2,6-bis(bromo-methyl)benzene to give the protected tetramine 2,6-bis{[bis(2-phthalimidoethyl)-amino]methyl}benzene (*54*). The removal of the protecting groups occurs by simple acidic cleavage (*54*) and 2,6-bis{[bis(2-aminoethyl)amino]methyl}benzene was obtained in almost quantitative yields.

The tridentate ligands DMEG$_3$tren and TMG$_3$tren were prepared according to literature procedures (*51*, *52*) To achieve a tridentate ligand with high steric demand, tris(2-aminoethyl)amine was reacted with three equivalents of the tetraethylchloroformamidinium chloride to give TEG$_3$tren. A schematic depiction of these polydentate ligands is given in Figure 5.

DMEG$_4$(baem)$_2$b R = Me, R' = -CH$_2$CH$_2$-
TMG$_4$(baem)$_2$b R = R' = Me

DMEG$_3$tren R = Me, R' = -CH$_2$CH$_2$-
TMG$_3$tren R = R' = Me
TEG$_3$tren R = Me, R' = Et
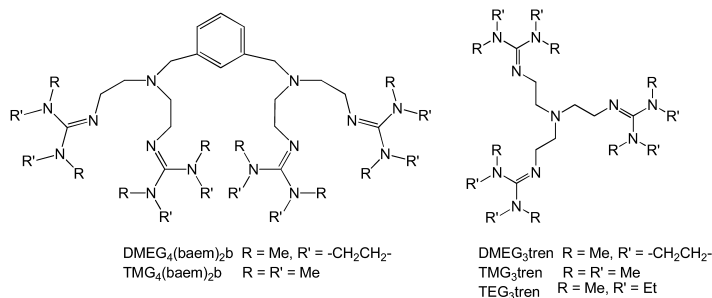
Figure 5. Schematic structure of polydentate guanidine ligands.
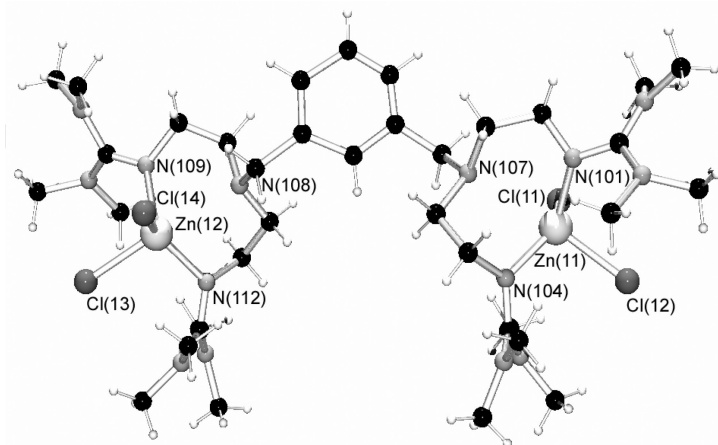
Figure 6. Crystal structure of [(TMG$_4$(baem)$_2$b)(ZnCl$_2$)$_2$] (14) as determined at 120 K.
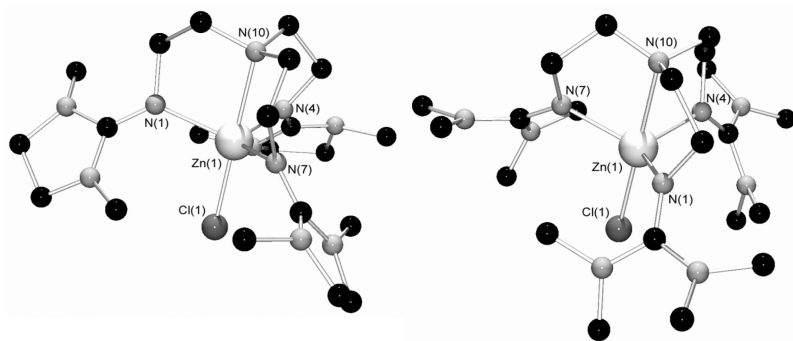
Figure 7. Molecular structure of [Zn(DMEG$_3$tren)Cl]$^+$ in crystals of [Zn(DMEG$_3$tren)Cl][Cl] (left, 15) and [Zn(TMG$_3$tren)Cl]$^+$ in crystals of [Zn(TMG$_3$tren)Cl][CF$_3$SO$_3$] (right, 17) as determined at 120 K. Hydrogen atoms were omitted due to reasons of clarity.

The complexes [(TMG$_4$(baem)$_2$b)(ZnCl$_2$)$_2$] (**14**), [Zn(DMEG$_3$tren)Cl][Cl] (**15**) and [Zn(TMG$_3$tren)Cl][Cl] (**16**) were obtained as colorless crystal solids in yields of 36-77% by stirring of the polydentate ligands with ZnCl$_2$ in dry THF. Single crystals of **14** and **15** were prepared by slow diffusion of ethyl ether in an acetonitrile solution of the complexes and their solid-state structures were determined by single crystal X-ray analysis (Figures 6 and 7). The crystal structures of **14** exhibit two molecules per asymmetric unit. Due to their high similarity, in the following only one structure is discussed as **14**. The crystals of **16** were strongly disordered and not suited for single crystal X-ray analysis. But the reaction of TMG$_3$tren with ZnCl$_2$ in the presence of triflate ions resulted in the formation of single crystals of [Zn(TMG$_3$tren)Cl][CF$_3$SO$_3$] which possess the same cationic structure motif as **16** and are discussed in the following as **17** (see Figure 7).

The polydentate ligand $TMG_4(baem)_2b$ in **14** does not coordinate one zinc atom fourfold, but two zinc atoms in a bidentate manner. The remaining coordination sites are occupied in each case by two chlorine atoms resulting in a distorted tetrahedral coordination geometry. The $Zn-N_{gua}$ distances are in each tetrahedron within the precision of measurements equal in length (av. 2.024 Å), whereas each tetrahedron exhibit one shorter (av. 2.302 Å) and one longer (av. 2.350 Å) Zn-Cl bond. Regarding the C-N bond lengths in the guanidine moiety, there is no clear trend observed within the precision of measurements.

The complexes **15** and **17** exhibit a trigonal-bipyramidal coordination geometry. The equatorial plane is defined by the N-donor atoms of the guanidine moieties ($Zn-N_{gua}$: av. 2.078 (**15**); av. 2.086 Å (**17**)), whereas the axial positions are taken by the amine nitrogen atom (Zn-N: 2.339(2) (**15**); 2.336(3) Å (**17**)) and the chlorido ligand (Zn-Cl: 2.332(2) (**15**); 2.356(1) Å (**17**)), respectively. The second chlorine atom or the triflate ion is far away from the metal center and acts as counter ion. Hence, the zinc atom is located in a molecular pocket formed by the N-donor ligands. This structure motif was also observed for the complexes $[Mn(TMG_3tren)Cl][Cl]$ and $[Zn(TMG_3tren)(CF_3SO_3)][CF_3SO_3]$ prepared by Sundermeyer et al. (*52*, *55*). The $C_{gua}-N_{gua}$ bonds are in each guanidine moiety with av. 1.311 (**15**) and av. 1.313 Å (**17**) equal in length and significantly shorter than the $C_{gua}-N$ bonds (**15**: av. 1.364; **17**: av. 1.364 Å). The kind of guanidine moiety shows no impact on the structural properties of the obtained complexes.

Selected bond lengths and angles of **14**, **15** and **17**are summarised in Table VIII.

The chlorido complexes **14**, **15** and **16** were tested for their ability to initiate the ring-opening polymerization of D,L-lactide according to the standard procedure (0.2 mol% catalyst calculated relative to the zinc centers, 150°C). In order to rate the catalytic activity of the complexes, the polymer yield, the molecular weights as well as the polydispersity of the PLA were determined (see Table IX). The tacticity was analysed by homonuclear decoupled ^1H NMR spectroscopy (*11*).

One idea concerning the preparation of zinc complexes stabilised by polydentate guanidine ligands was that the arms coordinating the zinc atom may release the metal atom easily when a substrate molecule approaches and that the guanidine function of the free arm supports the polymerization reaction and enhances the catalytic activity (*vide supra*). It is also supposable that the structure motif of a molecular pocket may influence the polymerization behaviour.

In contrast to these suggestions, the complexes **15** and **16** show neither an enhanced polymerization activity compared to other zinc guanidine systems nor can an impact on the microstructure be observed. Independent of the different ligands coordinated, they provide the same catalytic performance. PLAs were produced in respectable yields of around 70 % but the obtained chain length is smaller than it is in theory (e.g. $M_{w,exp.}$ = 22,000; $M_{w,theor.}$ = 50,000 g/mol). The chlorido complex **14** including tetrahedral coordinated zinc centers exhibits with yields of around 84 % higher polymerization activity than **15** and **16**. However, the M_w values of the produced polymer are also smaller than the theoretical values. This observation indicates the occurrence of side reactions leading to chain transfer or truncation. The polymerization activity of **15** and **16** may be affected by the

183

high steric hindrance of the guanidine units that hinder the accessibility to the zinc center and therefore the coordination and activation of lactide molecules. An impact on the stereo preference during the polymerization due to this high steric demand could not be observed for **15** and **16** (P_r = 0.53; 0.52.

Analogously to the precedent complexes, DFT is used to evaluate the influence of the amount of positive partial charge on the zinc center and negative charge on the guanidine N_{imine} atom on the activity in ROP. Table X summarizes the most important geometrical parameters whereas Table XI collects the NBO charges of these complexes. These tables show that the DFT methodology reproduces the experimental structures reasonably. The coordinational environment is in good agreement with the solid-state structure and the ligand structure with the complexes is in excellent agreement.

Table VIII. Selected bond lengths (Å) and bond angles (°) of 14, 15 and 17

	14	*15*	*17*
Zn-N$_{gua}$	2.001(10), 2.041(11), 2.012(10), 2.043(10)	2.074(2), 2.076(2), 2.084(2)	2.075(3), 2.085(3), 2.098(3)
Zn-N		2.339(2)	2.336(3)
Zn-Cl	2.301(3), 2.333(4), 2.302(4), 2.366(4)	2.332(1)	2.356(1)
C$_{gua}$-N$_{gua}$	1.332(15), 1.314(15), 1.310(17), 1.273(16)	1.307(2), 1.312(2), 1.313(2)	1.310(4), 1.316(4), 1.314(4)
C$_{gua}$-N	1.365(16), 1.305(16), 1.342(15), 1.353(15), 1.322(17), 1.385(17), 1.402(15), 1.356(15)	1.373(2), 1.350(2), 1.365(2), 1.380(2), 1.341(2), 1.376(2)	1.349(4), 1.372(4), 1.367(4), 1.360(4), 1.362(4), 1.372(4)
N-Zn-N	117.7(4), 118.1(4)		
Cl-Zn-Cl	104.1(1), 101.5(1)		
Đ (ZnCl$_2$, ZnN$_2$)	82.3, 83.1		
Structural parameter ρ	n/a	0.97, 0.96, 0.96	0.97, 0.96, 0.96

Table IX. Polymerization of D,L-lactide initiated by 14, 15 and 16

Initiator		Time[a]	Yield	M_w	PD[b]	P_r[c]
		[h]	[%]	[g/mol]		
$[TMG_4(baem)_2b(ZnCl_2)_2]$	**14**	24	81	36,000	1.9	0.54
$[TMG_4(baem)_2b(ZnCl_2)_2]$	**14**	48	86	33,000	1.9	
$[Zn(DMEG_3tren)Cl][Cl]$	**15**	24	72	21,000	1.8	0.53
$[Zn(DMEG_3tren)Cl][Cl]$	**15**	48	70	22,000	1.8	
$[Zn(TMG_3tren)Cl][Cl]$	**16**	24	71	22,000	1.9	0.52
$[Zn(TMG_3tren)Cl][Cl]$	**16**	48	69	21,000	1.8	

Reaction conditions: Catalyst (0.2 mol%, calculated per zinc center), 150 °C. [a] reaction times were not necessarily optimised. [b] PD = M_w/M_n where M_n is the number-average molar mass. [c] From analysis of the ^{1}H homonuclear decoupled NMR spectrum using the equation $P_r^2 = 2$ [sis] (*11*).

Complex **14** exhibits a smaller positive partial charge on the zinc center which is indicative for a decreased ROP activity. In fact, in spite of the polydentate ligand nature, both zinc centers seem to act as single initiation centers due to the special coordination motif with two dichloride zinc complex units. In the complexes **15** and **17**, the zinc center displays a positive charge which is comparable to that in the active acetato complexes **5 – 8**. Nevertheless, the activity of these complexes is rather mediocre which can be related to the steric hindrance around the zinc center. Three guanidine units encumber the access to the zinc center for the approaching lactide molecule. A special influence of the negative charge on the guanidine N_{imine} atom can not be derived here.

In this section the synthesis of the polydentate ligands $DMEG_4(baem)_2b$, $TMG_4(baem)_2b$ and TEG_3tren is reported. The zinc complexes stabilised by $TMG_4(baem)_2b$, $DMEG_3tren$ and TMG_3tren were prepared and tested for their catalytic activity in the ring-opening polymerization of D,L-lactide. They were all proven to be active initiators in lactide polymerization but positive influences characteristic for polydentate initiator systems like enhanced polymerization activity or impact on the PLA microstructure could not be observed. Instead, again the important role of sufficient positive partial charge on the zinc center and a good accessibility to the zinc center could be highlighted as essential prerequisites for lactide activation for ring-opening reactions.

Table X. Key geometrical parameters of complexes 14 - 17 calculated by DFT (RB3LYP/6-31G(d))

	14	*15*	*17*
Zn-N$_{gua}$	2.043, 2.044, 2.059, 2.059	2.070, 2.086, 2.156	2.055, 2.116, 2.153
Zn-N		2.342	2.336
Zn-Cl	2.304, 2.368, 2.304, 2.368	2.395	2.493
C$_{gua}$-N$_{gua}$	1.318, 1.322, 1.318, 1.322	1.310, 1.316, 1.317	1.317, 1.320, 1.326
C$_{gua}$-N	1.378, 1.367, 1.364, 1.384, 1.378, 1.367, 1.364, 1.384	1.399, 1.360, 1.368, 1.373, 1.363, 1.398	1.386, 1.366, 1.373, 1.378, 1.357, 1.382
N-Zn-N	116.5, 116.5		
Cl-Zn-Cl	108.1, 108.2		
Đ (ZnCl$_2$, ZnN$_2$)	80.5, 80.5		
Structural parameter ρ	0.96	0.96, 0.95, 0.95	0.97, 0.96, 0.96

Table XI. NBO charges in electron units (charge of electron is equal to 1) of complex 14 - 17 (RB3LYP/6-31G(d))

	14	*15*	*17*
Zn	1.083, 1.083	1.195	1.218
N$_{apical}$		-0.589	-0.590
N$_{gua}$	-0.755, -0.767 -0.755, -0.767	-0.761, -0.783, -0.804	-0.744, -0.760, -0.784
C$_{gua}$	0.693, 0.689, 0.693, 0.689	0.700, 0.715, 0.699	0.684, 0.685, 0.695

Continued on next page.

Table XI. (Continued). NBO charges in electron units (charge of electron is equal to 1) of complex 14 - 17 (RB3LYP/6-31G(d))

	14	*15*	*17*
N_{amine}	-0.451, -0.487, -0.450, -0.478 -0.451, -0.487 -0.450, -0.478	-0.425, -0.485 -0.435, -0.480 -0.444, -0.463	-0.451, -0.485 -0.463, -0.473 -0.426, -0.486
Cl	-0.675, -0.699 -0.675, -0.699	-0.694	-0.700

Conclusion

In summary, the monodentate acting guanidine-pyridine ligands DMEGpico and TMGpico as well as the polydentate guanidine ligands $DMEG_4(baem)_2b$, $TMG_4(baem)_2b$ and TEG_3tren were synthesized and completely characterized. The zinc complexes $[Zn(DMEGpico)_2Cl_2]$ (**11**), $[Zn(TMGpico)_2Cl_2]$ (**12**), $[(TMGpico)_2Zn_3(CH_3COO)_6]$ (**13**), $[(TMG_4(baem)_2b)(ZnCl_2)_2]$ (**14**), $[Zn(DMEG_3tren)Cl][Cl]$ (**15**) and $[Zn(TMG_3tren)Cl][Cl]$ (**16**) were obtained as colorless crystals and the chlorido complexes were tested towards their ability to initiate the ring-opening polymerization of D,L-lactide. They all were proven to be active initiators.

It could be shown that the different ligand classes have crucial impact on the molecular structure of the corresponding complexes and that this ligand effect has significant impact on the lactide polymerization activity. Four major points can be derived from this integrated study: i) in complexes with very small ligand bite, the ligand bite prevents the guanidine function from coordination to the zinc center, ii) the uncoordinated guanidine function next to the reaction center neither promotes the initiation of lactide polymerization nor increases the catalytic activity, iii) the tetradentate ligand $TMG_4(baem)_2b$ stabilises a complex which acts as two independent zinc complexes without especially enhanced positive charge on zinc or increased ROP activity, iv) the trisguanidine ligands $DMEG_3tren$ and TMG_3tren support a higher positive charge on the zinc center but the decreased substrate accessibility lowers the potential ROP activity. Furthermore, the important role of the amount of positive charge on the zinc center for the ROP activity has again been positively evaluated. Bearing these trends in mind, more active zinc guanidine catalysts can now be designed.

Acknowledgments

Materials and Methods

All manipulations were performed under nitrogen (99.996%) dried with P_4O_{10} granulate using Schlenk techniques. Solvents were purified according to literature procedures and also kept under nitrogen. Triethylamine (99%, Aldrich), 2-amino-3-picoline (95%, Aldrich), tris(2-aminoethyl)amine (96%, Aldrich), zinc(II) chloride (99.99%, Acros) and D,L-Lactide (3,6-Dimethyl-1,4-dioxane-2,5-dione, Purac) were used as purchased. The chloroform-amidiniumchlorides N,N,N′,N′-dimethylethylenechloroformamidiniumchloride (DMEG), N,N,N′,N′-tetramethylchloroformamidinium chloride (TMG), N,N,N′,N′-tetraethylchloroformamidinium chloride (TEG) (*46*), the amine 2,6-bis{[bis(2-aminoethyl)amino]methyl}benzene (*53*, *54*) as well as the ligands 1,1,1-tris{2-[2N-(1,3-dimethylethylenguanidino)]ethyl}amine (DMEG₃tren) (*51*) and 1,1,1-tris{2-[N²-(1,1,3,3-tetramethylguanidino)]ethyl}amine (TMG₃tren) (*52*) were prepared according to literature procedures. The dehydration of zinc(II) acetate (99.99%, Acros) was done on the basis of the orthoester method described by van Leeuwen and Groeneveld (*56*) for Co(II) and Ni(II) compounds.

Physical Measurements

Spectra were recorded with the following spectrometers: NMR: Bruker Avance 500. The NMR signals were calibrated to the residual signals of the deuterated solvents ($\delta_H(CDCl_3) = 7.26$ ppm, $\delta_H(CD_3CN) = 1.94$ ppm). Samples for homonuclear decoupling were prepared by dissolving 10 mg of the polymer in 1 ml of $CDCl_3$ and the samples were left for 2 hours to ensure full dissolution (*57*). The ^1H homonuclear decoupled spectra were recorded on a Bruker Avance 400 MHz spectrometer and referenced to residual solvent peaks. The parameter P_r (probability of heterotactic enchainment) was determined via analysis of the respective integrals of the tetrads, using $P_r^2 = 2$ [sis]. For the NMR analysis of the respective integrals of the tetrads [sis], see the work of Coates et al. (*11*). – IR: Nicolet P510. – MS (EI, 70eV): Finnigan MAT 95. –Elemental analyses: elementar vario MICRO cube.

Crystal Structure Analyses

Crystal data for compounds **11** to **15** and **17** are presented in Table XII and XIII. Data were collected with a Bruker-AXS SMART (*58*) APEX CCD, using MoKα radiation ($\lambda = 0.71073$ Å) and a graphite monochromator. Data reduction and absorption correction were done with SAINT and SADABS (*58*). The structures were solved by direct and conventional Fourier methods and all non-hydrogen atoms refined anisotropically with full-matrix least-squares based on F² (SHELXTL (*58*)). Hydrogen atoms were derived from difference Fourier maps and placed at idealized positions, riding on their parent C atoms, with isotropic displacement parameters $U_{iso}(H) = 1.2U_{eq}(C)$ and $1.5U_{eq}(C$ methyl). All methyl groups were allowed to rotate but not to tip. Full crystallographic data (excluding structure factors) for all complexes have been deposited with the Cambridge Crystallographic Data Center as supplementary no. CCDC-789410

(**11**), -789407 (**12**), -789409 (**13**), -789406 (**14**), -789411 (**15**) and -789408 (**17**). Copies of the data can be obtained free of charge on application to CCDC, 12 Union Road, Cambridge CB2 1EZ, UK (fax: (+44)1223-336-033; e-mail: deposit@ccdc.cam.ac.uk).

Table XII. Crystallographic data for the compounds 11 - 13

	11	*12*	*13* ·*THF*
Empirical formula	$C_{22}H_{32}Cl_2N_8Zn$	$C_{22}H_{36}Cl_2N_8Zn$	$C_{38}H_{62}N_8O_{13}Zn_3$
Formula weight / g mol^{-1}	544.83	548.86	1035.07
Temperature / K	120(2)	120(2)	120(2)
Crystal system	Monoclinic	Monoclinic	Monoclinic
Space group	$P2_1/n$	$P2_1/c$	$C2/c$
Unit cell dimensions:			
a / Å	9.924(2)	17.266(2)	12.020(3)
b / Å	20.210(5)	20.032(3)	14.228(3)
c / Å	13.221(3)	17.113(2)	27.944(7)
α /°			
β /°	101.611(6)	114.990(2)	96.850(5)
γ /°			
Volume / Å^3	2597.4(11)	5364.9(12)	4744.7(19)
Z	4	8	4
D_{calc} / Mg cm^{-3}	1.393	1.359	1.449
μ / mm^{-1}	1.177	1.140	1.571
F(000)	1136	2304	2160
Crystal size / mm^{-3}	0.31 x 0.26 x 0.23	0.42 x 0.40 x 0.07	0.37 x 0.35 x 0.26
θ_{max} / °	27.88	27.88	27.88
Index ranges	-11≤h≤13, -26≤k≤26, -17≤l≤17	-22≤h≤22, -26≤k≤24, -22≤l≤22	-15≤h≤15, -18≤k≤18, -36≤l≤36
Reflections collected	22905	46972	20336
Independent reflections	6194 [R(int) = 0.1621]	12788 [R(int) = 0.0366]	5666 [R(int) = 0.0679]
Absorption correction	Semi-empirical from equivalents		

Table XII. (Continued). Crystallographic data for the compounds 11 - 13

	11	*12*	*13 ·THF*
Transmission (max. and min.)	0.7734 and 0.7116	0.9244 and 0.6459	0.6855 and 0.5941
Refinement method		Full-matrix least-squares on F^2	
Data / restraints / parameters	6194 / 0 / 304	12788 / 0 / 615	5666 / 0 / 267
Goodness-of-fit on F^2	0.849	1.021	0.986
R1 [$I \geq 2\sigma(I)$]	0.0567	0.0347	0.0519
wR2 (all data)	0.1297	0.0861	0.1307
Largest diff. peak, hole / e $Å^{-3}$	0.862, -0.697	0.427, -0.273	0.906, -0.433

Table XIII. Crystallographic data for the compounds 14, 15 and 17

	14 ·MeCN ·2.5 Et$_2$O	*15*	*17*
Empirical formula	$C_{47}H_{98.5}Cl_4N_{14.5}O_{2.5}Zn_2$	$C_{21}H_{42}Cl_2N_{10}Zn$	$C_{22}H_{48}ClF_3N_{10}O_3SZn$
Formula weight / g mol^{-1}	1179.44	570.92	690.58
Temperature / K	293(2)	120(2)	120(2)
Crystal system	Triclinic	Monoclinic	Monoclinic
Space group	P1	P2$_1$/n	P2$_1$/n
Unit cell dimensions:			
a / Å	14.634(5)	12.7319(5)	8.8569(10)
b / Å	19.394(6)	12.2079(5)	16.9582(19)
c / Å	19.710(6)	21.2143(7)	21.296(2)
α /°	85.469(7)		
β /°	88.673(6)	126.773(2)	98.555(3)
γ /°	71.414(6)		
Volume / $Å^3$	5286(3)	2641.21(17)	3163.1(6)
Z	4	4	4
D$_{calc}$ / Mg cm^{-3}	1.482	1.436	1.450
μ / mm^{-1}	1.165	1.163	0.987
F(000)	2520	1208	1456

Continued on next page.

Table XIII. (Continued). Crystallographic data for the compounds 14, 15 and 17

	14 ·MeCN ·2.5 Et₂O	*15*	*17*
Crystal size / mm⁻³	0.42 x 0.41 x 0.10	0.35 x 0.29 x 0.19	0.47 x 0.09 x 0.08
θ_{max} / °	27.88	27.88	27.88
Index ranges	-19≤h≤19, -25≤k≤25, -25≤l≤25	-16≤h≤16, -16≤k≤16, -27≤l≤27	-11≤h≤11, -20≤k≤22, -28≤l≤28
Reflections collected	46209	24158	27710
Independent reflections	25018 [R(int) = 0.1927]	6295 [R(int) = 0.0334]	7533 [R(int) = 0.1098]
Absorption correction	Semi-empirical from equivalents		
Transmission (max. and min.)	0.8924 and 0.6403	0.8093 and 0.6863	0.9252 and 0.6542
Refinement method	Full-matrix least-squares on F²		
Data / restraints / parameters	25018 / 0 / 1069	6295 / 0 / 313	7533 / 0 / 383
Goodness-of-fit on F²	0.764	1.029	0.967
R1 [I ≥ 2σ(I)]	0.0883	0.0311	0.0582
wR2 (all data)	0.2658	0.0792	0.1184
Largest diff. peak, hole / e Å⁻³	1.087 and -0.695	0.537 and -0.271	0.870 and -0.396

Computational Details

Density functional theory (DFT) calculation: The calculations were performed with the program suite Gaussian03 (*59*). All geometries were optimised without constraints by using the B3LYP hybrid DFT functional and the 6-31g(d) basis sets implemented in Gaussian on all atoms. Tight conversion criteria were applied. Each stationary point has been characterized with frequency analysis at no negative eigenvalues

Gel Permeation Chromatography

The molecular weight and molecular weight distribution of obtained polylactide samples were determined by gel permeation chromatography (GPC) in THF as mobile phase at a flow rate of 1 mL/min. A combination of PSS SDV

columns with porosities of 10^5 Å and 10^3 Å were used together with a HPLC pump (L6200, Merck Hitachi) and a refractive index detector (Smartline RI Detector 2300, Knauer) detector. Universal calibration was applied to evaluate the chromatographic results. Kuhn-Mark-Houwink (KMH) parameters for the polystyrene standards (K_{PS} = 0.011 ml/g, a_{PS} = 0.725) were taken from literature (*60*). Previous GPC measurements utilizing online viscosimetry detection revealed the KMH parameters for polylactide (K_{PLa} = 0.053 ml/g, a_{PLa} = 0.610) (*25*).

Preparation of Compounds

General Synthesis of Guanidine Ligands with Chloroformamidinium Chlorides

A solution of the chloroformamidinium chloride (for guanidine-amine hybrid: 30 mmol, for trisguanidine: 90 mmol, for tetrakisguanidine: 120 mmol) in dry MeCN was added dropwise under vigorous stirring to an ice-cooled solution of an amine (30 mmol) and triethylamine (equimolar to the amount of chloroformamidiniumchloride) in dry MeCN. After 3 - 8h at reflux, an aqueous solution of NaOH (equimolar to the amount of chloroformamidinium chloride) was added. The solvent and NEt_3 were then evaporated under vacuum. In order to deprotonate the guanidine hydrochloride, 50 wt.% KOH (aq., 15 mL) was added and the free base was extracted into the MeCN phase (3 x 30 mL). The organic phase was dried withNa_2SO_4 and after filtration, the solvent was evaporated under reduced pressure.

N-(1,3-Dimethylimidazolidin-2-ylidene)-3-methylpyridin-2-amine (DMEGpico)

$C_{11}H_{16}N_4$ (M = 204.27 g/mol): Dark red solid; **Yield**: 3.86 g = 18.9 mmol = 63 %. **^{1}H-NMR** (500 MHz, CDCl$_3$, 25 °C): δ [ppm] = 2.18 (s, 3H, C*H$_3$*), 2.65 (s, 6H, C*H$_3$*), 3.35 (s, 4H, C*H$_2$*), 6.62 (m, 1H, C*H*), 7.29 (m, 1H, C*H*), 8.09 (m, 1H, C*H*). **^{13}C-NMR** (125MHz, CDCl$_3$, 25 °C): δ [ppm] = 18.5 (CH$_3$), 34.6 (CH$_3$), 48.3 (CH$_2$), 115.3 (CH), 125.2 (C), 137.1 (CH), 145.5 (CH), 156.8 (C), 160.9 (C). **IR** (KBr, $\tilde{v}$ [cm^{-1}]): 3059 vw (ν(C-H$_{arom.}$)), 3032 vw (ν(C-H$_{arom.}$)), 2993 w (ν(C-H$_{aliph.}$)), 2972 w (ν(C-H$_{aliph.}$)), 2927 w (ν(C-H$_{aliph.}$)), 2873 w (ν(C-H$_{aliph.}$)), 1620 s (ν(C=N)), 1577 vs (ν(C=N)), 1508 m, 1489 m, 1462 m, 1437 s, 1394 m, 1375 m, 1290 m, 1269 w, 1241 m, 1201 w, 1103 w, 1080 w, 1036 m, 974 m, 928 vw, 891 vw, 798 w, 787 w, 766 m, 735 w, 690 w, 654 w, 602 vw, 565 w, 534 vw. **EI-MS** (m/z, (%)): 204 (34) [M$^+$], 189 (100) [M$^+$ - CH$_3$], 119(8) [M$^+$ - (CH$_3$)$_2$NCH$_2$CH$_2$N(CH$_3$)$_2$ +H], 114 (10) [M$^+$ - C$_6$H$_6$N +2H], 108 (94), 106 (22), 92(13) [C$_6$H$_6$N$^+$], 81 (14), 80 (43), 65 (9), 42 (8).

1,1,3,3-Tetramethyl-2-(3-methylpyridin-2-yl)guanidine (TMGpico)

$C_{11}H_{18}N_4$ (M = 206.29 g/mol): Orange colored oil; Yield: 4.64 g =22.5 mmol = 75 %. **¹H-NMR** (500 MHz, CDCl₃, 25 °C): δ [ppm] =2.16 (s, 3H, C*H*₃), 2.71 (s, 12H, C*H*₃), 6.62 (m, 1H, C*H*), 7.30 (m, 1H, C*H*), 8.07 (m, 1H, C*H*). **¹³C-NMR** (125MHz, CDCl₃, 25 °C): δ [ppm] = 18.5 (CH₃), 39.5 (CH₃), 115.2 (CH), 124.4 (C), 137.4 (CH), 145.9 (CH), 161.6 (C), 162.7 (C). **IR** (film between NaCl plates, $\tilde{\nu}$ [cm⁻¹]): 3059 vw (ν(C-H_arom.)), 3001 w (ν(C-H_arom.)), 2931 m (ν(C-H_aliph.)), 2885 m (ν(C-H_aliph.)), 2812 vw (ν(C-H_aliph.)), 2792 vw (ν(C-H_aliph.)), 1601 m (ν(C=N)), 1564 vs (ν(C=N)), 1512 m, 1460 m, 1441 m, 1417 s, 1381 s, 1286 w, 1269 w, 1227 m, 1178 m, 1146 m,1105 m, 1059 m, 1022 s. **EI-MS** (m/z, (%)): 206 (66) [M⁺], 191 (92) [M⁺ - CH₃], 162 (69) [M⁺ - N(CH₃)₂], 148 (62), 119 (100) [M⁺ - 2 N(CH₃)₂ +H], 107 (16), 93 (17) [C₆H₆N⁺ +H], 92 (85)[C₆H₆N⁺], 85 (12), 65 (34), 44 (16) [N(CH₃)₂⁺], 42 (22).

2,6-Bis[bis(2-Aminoethyl)1,3-dimethylimidazolidin-2-ylidene]methylbenzene (DMEG₄(beam)₂b)

$C_{36}H_{64}N_{14}$ (M = 692.99 g/mol): Yellow oil; **Yield**: 18.92 g = 27.3 mmol =91 %. **¹H-NMR** (500 MHz, CDCl₃, 25 °C): δ [ppm] = 2.72 (m, 24+8H, C*H*₃+C*H*₂), 3.11 (m, 16H, C*H*₂), 3.49 (m, 8H, C*H*₂), 3.70 (m, 4H, C*H*₂), 7.20 (m, 4H, C*H*). **¹³C-NMR** (125 MHz, CDCl₃, 25 °C): δ [ppm] = 39.9 (CH₃), 49.4 (CH₂), 46.4 (CH₂), 58.1 (CH₂), 60.1 (CH₂), 127.0 (CH), 128.1 (CH), 129.2 (CH), 140.5 (C), 157.4 (C). **IR** (film between NaCl plates, $\tilde{\nu}$ [cm⁻¹]): 3352 m (ν(C-H_arom.)), 3294 m (ν(C-H_arom.)), 2933 s (ν(C-H_aliph.)), 2835 s (ν(C-H_aliph.)), 1662 vs (ν(C=N)), 1483 m, 1441 m, 1414 m, 1383 m, 1265 s, 1198 m, 1138 m, 1120 m, 1066 m, 1018 s. **EI-MS** (m/z,(%)): 693 (9) [M⁺], 596 (24) [M⁺ - C₅H₁₀N₂ +H], 566 (38) [M⁺ - C₆H₁₂N₃⁺ -H], 500 (22), 483 (55) [M⁺ - C₅H₁₀N₂ - C₅H₁₀N₃], 471 (70) , 470 (91) [M⁺ - 2 C₅H₁₀N₃ +H], 466 (26), 456 (20), 453 (16), 440 (10) [M⁺ - 2 C₆H₁₂N₃⁺ -H], 427 (29), 397 (9), 387 (13), 374 (79), 360 (10), 357 (27), 331 (12), 301 (22), 286 (6), 272 (12), 198 (8), 182 (6), 169 (25), 167 (10), 149 (88), 127 (51) [C₆H₁₂N₃⁺ +H], 126 (100) [C₆H₁₂N₃⁺], 114 (17) [C₅H₁₀N₃⁺ +2H], 105 (18), 98 (10) [C₅H₁₀N₂⁺],70 (10) [CH₂CH₂NCH₂CH₂⁺], 56 (30).

2,6-Bis[bis(2-Aminoethyl)tetramethyl-guanidino]methylbenzene (TMG₄(baem)₂b)

$C_{36}H_{72}N_{14}$ (M = 701,06 g/mol): Orange colored oil; Yield: 18.30 g = 26.1mmol = 87 %. **¹H-NMR** (500 MHz, CDCl₃, 25 °C): δ [ppm] = 2.62 (m, 48+8H, C*H*₃+C*H*₂), 3.17 (m, 8H, C*H*₂), 3.57 (s, 4H, C*H*₂), 7.11 (m, 4H, C*H*). **¹³C-NMR** (125 MHz, CDCl₃, 25 °C): δ [ppm] = 38.5 (CH₃), 38.9 (CH₃), 39.2 (CH₃), 39.6 (CH₃), 47.9 (CH₂), 57.3 (CH₂), 59.8 (CH₂), 127.0 (CH), 128.1 (CH), 129.1 (CH), 140.3 (C), 160.3 (C). **IR** (KBr, $\tilde{\nu}$ [cm⁻¹]): 2997 m (ν(C-H_arom.)), 2929 m (ν(C-H_aliph.)), 2891 m (ν(C-H_aliph.)), 2841 m (ν(C-H_aliph.)), 2802 m (ν(C-H_aliph.)),

1616 vs (ν(C=N)), 1496 m, 1452 m, 1404 m, 1369 m, 1313 w, 1236 w, 1132 m, 1063w, 993 w, 912 w, 796 vw, 746 w, 704 w, 669 vw, 592 w. **EI-MS** (m/z, (%)): 702 (21) [M⁺], 701 (52) [M⁺], 586 (9) [M⁺ - HN(C(N(CH₃)₂)₂)], 573 (70) [M⁺ - CH₂N(C(N(CH₃)₂)₂)], 572 (100) [M⁺ - CH₃N(C(N(CH₃)₂)₂)], 558 (16), 470 (19), 457 (49), 432 (15), 401 (15) [M⁺ - 3 C(N(CH₃)₂)], 274 (16), 142 (77), 128 (54) [CH₂N(C(N(CH₃)₂)₂)⁺], 85 (96), 77 (23) [C₆H₅⁺], 58 (30) [C(N(CH₃)₂⁺ +2H].

2′,2′,2′′-(2,2′,2′′-Nitrilotris(ethane-2,1-diyl))tris(1,1,3,3-tetraethylguanidine) (TEG₃tren)

C₃₃H₇₂N₁₀ (M = 609.00 g/mol): Yellow oil; **Yield**: 11.69 g = 19.2 mmol = 64 %. **¹H-NMR** (500 MHz, CDCl₃, 25 °C): δ [ppm] = 1.00 (t, 36H, C*H*₃, ³J =7.1 Hz), 2.72 (m, 6H, C*H*₂), 3.02 (q, 12H, C*H*₂, ³J = 7.1Hz), 3.10 (q, 12H, C*H*₂, ³J = 7.1 Hz), 3.25 (m, 6H, C*H*₂). **¹³C-NMR** (125 MHz, CDCl₃, 25 °C): δ [ppm] = 13.0 (CH₃), 13.8 (CH₃), 41.6 (CH₂), 42.6 (CH₂), 48.6 (CH₂), 58.2 (CH₂), 158.4 (C). **IR** (Film between NaCl plates, ν̃[cm⁻¹]): 2966 s (ν(C-H_aliph.)), 2929 m (ν(C-H_aliph.)), 2868 m (ν(C-H_aliph.)), 1612 vs (ν(C=N)), 1460 m, 1402 m, 1375 m, 1358 m, 1338 m, 1302 m, 1261 s, 1219 m, 1205 m, 1130 m, 1068 s. **EI-MS** (m/z, (%)): 610 (4) [M⁺], 438 (10) [M⁺ - C₉H₂₀N₃ - H], 424 (97) [M⁺ - C₁₀H₂₂N₃ - H], 266 (97), 253 (10), 240 (13), 198 (48) [C₁₁H₂₄N₃⁺], 184 (72) [C₁₀H₂₂N₃⁺], 168 (33), 156 (29) [C₉H₂₀N₂⁺], 154 (11), 127 (24), 113 (100), 100 (13) [N(CH₂CH₂)₃⁺ +2H], 99 (13) [N(CH₂CH₂)₃⁺ +H], 86 (22), 72 (18) [C₄H₁₀N⁺], 57 (11).

General Synthesis of Zinc Complexes with Guanidine Ligands

A solution of the ligand (1.1 mmol) in dry MeCN or THF was added to a suspension of the zinc compound (1 mmol or less, depending on the molar ratio given in the complex) in a dry aprotic solvent (MeCN, THF) with stirring. The resulting reaction mixture was stirred for 20 min or longer. In the case of a clear solution, single crystals could be obtained by diffusion of diethyl ether, diisopropyl ether or pentane. When the complex precipitated, the reaction mixture was slowly heated under reflux to give a clear solution. Single crystals could be obtained by slowly cooling to room temperature.

[(DMEGpico)₂ZnCl₂] (11)

C₂₂H₃₂N₈ZnCl₂ (M = 544.86 g/mol): Colorless crystals; **Yield**: 0.264 g = 0.49 mmol = 97 %; **m.p.** 206°C. **¹H-NMR** (500 MHz, CD₃CN, 25 °C): δ [ppm] = 2.02 (s, 6H, C*H*₃), 2.41 (s, 12H, C*H*₃), 3.20 (s, 8H, C*H*₂), 7.30 (dd, 2H, C*H*, ³J = 5.7 Hz, ³J = 7.2 Hz), 7.83(d, 2H, C*H*, ³J = 7.2 Hz,), 8.44 (m, 2H, C*H*). **¹³C-NMR** (125 MHz, CD₃CN, 25 °C): δ [ppm] = 16.8 (CH₃), 33.2 (CH₃), 47.7 (CH₂), 115.5 (CH), 126.2 (C), 139.7 (CH), 144.4 (CH), 154.5 (C), 160.9 (C). **IR** (KBr, ν̃[cm⁻¹]): 3070 w (ν(C-H_arom.)), 3053 w (ν(C-H_arom.)), 2939 m (ν(C-H_aliph.)), 2860

m (ν(C-H$_{aliph.}$)), 1651 vs (ν(C=N)), 1599 s (ν(C=N)), 1562 s (ν(C=N)), 1506 s,1471 s, 1446 s, 1433 s, 1404 s, 1381 m, 1333 m, 1284 s, 1240 m, 1188 m, 1122 m, 1080 m, 1034 s, 995 m, 970 m, 899 w, 849 vw, 810 w, 787 m, 715 m, 708 m, 698 m, 654 w, 607 w, 592 vw, 532 vw. **EI-MS** (m/z, (%)): 307 (3) [C$_{11}$H$_{16}$N$_4$ZnCl$^+$], 305 (4) [C$_{11}$H$_{16}$N$_4$ZnCl$^+$], 303 (5) [C$_{11}$H$_{16}$N$_4$ZnCl$^+$],204 (92) [C$_{11}$H$_{16}$N$_4^+$], 189 (100) [C$_{11}$H$_{16}$N$_4^+$ -CH$_3$], 148 (9), 119 (10) [C$_7$H$_6$N$_2^+$ +H], 98 (15) [C$_5$H$_{10}$N$_2^+$], 92 (19) [C$_6$H$_6$N$^+$], 65 (10). **CI-MS** (m/z, (%)): 511 (0.1) [M$^+$ - Cl], 509 (0.4) [M$^+$ - Cl], 507 (0.2) [M$^+$ - Cl], 410 (2), 409 (6) [M$^+$ -Cl - C$_5$H$_{10}$N$_2$], 307 (0.5) [C$_{11}$H$_{16}$N$_4$ZnCl$^+$], 305 (1) [C$_{11}$H$_{16}$N$_4$ZnCl$^+$], 303 (0.8) [C$_{11}$H$_{16}$N$_4$ZnCl$^+$], 205 (100) [C$_{11}$H$_{16}$N$_4^+$ +H], 204 (39) [C$_{11}$H$_{16}$N$_4^+$], 57 (100). **CHN analysis**: calculated: C 48.45, H 5.87, N 20.56; found: C 48.83, H 5.99, N 20.50.

[(TMGpico)$_2$ZnCl$_2$] (12)

C$_{22}$H$_{36}$N$_8$ZnCl$_2$ (M = 548.89 g/mol): Colorless crystals; **Yield**: 0.270 g = 0.49 mmol = 98 %; **m.p.** 232°C. **^{1}H-NMR** (500 MHz, CD$_3$CN, 25 °C): δ [ppm] = 2.24 (s, 6H, C*H*$_3$), 2.99 (s, 24H, C*H*$_3$), 7.30 (m, 2H, C*H*), 7.83 (m, 2H, C*H*), 8.45 (m, 2H, C*H*). **^{13}C-NMR** (125 MHz, CD$_3$CN, 25 °C): δ [ppm] = 16.3 (CH$_3$), 39.8 (CH$_3$), 121.3 (CH), 126.0 (C, b), 141.9 (CH, c), 146.2 (CH, e), 159.0 (C), 166.2 (C). **IR** (KBr, $\tilde{\nu}$[cm^{-1}]): 3199 m (ν(C-H$_{arom.}$)), 3161 m (ν(C-H$_{arom.}$)), 3124 m (ν(C-H$_{arom.}$)), 3101 m (ν(C-H$_{arom.}$)), 3057 m (ν(C-H$_{arom.}$)), 3022 m (ν(C-H$_{arom.}$)), 2974 m (ν(C-H$_{aliph.}$)), 2947 m (ν(C-H$_{aliph.}$)), 2914 m (ν(C-H$_{aliph.}$)), 2806 m, 1633 vs (ν(C=N)), 1603 s (ν(C=N)), 1585 m (ν(C=N)), 1562 vs (ν(C=N)), 1508 w, 1458 s, 1442 s, 1419 m,1410 s, 1396 s, 1311 m, 1284 m, 1267 w, 1228 m, 1190 m, 1169 m, 1151 m, 1122 m, 1068 m, 1039 m, 1001 m, 926 m, 879 m, 810 m, 789 m, 733 m, 700 m, 687 m, 650 m, 592 w, 552 w. **EI-MS** (m/z, (%)): 305 (21) [Zn^{37}ClC$_{11}$H$_{18}$N$_4^+$], 303 (30) [Zn^{35}ClC$_{11}$H$_{18}$N$_4^+$], 206 (93) [C$_{11}$H$_{18}$N$_4$+], 191 (100) [C$_{11}$H$_{18}$N$_4^+$ -CH$_3$], 190 (26), 162 (84) [C$_{11}$H$_{18}$N$_4^+$ -N(CH$_3$)$_2$], 148 (41), 119 (89) [C$_{11}$H$_{18}$N$_4^+$ -2N(CH$_3$)$_2$ +H], 107 (14), 92 (17) [C$_6$H$_6$N$^+$], 65 (32). **CHN analysis**: calculated: C 48.10, H 6.56, N 20.40; found: C 48.05, H 6.54, N 20.21.

[(TMGpico)$_2$Zn$_3$(CH$_3$COO)$_6$] (13)

C$_{34}$H$_{54}$N$_8$Zn$_3$O$_{12}$ (M= 963.01 g/mol): Colorless crystals; **Yield**: 0.968 g =1.01 mmol = 67 %; **m.p.** 88°C. **^{1}H-NMR** (500 MHz, CD$_3$CN, 25 °C): δ [ppm] = 1.96 (s, 18H, C*H*$_3$), 2.08 (s, 6H, C*H*$_3$), 2.79 (s, 24H, C*H*$_3$), 6.91 (dd, 2H, C*H*, ^{3}J =7.4Hz, ^{3}J = 5.1Hz), 7.60 (dd, 2H, C*H*, ^{3}J =7.4 Hz, ^{4}J = 0.9 Hz), 8.07 (dd, 2H, C*H*, ^{3}J= 5.1 Hz, ^{4}J = 0.9 Hz). **^{13}C-NMR** (125MHz, CD$_3$CN, 25 °C): δ [ppm] = 16.6 (CH$_3$), 22.1 (CH$_3$), 39.0 (CH$_3$), 116.9 (CH), 124.4 (C), 140.4 (CH), 144.26 (CH), 159.4 (C), 168.3 (C), 179.2 (C). **IR** (KBr, $\tilde{\nu}$[cm^{-1}]): 3005 m (ν(C-H$_{arom.}$)), 2931 m (ν(C-H$_{aliph.}$)), 2802 w (ν(C-H$_{aliph.}$)), 1589 vs (ν(C=N)), 1552 s, 1427 s, 1390 s, 1335 m, 1273 vw, 1234 w, 1221 w, 1186 w, 1153 w, 1065 vw, 1029 m, 995 vw, 926 vw, 887 vw, 798 w, 741 vw, 673 m, 617 w, 561 vw, 538 vw. **EI-MS** (m/z, (%)): 206 (56) [C$_{11}$H$_{18}$N$_4^+$],191 (97) [C$_{11}$H$_{18}$N$_4^+$ -CH$_3$], 162 (65) [C$_{11}$H$_{18}$N$_4^+$ -N(CH$_3$)$_2$], 148

(51), 119 (100) [$C_{11}H_{18}N_4^+$ -2 N(CH$_3$)$_2$ +H], 107 (16), 93 (17) [$C_6H_6N^+$ +H], 92 (82) [$C_6H_6N^+$], 65 (31). **CHN analysis**: calculated: C 42.37, H 5.61, N 11.63; found: C 42.04, H 5.47, N 11.52.

[TMG$_4$(beam)$_2$b(ZnCl$_2$)$_2$] (14)

$C_{36}H_{72}N_{14}Zn_2Cl_4$ (M= 973.67 g/mol): Colorless crystals; **Yield**: 1.499 g = 1.54 mmol = 77 %; **m.p.** 158°C. **¹H-NMR** (500 MHz, CD$_3$CN, 25 °C): δ [ppm] = 2.61 (m, 8H, CH$_2$), 2.81 (m, 24H, C*H*$_3$), 2.87 (m, 24H, C*H*$_3$), 3.18 (m, 8H, C*H*$_2$), 4.03 (s, 4H, C*H*$_2$), 7.35 (m, 3H, C*H*), 7.59 (s, 1H, C*H*). **¹³C-NMR** (125 MHz, CD$_3$CN, 25 °C): δ [ppm] = 38.9 (CH$_3$), 39.2 (CH$_3$), 46.5 (CH$_2$), 53.8 (CH$_2$), 59.2 (CH$_2$), 127.9 (CH), 130.2 (CH), 133.9 (CH), 135.6 (C), 166.6 (C). **IR** (KBr, $\bar{\nu}$[cm^{-1}]): 3003 w (ν(C-H$_{arom.}$)), 2931 m (ν(C-H$_{aliph.}$)), 2898 m (ν(C-H$_{aliph.}$)), 2854 m (ν(C-H$_{aliph.}$)), 1618 s (ν(C=N)), 1577 vs (ν(C=N)), 1533 m, 1458 m, 1425 m, 1400 m, 1394 m, 1361 w, 1346 w, 1261 vw, 1238 w, 1159 m, 1147 m, 115 vw, 1066 w, 1049 w, 1022 vw, 987 vw, 893 w, 808 vw, 768 w, 742 vw, 719 w, 669 w, 617 w, 586 w. **EI-MS** (m/z, (%)): 701 (44) [M$^+$ - 2 ZnCl$_2$], 586 (8) [M$^+$ -HN(C(N(CH$_3$)$_2$)$_2$) -2 ZnCl$_2$], 572 (100) [M$^+$ -CH$_3$N(C(N(CH$_3$)$_2$)$_2$) -2 ZnCl$_2$], 558 (13), 470 (17), 457 (42), 432 (9), 401 (14) [M$^+$ -3 C(N(CH$_3$)$_2$) -2 ZnCl$_2$], 274 (15), 180 (26), 142 (73), 128 (36) [CH$_2$N(C(N(CH$_3$)$_2$)$_2$)$^+$], 85 (89), 72 (22), 58 (25) [C(N(CH$_3$)$_2^+$ + 2H]. **CHN analysis**: calculated: C 44.37, H 7.39, N 20.13; found: C 44.18, H 7.47, N 18.35.

[Zn(DMEG$_3$tren)Cl][Cl] (15)

$C_{21}H_{42}N_{10}ZnCl_2$ (M = 570.94 g/mol): Colorless crystals; **Yield**: 0.347 g = 0.61 mmol = 61 % ; **m.p.** 230°C. **¹H-NMR** (500 MHz, CD$_3$CN, 25 °C): δ [ppm] = 2.61 (s, 6H, C*H*$_2$), 2.82(s, 18H, C*H*$_3$), 3.32 (br, 6H, C*H*$_2$), 3.43 (s, 12H, C*H*$_2$). **¹³C-NMR** (125 MHz, CD$_3$CN, 25 °C): δ [ppm] = 35.8 (CH$_3$), 46.3(CH$_2$), 48.8 (CH$_2$), 56.0 (CH$_2$), 166.8 (C). **IR** (KBr, $\bar{\nu}$[cm^{-1}]): 2945 s (ν(C-H$_{aliph.}$)), 2858 s (ν(C-H$_{aliph.}$)), 1653 vs (ν(C=N)), 1645 vs (ν(C=N)), 1635 vs (ν(C=N)), 1616 vs (ν(C=N)), 1597 vs (ν(C=N)), 1560 s, 1543 m, 1508 s, 1491 s, 1458 s, 1421 s, 1406 s, 1383 m, 1342 m, 1298 s, 1271 s, 1232 m, 1167 m, 1138 m, 1124 m, 1078 m, 1053 m, 1020 m, 976 m, 939 w, 910 m, 895 w, 851 vw, 770 m, 725 m, 702 m, 648 m, 604 m, 554 m, 525 m. **EI-MS** (m/z,(%)): 537 (1) [M$^+$: $C_{21}H_{42}N_{10}{}^{66}Zn^{37}Cl$, $C_{21}H_{42}N_{10}{}^{68}Zn^{35}Cl$], 535 (2) [M$^+$: $C_{21}H_{42}N_{10}{}^{66}Zn^{35}Cl$, $C_{21}H_{42}N_{10}{}^{64}Zn^{37}Cl$], 533 (2) [M$^+$: $C_{21}H_{42}N_{10}{}^{64}Zn^{35}Cl$], 435 (2) [M$^+$ -ZnCl], 308 (41) [M$^+$ -ZnCl - N$_3$C$_6$H$_{10}^+$ -H], 208 (19), 195 (38) [N$_4$C$_{10}$H$_{20}^+$ -H], 169 (14) [N$_4$C$_8$H$_{16}^+$ +H], 140 (34) [N$_3$C$_7$H$_{14}^+$], 126 (100) [N$_3$C$_6$H$_{10}^+$], 98 (11) [N$_2$C$_5$H$_{10}^+$]. **CHN analysis**: calculated: C 44.14, H 7.36, N 24.52; found: C 43.38, H 7.34, N 24.02.

[Zn(TMG₃tren)Cl][Cl] (16)

C$_{21}$H$_{48}$N$_{10}$ZnCl$_2$ (M = 576.98 g/mol): Colorless crystals; **Yield**: 0.207 g = 0.36 mmol = 36 %; **m.p.** 180°C. **¹H-NMR** (500MHz, CD$_3$CN, 25 °C): δ [ppm] = 2.63 (m, 6H, C*H*$_2$), 2.67 (s, 8H, C*H*$_3$), 2.75 (s, 9H, C*H*$_3$), 2.82 (s, 10H, C*H*$_3$), 2.85 (m, 3H, C*H*$_2$), 2.92 (s, 9H, C*H*$_3$), 3.40 (m, 3H, C*H*$_2$). **¹³C-NMR** (125 MHz, CD$_3$CN, 25 °C): δ [ppm] = 37.9 (CH$_3$), 38.6 (CH$_3$), 39.2 (CH$_3$), 39.4 (CH$_3$), 46.2 (CH$_2$), 54.2 (CH$_2$), 166.0 (C). **IR** (KBr, $\tilde{v}$[cm^{-1}]): 2991 m (ν(C-H$_{aliph.}$)), 2945 s (ν(C-H$_{aliph.}$)), 2887 s (ν(C-H$_{aliph.}$)), 2854 m (ν(C-H$_{aliph.}$)), 1556 vs (ν(C=N)), 1468 s, 1444 m, 1425 s, 1394 vs, 1344 s, 1282 m, 1257 m, 1248 m, 1232 m, 1165 s, 1149 s, 1119 w, 1080 m, 1066 m, 1051 m, 1026 w, 1011 m, 985 m, 908 m, 893 m, 766 m, 743 w, 721 w, 590 w, 559 w, 532 w. **EI-MS** (m/z, (%)): 543 (1) [M$^+$: C$_{21}$H$_{48}$N$_{10}$^{66}Zn^{37}Cl, C$_{21}$H$_{48}$N$_{10}$^{68}Zn^{35}Cl], 541 (1) [M$^+$: C$_{21}$H$_{48}$N$_{10}$^{66}Zn^{35}Cl, C$_{21}$H$_{48}$N$_{10}$^{64}Zn^{37}Cl], 539 (2) [M$^+$: C$_{21}$H$_{48}$N$_{10}$^{64}Zn^{35}Cl], 439 (1) [M$^+$ - ZnCl - H], 396 (2) [N$_9$C$_{19}$H$_{42}$$^+$], 313 (31), 312 (95) [N$_7C_{15}H_{34}$$^+$], 255 (20), 222 (15), 210 (93), 197 (20), 171 (20), 142 (83) [N$_3$C$_7$H$_{16}$$^+$], 128 (91) [N$_3C_6H_{14}$$^+$], 126 (45), 111 (21), 100 (20) [N$_2$C$_5$H$_{12}$$^+$], 97(22), 85 (100). **CHN analysis**: calculated: C 43.68, H 8.32, N 24.26; found: C 43.46, H 8.08, N 23.67.

General Procedure for D,L-Lactide Polymerization

D,L-Lactide (3,6-dimethyl-1,4-dioxane-2,5-dione, 3.603 g, 25 mmol, used as purchased) and the initiator (I/M ratio 1/500) were weighed into a 50 mL flask, which was flushed with argon and closed with a glass stopper. The reaction vessel was then heated at 150 °C. After the reaction time the polymer melt was allowed to cool to room temperature and then was dissolved in 25 mL of dichloromethane. The PLA was precipitated in 350 mL of ice-cooled ethanol und dried under vacuum at 50 °C.

References

1. Platel, R. H.; Hodgson, L. M.; Williams, C. K. *Polym. Rev.* **2008**, *48*, 11–63.
2. Gupta, B.; Revagade, N.; Hilborn, J. *Prog. Polym. Sci.* **2007**, *32*, 455–482.
3. Dechy-Cabaret, O.; Martin-Vaca, B.; Bourissou, D. *Chem. Rev.* **2004**, *104*, 6147–6176.
4. Wu, J.; Yu, T.-L.; Chen, C.-T.; Lin, C.-C. *Coord. Chem. Rev.* **2006**, *250*, 602–626.
5. Drumwright, R. W.; Gruber, P. R.; Henton, D. E. *Adv. Mat.* **2000**, *12*, 1841–1846.
6. Kricheldorf, H. R. *Chemosphere* **2001**, *43*, 49–54.
7. Wheaton, C. A.; Hayes, P. G.; Ireland, B. J. *Dalton Trans.* **2009**, 4832–4846.
8. Garlotta, D. *J. Polym. Environ.* **2001**, *9*, 63–84.
9. Dove, A. P.; Gibson, V. C.; Marshall, E. L.; Rzepa, H. S.; White, A. J. P.; Williams, D. J. *J. Am. Chem. Soc.* **2006**, *128*, 9834–9843.

10. Williams, C. K.; Breyfogle, L. E.; Choi, S. K.; Nam, W.; Young, V. G.; Hillmyer, M. A.; Tolman, W. B. *J. Am. Chem. Soc.* **2003**, *125*, 11350–11359.

11. Chamberlain, B. M.; Cheng, M.; Moore, D. R.; Ovitt, T. M.; Lobkovsky, E. B.; Coates, G. W. *J. Am. Chem. Soc.* **2001**, *123*, 3229–3238.

12. Ejfler, J.; Szafert, S.; Mierzwicki, K.; Jerzykiewicz, L. B.; Sobota, P. *Dalton Trans.* **2008**, 6556–6562.

13. Wu, J.-C.; Huang, B.-H.; Hsueh, M.-L.; Lai, S.-L.; Lin, C.-C *Polymer* **2005**, *46*, 9784–9792.

14. (a) Zhong, Z. Y.; Dijkstra, P. J.; Feijen, J. *Angew. Chem.* **2002**, *114*, 4692-4695. (b) *Angew. Chem., Int. Ed.* **2002**, *41*, 4510-4513.

15. Zhong, Z. Y.; Dijkstra, P. J.; Feijen, J. *J. Am. Chem. Soc.* **2003**, *125*, 11291–11298.

16. Ma, H.; Spaniol, T. P.; Okuda, J. *Inorg. Chem.* **2008**, *47*, 3328–3339.

17. (a) Ma, H.; Spaniol, T. P.; Okuda, J. *Angew. Chem.* **2006**, *118*, 7982-7985. (b) *Angew. Chem. Int. Ed.* **2006**, *45*, 7818-7821.

18. Peckermann, I.; Kapelski, A.; Spaniol, T. P.; Okuda, J. *Inorg. Chem.* **2009**, *48*, 5526–5534.

19. Lian, B.; Ma, H.; Spaniol, T. P.; Okuda, J. *Dalton Trans.* **2009**, 9033–9042.

20. (a) Amgoune, A.; Thomas, C. M.; Ilinca, S.; Roisnel, T.; Carpentier, J. F. *Angew. Chem.* **2006**, *118*, 2848-2850. (b) *Angew. Chem., Int. Ed.* 2006, *45*, 2782-2784.

21. Pratt, R. C.; Lohmeijer, B. G. G.; Long, D. A.; Waymouth, R. M.; Hedrick, J. L. *J. Am. Chem. Soc.* **2006**, *128*, 4556–4557.

22. Chuma, A.; Horn, H. W.; Swope, W. C.; Pratt, R. C.; Zhang, L.; Lohmeijer, B. G. G.; Wade, C. G.; Waymouth, R. M.; Hedrick, J. L.; Rice, J. E. J. *Am. Chem. Soc.* **2008**, *130*, 6749–6754.

23. Becker, J. M.; Tempelaar, S.; Stanford, M. J.; Pounder, R. J.; Covington, J. A.; Dove, A. P. *Chem. Eur J.* **2010**, DOI: 10.1002/chem.200902518.

24. Börner, J.; Herres-Pawlis, S.; Flörke, U.; Huber, K. *Eur. J. Inorg. Chem.* **2007**, 5645–5651.

25. Börner, J.; Flörke, U.; Huber, K.; Döring, A.; Kuckling, D.; Herres-Pawlis, S. *Chem. Eur. J.* **2009**, *15*, 2362–2376.

26. Börner, J.; Flörke, U.; Glöge, T.; Bannenberg, T.; Tamm, M.; Jones, M. D.; Döring, A.; Kuckling, D.; Herres-Pawlis, S. *J. Mol. Catal. A: Chem.* **2010**, *316*, 139–145.

27. Wheaton, C. A.; Ireland, B. J.; Hayes, P. G. *Organometallics* **2009**, *28*, 1282–1285.

28. Ireland, B. J.; Wheaton, C. A.; Hayes, P. G. *Organometallics* **2010**, *29*, 1079–1084.

29. Wheaton, C. A.; Hayes, P. G. *Dalton Trans.* **2010**, 3861–3869.

30. Raab, V.; Harms, K.; Sundermeyer, J.; Kovacevic, B.; Maksic, Z. B. *J. Org. Chem.* **2003**, *68*, 8790–8797.

31. Herres-Pawlis, S.; Flörke, U.; Henkel, G. *Eur. J. Inorg. Chem.* **2005**, 3815–3824.

32. Herres-Pawlis, S.; Verma, P.; Haase, R.; Kang, P.; Lyons, C. T.; Wasinger, E. C.; Flörke, U.; Henkel, G.; Stack, T. D. P. *J. Am. Chem. Soc.* **2009**, *131*, 1154–1169.

33. Ng, J. J.; Durr, C. B.; Lance, J. M.; Bunge, S. D. *Eur. J. Inorg. Chem.* **2010**, *9*, 1424–1430.

34. Ajellala, N.; Carpentier, J.-F.; Guillaumea, C.; Guillaume, S. M.; Heloua, M.; Poiriera, V.; Sarazina, Y.; Trifonov, A. *Dalton Trans.* **2010**, DOI: 10.1039/c001226b.

35. Sousa, S. F.; Carvalho, E. S.; Ferreira, D. M.; Tavares, I. S.; Fernandes, P. A.; Ramos, M. J.; Gomes, J. A. N. F. *J. Comput. Chem.* **2009**, *30*, 2752–2763.

36. Picot, D.; Ohanessian, G.; Frison, G. *Inorg. Chem.* **2008**, *47*, 8167–8178.

37. Frison, G.; Ohanessian, G. *J. Comput. Chem.* **2008**, *29*, 416–433.

38. Amin, E. A.; Truhlar, D. G. *J. Chem. Theory Comput.* **2008**, *4*, 75–85.

39. Eger, W. A.; Jahn, B. O.; Anders, E. *J. Mol. Model.* **2009**, *15*, 433–446.

40. Ling, J.; Shen, J.; Hogen-Esch, T. E. *Polymer* **2009**, *50*, 3575–3581.

41. Marshall, E. L.; Gibson, V. C.; Rzepa, H. S. *J. Am. Chem. Soc.* **2005**, *127*, 6048–6051.

42. von Schenck, H.; Ryner, M.; Albertsson, A.-C.; Svensson, M. *Macromolecules* **2002**, *35*, 1556–1562.

43. Ryner, M.; Stridsberg, K.; Albertsson, A.-C.; von Schenck, H.; Svensson, M. *Macromolecules* **2001**, *34*, 3877–3881.

44. Foster, J.; Weinhold, F. *J. Am. Chem. Soc.* **1980**, *102*, 7211–7218.

45. Reed, A.; Curtis, L.; Weinhold, F. *Chem. Rev.* **1988**, *88*, 899–926.

46. Herres-Pawlis, S.; Neuba, A.; Seewald, O.; Seshadri, T.; Egold, H.; Flörke, U.; Henkel, G. *Eur. J. Org. Chem.* **2005**, 4879–4890.

47. Kantlehner, W.; Haug, E.; Mergen, W.; Speh, P.; Maier, T.; Kapassakalidis, J.; Bräuner, H.-J.; Hagen, H. *Liebigs Ann. Chem.* **1984**, *1*, 108–125.

48. Börner, J.; dos Santos Vieira, I.; Flörke, U.; Döring, A.; Kuckling, D.; Herres-Pawlis, S. *Polym. Prepr. (Am. Chem. Soc., Div. Polym. Chem.)* **2010**, *51*, 743–744.

49. Börner, J.; Flörke, U.; Döring, A.; Kuckling, D.; Jones, M. D.; Herres-Pawlis, S. *Sustainability* **2009**, *1*, 1226–1239.

50. Otero, A.; Fernandez-Baeza, J.; Lara-Sanchez, A.; Alonso-Moreno, C.; Marquez-Segovia, I.; Sanchez-Barba, L. F.; Rodriguez, A. M. *Angew. Chem.* **2009**, *121*, 2210–2213.

51. Gauchenova, E. V. Ph.D. Thesis, Universität Marburg, 2006.

52. Wittmann, H.; Raab, V.; Schorm, A.; Plackmeyer, J.; Sundermeyer, J. *Eur. J. Inorg. Chem.* **2001**, 1937–1948.

53. Miranda, C.; Escarti, F.; Lamarque, L.; Yunta, M.; Navarro, P.; Garcia-Espana, E.; Jimeno, M. *J. Am. Chem. Soc.* **2004**, *126*, 823–833.

54. Formica, M.; Giorgi, L.; Fusi, V.; Micheloni, M.; Pontellini, R. *Polyhedron* **2002**, *21*, 1351–1356.

55. Sundermeyer, J.; Raab, V.; Gaoutchenova, E.; Garrelts, U.; Abacilar, N.; Harms, K. In *Activating Unreactive Substrates*; Bolm, C., Ekkehardt-Hahn, F., Eds.; Wiley-VCH: Weinheim, Germany, 2009; Chapter 2, pp 17−38.

56. van Leeuwen, P. W. N. M.; Groeneveld, W. L. *Inorg. Nucl. Chem. Lett.* **1967**, *3*, 145–146.

57. Zell, M.; Padden, B.; Paterick, A.; Thakur, K.; Kean, R.; Hillmyer, M.; Munson, E. *Macromolecules* **2002**, *35*, 7700−7707.

58. SMART (Version 5.62), SAINT (Version 6.02), SHELXTL (Version 6.10), and SADABS (Version 2.03); Bruker AXS, Inc., Madison, WI, 2002

59. Gaussian 03, Revision E.01; Frisch, M. J.; Trucks, G. W.; Schlegel, H. B.; Scuseria, G. E.; Robb, M. A.; Cheeseman, J. R.; Montgomery, J. A., Jr.; Vreven, T.; Kudin, K. N.; Burant, J. C.; Millam, J. M.; Iyengar, S. S.; Tomasi, J.; Barone, V.; Mennucci, B.; Cossi, M.; Scalmani, G.; Rega, N.; Petersson, G. A.; Nakatsuji, H.; Hada, M.; Ehara, M.; Toyota, K.; Fukuda, R.; Hasegawa, J.; Ishida, M.; Nakajima, T.; Honda, Y.; Kitao, O.; Nakai, H.; Klene, M.; Li, X.; Knox, J. E.; Hratchian, H. P.; Cross, J. B.; Bakken, V.; Adamo, C.; Jaramillo, J.; Gomperts, R.; Stratmann, R. E.; Yazyev, O.; Austin, A. J.; Cammi, R.; Pomelli, C.; Ochterski, J. W.; Ayala, P. Y.; Morokuma, K.; Voth, G. A.; Salvador, P.; Dannenberg, J. J.; Zakrzewski, V. G.; Dapprich, S.; Daniels, A. D.; Strain, M. C.; Farkas, O.; Malick, D. K.; Rabuck, A. D.; Raghavachari, K.; Foresman, J. B.; Ortiz, J. V.; Cui, Q.; Baboul, A. G.; Clifford, S.; Cioslowski, J.; Stefanov, B. B.; Liu, G.; Liashenko, A.; Piskorz, P.; Komaromi, I.; Martin, R. L.; Fox, D. J.; Keith, T.; Al-Laham, M. A.; Peng, C. Y.; Nanayakkara, A.; Challacombe, M.; Gill, P. M. W.; Johnson, B.; Chen, W.; Wong, M. W.; Gonzalez, C.; Pople, J. A. Gaussian, Inc.: Wallingford, CT, 2004.

60. Mark, J. E. *Polymer Data Handbook*; Oxford University Press: New York, 1999.

Subject Index